TIME-DEPENDENT MODELING OF RADIATIVE PROCESSES IN MAGNETIZED ASTROPHYSICAL PLASMAS

INDREK VURM

Division of Astronomy
Department of Physics
University of Oulu
Finland

Academic Dissertation to be presented with the assent of the Faculty of Science, University of Oulu, for public discussion in the Auditorium Anttilansali, Linnanmaa, on October 22nd, 2010, at 12 o'clock.

OULU 2010 • UNIVERSITY OF OULU

Vurm, Indrek: The doctoral thesis at the Division of Astronomy, Department of Physics

Department of Physics
P.O. Box 3000
FIN-90014 University of Oulu
FINLAND

Supervisors
Prof. Juri Poutanen, University of Oulu, Finland
Dr. Tõnu Viik, Tartu Observatory, Estonia

Reviewers
Dr. Gabriele Ghisellini, Brera Astronomical Observatory, Merate, Italy
Prof. Andrzej A. Zdziarski, N. Copernicus Astronomical Centre, Warsaw, Poland

Opponent
Dr. Gabriele Ghisellini, Brera Astronomical Observatory, Merate, Italy

Custos
Prof. Juri Poutanen, University of Oulu, Finland

Cover artwork: “Gamma-ray burst”
Credit: ESO/A. Roquette

ISBN 978-951-42-6331-6
ISBN 978-951-42-6333-0 (PDF)

OULU UNIVERSITY PRESS
Oulu 2010

Abstract

A variety of different classes of astrophysical sources exhibit spectra that span many orders of magnitude in photon energy, ranging from radio wavelengths to high-energy gamma-rays. Such objects can often be associated with a compact object (black hole or a neutron star) and include relativistic jets from active galaxies, gamma-ray bursts, accreting black holes and neutron stars in X-ray binaries etc. The formation of the broad-band spectrum typically takes place in hot plasma through different processes like synchrotron radiation, inverse Compton scattering, photon–photon pair production. Understanding the physical conditions in these objects requires detailed modeling of the particle–photon interactions.

Numerical simulations of radiative processes in magnetized compact sources are complicated because both particle and photon distributions span several orders of magnitude in energy, the distributions strongly depend on each other, the radiative processes behave significantly differently depending on the energy regime, and, finally, due to the enormous difference in the time-scales of the processes. We have developed a novel computer code for time-dependent simulations that overcomes these problems. The processes taken into account are Compton scattering, electron–positron pair production and annihilation, Coulomb scattering as well as synchrotron emission and absorption. The relevant kinetic equations are discussed in detail. Analytic expressions for the rates of all included physical processes are calculated without approximations. We solve coupled integro-differential kinetic equations for photons and electrons/positrons without any limitations on the photon and lepton energies. A numerical scheme is proposed to guarantee energy conservation when dealing with synchrotron processes in electron and photon equations. The code is tested using several problems described previously in the literature. Good agreement with previous works is found in the parameter regimes where comparison is feasible, with the differences attributable to our improved treatment of the microphysics.

We apply the code to study two different astrophysical problems: prompt gamma-ray burst emission from neutron-loaded flows and spectral states of black hole X-ray binaries.

Nuclear collisions in neutron-loaded gamma-ray burst outflows can dissipate a significant fraction of the flow energy, resulting in heating as well as high-energy injection of electron–positron pairs. We use our time-dependent code to self-consistently follow the evolution of particle and photon distributions along the flow and find that the emerging Comptonized spectra resemble those typically observed in gamma-ray bursts, peaking close to 1 MeV. Hard observed spectra below the peak that present a problem to (synchrotron) shock models are easily reproduced. The high-energy spectrum extends to several GeV without a cutoff. Magnetization of the flow will lead to softer spectra peaking at somewhat lower energies. An additional synchrotron spectral component below $\sim$ 50 keV (soft excess) is also produced.

We discuss the origin of dramatically different electron distributions responsible for Comptonization in black hole X-ray binaries in their various states. In the absence of external soft photons, the electrons are efficiently thermalized by synchrotron self-absorption and Coulomb scattering even for pure non-thermal electron injection. The resulting quasi-thermal synchrotron self-Compton spectra have very stable slopes and electron temperatures similar to the hard states of black hole binaries. The observed hard X-ray spectral slopes, the cutoff at 100 keV, and the MeV tail together require low magnetic fields ruling out the magnetic dissipation mechanism. The motion of the accretion disk towards the black hole results in larger Compton cooling and lower equilibrium electron temperature. Our self-consistent simulations show that in this case both electron and photon distributions attain a power-law-dominated shape similar to what is observed in the soft state. The electron distribution in the Cyg X-1 soft state might require a strong magnetic field, being consistent with the magnetically-dominated corona.

Acknowledgments

The present work was carried out at the Department of Physics, University of Oulu.

I would first like to thank Dr. Tõnu Viik, who first sparked my interest in astronomy and gave me my first project. He is also the person who introduced me to Prof. Juri Poutanen, who became the main supervisor of the present thesis. I am deeply indebted to Prof. Juri Poutanen, whose day-to-day advice and unfailing support helped me through some very difficult times. Without his help this thesis would never have been completed.

I am grateful to Prof. Andrei M. Beloborodov for his support and advice regarding the gamma-ray burst project, as well as for the chance to visit and work with him at the Columbia University, New York. I also wish to thank Dr. Gabriele Ghisellini and Prof. Andrzej Zdziarski for pre-examining the thesis and giving some useful comments.

My gratitude also goes to Askar Ibragimov, Alexandra Veledina, Jari Kajava and Marja Annala at the University of Oulu for their friendship and support during the work that led to the completion of this thesis.

I thank the Department of Physics, University of Oulu, for placing at my disposal the facilities necessary to carry out this research. I thank CIMO, Academy of Finland and the Wihuri Foundation for financial support.

I am also grateful to my parents for their support, both personal and financial, especially at the initial stages of my studies. Finally, my greatest thanks go to my wife Liis Roosaar, who has stood by me and supported me throughout those years.

Oulu, September 2010 Indrek Vurm

List of original papers

The present thesis is partly based on the following papers:

Paper I: Vurm I., Poutanen J.: Electron thermalization and photon emission from magnetized compact sources, 2008, International Journal of Modern Physics D, 17, 1629

Paper II: Poutanen J., Vurm I.: On the Origin of Spectral States in Accreting Black Holes, 2009, Astrophysical Journal Letters, 690, L97

Paper III: Vurm I., Poutanen J.: Time-Dependent Modeling of Radiative Processes in Hot Magnetized Plasmas, 2009, Astrophysical Journal, 698, 293

Paper IV: Poutanen J., Vurm I.: Theory of Compton scattering by anisotropic electrons, 2010, Astrophysical Journal Supplement Series, 189, 286.

Paper V: Vurm I., Beloborodov A. M., Poutanen J.: Gamma-ray bursts from magnetized neutron-loaded flows, 2010, in preparation.

Contents

Introduction

Spectral energy distributions of a number of compact, magnetized, high-energy sources such as relativistic jets from active galaxies, gamma-ray bursts, black hole accretion disk–coronae are strongly affected and shaped by Compton scattering, synchrotron radiation and electron–positron pair production (see e.g. Gierliński et al. 1999; Ghisellini et al. 2002; Zdziarski & Gierliński 2004; Stern & Poutanen 2004). Understanding the physical conditions in these sources requires detailed modeling of the interactions between the particles and photons, which is not an easy task. The basic problem is that we cannot compute radiative processes from a given a priori lepton distribution (e.g. Maxwellian or a power-law), because it depends strongly on the radiation field, which in its turn is determined by the particle distribution. Another problem is that the time-scales for various processes differ by orders of magnitude. The energy range of particles and photons responsible for the emission also spans many orders of magnitude, with different processes making dominant contributions to the emergent spectrum in different bands. One of the main difficulties in calculating radiative processes over a wide range of energies is that a particular radiative process may behave significantly differently depending on the energy regime, the most well-known example of such processes being also the most important in relativistic plasma, namely Compton scattering. Depending on the energies of the interacting particles, an electron or a photon can lose (or gain) a significant or negligible fraction of its initial energy in one scattering. The former case has to be accounted for by the integral scattering terms in the kinetic equations, while the latter necessitates the Fokker-Planck treatment.

The treatment of radiative processes in relativistic plasmas has been the subject of several works. There are two basic approaches: Monte Carlo methods (e.g. Stern et al. 1995a; Pilla & Shaham 1997) and solving the relevant kinetic equations (e.g. Lightman & Zdziarski 1987; Coppi 1992, 1999; Nayakshin & Melia 1998; Pe'er & Waxman 2005; Belmont et al. 2008). Both have their own advantages and disadvantages. Monte Carlo treatment makes it easy to take into account radiative transfer effects, on the other hand it usually suffers from poor photon statistics at high energies. Another problem can arise at very low energies, where the optical thickness to synchrotron absorption can be enormous. In the kinetic theory approach photon statistics is not an issue, the sole difficulty lies in solving the relevant integro-differential equations. In this work we have chosen to follow the second approach.

Due to the difficulties in solving the exact Boltzmann equations of the kinetic theory, different simplifying approximations have been made in earlier works. They fall in three basic categories: ad hoc assumptions about the particle energy distributions, approximate treatment of different physical processes, and simplified treatment of radiative transport. Various approximations invoked to simplify the treatment of radiative processes at the same time limit the range of their applicability. One commonly employed approximation concerns Compton scattering, which is assumed to take place in the Thomson regime (e.g. Ghisellini et al. 1998) and is accounted for by a simple cooling term in the electron equation. This sets two restrictions that the photon energy in the electron rest frame is smaller than the electron rest energy and the average photon energy is much lower than the electron kinetic energy. Otherwise all photons would not contribute to electron cooling, the higher energy ones being downscattered via Compton scattering. This means that one is unable to treat cases when Comptonization approaches saturation, which may be relevant at high compactnesses, and to study electron heating by external radiation. Other works account for Klein-Nishina corrections to the electron cooling rate, but still neglect the diffusive nature of the process when electron and photon energies are comparable (Coppi 1992; Moderski et al. 2005; Pe'er & Waxman 2005), which works towards establishing an equilibrium Maxwellian distribution. Another useful approximation, when the integral terms describing Compton scattering are accounted for, is to consider ultrarelativistic electrons and very low energy photons (e.g. Zdziarski 1988; Moderski et al. 2005). This, however, becomes increasingly inaccurate when the electrons cool to sufficiently low energies.

The cyclo-synchrotron process also exhibits qualitatively different behavior depending on the energy of the radiating particles. If the emitting particles are relativistic, the emission spectrum is smooth and can span several orders of magnitude in energy, while in the non-relativistic case the energy is radiated at discrete cyclotron harmonics and most of this radiation might be strongly self-absorbed. In the first case, the radiating particle (electron or positron) mostly loses its energy in a continuous fashion, while in the second case it can gain energy by absorbing the cyclo-synchrotron photons emitted by other particles. This process is a dominant particle thermalization mechanism in compact magnetized sources (Ghisellini et al. 1988). Its proper account requires accurate emissivities in the transrelativistic regime, because electron thermalization usually takes place at mildly relativistic energies. Some codes for computing radiative processes in relativistic plasma (e.g. EQPAIR described in Coppi 1992, 1999) neglect this process completely as the electrons are *assumed* to be thermal at low energies or account for thermalization by Coulomb collisions only (Nayakshin & Melia 1998). In other approaches synchrotron thermalization is computed (Ghisellini et al. 1998), but Compton scattering is then considered only approximately.

Owing to the fact that proper treatment of transport processes for all types of particles would make the task prohibitively difficult, and partly due to our igno-

rance of the exact geometry of the problem, it is rather common practice to neglect radiative transport altogether (e.g. Lightman & Zdziarski 1987; Coppi 1992) and assume spatially homogeneous and isotropic particle distributions. In this case particle and photon loss from the system is modeled in terms of simple escape probabilities. We also follow this approach here.

The main purpose of this project has been to develop a new numerical code that can overcome the aforementioned difficulties and accurately treat the evolution of particle and photon distributions in relativistic plasmas interacting via Compton scattering, synchrotron emission and absorption, electron-positron pair production and annihilation as well as Coulomb scattering. No approximations have been made regarding the treatment of physical processes, thus the code can handle a practically unlimited range of particle/photon energies. The code can treat particle thermalization by synchrotron self-absorption, Coulomb (Møller) scattering as well as Compton scattering. It can also handle pair-cascades irrespective of their type (for classification of pair cascades, see Svensson 1987). Good energy conservation, wide energy range as well as the inclusion of all the most important radiative processes in hot plasma make the code applicable to a large variety of astrophysical phenomena, two of which are considered in this work.

The thesis is divided into three parts. In Part I we consider separately all the included physical processes. Starting from the general form of the kinetic equations for electrons, positrons and photons, we rewrite them for each process in a form that is directly "usable", which depends on the peculiarities of a particular process. As a result, the resulting kinetic equations will contain both integral and up to second-order differential terms, accounting for both discrete as well as continuous energy exchange mechanisms. The inclusion of second-derivative terms also enables us to treat diffusion in energy space and consequently particle thermalization. We derive exact explicit expressions for all the relevant rates, cross-sections, emissivities etc., without limitations on the particles' energies.

In Part II we describe in detail the numerical code that solves the coupled integro-differential kinetic equations describing time evolution of the photon and lepton distributions. The numerical scheme was developed with two main goals in mind: accurate energy conservation and relaxation to correct equilibrium distributions. The former goal necessitates special care for some processes. For example, extreme caution has to be taken when dealing with synchrotron self-absorption, because of cancellation of large, almost equal terms, which can result in inaccuracies and huge energy sinks. Also, accurate treatment of Compton scattering requires the substitution of Fokker-Planck differential terms instead of integral terms in regimes where the energy gain/loss in a single scattering becomes small compared to the energy bin size. The coefficients in the Fokker-Planck equation in this case are computed exactly from the moments of the integral equation, ensuring energy conservation. Numerical simulations show that our code conserves energy with about 1% accuracy. We present an extensive testing of the code using

some problems described previously in the literature. Processes involving bremsstrahlung can be easily added to the code, while for the conditions considered in this work, they are not important.

In Part III we consider two astrophysical problems where the kinetic code finds its application. First, we study radiative processes in relativistic diverging outflows under conditions characteristic of gamma-ray bursts. This is done in the framework of a so-called neutron-loaded fireball model (Beloborodov 2010). An initially optically thick radiation-dominated flow accelerates to relativistic velocities at the expense of its internal energy. At a certain radius the proton and neutron components of the flow decouple, which can lead two embedded flows with different Lorentz factors. Nuclear collisions in such compound flows can dissipate a significant fraction of the total flow energy. Detailed numerical modeling of radiative processes in these flows lead to prompt emission spectra resembling the Band spectrum (Band et al. 1993), with hard low-energy slopes. Significant GeV emission is also predicted, along with a Lorentz-boosted annihilation line.

As another application we study the radiative mechanisms giving rise to different spectral states in black hole X-ray binaries. We discuss the origin of the dramatically different distributions of the Comptonizing electrons in various states. Studying the interplay between electron thermalization and radiative cooling lends support to the scenario in which spectral state transitions are the result of a variable amount of soft photons entering the active region from the cool accretion disk, associated with a changing inner disk radius.

Part I

Physical processes

Chapter 1

Theory of Compton scattering by anisotropic electrons

1.1 Introduction

Compton scattering is one of the most important radiative processes that shapes the spectra of various sources: black holes and neutron stars in X-ray binaries, pulsars and pulsar wind nebulae, jets from active galactic nuclei, and the early universe. Compton scattering kernel takes a simple form if electrons are ultra-relativistic with the Lorentz factor $\gamma \gg 1$ (Blumenthal & Gould 1970). In a general case, when no restrictions are made on the energies of photon and electrons, Jones (1968) derived the kernel for isotropic electrons and photons. The formulae there contain a few misprints, but even by correcting those (see e.g. Pe'er & Waxman 2005) they cannot be used for calculations because of a number of numerical cancellations (see e.g. Belmont 2009). An alternative derivation to that kernel was given by Brinkmann (1984) and Nagirner & Poutanen (1994), who showed how to extend the numerical scheme to cover all photon and electron energies of interest in astrophysical sources.

In real astrophysical environments, the radiation field does not need to be isotropic and a more general redistribution function is required to describe angle-dependent Compton scattering. Nagirner & Poutanen (1994) extended previous results to the situation when the photon distribution can be represented as a linear function of some polar angle cosine (Eddington approximation), deriving an analytical formula for the first moment of the kernel. Aharonian & Atoyan (1981) were the first to derive a redistribution function for arbitrary photon angular dependence (see also Prasad et al. 1986). Kershaw et al. (1986) and Kershaw (1987) have developed numerical methods to compute the kernel efficiently and with a high accuracy. All these works neglect the effect of photon polarization.

Nagirner & Poutanen (1993) have derived a general Compton scattering redistribution matrix for Stokes parameters assuming an isotropic electron distribution. A general relativistic kinetic equation incorporating the effects of induced scatter-

ing and polarization of photons as well as electron polarization and degeneracy has been derived by Nagirner & Poutanen (2001).

In this chapter we propose a method to extend previous results to the case where the electron distribution is no longer isotropic, but can have weak anisotropies which can be represented as a second order polynomial of the cosine of some polar angle. The proposed formalism can find its application in a number of astrophysical problems. The distortion of the cosmic microwave background (CMB) caused by the hot electron gas in clusters of galaxies (i.e. the kinematic and thermal Sunyaev-Zeldovich effect) is an obvious application. The electron distribution, isotropic in the cluster frame, can be Lorentz transformed to the CMB frame, resulting in a dipole term linear in cluster velocity and a small quadrupole correction. Compton scattering then can be directly computed in the CMB frame. Another possible application concerns the models of outflowing accretion disk-coronae or jets (Beloborodov 1999; Malzac et al. 2001). If the outflow velocities are non-relativistic, the radiation transport can be considered directly in the accretion disk frame following recipe by Poutanen & Svensson (1996), with the Lorentz transformed electron distribution.

Weak anisotropies in the electron distribution can arise in high-energy sources with ordered magnetic field, because of the pitch angle-dependence of the synchrotron cooling rate and/or anisotropic injection of high-energy electrons (e.g. Bjornsson 1985; Roland et al. 1985; Crusius-Waetzel & Lesch 1998; Schopper et al. 1998). An anisotropic electron distribution is also a very natural outcome of the photon breeding operation in relativistic jets with the toroidal magnetic field (Stern & Poutanen 2006, 2008), because the electron-positron pairs born inside the jet by the external high-energy photons move perpendicularly to the field.

Our method is also extendable to the polarized radiation using the techniques developed in Nagirner & Poutanen (1993). It is also in principle possible to calculate the scattering redistribution function in the case when the electron distribution is expressible as an arbitrary order expansion over the polar angle cosine. Unfortunately, in the latter case the analytical expressions become extremely cumbersome and the advantage over direct numerical integration becomes small.

Although here we consider only photon scattering it is also possible to apply the same method for electrons interacting with the photons in the case when photon angular distribution is expressible as an expansion of powers of the polar angle cosine. This can be of interest only in the deep Klein-Nishina regime where the electron can lose or gain a large fraction of its initial energy in one scattering and continuous energy loss approach is not applicable.

This chapter is organized as follows. In Section 1.2 we introduce the relativistic kinetic equation for Compton scattering and define the redistribution function and total cross-section. The expressions for the total cross-section, the mean energy and dispersion of scattered photons, and the radiation pressure force are given in Section 1.3. The exact analytical formulae for the redistribution function for mono-energetic anisotropic electrons as well as approximate formulae

valid in the Thomson regime are derived in Section 1.4. We present the numerical examples of redistribution functions in Section 1.5, the relativistic theory of the Sunyaev-Zeldovich effect is developed in Section 1.6. We summarize our findings in Section 1.7.

1.2 Relativistic kinetic equation

Let us define the dimensionless photon four-momentum as $\underline{x} = \{x, \boldsymbol{x}\} = x\{1, \boldsymbol{\omega}\}$, where $\boldsymbol{\omega}$ is the unit vector in the photon propagation direction and $x \equiv h\nu/m_{\rm e}c^2$. The photon distribution will be described by the occupation number n. The dimensionless electron four-momentum is $\underline{p} = \{\gamma, \boldsymbol{p}\} = \{\gamma, p\boldsymbol{\Omega}\} = \gamma\{1, \beta\boldsymbol{\Omega}\}$, where $\boldsymbol{\Omega}$ is the unit vector along the electron momentum, γ and $p = \sqrt{\gamma^2 - 1}$ are the electron Lorentz factor and its momentum in units of $m_{\rm e}c$, and $\beta = p/\gamma$ is the electron velocity in units of speed of light. The momentum distribution of electrons is described by the relativistically invariant distribution function $f_{\rm e}(\boldsymbol{p})$ (see Belyaev & Budker 1956; Nagirner & Poutanen 1994).

The interaction between photons and electrons via Compton scattering (in linear approximation, i.e. ignoring induced scattering and electron degeneracy) can be described by the explicitly covariant relativistic kinetic equation for photons (Pomraning 1973; Nagirner & Poutanen 1993; Nagirner & Poutanen 1994):

$$\begin{aligned} \underline{x} \cdot \underline{\nabla} n(\boldsymbol{x}) &= \frac{r_{\rm e}^2}{2} \int \frac{d^3p}{\gamma} \frac{d^3p_1}{\gamma_1} \frac{d^3x_1}{x_1} \, \delta^4(\underline{p}_1 + \underline{x}_1 - \underline{p} - \underline{x}) \, F \\ &\times \left[n(\boldsymbol{x}_1) f_{\rm e}(\boldsymbol{p}_1) - n(\boldsymbol{x}) f_{\rm e}(\boldsymbol{p}) \right], \end{aligned} \tag{1.1}$$

where $\underline{\nabla} = \{\partial/c\partial t, \boldsymbol{\nabla}\}$ is the four-gradient, $r_{\rm e}$ is the classical electron radius, F is the Klein-Nishina reaction rate (Berestetskii et al. 1982)

$$F = \left(\frac{1}{\xi} - \frac{1}{\xi_1} \right)^2 + 2 \left(\frac{1}{\xi} - \frac{1}{\xi_1} \right) + \frac{\xi}{\xi_1} + \frac{\xi_1}{\xi}, \tag{1.2}$$

and

$$\xi = \underline{p}_1 \cdot \underline{x}_1 = \underline{p} \cdot \underline{x}, \qquad \xi_1 = \underline{p}_1 \cdot \underline{x} = \underline{p} \cdot \underline{x}_1 \tag{1.3}$$

are the four-products of corresponding momenta. The second equalities in both equations (1.3) arise from the four-momentum conservation law. The invariant scalar product of the photon four-momenta can be written in the laboratory frame as well as in the frame related to a specific electron

$$q \equiv \underline{x} \cdot \underline{x}_1 = x x_1 (1 - \mu) = \xi \xi_1 (1 - \mu_0) = \xi - \xi_1, \tag{1.4}$$

where $\mu = \boldsymbol{\omega} \cdot \boldsymbol{\omega}_1$ is the cosine of the photon scattering angle in some frame and μ_0 is the corresponding cosine in the electron rest frame.

In any frame, the kinetic equation can be also put in the usual form of the radiative transfer equation (Nagirner & Poutanen 1993):

$$\left(\frac{1}{c}\frac{\partial}{\partial t} + \boldsymbol{\omega}\cdot\boldsymbol{\nabla}\right) n(\boldsymbol{x}) = -\sigma_{\rm T}\, N_{\rm e}\, \overline{s}_0(\boldsymbol{x})\, n(\boldsymbol{x}) + \sigma_{\rm T} N_{\rm e}\, \frac{1}{x}\int_0^\infty x_1 dx_1 \int d^2\omega_1\, R(\boldsymbol{x}_1 \rightarrow \boldsymbol{x}) n(\boldsymbol{x}_1), \quad (1.5)$$

where $N_{\rm e}$ is the electron density in that frame. Here we have defined the photon redistribution function

$$R(\boldsymbol{x}_1 \rightarrow \boldsymbol{x}) = \frac{3}{16\pi}\frac{1}{N_{\rm e}}\int \frac{d^3p}{\gamma}\frac{d^3p_1}{\gamma_1} f_{\rm e}(\boldsymbol{p}_1) F \delta^4(\underline{p}_1 + \underline{x}_1 - \underline{p} - \underline{x}) \quad (1.6)$$

and the total scattering cross-section (in units of Thomson cross-section $\sigma_{\rm T}$)

$$\overline{s}_0(\boldsymbol{x}) = \frac{3}{16\pi}\frac{1}{N_{\rm e}}\frac{1}{x}\int \frac{d^3p}{\gamma}\frac{d^3p_1}{\gamma_1}\frac{d^3x_1}{x_1} f_{\rm e}(\boldsymbol{p})\, F\, \delta^4(\underline{p}_1 + \underline{x}_1 - \underline{p} - \underline{x}). \quad (1.7)$$

1.2.1 Electron distribution and scattering geometry

Let us now consider a specific frame E. Our basic assumption is that the anisotropy of the electron distribution in this frame can be expressed as a second order polynomial expansion in the cosine of the polar angle in some coordinate system $(\boldsymbol{l}_1, \boldsymbol{l}_2, \boldsymbol{l}_3)$:

$$\frac{1}{N_{\rm e}} f_{\rm e}(\boldsymbol{p}) = f_{\rm e}(\gamma, \eta_{\rm e}) = \sum_{k=0}^{2} f_k(\gamma) P_k(\eta_{\rm e}), \quad (1.8)$$

where $N_{\rm e}$ is the electron density in frame E, $\eta_{\rm e} = \boldsymbol{\Omega}\cdot\boldsymbol{l}_3$ is the cosine of the polar angle of the electron momentum, $P_k(\eta_{\rm e})$ are the Legendre polynomials, and we now switched to the dimensionless distribution function $f_{\rm e}(\gamma, \eta_{\rm e})$ normalized to unity:

$$\int d^2\Omega \int f_{\rm e}(\gamma, \eta_{\rm e})\, p^2 dp = 1. \quad (1.9)$$

The moments f_0, f_1 and f_2 determine the energy spectrum of electrons and the relative magnitudes of the isotropic and anisotropic components. The distribution function for mono-energetic electrons of energy γ_0 can be described by

$$f_{\rm e}(\gamma, \eta_{\rm e}) = \frac{1}{4\pi\, p\gamma}\delta(\gamma - \gamma_0)\left[1 + \frac{f_1}{f_0}\eta_{\rm e} + \frac{f_2}{f_0}P_2(\eta_{\rm e})\right], \quad (1.10)$$

where the ratios f_1/f_0 and f_2/f_0 are constants.

The directions of photons in this coordinate system (see Figure 1.1) are given by

$$\boldsymbol{\omega} = \sqrt{1-\eta^2}\cos\phi\, \boldsymbol{l}_1 + \sqrt{1-\eta^2}\sin\phi\, \boldsymbol{l}_2 + \eta\, \boldsymbol{l}_3, \quad (1.11)$$

$$\boldsymbol{\omega}_1 = \sqrt{1-\eta_1^2}\cos\phi_1\, \boldsymbol{l}_1 + \sqrt{1-\eta_1^2}\sin\phi_1\, \boldsymbol{l}_2 + \eta_1\, \boldsymbol{l}_3, \quad (1.12)$$

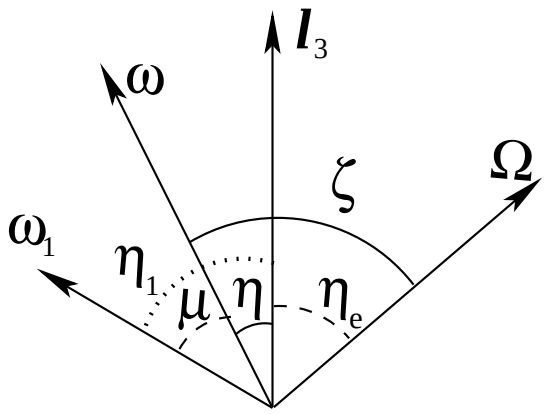

Figure 1.1: The scattering particles' momentum vectors and the vector $\boldsymbol{l}_3$. Note that the shown angular variables are the cosines of the respective angles.

so that the cosine of the scattering angle is

$$\mu = \boldsymbol{\omega} \cdot \boldsymbol{\omega}_1 = \eta\eta_1 + \sqrt{1-\eta^2}\sqrt{1-\eta_1^2}\cos(\phi - \phi_1). \tag{1.13}$$

1.3 Total cross section and mean powers of energies

1.3.1 Total cross-section

Let us simplify the expression for the total cross-section. We follow here the approach described in Nagirner & Poutanen (1994). We rewrite the cross-section as

$$\overline{s}_0(\boldsymbol{x}) = \frac{1}{x}\int s_0(\xi)\,\xi\; f_e(\gamma,\eta_e)\,\frac{d^3p}{\gamma}, \tag{1.14}$$

where

$$s_0(\xi) = \frac{3}{16\pi}\frac{1}{\xi}\int \frac{d^3p_1}{\gamma_1}\frac{d^3x_1}{x_1}\,F\,\delta^4(\underline{p}_1 + \underline{x}_1 - \underline{p} - \underline{x}). \tag{1.15}$$

Using the identity

$$\delta(\gamma_1 + x_1 - \gamma - x) = \gamma_1\,\delta\left(\underline{x}_1\cdot(\underline{p}+\underline{x}) - \underline{x}\cdot\underline{p}\right) \tag{1.16}$$

and taking the integral over $\boldsymbol{p}_1$ in equation (1.15), we get

$$\begin{aligned} s_0(\xi) &= \frac{3}{16\pi}\frac{1}{\xi}\int \frac{d^3x_1}{x_1}\,F\,\delta\left(\underline{x}_1\cdot(\underline{p}+\underline{x}) - \underline{x}\cdot\underline{p}\right) \\ &= \frac{3}{16\pi}\frac{1}{\xi}\int \xi_1 d\xi_1\,d\mu_0\,d\phi_0\;\; F\,\delta\left[\xi_1 + \xi\xi_1(1-\mu_0) - \xi\right] \\ &= \frac{3}{8\xi^2}\int_{\xi/(1+2\xi)}^{\xi} F\,d\xi_1, \end{aligned} \tag{1.17}$$

where we used invariant $x_1 dx_1 d^2\omega_1 = \xi_1 d\xi_1\, d\mu_0\, d\phi_0$ and the fact that F does not depend on azimuthal angle ϕ_0. Substituting F from equation (1.2) we get (Berestetskii, Lifshitz, & Pitaevskii 1982; Nagirner & Poutanen 1994)

$$s_0(\xi) = \frac{3}{8\xi^2}\left[4 + \left(\xi - 2 - \frac{2}{\xi}\right)\ln(1+2\xi) + 2\xi^2\frac{1+\xi}{(1+2\xi)^2}\right]. \qquad (1.18)$$

Putting $\xi \to x$, we, of course, get the total Klein-Nishina cross-section for a photon of energy x on electrons at rest.

To obtain the total scattering cross-section on an anisotropic electron distribution, we have to calculate the angular integrals over incoming electron directions in equation (1.14). We introduce the cosines between electron momentum and photons:

$$\zeta = \Omega \cdot \boldsymbol{\omega}, \quad \zeta_1 = \Omega \cdot \boldsymbol{\omega}_1 \qquad (1.19)$$

so that

$$\xi = x(\gamma - p\zeta), \quad \xi_1 = x_1(\gamma - p\zeta_1). \qquad (1.20)$$

We choose the spherical coordinate system and measure the polar angle from the direction of the *initial* photon $\boldsymbol{\omega}$, we get

$$\overline{s_0}(\boldsymbol{x}) = \overline{s_0}(x,\eta) = \frac{1}{x}\int_0^\infty \frac{p^2 dp}{\gamma}\int_{-1}^{1} d\zeta\; s_0(\xi)\int_0^{2\pi} d\Phi\; f_{\rm e}(\gamma,\eta_{\rm e}). \qquad (1.21)$$

Azimuth Φ is now defined as the difference between the azimuths of the electron momentum direction and the vector $\boldsymbol{l}_3$ in a frame with z-axis along $\boldsymbol{\omega}$. The angular variable $\eta_{\rm e}$ in the expansion (1.8) is expressed in this frame as

$$\eta_{\rm e} = \eta\zeta + \sqrt{1-\eta^2}\,\sqrt{1-\zeta^2}\cos\Phi. \qquad (1.22)$$

The physical meaning of equation (1.21) can also be understood if we consider a monoenergetic beam of electrons along $\boldsymbol{l}_3$ axis: $f_{\rm e}(\gamma,\eta_{\rm e}) = \delta(\eta_{\rm e}-1)\delta(\gamma - \gamma_0)/(2\pi p\gamma)$. Then

$$\overline{s_0}(x,\eta) = (1-\beta\eta)\, s_0(x'), \qquad (1.23)$$

where $x' = x\gamma(1-\beta\eta)$ is the photon energy in the electron rest frame (we omitted subscript 0 in γ and β). The factor $1-\beta\eta$ in equation (1.23) accounts for the reduced number of collision per unit length.

When calculating the azimuthal integral in equation (1.21) we just have to integrate $P_k(\eta_{\rm e})$ with $\eta_{\rm e}$ given by equation (1.22). The properties of the Legendre polynomials give us the average

$$\overline{P_k(\eta_{\rm e})} = P_k(\eta)\, P_k(\zeta), \qquad (1.24)$$

so that the averaged distribution function becomes

$$\overline{f_{\rm e}}(\gamma,\eta,\zeta) = \frac{1}{2\pi}\int_0^{2\pi} d\Phi\; f_{\rm e}(\gamma,\eta_{\rm e}) = \sum_{k=0}^{2} f_k(\gamma) P_k(\eta)\, P_k(\zeta). \qquad (1.25)$$

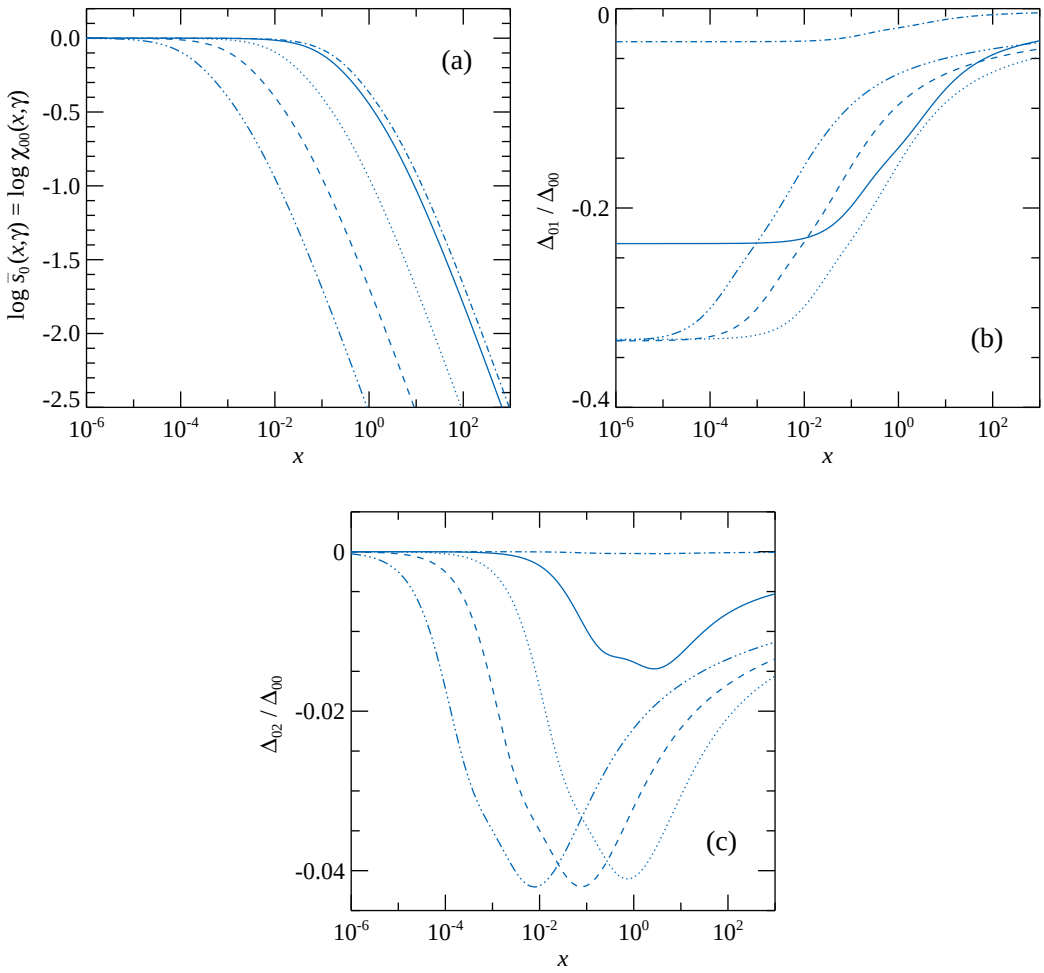

Figure 1.2: (a) Total cross-section $\chi_{00} = \Delta_{00}$ for isotropic mono-energetic electrons of various momenta $p = 0.1, 1, 10, 10^2, 10^3$ (from top to bottom, dot-dashed, solid, dotted, dashed, and triple-dot-dashed curves) as a function of photon energy x. (b) Relative correction to the cross-section arising from the dipole term in the electron distribution (1.8) for the same p as in panel (a). At small x the curves approach the asymptotic value in the Thomson limit $-\beta/3$. (c) Relative correction to the cross-section arising from the quadrupole term Δ_{02}/Δ_{00}.

The cross-section now can be written as

$$\overline{s_0}(x,\eta) = 4\pi \sum_{k=0}^{2} P_k(\eta) \int_1^\infty p\gamma \, d\gamma \; f_k \, \Delta_{0k}(x,\gamma), \tag{1.26}$$

where

$$\Delta_{0k}(x,\gamma) = \frac{1}{2\gamma x} \int_{-1}^{1} P_k(\zeta) \; \xi \; s_0(\xi) \, d\zeta. \tag{1.27}$$

Changing the integration variable and expressing P_k through ξ using equation (1.20), we get

$$\Delta_{0k}(x,\gamma) \;\; = \;\; \sum_{n=0}^{k} b_{nk} \, \chi_{0n}, \tag{1.28}$$

where

$$\chi_{0n}(x,\gamma) = \frac{1}{2\gamma p \, x^{2+n}} \int_{x(\gamma-p)}^{x(\gamma+p)} \xi^{n+1} \; s_0(\xi) \, d\xi. \tag{1.29}$$

and

$$\begin{aligned} b_{00} &= 1, \quad b_{01} = \frac{\gamma}{p}, \quad b_{11} = -\frac{1}{p}, \\ b_{02} &= \frac{1}{2p^2}(2\gamma^2+1), \quad b_{12} = -\frac{3\gamma}{p^2}, \quad b_{22} = \frac{3}{2p^2}. \end{aligned} \tag{1.30}$$

The zeroth function $\Delta_{00} = \chi_{00}$ coincides with the function $\Psi_0(x,\gamma)$ from Nagirner & Poutanen (1994). When electron distribution is isotropic (i.e. $f_1 = f_2 = 0$), expression (1.26) for the total cross-section is reduced to equation (3.4.1) from Nagirner & Poutanen (1994) and the dependence on η obviously disappears. Functions χ_{0n} of two arguments can be presented through the functions of one argument:

$$\chi_{0n}(x,\gamma) = \frac{1}{2\gamma p} \; \frac{u^{2+n}}{2+n} \psi_{n+1,0}(xu) \Big|_{u=\gamma-p}^{u=\gamma+p}, \tag{1.31}$$

where

$$\psi_{i0}(\xi) = \frac{i+1}{\xi^{i+1}} \int_0^\xi t^i s_0(t) dt. \tag{1.32}$$

The explicit expressions for the functions $\psi_{i0}(\xi)$ ($i = 1, 2, 3$) can be found in Appendix A.2 (see also Nagirner & Poutanen (1994)). Thus the total cross-section is given by a single integral over the electron energy (1.26) with all functions under the integral given by analytical expressions. Numerical calculations of functions Δ_{0k} can be separated into three regimes: (1) in the Thomson regime, $x\gamma \ll 1$, the series expansion (see Appendix A.4) can be used; (2) for $p \ll 1$, but x not sufficiently small for regime (1), we numerically take the integral in equation (1.27) using 5-point Gaussian quadrature to reach accuracy better than 1%; (3) in other cases, we use the sum in equation (1.28) and analytical expressions (1.31) for χ_{0n}.

For mono-energetic electron distribution of Lorentz factor γ given by equation (1.10), we can introduce the cross-section analogously to equation (1.26):

$$\overline{s_0}(x,\gamma,\eta) = \sum_{k=0}^{2} \frac{f_k}{f_0} P_k(\eta)\Delta_{0k}(x,\gamma). \tag{1.33}$$

For isotropic mono-energetic electrons, the total cross-section is shown in Figure 1.2(a). The relative corrections arising due to the dipole and quadrupole term in the electron distribution are shown in Figures 1.2(b) and 1.2(c), respectively. These have to be multiplied by the angle- and, possibly, the energy-dependent factor $P_k(\eta)\, f_k/\, f_0$ to obtain the final correction. In the Thomson limit, at small $x\gamma \ll 1$, the cross-section takes the form (see Appendix A.4)

$$\overline{s_0}(x,\gamma,\eta) \approx 1 - \frac{1}{3}\frac{f_1}{f_0}\,\eta\beta, \tag{1.34}$$

where the correction to unity term can be easily obtained by averaging the transport cross-section over electron directions (i.e. integrating $(1-\beta\zeta)\eta_e$ over the angles). This corresponds to the flattening in Figure 1.2(b) at $\Delta_{01}/\Delta_{00} = -\beta/3$. The correction from the quadrupole term in this regime as well as for non-relativistic electrons becomes negligible:

$$\Delta_{02}/\Delta_{00} \approx -\frac{4}{15}\,\beta^2\,(x\gamma). \tag{1.35}$$

1.3.2 Mean powers of scattered photon energy

In some situations, the full relativistic kinetic equations can be substituted by the approximate one obtained in the Fokker-Planck approximation. This requires knowledge of various moments of the redistribution function, such as total cross-section, the mean energy and dispersion of the scattered photons (see Nagirner & Poutanen 1994, Vurm & Poutanen 2009). It is often time-consuming to compute numerically the integrals of the redistribution function and instead direct calculations of the moments are preferable. Below we obtain analytical expressions for the mean energy and dispersion of the energy of scattered photons in frame E as a function of the initial photon energy x and the direction of its propagation relative to a symmetry axis of the electron distribution $\boldsymbol{l}_3$.

Following Nagirner & Poutanen (1994), we define the mean of powers of energy of scattered photons:

$$\overline{x_1^j}\overline{s}_0(\boldsymbol{x}) = \frac{1}{x}\int \langle x_1^j\rangle s_0(\xi)\,\xi\; f_e(\gamma,\eta_e)\,\frac{d^3p}{\gamma}, \tag{1.36}$$

where now

$$\begin{aligned}\langle x_1^j\rangle s_0(\xi) &= \frac{3}{16\pi}\frac{1}{\xi}\int \frac{d^3p_1}{\gamma_1}\frac{d^3x_1}{x_1} F\, x_1^j\,\delta^4(\underline{p}_1 + \underline{x}_1 - \underline{p} - \underline{x}) \\ &= \frac{3}{16\pi}\frac{1}{\xi}\int x_1^{j+1} dx_1 d^2\omega_1\, F\;\delta\{x_1[\gamma + x - \boldsymbol{\omega}_1\cdot(p\boldsymbol{\Omega} + x\boldsymbol{\omega})] - \xi\}\,.\end{aligned} \tag{1.37}$$

Averaging over photon directions

Quantities (1.37) are not invariants (except for $j = 0$), and we have to compute the scattered photon energy in a certain frame, which we choose to be frame E. Because of the additional term x_1^j under the integral, a simple change of variables to the electron rest frame as in equation (1.17) is not possible. Instead, we use the δ-function to take the integral over x_1:

$$\langle x_1^j \rangle s_0(\xi) = \frac{3}{16\pi}\frac{1}{\xi^2}\int x_1^{j+2}\, d^2\omega_1\, F\ . \tag{1.38}$$

Now we change the variables to those in the electron rest frame (with subscript 0). We choose the coordinate system with the polar axis along the direction of the incoming photon $\boldsymbol{\omega}_0$. In this frame, the cosine of the angle between the electron momentum and the incoming photon is ζ_0. The cosine of the angle between the outgoing photon momentum and the electron is then $\zeta_{10} = \zeta_0\mu_0 + \sqrt{1-\zeta_0^2}\sqrt{1-\mu_0^2}\cos\phi_0$.

We use invariants $x_1^2 d^2\omega_1 = \xi_1^2 d\mu_0 d\phi_0$ and the energy conservation law in the electron rest frame $\xi_1 = \xi/(1+\xi[1-\mu_0])$, to get (see Nagirner & Poutanen (1994))

$$x_1^2 d^2\omega_1 = d\xi_1 d\phi_0. \tag{1.39}$$

Finally, we have

$$\langle x_1^j \rangle s_0(\xi) = \frac{3}{16\pi}\frac{1}{\xi^2}\int_{\xi/(1+2\xi)}^{\xi} F\, d\xi_1 \int_0^{2\pi} x_1^j d\phi_0. \tag{1.40}$$

Because ξ_1 is the energy of scattered photon in the electron rest frame, the Doppler effect gives us

$$x_1 = \xi_1(\gamma + p\zeta_{10}) = \xi_1\left(\gamma + p\zeta_0\,\mu_0 + p\sqrt{1-\zeta_0^2}\sqrt{1-\mu_0^2}\cos\phi_0\right), \tag{1.41}$$

where we now can substitute

$$\mu_0 = 1 + \frac{1}{\xi} - \frac{1}{\xi_1}, \quad p\zeta_0 = \frac{x}{\xi} - \gamma, \tag{1.42}$$

which are consequences of the conservation law and of the Lorentz transformation $x = \xi(\gamma + p\zeta_0)$, respectively. The terms containing a linear combination of square roots and $\cos\phi_0$ will disappear after averaging over ϕ_0.

We now introduce moments of the invariant cross-section

$$s_j(\xi) = \frac{3}{8\,\xi^{j+2}}\int_{\xi/(1+2\,\xi)}^{\xi} \xi_1^j F\, d\xi_1. \tag{1.43}$$

For $j = 0$, we get of course the total cross-section s_0 given by equation (1.18). Nagirner & Poutanen (1994) derived the corresponding expressions for $j = 1, 2$:

$$s_1(\xi) = \frac{3}{8\,\xi^3}\left(l_\xi + \frac{4}{3}\,\xi^2 - \frac{3}{2}\xi - \frac{\xi}{2}\,R_\xi - \frac{\xi^2}{3}\,R_\xi^3\right), \tag{1.44}$$

$$s_2(\xi) = \frac{R_\xi}{16}\left(9 + R_\xi + 3\,R_\xi^2 + 3\,R_\xi^3\right), \tag{1.45}$$

where $l_\xi = \ln(1 + 2\,\xi)$, and $R_\xi = 1/(1 + 2\,\xi)$.

For the mean energy of the scattered photon we have then

$$\langle x_1 \rangle\, s_0(\xi) = \xi\,\left[\gamma\, S_1(\xi) + x\, S_2(\xi)\right], \tag{1.46}$$

and for the mean square of energy

$$\langle x_1^2 \rangle\, s_0(\xi) = \gamma^2\,\xi^2\, S_4(\xi) - \gamma\, x\,\xi\, S_5(\xi) + x^2\, S_6(\xi) - \xi^2\, S_7(\xi), \tag{1.47}$$

where

$$\begin{aligned}
S_1(\xi) &= \left[s_0(\xi) - s_1(\xi)\right]/\xi, \quad S_2(\xi) = \left[s_1(\xi) - S_1(\xi)\right]/\xi,\\
S_3(\xi) &= \left[s_1(\xi) - s_2(\xi)\right]/\xi, \quad S_4(\xi) = \left[S_1(\xi) - S_3(\xi)\right]/\xi,\\
S_5(\xi) &= 3\,S_4(\xi) - 4\,S_3(\xi), \quad S_7(\xi) = S_3(\xi) - S_4(\xi)/2,\\
S_6(\xi) &= s_2(\xi) - 3\,S_7(\xi).
\end{aligned} \tag{1.48}$$

All functions $S_j(\xi)$ are elementary. In addition, they are defined in such a way so that not to become zero at $\xi = 0$. The series expansion of functions s and S for small arguments are presented in Appendix A.1.

Averaging over electron directions

We need to integrate in equation (1.36) over anisotropic electron distribution. We follow the derivation of the total cross-section that lead from equation (1.21) to equation (1.26). Representing integral over electron momentum $d^3p = p^2 dp\, d\zeta\, d\Phi$ we get:

$$\overline{x_1^j\, s_0}(x, \eta) = 4\pi\, x^j \sum_{k=0}^{2} P_k(\eta) \int_1^\infty p\gamma\, d\gamma\; f_k\, \Delta_{jk}(x, \gamma), \tag{1.49}$$

where

$$\Delta_{jk}(x, \gamma) = \frac{1}{2\gamma x^{1+j}} \int_{-1}^{1} P_k(\zeta)\, \xi\, \langle x_1^j \rangle\, s_0(\xi)\, d\zeta = \sum_{n=0}^{k} b_{nk}\, \chi_{jn} \tag{1.50}$$

and

$$\chi_{jn}(x, \gamma) = \frac{1}{2\gamma p x^{2+j+n}} \int_{x(\gamma-p)}^{x(\gamma+p)} \langle x_1^j \rangle s_0(\xi)\;\; \xi^{n+1}\, d\xi. \tag{1.51}$$

Functions $\chi_{j0} = \Delta_{j0}$ coincide with functions $\Psi_j(x, \gamma)$ introduced by Nagirner & Poutanen (1994), while functions χ_{0n} are given by equation (1.31). The explicit

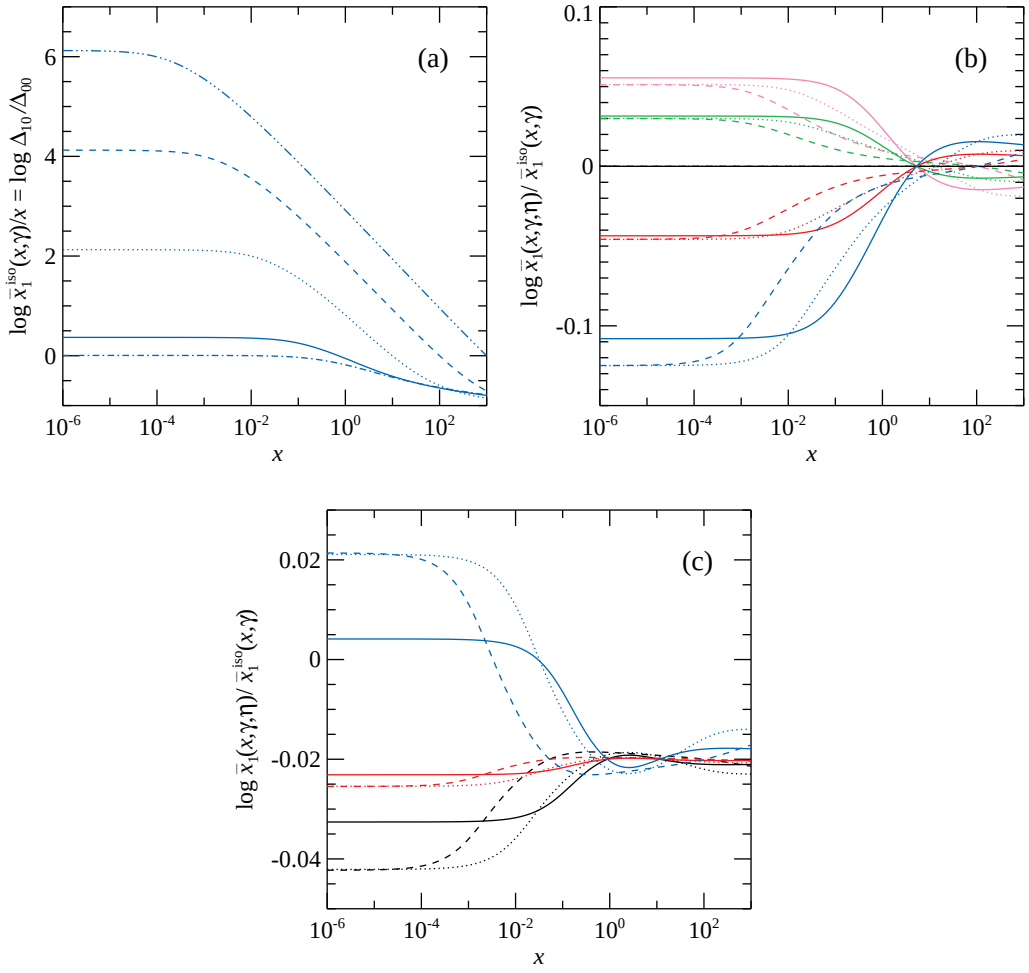

Figure 1.3: (a) Mean energy of scattered photons in units of the incident photon energy $\overline{x_1}^{\rm iso}(x,\gamma)/x = \Delta_{10}/\Delta_{00}$ as a function of x for isotropic mono-energetic electrons of various momenta $p = 0.1, 1, 10, 10^2, 10^3$ (from bottom to top, dot-dashed, solid, dotted, dashed, and triple-dot-dashed curves). The asymptotic value at small x in Thomson approximation is $1 + \frac{4}{3}p^2$. (b) A correction to the mean energy (in units of $\overline{x_1}^{\rm iso}$) arising from the linear term in the electron distribution (1.8) with $f_1/f_0 = 1$. Solid, dotted and dashed curves correspond for $p = 1, 10, 100$, respectively. The curves from top to bottom correspond to $\eta = -1, -0.5, 0, 0.5, 1$. At small x, the curves approach the limiting value given by equation (1.58). (c) Same as (b), but for the quadrupole term in the electron distribution (1.8) with $f_2/f_0 = 1$. These are even functions of η, the curves from the bottom to the top correspond to $\eta = 0, 0.5, 1$. At small x, the curves approach the limiting value given by equation (1.59).

expressions for the function χ_{jn} for $j = 1, 2$ (which are analogous to functions Ψ_1 and Ψ_2 from Nagirner & Poutanen (1994)) can be obtained using expression for mean powers of energies (1.46) or (1.47):

$$\chi_{1n}(x,\gamma) = \frac{1}{2\gamma p}\,\frac{u^{3+n}}{3+n}\left[\gamma\,\Psi_{2+n,1}(xu) + x\,\Psi_{2+n,2}(xu)\right]\Bigg|_{u=\gamma-p}^{u=\gamma+p}, \tag{1.52}$$

$$\begin{aligned}\chi_{2n}(x,\gamma) &= \frac{1}{2\gamma p}\left[\gamma^2\frac{u^{4+n}}{4+n}\Psi_{3+n,4}(xu) - \gamma\frac{u^{3+n}}{3+n}\Psi_{2+n,5}(xu)\right.\\ &+ \left.\frac{u^{2+n}}{2+n}\Psi_{1+n,6}(xu) - \frac{u^{4+n}}{4+n}\Psi_{3+n,7}(xu)\right]\Bigg|_{u=\gamma-p}^{u=\gamma+p},\end{aligned} \tag{1.53}$$

where

$$\Psi_{ij}(\xi) = \frac{i+1}{\xi^{i+1}}\int_0^\xi t^i S_j(t)dt. \tag{1.54}$$

These are related to functions

$$\psi_{ij}(\xi) = \frac{i+1}{\xi^{i+1}}\int_0^\xi t^i s_j(t)dt, \tag{1.55}$$

because functions S_j are expressed through s_j. The explicit expressions for both type of these functions as well as their series expansions for small arguments are given in Appendix A.2.

As in the case of functions Δ_{0k}, for calculating Δ_{jk}, we consider three regimes: (1) $x\gamma \ll 1$, when we use the series expansion (see Appendix A.4); (2) for $p \ll 1$ we numerically take the integral in equation (1.50) using Gaussian quadrature; (3) in other cases, we use the sum in equation (1.50) and analytical expressions for χ_{jn}.

For mono-energetic electron distribution (1.10) of Lorentz factor γ, we can introduce the mean powers of photon energy analogously to equation (1.49):

$$\overline{x_1^j}\,\overline{s_0}(x,\gamma,\eta) = x^j\sum_{k=0}^{2}\frac{f_k}{f_0}\,P_k(\eta)\,\Delta_{jk}. \tag{1.56}$$

The mean energy of scattered photons for such electrons for a scattering act is given by the ratio of equations (1.56) and (1.33). It is shown in Figure 1.3(a). In the low-energy (Thomson) limit the energy gain factor is given by a well known expression $\overline{x_1}^{\rm iso}/x = 1+4p^2/3$, which translated to $\frac{4}{3}\gamma^2$ at large γ. The relative corrections arising due to the dipole and quadrupole terms in the electron distribution are shown in Figures 1.3(b) and 1.3(c), respectively. Using asymptotic expansions of Δ_{jk} in the Thomson limit (see Appendix A.4), we get the asymptotic value

$$\frac{\overline{x_1}(x,\gamma,\eta)}{\overline{x_1}^{\rm iso}(x,\gamma)} = \frac{\gamma^2\left(1+\frac{1}{3}\beta^2\right) - \frac{2}{3}\beta\gamma^2\frac{f_1}{f_0}\eta + \frac{2}{15}\beta^2\gamma^2\frac{f_2}{f_0}P_2(\eta)}{\gamma^2\left(1+\frac{1}{3}\beta^2\right)\left(1-\frac{1}{3}\beta\frac{f_1}{f_0}\eta\right)}. \tag{1.57}$$

Thus in non-relativistic limit $\beta \ll 1$, the correction is negligible. In the relativistic limit $\gamma \gg 1$, the relative corrections arising from the two terms are

$$\frac{\overline{x_1}(x,\gamma,\eta)}{\overline{x_1}^{\rm iso}(x,\gamma)} = \frac{1-\frac{1}{2}\frac{f_1}{f_0}\eta}{1-\frac{1}{3}\frac{f_1}{f_0}\eta}, \tag{1.58}$$

$$\frac{\overline{x_1}(x,\gamma,\eta)}{\overline{x_1}^{\rm iso}(x,\gamma)} = 1+\frac{1}{10}\frac{f_2}{f_0}P_2(\eta). \tag{1.59}$$

1.3.3 Energy exchange and dispersion

The difference of the photon energies before and after scattering $x-x_1$ is of course just the energy transfer to the electron gas. For the fixed angle between electrons and incident photons ζ (and fixed electron energy γ), the energy loss averaged over the directions of scattered photons is $x-\langle x_1\rangle$. The product $(x-\langle x_1\rangle)N_{\rm e}\sigma_{\rm T}\, s_0(\xi)$ is then the energy loss on a unit length. From equation (1.46) we can easily get (see also Nagirner & Poutanen (1994)):

$$(x-\langle x_1\rangle)\, s_0(\xi) = x s_0(\xi) - \gamma\xi S_1(\xi) - x\xi S_2(\xi) = (x + x\xi - \gamma\xi)S_1(\xi). \tag{1.60}$$

The corresponding energy loss (per unit length and in units $N_{\rm e}\sigma_{\rm T}$) averaged over the electron directions (and integrated over electron energies) becomes [see equations (1.26) and (1.49)]:

$$(x-\overline{x_1})\,\overline{s_0}(x,\eta) = 4\pi x \sum_{k=0}^{2} P_k(\eta) \int_1^\infty p\gamma\, d\gamma\; f_k\; (\Delta_{0k}-\Delta_{1k})\,. \tag{1.61}$$

The heating rate per unit volume is then

$$\dot{E} = N_{\rm e}\sigma_{\rm T} \int dx \int d^2\omega\; I(x,\omega)\left(1-\frac{\overline{x_1}}{x}\right)\overline{s_0}(x,\eta), \tag{1.62}$$

where $I(x,\omega)$ is the specific intensity of radiation in a given direction. This expression can be positive (so called Compton heating) when the photons typically have larger energies than the electron gas, or negative (Compton cooling) when one considers cooling of the relativistic electron gas by soft radiation.

The dispersion of the scattered photon energy is given by the usual expression $\overline{D}(x) = \overline{x_1^2} - \overline{x_1}^2$, which of course depends on the electron momentum distribution. For mono-energetic electrons we can define the dispersion as

$$\overline{D}(x,\gamma,\eta) = \overline{x_1^2}(x,\gamma,\eta) - \overline{x_1}^2(x,\gamma,\eta), \tag{1.63}$$

where $\overline{x_1^j}(x,\gamma,\eta)$ are given by equation (1.56). The dispersion for isotropic electrons is shown in Figure 1.3(a). The low-energy (Thomson) limit for $x \ll 1/\gamma$ is (see Nagirner & Poutanen (1994))

$$\overline{D}(x,\gamma) = x^2\frac{2}{45}\left(23\gamma^2-8\right)p^2. \tag{1.64}$$

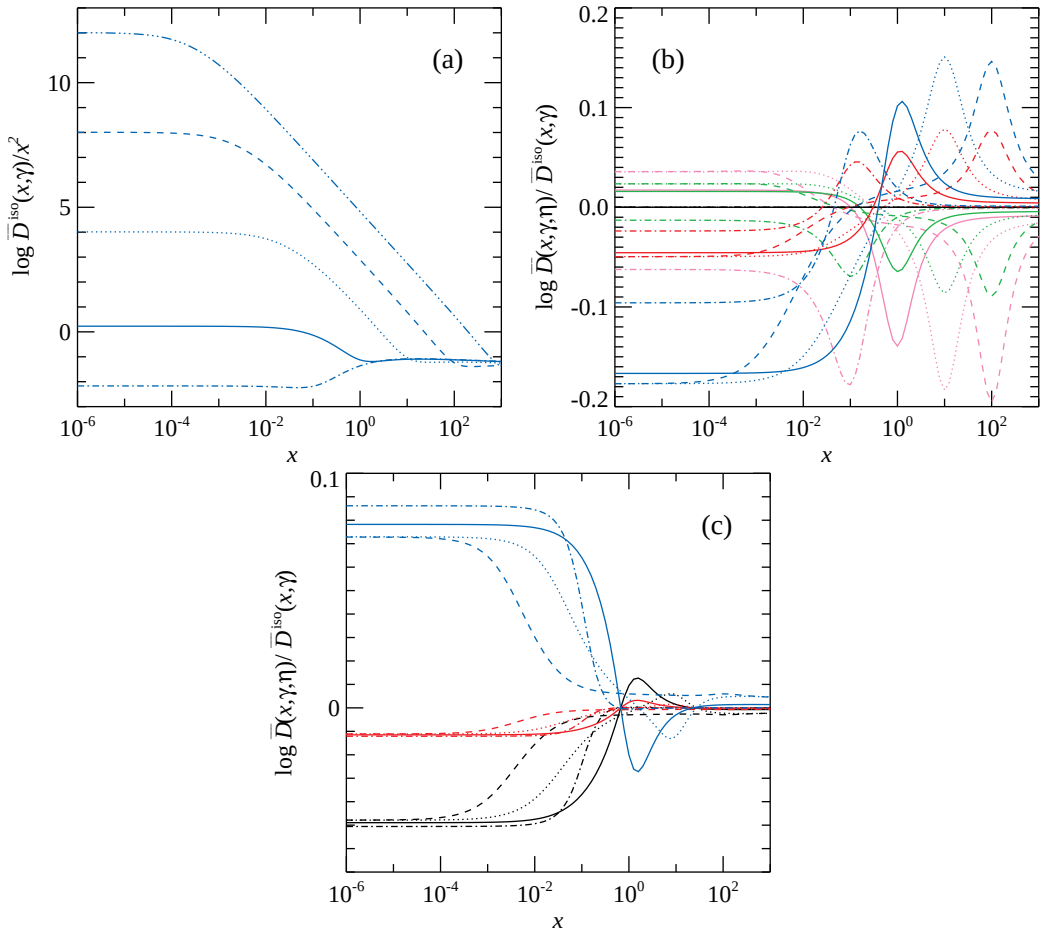

Figure 1.4: (a) Dispersion of the energy of scattered photons (in units of x^2) for isotropic mono-energetic electrons of $p = 0.1, 1, 10, 10^2, 10^3$ (from bottom to top). The asymptotic value of $\overline{D}/x^2$ at small x in the Thomson approximation is $\frac{2}{45}(23\gamma^2 - 8)p^2$. (b) A correction to the dispersion (in terms of the isotropic quantity) arising from the linear term in the electron distribution (1.8) with $f_1/f_0 = 1$. Solid, dotted and dashed curves correspond to $p = 1, 10, 100$, respectively. The curves from top to bottom correspond to $\eta = -1, -0.5, 0, 0.5, 1$. (c) A correction to the dispersion arising from the quadrupole term in the electron distribution (1.8) with $f_2/f_0 = 1$ for the same p and η as in panel (b). These are even functions of η, the curves from bottom to top correspond to $\eta = 0, 0.5, 1$.

The relative corrections arising due to the dipole and quadrupole term in the electron distribution reach about 50 % and are shown in Figures 1.4(b) and 1.4(c), respectively.

1.3.4 Radiation force

Now we would like to derive analytic expression for the radiation force acting on the electron gas. Nagirner & Poutanen (1994) have developed a formalism appropriate for isotropic electron distribution, when the averaged transferred momentum is along the momentum of the incoming photons, because of the symmetry. For the electron distribution described by equation (1.8), the momentum is transferred in the plane containing the initial photon momentum and the symmetry axis $\boldsymbol{l}_3$. If the incident photons are axially symmetric around $\boldsymbol{l}_3$, then obviously, the total momentum transferred to the electrons has to be parallel to $\boldsymbol{l}_3$ by symmetry. We derive here more general formulae for the total momentum transferred by a beam of photons propagating along direction $\boldsymbol{\omega}$ (such as $\boldsymbol{\omega} \cdot \boldsymbol{l}_3 = \eta$), as well as its projections to $\boldsymbol{l}_3$ and perpendicular direction.

Let us introduce the vector basis:

$$\boldsymbol{e}_1(\boldsymbol{\omega}, \boldsymbol{l}_3) = \frac{\boldsymbol{l}_3 - \eta\,\boldsymbol{\omega}}{\sqrt{1-\eta^2}}, \quad \boldsymbol{e}_2(\boldsymbol{\omega}, \boldsymbol{l}_3) = \frac{\boldsymbol{\omega} \times \boldsymbol{l}_3}{\sqrt{1-\eta^2}}, \quad \boldsymbol{e}_3 = \boldsymbol{\omega}. \tag{1.65}$$

In a single scattering act the momentum transferred is

$$\boldsymbol{Q} = x\boldsymbol{\omega} - x_1\boldsymbol{\omega}_1. \tag{1.66}$$

The components of the momentum transferred to the electron gas along and perpendicular to $\boldsymbol{\omega}$ are:

$$Q_3 = x - x_1\,\boldsymbol{\omega}_1 \cdot \boldsymbol{e}_3 = x - x_1\mu, \tag{1.67}$$

$$Q_1 = -x_1\,\boldsymbol{\omega}_1 \cdot \boldsymbol{e}_1 = -x_1\frac{\eta_1 - \eta\mu}{\sqrt{1-\eta^2}}. \tag{1.68}$$

Analogously to equation (1.36), we define the mean transferred momentum as

$$\overline{\boldsymbol{Q}}\,\overline{s}_0(\boldsymbol{x}) = \frac{1}{x}\int \langle \boldsymbol{Q} \rangle s_0(\xi)\,\xi\; f_{\rm e}(\gamma, \eta_{\rm e})\,\frac{d^3p}{\gamma}, \tag{1.69}$$

where

$$\langle \boldsymbol{Q} \rangle s_0(\xi) = \frac{3}{16\pi}\frac{1}{\xi}\int \frac{d^3p_1}{\gamma_1}\frac{d^3x_1}{x_1}\; F\;\boldsymbol{Q}\;\delta^4(\underline{p}_1 + \underline{x}_1 - \underline{p} - \underline{x}) \tag{1.70}$$

$$= \frac{3}{16\pi}\frac{1}{\xi}\int x_1 dx_1 d^2\omega_1\, F\,\boldsymbol{Q}\;\delta\{x_1[\gamma + x - \boldsymbol{\omega}_1\cdot(p\boldsymbol{\Omega} + x\boldsymbol{\omega})] - \xi\}\,.$$

Averaging over photon directions

Let us introduce a vector basis defined by the photon and electron momenta:

$$\boldsymbol{e}_1(\boldsymbol{\omega},\boldsymbol{\Omega}) = \frac{\boldsymbol{\Omega} - \zeta\,\boldsymbol{\omega}}{\sqrt{1-\zeta^2}},\quad \boldsymbol{e}_2(\boldsymbol{\omega},\boldsymbol{\Omega}) = \frac{\boldsymbol{\omega}\times\boldsymbol{\Omega}}{\sqrt{1-\zeta^2}},\quad \boldsymbol{e}_3 = \boldsymbol{\omega}, \tag{1.71}$$

where $\zeta = \boldsymbol{\omega}\cdot\boldsymbol{\Omega}$, therefore $\boldsymbol{\Omega} = \sqrt{1-\zeta^2}\,\boldsymbol{e}_1(\boldsymbol{\omega},\boldsymbol{\Omega}) + \zeta\,\boldsymbol{e}_3$. Fixing the angle $\arccos\zeta$ between the electrons of momentum $p\,\boldsymbol{\Omega}$ and the incident photon momentum and averaging over directions of scattered photons, we can get the mean momentum transmitted in the direction $\boldsymbol{\omega}$:

$$\langle Q_3\rangle\, s_0(\xi) = \langle x - x_1\rangle\, s_0(\xi) + \langle x_1\,(1-\mu)\rangle\, s_0(\xi). \tag{1.72}$$

The first term is given by equation (1.60), the second term is

$$\begin{aligned}\langle x_1(1-\mu)\rangle\, s_0(\xi) &= \frac{3}{16\pi\xi^2}\int x_1^3(1-\mu)F d^2\omega_1\\ &= \frac{3}{16\,\pi\,x\,\xi}\int \xi_1\,(1-\mu_0)\,F\,d\xi_1\,d\phi_0\\ &= \frac{3}{8\,x\,\xi^2}\int_{\xi/(1+2\,\xi)}^{\xi}(\xi-\xi_1)\,F\,d\xi_1 = \frac{\xi}{x}\,[s_0(\xi)-s_1(\xi)] = \frac{\xi^2}{x}\,S_1(\xi),\end{aligned} \tag{1.73}$$

where we have used the invariant given by equation (1.4) and changed the variables according to equation (1.39). Thus, for the fixed electron and photon energies and the angle between their momenta, the mean momentum transmitted to the electron gas in the direction of the initial photon propagation $\boldsymbol{\omega}$, in accordance with equations (1.48), (1.46) and (1.73), is (Nagirner & Poutanen 1994)

$$\langle Q_3\rangle s_0(\xi) = \langle x - x_1\,\mu\rangle s_0(\xi) = \left(x + x\,\xi - \gamma\,\xi + \frac{\xi^2}{x}\right) S_1(\xi). \tag{1.74}$$

In contrast to Nagirner & Poutanen (1994), we are now interested to know the total momentum transfer. Obviously, by symmetry, it has to lie in the $(\boldsymbol{\Omega},\boldsymbol{\omega})$ plane. Averaging expression (1.68) for Q_1 over angles is not easy, but we can compute the momentum transferred along the electron momentum: $Q_\Omega \equiv x\zeta - x_1\zeta_1$. Using identity $x_1\zeta_1 = (\gamma x_1 - \xi_1)/p$ and substituting equation (1.41) and (1.42), similarly to equation (1.40), we get

$$\begin{aligned}\langle x_1\zeta_1\rangle s_0(\xi) &= \frac{3}{16\pi}\frac{1}{\xi^2}\int_{\xi/(1+2\xi)}^{\xi} F\,d\xi_1\int_0^{2\pi} x_1\zeta_1 d\phi_0\\ &= \frac{3}{8\xi^2}\int_{\xi/(1+2\xi)}^{\xi} F\,d\xi_1\frac{1}{p}\left[\left(\frac{\gamma x}{\xi}+\frac{\gamma x}{\xi^2}-\frac{\gamma^2}{\xi}-1\right)\xi_1 + \gamma\left(\gamma-\frac{x}{\xi}\right)\right]\\ &= \frac{1}{p}\left(\gamma x + \frac{\gamma x}{\xi} - \gamma^2 - \xi\right) s_1(\xi) + \frac{\gamma}{p}\left(\gamma - \frac{x}{\xi}\right) s_0(\xi)\\ &= \frac{1}{p}\left[\gamma^2\xi\,S_1(\xi) + \gamma x\,\xi\,S_2(\xi) - \xi\,s_1(\xi)\right],\end{aligned} \tag{1.75}$$

and using identity $x\zeta = (\gamma x - \xi)/p$, we finally obtain

$$\langle Q_\Omega \rangle s_0(\xi) = \langle x\zeta - x_1\zeta_1 \rangle s_0(\xi) = \frac{1}{p}\left(\gamma x + \gamma x\,\xi - \gamma^2\xi - \xi^2\right) S_1(\xi). \tag{1.76}$$

The momentum along $\boldsymbol{e}_1(\boldsymbol{\omega}, \boldsymbol{\Omega})$ is then simply

$$\begin{aligned}\langle Q_1 \rangle s_0(\xi) &= \frac{\langle Q_\Omega \rangle - \zeta \langle Q_3 \rangle}{\sqrt{1-\zeta^2}} s_0(\xi) \\ &= \frac{S_1(\xi)}{p\sqrt{1-\zeta^2}}\left(\xi - 2\gamma\frac{\xi^2}{x} + \frac{\xi^3}{x^2}\right) = -p\sqrt{1-\zeta^2}\,\xi\, S_1(\xi).\end{aligned} \tag{1.77}$$

Thus the total transferred momentum $\boldsymbol{Q}$ averaged over directions of scattered photons can be decomposed into two components along basis vectors:

$$\langle \boldsymbol{Q} \rangle = \langle Q_1 \rangle\, \boldsymbol{e}_1(\boldsymbol{\omega}, \boldsymbol{\Omega}) + \langle Q_3 \rangle\, \boldsymbol{e}_3. \tag{1.78}$$

Averaging over electron directions

As in previous sections, we choose to measure the azimuth of the electron momentum Φ in the frame defined by equations (1.65) from the projection of vector $\boldsymbol{l}_3$ onto the plane perpendicular to $\boldsymbol{\omega}$. Therefore,

$$\langle \boldsymbol{Q} \rangle = \langle Q_1 \rangle \left[\cos\Phi\, \boldsymbol{e}_1(\boldsymbol{\omega}, \boldsymbol{l}_3) + \sin\Phi\, \boldsymbol{e}_2(\boldsymbol{\omega}, \boldsymbol{l}_3)\right] + \langle Q_3 \rangle\, \boldsymbol{e}_3. \tag{1.79}$$

The total momentum transfer averaged over the electron distribution is obtained from equation (1.69):

$$\overline{\boldsymbol{Q}}\,\overline{s_0}(x,\eta) = \frac{1}{x}\int_1^\infty p\,d\gamma \int_{-1}^1 d\zeta\,\xi \int_0^{2\pi} d\Phi\, \langle \boldsymbol{Q} \rangle s_0(\xi)\, f_\mathrm{e}(\gamma, \eta_\mathrm{e}). \tag{1.80}$$

Obviously, the component along $\boldsymbol{e}_2(\boldsymbol{\omega}, \boldsymbol{l}_3)$ becomes zero, as f_e is an even function of Φ. The term along $\boldsymbol{e}_1(\boldsymbol{\omega}, \boldsymbol{l}_3)$ involves integration of f_e over azimuth with the weight $\cos\Phi$, and its averaged value is

$$\overline{f_\mathrm{e}\cos\Phi} = \sum_{k=1}^{2} \frac{f_k}{k(k+1)} P_k^1(\eta) P_k^1(\zeta), \tag{1.81}$$

where P_k^1 are the associated Legendre functions:

$$P_1^1(u) = \sqrt{1-u^2}, \quad P_2^1(u) = 3\,u\,\sqrt{1-u^2}. \tag{1.82}$$

It is worth mentioning that the isotropic component of the electron distribution f_0 does not contribute to the momentum transferred perpendicular to $\boldsymbol{\omega}$ by

symmetry. Substituting expression (1.77) into equation (1.80), we get the first component of the vector

$$\overline{Q}_1\overline{s_0}(x,\eta) = 4\pi x \sum_{k=1}^{2} P_k^1(\eta) \int_1^\infty p\gamma \, d\gamma \, f_k \, \Delta_{1k}^\perp(x,\gamma), \tag{1.83}$$

where

$$\Delta_{1k}^\perp(x,\gamma) = \frac{1}{k(k+1)} \frac{1}{2\gamma x^2} \int_{-1}^{1} P_k^1(\zeta) \, \xi \, \langle Q_1 \rangle \, s_0(\xi) \, d\zeta. \tag{1.84}$$

Changing the integration variable to ξ, and introducing a set of functions

$$\begin{aligned} \chi_{1n}^\perp(x,\gamma) &= \frac{1}{2\gamma p \; x^{3+n}} \int_{x(\gamma-p)}^{x(\gamma+p)} \sqrt{1-\zeta^2} \, \langle Q_1 \rangle s_0(\xi) \;\; \xi^{n+1} \, d\xi \\ &= \frac{1}{2\gamma p} \frac{1}{p} \left[\frac{u^{3+n}}{3+n} \Psi_{2+n,1}(xu) - 2\gamma \frac{u^{4+n}}{4+n} \Psi_{3+n,1}(xu) \right. \\ &+ \left. \frac{u^{5+n}}{5+n} \Psi_{4+n,1}(xu) \right] \Bigg|_{u=\gamma-p}^{u=\gamma+p}, \; n = 0, 1, \end{aligned} \tag{1.85}$$

we get

$$\Delta_{11}^\perp = \frac{1}{2} \chi_{10}^\perp, \quad \Delta_{12}^\perp = \frac{1}{2p} \left(\gamma \chi_{10}^\perp - \chi_{11}^\perp \right). \tag{1.86}$$

Now let us evaluate the component of vector (1.80) along $\boldsymbol{e}_3$. Because $\langle Q_3 \rangle$ does not depend on azimuth Φ, the azimuthal integration just gives the averaged electron distribution given by equation (1.25). Thus we get

$$\overline{Q}_3 \, \overline{s_0}(x,\eta) = 4\pi x \sum_{k=0}^{2} P_k(\eta) \int_1^\infty p\gamma \, d\gamma \, f_k \, \left(\Delta_{0k} - \Delta_{1k} + \Delta_{1k}^* \right), \tag{1.87}$$

where

$$\Delta_{1k}^*(x,\gamma) = \frac{1}{2\gamma x^2} \int_{-1}^{1} P_k(\zeta) \, \xi \, \langle x_1(1-\mu) \rangle s_0(\xi) \, d\zeta = \sum_{n=0}^{k} \; b_{nk} \chi_{1n}^*, \tag{1.88}$$

and

$$\begin{aligned} \chi_{1n}^*(x,\gamma) &= \frac{1}{2\gamma p \; x^{3+n}} \int_{x(\gamma-p)}^{x(\gamma+p)} \langle x_1(1-\mu) \rangle \, s_0(\xi) \, \xi^{n+1} \, d\xi \\ &= \frac{1}{2\gamma p} \; \frac{u^{4+n}}{4+n} \Psi_{3+n,1}(xu) \Big|_{u=\gamma-p}^{u=\gamma+p}, \; n = 0, 1, 2. \end{aligned} \tag{1.89}$$

For isotropic electron distribution, the only function of interest is Δ_{10}^* which coincides with function $\Psi_1^*(x,\gamma)$ introduced by Nagirner & Poutanen (1994). Now

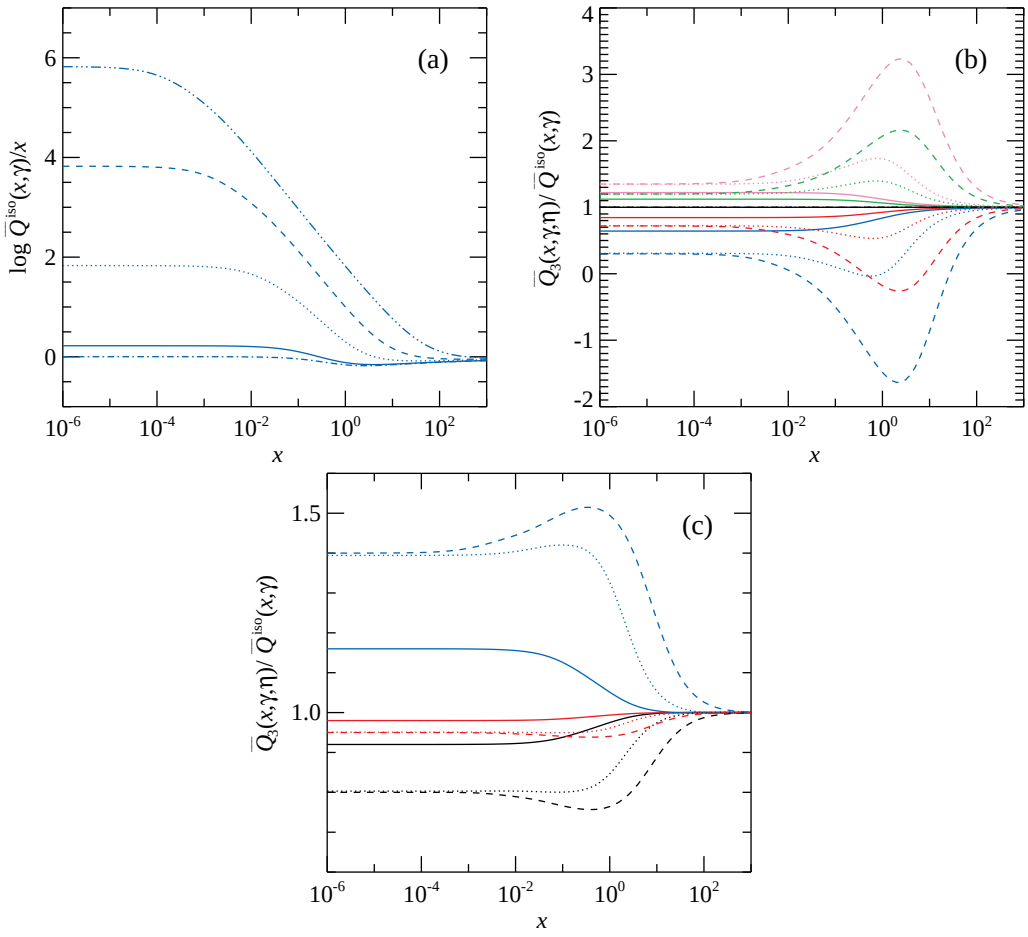

Figure 1.5: (a) Average momentum transferred to the electron gas per scattering $\overline{Q}^{\rm iso}$ (in units of x) for isotropic mono-energetic electrons (with $f_1 = f_2 = 0$). Curves from bottom to top correspond to the electron momenta $p = 0.1, 1, 10, 10^2, 10^3$. The asymptotic value at small x in the Thomson approximation is $1 + 2p^2/3$ [Nagirner & Poutanen (1994); see equation (1.95)]. (b) The momentum transferred along ω for anisotropic electrons with $f_1/f_0 = 1$ in units of the isotropic quantity $\overline{Q}^{\rm iso}$. Solid, dotted and dashed curves correspond to $p = 1, 10, 100$, respectively. The curves from top to bottom correspond to $\eta = -1, -0.5, 0, 0.5, 1$ (pink, green, black, red, and blue curves, respectively). (c) Same as (b), but for the electron distribution (1.8) with the quadrupole term with $f_2/f_0 = 1$ for the same p and η as in panel (b). These are even functions of η, the curves from the bottom to the top correspond to $\eta = 0, 0.5, 1$. The flat parts of the curves correspond to the Thomson limit given by equation (1.95).

combining equations (1.83) and (1.87), we get the momentum transfer along the symmetry axis of the electron distribution $\boldsymbol{l}_3$ and perpendicular to it:

$$\overline{Q}_{\parallel} = \sqrt{1-\eta^2}\,\overline{Q}_1 + \eta\,\overline{Q}_3, \tag{1.90}$$

$$\overline{Q}_{\perp} = -\eta\,\overline{Q}_1 + \sqrt{1-\eta^2}\,\overline{Q}_3. \tag{1.91}$$

Expressions (1.87), (1.83) and (1.90) give the momentum transferred to the electron gas (in terms of one integral over the electron energy) along $\boldsymbol{\omega}$, perpendicular to that direction as well as along vector $\boldsymbol{l}_3$ and perpendicular to it.

Similarly to equation (1.62), we can also get the two components of the momentum transfer rate per unit volume:

$$\dot{P}_{1,3} = \frac{N_{\rm e}\sigma_{\rm T}}{c}\int\frac{d\,x}{x}\int d^2\omega\; I(x,\eta)\;\overline{Q}_{1,3}\,\overline{s_0}(x,\eta). \tag{1.92}$$

For mono-energetic electron distribution of Lorentz factor γ given by equation (1.10), the momenta transferred along ω and perpendicular to it are

$$\overline{Q}_3\,\overline{s_0}(x,\gamma,\eta) = x\sum_{k=0}^{2}\frac{f_k}{f_0}\,P_k(\eta)\;\left(\Delta_{0k}-\Delta_{1k}+\Delta_{1k}^{*}\right), \tag{1.93}$$

$$\overline{Q}_1\,\overline{s_0}(x,\gamma,\eta) = x\sum_{k=1}^{2}\frac{f_k}{f_0}\,P_k^1(\eta)\;\Delta_{1k}^{\perp}, \tag{1.94}$$

where we kept the notations for the functions $\overline{Q}_3$ and $\overline{Q}_1$, but added the argument γ. To get the average momentum transferred in a single scattering act, one needs to divide these expression by the total cross-section $\overline{s_0}(x,\gamma,\eta)$. The ω component of the transferred momentum for isotropic electrons is shown in Figure 1.5(a). As shown by Nagirner & Poutanen (1994), the low-energy (Thomson) limit is given by $x(1+2p^2/3)$. The angular dependent corrections arising due to the dipole and quadrupole term in the electron distribution are shown in Figures 1.5(b) and 1.5(c), respectively. While the component perpendicular to ω is zero for isotropic electrons, a substantial momentum component arises in the anisotropic case. For a large linear term of the electron distribution with $f_1/f_0 = 1$, the momentum transferred in that direction is shown in Figure 1.6(a). Similar results in the case of the quadrupole term with $f_2/f_0 = 1$ are shown in Figure 1.6(b). In the Thomson limit, we get (see Appendix A.4)

$$\overline{Q}_3\,\overline{s_0}(x,\gamma,\eta) = x\left[1+\frac{2}{3}p^2-\frac{f_1}{f_0}\eta\beta\,\frac{2}{15}(4\gamma^2+1)+\frac{f_2}{f_0}\,P_2(\eta)\,\frac{4}{15}\,p^2\right], \tag{1.95}$$

$$\overline{Q}_1\,\overline{s_0}(x,\gamma,\eta) = x\gamma^2\beta\sqrt{1-\eta^2}\left[-\frac{f_1}{f_0}\frac{1}{3}\left(1+\frac{\beta^2}{5}\right)+\frac{2}{5}\frac{f_2}{f_0}\eta\beta\right]. \tag{1.96}$$

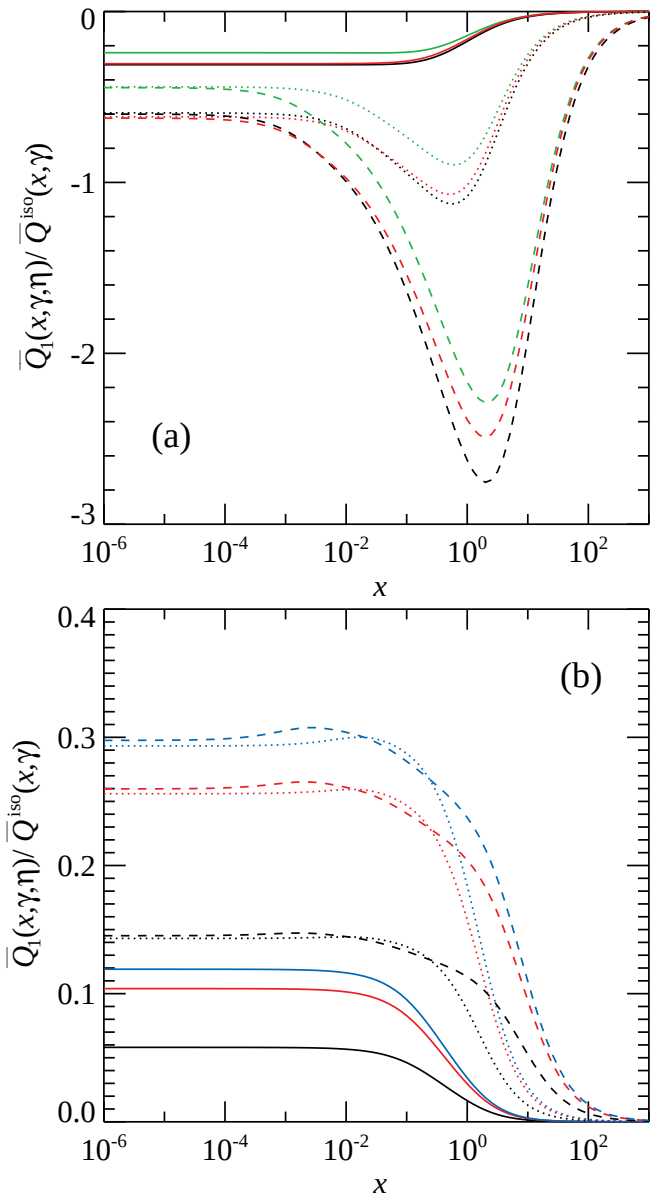

Figure 1.6: (a) Momentum transferred in the direction perpendicular to ω (in units of the momentum along ω for isotropic distribution) arising from the linear term in the electron distribution (1.8) with $f_1/f_0 = 1$. For $\eta = \pm 1$, the momentum is zero by symmetry. From the top to the bottom curves correspond to $\eta = -0.5$ (green), 0.5 (red), 0 (black). Solid, dotted and dashed curves correspond to $p = 1, 10, 100$, respectively. (b) Momentum transferred in the direction perpendicular to ω arising from the quadrupole term in the electron distribution (1.8) with $f_2/f_0 = 1$ for the same p as in panel (a). The curves from bottom to top correspond to $\eta = \pm 0.25, 0.5, 0.75$ (black, red, blue curves). The momentum is zero for $\eta = -1, 0, 1$ because of the symmetry. The flat parts of the curves correspond to the Thomson limit given by equation (1.96).

1.4 Redistribution functions for anisotropic electrons

We would like to reduce the expression for the redistribution function (1.6) to a form suitable for calculations. For the electron distribution of the form (1.8), this function should depend on the energies of incoming and scattered photons x_1 and x, the corresponding (cosines of) polar angles η_1 and η as well as the difference in azimuth $\phi - \phi_1$ (or cosine of the scattering angle μ).

1.4.1 Integration over electron directions

The three-dimensional integral over $\boldsymbol{p}$ in equation (1.6) disappears due to the δ-function. For further simplifications we can also use the identity

$$\delta(\gamma_1 + x_1 - \gamma - x) = \gamma\delta\left(\underline{x}\cdot(\underline{p}_1 + \underline{x}_1) - \underline{x}_1\cdot\underline{p}_1\right). \tag{1.97}$$

At this stage, we drop subscript 1 with the electron quantities and get

$$R(\boldsymbol{x}_1 \to \boldsymbol{x}) = \frac{3}{16\,\pi}\int\frac{d^3p}{\gamma}\,\delta(\Gamma)\;f_{\rm e}(\gamma,\eta_{\rm e})\,F. \tag{1.98}$$

where

$$\Gamma = \gamma(x_1 - x) - p(x_1\boldsymbol{\omega}_1 - x\boldsymbol{\omega})\cdot\boldsymbol{\Omega} - q. \tag{1.99}$$

The angular integrals in equation (1.98) need the introduction of a suitable coordinate system. Often the polar axis is taken along the direction of the scattered photon $\boldsymbol{\omega}$ (see e.g. Nagirner & Poutanen 1993, 1994). However, the easiest and the most transparent way, is to choose the polar axis along the direction of the transferred momentum as was proposed by Aharonian & Atoyan (1981) (see also Prasad et al. 1986)

$$\boldsymbol{n} \equiv (x_1\boldsymbol{\omega}_1 - x\boldsymbol{\omega})\,/Q, \tag{1.100}$$

where

$$Q^2 = (x_1\boldsymbol{\omega}_1 - x\boldsymbol{\omega})^2 = x^2 + x_1^2 - 2xx_1\mu = (x - x_1)^2 + 2q. \tag{1.101}$$

With this definition we get:

$$\cos\kappa \equiv \boldsymbol{n}\cdot\boldsymbol{\omega} = (x_1\mu - x)\,/Q, \quad \sin\kappa = x_1\sqrt{1-\mu^2}/Q \tag{1.102}$$

and

$$\cos\alpha \equiv \boldsymbol{n}\cdot\boldsymbol{l}_3 = (x_1\eta_1 - x\eta)\,/Q. \tag{1.103}$$

Thus one of the integration variables becomes $\cos\theta = \boldsymbol{\Omega}\cdot\boldsymbol{n}$ and another is azimuth Φ. The redistribution function (1.98) then can be written as

$$R(\boldsymbol{x}_1 \to \boldsymbol{x}) = \frac{3}{16\pi}\int_1^\infty p\,dp\int_{-1}^1 d\cos\theta\int_0^{2\pi} d\Phi\;f_{\rm e}(\gamma,\eta_{\rm e})\,F\,\delta(\Gamma), \tag{1.104}$$

where now

$$\Gamma = \gamma(x_1 - x) - q - pQ\cos\theta. \tag{1.105}$$

Integrating first over $\cos\theta$ using the δ-function we get

$$R(\boldsymbol{x}_1 \to \boldsymbol{x}) = \frac{3}{16\,\pi}\int_{\gamma_*}^{\infty} d\gamma \frac{1}{Q}\int_0^{2\pi} d\Phi\; f_{\rm e}(\gamma,\eta_{\rm e})\,F, \tag{1.106}$$

where we need to substitute

$$\cos\theta = \frac{\gamma(x_1 - x) - q}{pQ} \tag{1.107}$$

to the expressions for $\eta_{\rm e}$ and F (see below). This yields

$$\sin\theta = \frac{b}{\sqrt{r}\;pQ}, \tag{1.108}$$

where

$$b = \sqrt{r}\,\sqrt{p^2Q^2 - [\gamma(x_1 - x) - q]^2}, \quad r = \frac{1+\mu}{1-\mu}. \tag{1.109}$$

The lower limit for the integral over γ comes from the requirement that $|\cos\theta| \le 1$:

$$\gamma \ge \gamma_*(x, x_1, \mu) = \frac{1}{2}\left(x - x_1 + Q\sqrt{1 + 2/q}\right). \tag{1.110}$$

1.4.2 Integration over the azimuth

In order to calculate the azimuthal integral in equation (1.106) we have to express ξ and ξ_1 (that enter the expression for F) and $\eta_{\rm e}$ in terms of the integration variable Φ. We measure the azimuth Φ from the projection of $\boldsymbol{\omega}$ onto the plane normal to $\boldsymbol{n}$, so that in this system

$$\boldsymbol{\omega} = (\sin\kappa, 0, \cos\kappa) \tag{1.111}$$

and the unit vector along the electron momentum is

$$\boldsymbol{\Omega} = (\sin\theta\cos\Phi, \sin\theta\sin\Phi, \cos\theta). \tag{1.112}$$

Thus we can express the angle between the electron momentum and $\boldsymbol{l}_3$ (see Figure 1.1) through Φ:

$$\eta_{\rm e} \equiv \boldsymbol{\Omega}\cdot\boldsymbol{l}_3 = \cos\theta\;\cos\alpha + \sin\theta\;\sin\alpha\cos(\chi - \Phi), \tag{1.113}$$

where χ is the azimuth of the vector $\boldsymbol{l}_3$ in the $\boldsymbol{n}$ frame. We can also write

$$\eta \equiv \boldsymbol{\omega}\cdot\boldsymbol{l}_3 = \cos\kappa\;\cos\alpha + \sin\kappa\;\sin\alpha\cos\chi, \tag{1.114}$$

and use this expression to obtain $\cos\chi$. Substituting it to equation (1.113) we thus express the electron polar angle $\eta_{\rm e}$ in equation (1.8) through the integration variable Φ.

The kernel F depends on the four-products ξ and ξ_1, which can be rewritten as

$$\xi_1 = x(\gamma - p\zeta), \quad \xi = q + \xi_1, \tag{1.115}$$

where

$$\zeta \equiv \mathbf{\Omega} \cdot \boldsymbol{\omega} = \cos\theta\ \cos\kappa + \sin\theta \sin\kappa \cos\Phi. \tag{1.116}$$

Equation (1.115) then can be transformed to

$$\xi_1 = \frac{q}{Q^2}(d_- - b\cos\Phi), \quad \xi = \frac{q}{Q^2}(d_+ - b\cos\Phi), \tag{1.117}$$

where we defined

$$\begin{aligned} d_- &= \gamma(x + x_1) - x(x - x_1\mu)\,, \\ d_+ &= \gamma(x + x_1) + x_1(x_1 - x\mu) = d_- + Q^2, \end{aligned} \tag{1.118}$$

which have the following property:

$$\begin{aligned} \left(d_-^2 - b^2\right)/Q^2 &= (\gamma - x)^2 + r \equiv a_-^2, \\ \left(d_+^2 - b^2\right)/Q^2 &= (\gamma + x_1)^2 + r \equiv a_+^2. \end{aligned} \tag{1.119}$$

Function F in the azimuthal integral in equation (1.106) is an even function of Φ. Therefore the terms in f_e containing $\sin\Phi$ give zero contribution. Neglecting these terms we can express the azimuthal integral as

$$\int_0^{2\pi} \eta_\mathrm{e} F d\Phi = \int_0^{2\pi} \overline{\eta_\mathrm{e}} F d\Phi, \tag{1.120}$$

$$\int_0^{2\pi} \eta_\mathrm{e}^2 F d\Phi = \int_0^{2\pi} \overline{\eta_\mathrm{e}^2} F d\Phi, \tag{1.121}$$

where

$$\overline{\eta_\mathrm{e}} = \cos\theta\ \cos\alpha + \sin\theta\ \sin\alpha\ \cos\chi\ \cos\Phi, \tag{1.122}$$

$$\begin{aligned} \overline{\eta_\mathrm{e}^2} &= \cos^2\theta\ \cos^2\alpha + \sin^2\theta \sin^2\alpha \sin^2\chi \\ &+ 2\sin\theta\sin\alpha\ \cos\theta\ \cos\alpha\ \cos\chi\ \cos\Phi \\ &+ \sin^2\theta\ \sin^2\alpha\ \cos 2\chi\ \cos^2\Phi. \end{aligned} \tag{1.123}$$

Thus the expansion (1.8) (with η_e and η_e^2 substituted by $\overline{\eta_\mathrm{e}}$ and $\overline{\eta_\mathrm{e}^2}$, respectively) is a quadratic function of $\cos\Phi$. Expressing

$$\cos\Phi = -\frac{Q^2}{2b}\frac{\xi + \xi_1}{q} + \frac{d_- + d_+}{2b}, \tag{1.124}$$

$$\cos^2\Phi = \frac{Q^4}{b^2}\frac{\xi\xi_1}{q^2} - \frac{Q^2(d_+ + d_-)}{2b^2}\frac{\xi + \xi_1}{q} + \frac{d_+^2 + d_-^2}{2b^2}$$

and using the identity $\xi = \xi_1 + q$, we obtain an expansion of f_e that is symmetric in ξ and ξ_1:

$$\overline{f_e}(\gamma) = c_0 + c_\Sigma \frac{\xi + \xi_1}{q} + c_\Pi \frac{\xi\xi_1}{q^2}. \tag{1.125}$$

The coefficients c_0, c_Σ and c_Π can be represented in the form:

$$\begin{aligned} c_0 &= f_0 + c_{01} f_1 + c_{02} f_2, \\ c_\Sigma &= c_{11} f_1 + c_{12} f_2, \\ c_\Pi &= c_{22} f_2, \end{aligned} \tag{1.126}$$

where the coefficients in front of $f_{0,1,2}$ can easily be derived after lengthy but straightforward calculation:

$$\begin{aligned} c_{01} &= \frac{2\rho - \epsilon + \epsilon_1}{2p(1+\mu)}, \\ c_{11} &= -\frac{\epsilon + \epsilon_1}{2p(1+\mu)}, \\ c_{02} &= \frac{3}{4p^2(1+\mu)^2}\left[(\epsilon-\rho)^2 + (\epsilon_1+\rho)^2 + \lambda(a_-^2 + a_+^2)\right] - \frac{1}{2}, \\ c_{12} &= -\frac{3}{4p^2(1+\mu)^2}\left[(\epsilon+\epsilon_1)(2\rho - \epsilon + \epsilon_1) + \lambda(d_- + d_+)\right], \\ c_{22} &= \frac{3}{2p^2(1+\mu)^2}\left[(\epsilon+\epsilon_1)^2 + \lambda Q^2\right]. \end{aligned} \tag{1.127}$$

Here we defined

$$\begin{aligned} \epsilon &\equiv x(\eta_1 - \eta\mu), \quad \epsilon_1 \equiv x_1(\eta - \eta_1\mu), \quad \rho = \gamma(\eta + \eta_1), \\ \lambda &= \mu^2 + \eta^2 + \eta_1^2 - 2\mu\eta\eta_1 - 1. \end{aligned} \tag{1.128}$$

The redistribution function (1.106) is then expressed as

$$R(x_1, \omega_1 \to x, \omega) = \frac{3}{8} \int\limits_{\gamma_*(x, x_1, \mu)}^{\infty} d\gamma \left[c_0 R_0 + c_\Sigma R_\Sigma + c_\Pi R_\Pi\right], \tag{1.129}$$

where we have introduced three functions

$$R_0(x, x_1, \mu, \gamma) = \frac{1}{\pi Q} \int_0^\pi F \, d\Phi, \tag{1.130}$$

$$R_\Sigma(x, x_1, \mu, \gamma) = \frac{1}{\pi Q\, q} \int_0^\pi (\xi + \xi_1) F \, d\Phi, \tag{1.131}$$

$$R_\Pi(x, x_1, \mu, \gamma) = \frac{1}{\pi Q\, q^2} \int_0^\pi \xi\xi_1 F \, d\Phi. \tag{1.132}$$

Alternatively, we can represent the redistribution function as a sum of three terms arising from the corresponding three terms in the electron distribution:

$$R(x_1, \omega_1 \to x, \omega) = \frac{3}{8} \int\limits_{\gamma_*(x, x_1, \mu)}^{\infty} d\gamma \left[f_0 R_0 + f_1 R_1 + f_2 R_2 \right], \tag{1.133}$$

where

$$\begin{aligned} R_1(x, \eta; x_1, \eta_1; \mu; \gamma) &= c_{01} R_0 + c_{11} R_\Sigma \,, \\ R_2(x, \eta; x_1, \eta_1; \mu; \gamma) &= c_{02} R_0 + c_{12} R_\Sigma + c_{22} R_\Pi \,. \end{aligned} \tag{1.134}$$

Using the Klein-Nishina cross-section (1.2) in the form

$$F = 2 + \frac{q^2 - 2q - 2}{q} \left(\frac{1}{\xi_1} - \frac{1}{\xi} \right) + \frac{1}{\xi^2} + \frac{1}{\xi_1^2}, \tag{1.135}$$

(and remembering that $\xi = \xi_1 + q$), we see that the integrals (1.130)–(1.132) involve integrals of types

$$\int_0^\pi \xi^s \, d\Phi, \quad \int_0^\pi \xi_1^s \, d\Phi, \tag{1.136}$$

where $s = -2, ..., 2$. The integrals over non-negative powers of ξ and ξ_1 are trivial. For the negative powers, using equations (1.117) and (1.119) we get (see Nagirner & Poutanen 1993, for details):

$$\int_0^\pi \frac{d\Phi}{\xi_1} = \frac{\pi Q}{q} \frac{1}{a_-}, \quad \int_0^\pi \frac{d\Phi}{\xi_1^2} = \frac{\pi Q}{q^2} \frac{d_-}{a_-^3} \tag{1.137}$$

and similar equations for ξ which we get by substituting ξ, a_+ and d_+ for ξ_1, a_- and d_-, respectively.

After some straightforward algebra we get the expressions for R_0, R_Σ and R_Π:

$$R_0 = \frac{2}{Q} + \frac{q^2 - 2q - 2}{q^2} \left(\frac{1}{a_-} - \frac{1}{a_+} \right) + \frac{1}{q^2} \left(\frac{d_-}{a_-^3} + \frac{d_+}{a_+^3} \right), \tag{1.138}$$

which was obtained by Aharonian & Atoyan (1981) (see also Nagirner & Poutanen 1993),

$$R_\Sigma = \frac{2}{Q^3} (d_- + d_+) + \left(1 - \frac{2}{q} \right) \left(\frac{1}{a_-} + \frac{1}{a_+} \right) + \frac{1}{q^2} \left(\frac{d_-}{a_-^3} - \frac{d_+}{a_+^3} \right) \tag{1.139}$$

and

$$R_\Pi = \frac{2}{Q^5} \left(d_- d_+ + \frac{b^2}{2} \right) + \left(1 - \frac{2}{q} \right) \frac{1}{Q} + \frac{1}{q^2} \left(\frac{1}{a_-} - \frac{1}{a_+} \right). \tag{1.140}$$

Equation (1.129) (or alternatively equations (1.133) and (1.134)) together with our computed redistribution functions (1.138)–(1.140) and the coefficients (1.126)–(1.128) give the full analytical solution for the redistribution function describing scattering of arbitrary photons from the electron gas which anisotropy can be described by equation (1.8).

1.4.3 Alternative redistribution functions

An alternative expression for the redistribution function $R(\boldsymbol{x}_1 \rightarrow \boldsymbol{x})$ can be obtained if we compute the moments

$$\begin{aligned} R_\phi(x, x_1, \mu, \gamma) &= \frac{1}{\pi Q}\int_0^\pi \cos\Phi\ F\ d\Phi \\ &= \frac{q^2-2q-2}{q^2}\frac{1}{b}\left(\frac{d_-}{a_-}-\frac{d_+}{a_+}\right)+\frac{b}{q^2}\left(\frac{1}{a_-^3}+\frac{1}{a_+^3}\right), \qquad (1.141) \\ R_{\phi\phi}(x, x_1, \mu, \gamma) &= \frac{1}{\pi Q}\int_0^\pi \cos^2\Phi\ F\ d\Phi \\ &= \frac{1}{Q}+\frac{Q^3}{b^2}\left(1-\frac{2}{q}\right)+\frac{q^2-2q-2}{q^2}\frac{1}{b^2}\left(\frac{d_-^2}{a_-}-\frac{d_+^2}{a_+}\right) \\ &- \frac{Q^2}{q^2b^2}\left(\frac{d_-}{a_-}+\frac{d_+}{a_+}\right)+\frac{1}{q^2}\left(\frac{d_-}{a_-^3}+\frac{d_+}{a_+^3}\right). \qquad (1.142) \end{aligned}$$

The expressions for R_1 and R_2 then take the form:

$$\begin{aligned} R_1 &= d_{01}R_0 + d_{11}R_\phi\ , \qquad (1.143) \\ R_2 &= d_{02}R_0 + d_{12}R_\phi + d_{22}R_{\phi\phi}\ , \end{aligned}$$

where

$$\begin{aligned} d_{01} &= \cos\theta\ \cos\alpha, \\ d_{11} &= \sin\theta\ \sin\alpha\ \cos\chi = \frac{b}{p(1+\mu)Q^2}\left(\epsilon+\epsilon_1\right), \\ d_{02} &= \frac{3}{2}\left(\cos^2\theta\ \cos^2\alpha+\sin^2\theta\ \sin^2\alpha\ \sin^2\chi\right)-\frac{1}{2} \\ &= \frac{3}{2}\left(2d_{01}^2-d_{11}^2+\sin^2\theta-\cos^2\alpha\right)-\frac{1}{2}, \qquad (1.144) \\ d_{12} &= 3\cos\theta\ \cos\alpha\sin\theta\ \sin\alpha\ \cos\chi = 3\ d_{01}\ d_{11}, \\ d_{22} &= \frac{3}{2}\sin^2\theta\ \sin^2\alpha\ \cos 2\chi \\ &= \frac{3}{2}\left(2d_{11}^2-d_{01}^2-\sin^2\theta+\cos^2\alpha\right). \end{aligned}$$

1.4.4 Approximate redistribution functions

Approximate forms of equations (1.138)–(1.140) can be obtained by making certain simplifying assumptions about the scattering. For example, in the Thomson regime in the electron rest frame the Klein-Nishina kernel F is just $1+\mu_0^2$. Assuming further isotropic scattering in that frame and substituting F by $4/3$, we now

get for the integrals (1.130)–(1.132):

$$R_0 \approx \frac{4}{3Q}, \tag{1.145}$$

$$R_\Sigma \approx \frac{4}{3Q^3}\left(d_- + d_+\right), \tag{1.146}$$

$$R_\Pi \approx \frac{4}{3Q^5}\left(d_- d_+ + \frac{b^2}{2}\right). \tag{1.147}$$

The expression for R_0 was derived by Arutyunyan & Nikogosyan (1980). For the alternative functions (1.141), (1.142), we then have

$$R_\phi = 0, \qquad R_{\phi\phi} = \frac{2}{3Q}. \tag{1.148}$$

These then give

$$R_1 \approx d_{01} R_0 = \cos\theta \cos\alpha \, R_0, \tag{1.149}$$

$$R_2 \approx \left(d_{02} + \frac{1}{2} d_{22}\right) R_0 = P_2(\cos\theta)\, P_2(\cos\alpha)\, R_0, \tag{1.150}$$

with $\cos\theta$ and $\cos\alpha$ given by equations (1.107) and (1.103), respectively. The approximate expressions are better than 50 % accurate in the Thomson regime for $x_1\gamma < 0.1$ at all scattered photon energies.

1.4.5 Relation to the mean powers of photon energies

The relation between the redistribution function averaged over any electron distribution and the mean powers of photon energies follows directly from their definitions (1.6), (1.7) and (1.36):

$$\overline{x_1^j}\,\overline{s_0}(x,\eta) = \frac{1}{x}\int x_1^{j+1} dx_1 \int d^2\omega_1 \, R(\boldsymbol{x} \to \boldsymbol{x}_1). \tag{1.151}$$

This relation is valid for any electron distribution. Comparing equations (1.133) and (1.49), we get a relation between the functions depending on the electron energy:

$$\Delta_{jk}(x,\gamma) P_k(\eta) = \frac{3}{32\pi\gamma p x^{j+1}} \times \int_{x^-(x,\gamma)}^{x_\mathrm{m}(x,\gamma)} x_1^{j+1} dx_1 \int R_k(x_1,\eta_1; x,\eta; \mu; \gamma)\, d^2\omega_1, \tag{1.152}$$

where $\eta_1 = \eta\mu + \sqrt{1-\eta^2}\sqrt{1-\mu^2}\cos\Phi$ and R_0 depends only on the scattering angle μ, but not η, η_1. The integrals over the solid angle can be represented as

the integrals over $d\mu$ and $d\Phi$, where $\Phi \in [0, 2\pi]$ and the limits on μ, $\mu_{\rm m}(x_1, x, \gamma)$ and $\mu^{+}(x_1, x, \gamma)$, are given by equations (A.39)–(A.40) with the arguments x and x_1 reversed. Using equations (1.87) and (1.84), we also get

$$\Delta^{*}_{1k}(x,\gamma)P_k(\eta) = \frac{3}{32\pi\gamma p x^2}\int x_1^2 dx_1 \int (1-\mu)\, R_k\, d^2\omega_1, \tag{1.153}$$

$$\Delta^{\perp}_{1k}(x,\gamma)P^1_k(\eta) = \frac{3}{32\pi\gamma p x^2}\int x_1^2 dx_1 \int \sqrt{1-\mu^2}\cos\Phi\, R_k d^2\omega_1. \tag{1.154}$$

In order to check the accuracy of our derivations we compared the left hand sides of equations (1.152)–(1.154) to the right-hand sides, where the integrals were performed numerically and obtained consistent results.

1.5 Examples of redistribution functions

Now we demonstrate the properties of the derived redistribution functions. We consider a volume filled by electrons with the angular distribution given by equation (1.8). The emissivity in a direction $\boldsymbol{\omega}$ at energy x can be obtained from the radiative transfer equation (1.5) and is given by the integral over the redistribution function

$$\epsilon(\boldsymbol{x}) = \sigma_{\rm T} N_{\rm e}\, x^2 \int_0^\infty \frac{dx_1}{x_1^2}\int d^2\omega_1\, I(\boldsymbol{x}_1)\, R(x_1, \boldsymbol{\omega}_1 \to x, \boldsymbol{\omega}), \tag{1.155}$$

where $I(\boldsymbol{x}_1) = 2m_{\rm e}(m_{\rm e}c^2/h)^3 x_1^3 n(\boldsymbol{x}_1)$ is the specific intensity of the incident radiation normalized to the photon density as

$$N_{\rm ph} = \frac{1}{m_{\rm e}c^3}\int d^2\omega \int I(\boldsymbol{x})\,\frac{dx}{x}. \tag{1.156}$$

Let us consider mono-energetic (with energy γ) electron distribution (1.10). Consider also a monochromatic source of isotropic seed photons at energy x_1 with total photon number density $N_{\rm ph}$. According to equation (1.133) we can write the emissivity at an observer direction η for a given scattering angle as

$$\overline{\epsilon}(x,\eta,\mu) = \frac{3}{32\pi} m_{\rm e}c^3\sigma_{\rm T}N_{\rm e}N_{\rm ph}\frac{x^2}{x_1}\frac{1}{p\gamma}\left[R_0 + \frac{f_1}{f_0}\overline{R}_1 + \frac{f_2}{f_0}\overline{R}_2\right], \tag{1.157}$$

which is related to the scattering angle-averaged emissivity as $\epsilon(\boldsymbol{x}) = \frac{1}{2}\int \overline{\epsilon}(x,\eta,\mu)d\mu$, and where (for $k = 1, 2$)

$$\overline{R}_k(x,\eta;x_1;\mu;\gamma) = \frac{1}{2\pi}\int_0^{2\pi} d\Phi\, R_k(x,\eta;x_1,\eta_1;\mu;\gamma) \tag{1.158}$$

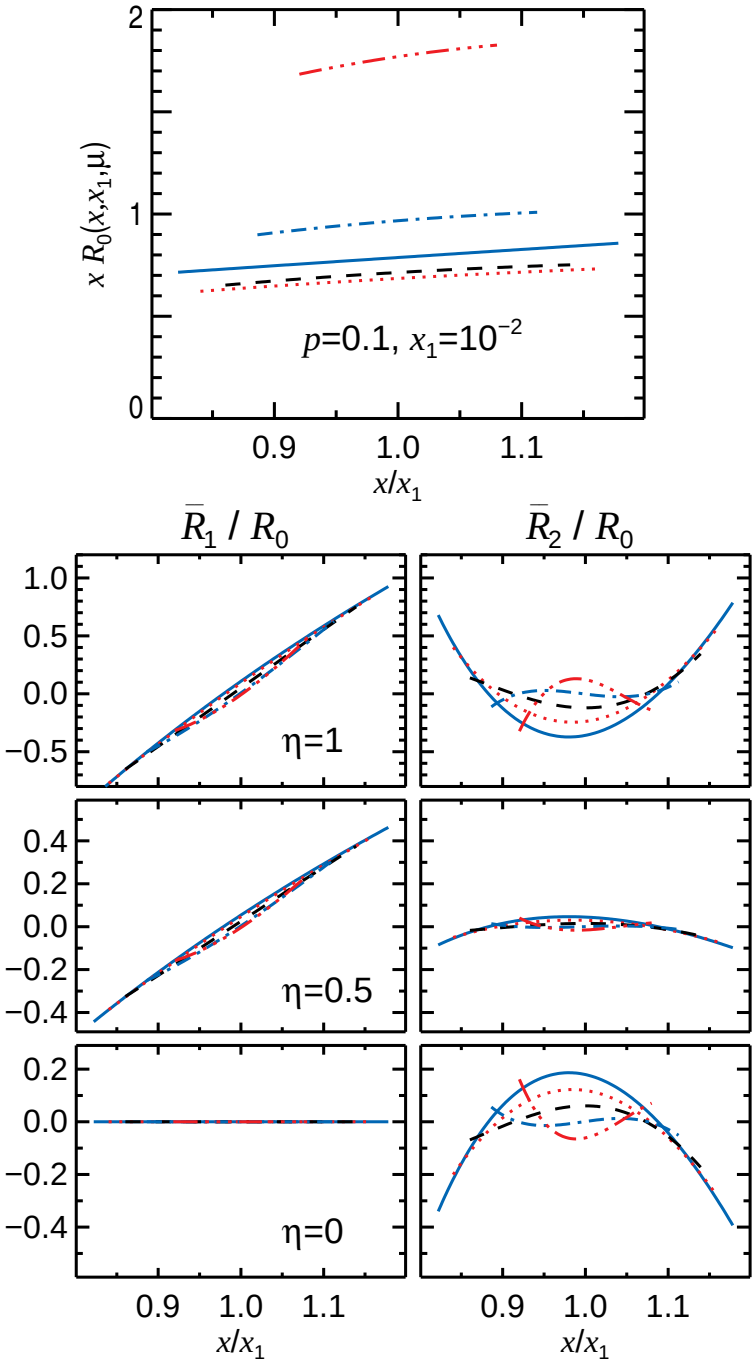

Figure 1.7: Redistribution functions for anisotropic electrons at a given scattering angle. The incident photon energy is $x_1 = 10^{-2}$ and the electron momentum $p = 0.1$. The upper panel shows the photon (number) emissivity for isotropic electrons. The solid, dotted, dashed, dot-dashed and dot-dot-dashed curves correspond to the cosine of scattering angle $\mu = -2/3, -1/3, 0, 1/3, 2/3$, respectively. The lower left panels show the ratio $\overline{R}_1/R_0$, while the right panels show $\overline{R}_2/R_0$ as a function of the ratio of the scattered to the incident photon energies. The three row of panels corresponds to the different observer directions $\eta = 1, 0.5, 0$.

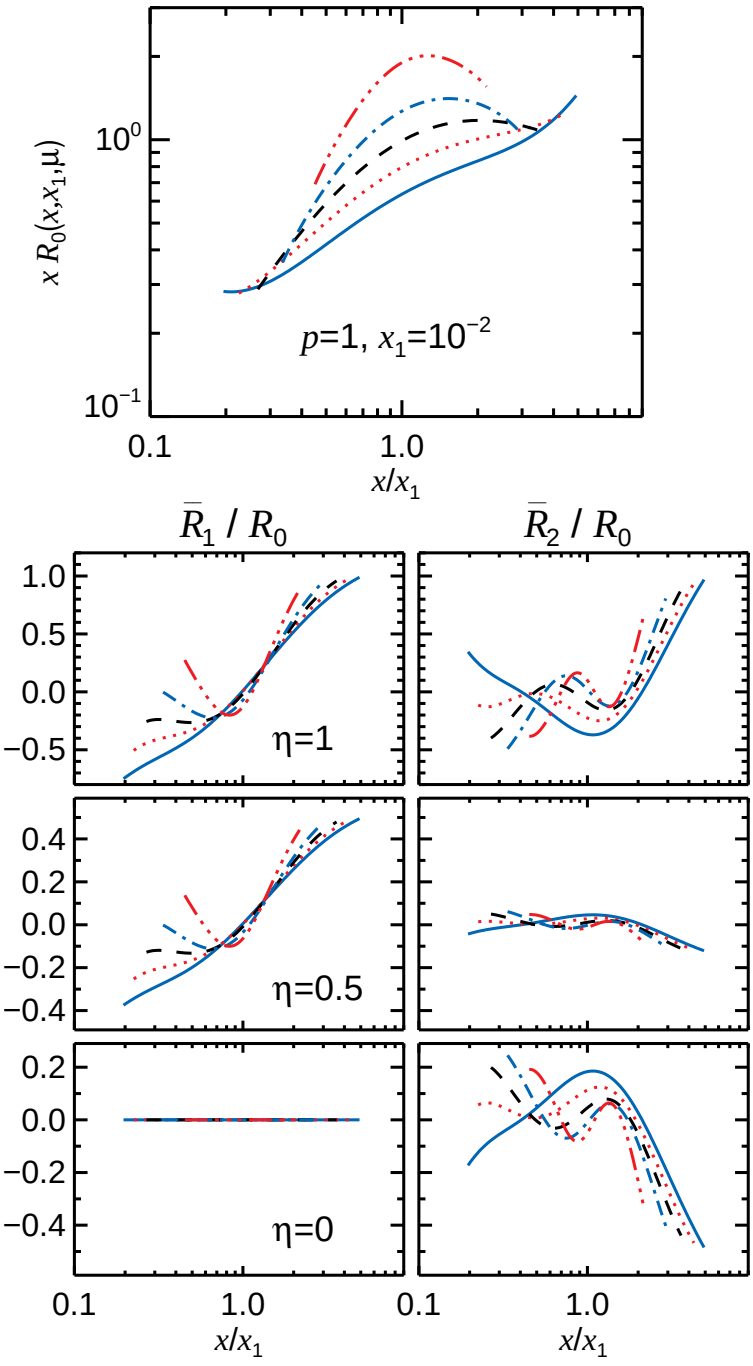

Figure 1.8: Same as Figure 1.7, but for $p = 1$. Note, that here the axes are in logarithmic units.

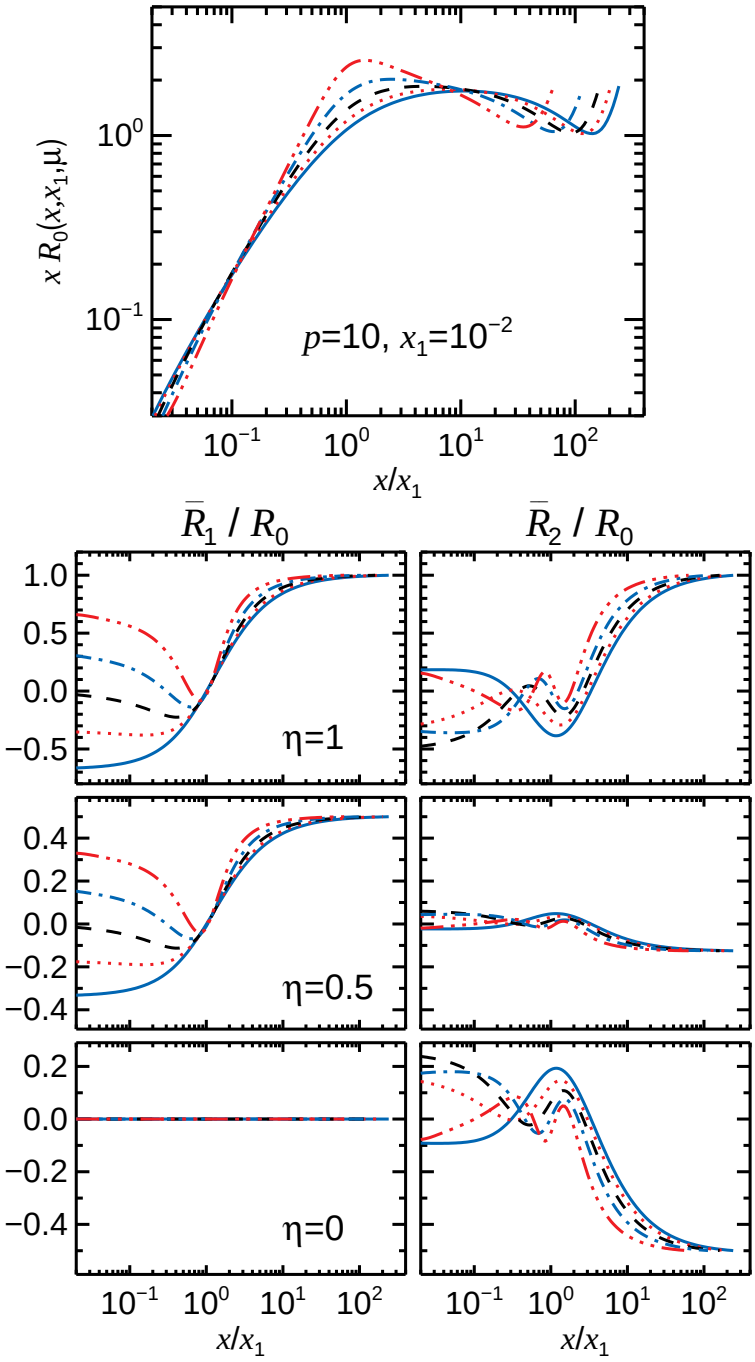

Figure 1.9: Same as Figure 1.8, but for $p = 10$.

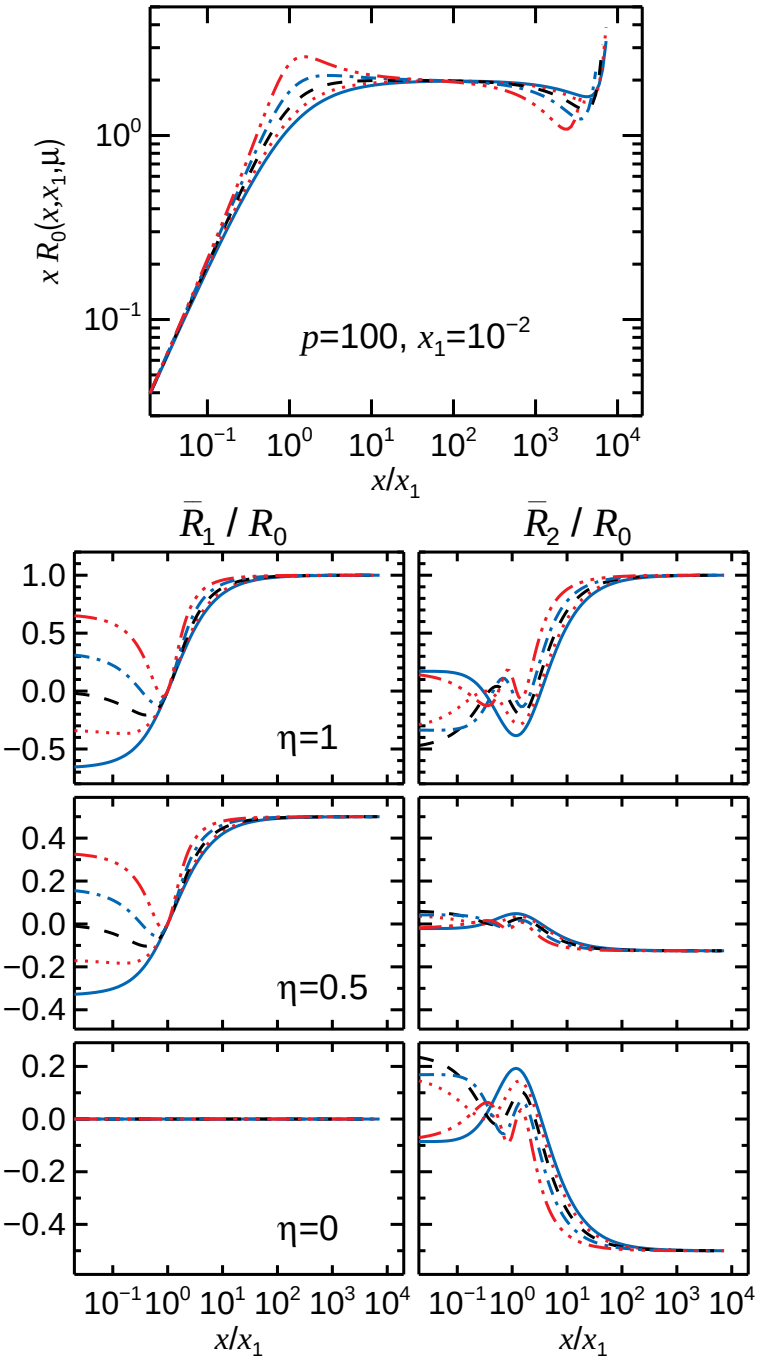

Figure 1.10: Same as Figure 1.8, but for $p = 100$.

and $\eta_1 = \eta\mu + \sqrt{1-\eta^2}\sqrt{1-\mu^2}\cos\Phi$. These functions obviously possess symmetry properties:

$$\overline{R}_1(x,-\eta;x_1;\mu;\gamma) = -\overline{R}_1(x,\eta;x_1;\mu;\gamma), \quad (1.159)$$

$$\overline{R}_2(x,-\eta;x_1;\mu;\gamma) = \overline{R}_2(x,\eta;x_1;\mu;\gamma). \quad (1.160)$$

We compute separately the emissivities resulting from three terms in the electron distribution, i.e. functions $R_0, \overline{R}_1, \overline{R}_2$ (see equation (1.157)), and show in Figures 1.7–1.10 the function R_0 multiplied by x (i.e. quantity proportional to the photon number emissivity) for better visibility as well as the ratios $\overline{R}_1/R_0$ and $\overline{R}_2/R_0$. The main behavior of the functions can easily be understood using formulae (1.149)–(1.150) derived in the Thomson limit and isotropic scattering approximation. Averaging them over the azimuth and using relation $\overline{P_k(\eta_1)} = P_k(\eta)P_k(\mu)$, we get

$$\frac{\overline{R}_1}{R_0} \approx \frac{x_1\mu - x}{Q}\,\eta\,\cos\theta\,, \quad (1.161)$$

$$\frac{\overline{R}_2}{R_0} \approx \frac{x_1^2 P_2(\mu) - 2xx_1\mu + x^2}{Q^2}\,P_2(\eta)\,P_2(\cos\theta)\,. \quad (1.162)$$

These approximate expressions become extremely accurate for high p (i.e. accuracy is about 10^{-3} at $p = 100$).

For a small electron momentum $p = 0.1$ and low photon energies $x_1 = 10^{-2}$, the exact redistribution functions are shown in Figure 1.7. In this regime, scattering is nearly coherent with the scattered photon energies bounded by (see equation (A.35)) $x^{\pm}/x_1 \approx 1 \pm p\sqrt{2(1-\mu)}$. In this regime, $|x - x_1|^2 \ll q \ll x, x_1$ and $\cos\theta \approx (x_1 - x)/pQ$ is a nearly linear function of x/x_1, because $Q/x_1 \approx \sqrt{2(1-\mu)}$. For μ not too close to 1, the azimuth averaging of $\cos\alpha$ gives $-\eta\sqrt{(1-\mu)/2}$ and thus $\overline{R}_1/R_0 \approx (1 - x/x_1)\eta/(2p)$. For $\eta = 0$, the function is always zero, because of the symmetry. Similarly, the nearly quadratic dependence of $\overline{R}_2/R_0$ on energy results from the $\cos^2\theta$ term, while at $\mu \approx 1/3$ the function becomes more complicated because of the cancellation in the $\overline{P_2(\cos\alpha)}$ term.

In the opposite limit of the relativistic electrons (see Figures 1.9 and 1.10), the approximation (1.145) for the function R_0 works fine up to $x_1\gamma \lesssim 0.1$, while as said above the ratios $\overline{R}_1/R_0$ and $\overline{R}_2/R_0$ are very close to those given by equations (1.161) and (1.162) for any photon and electron energies. At small scattered photon energies $x \ll x_1$, $xR_0 \propto x/x_1$, and

$$\overline{R}_1/R_0 \approx \eta\mu\cos\theta, \quad \overline{R}_2/R_0 \approx P_2(\eta)P_2(\mu)P_2(\cos\theta), \quad (1.163)$$

with $\cos\theta \approx 1 - x/x_1$. At high scattered photon energies $x \gg x_1$, the photons are scattered at large angles in the electron rest frame and therefore they are beamed in the direction of the incoming electrons. In that case, the angular distribution of the scattered photons resemble that of the electrons. In this regime $xR_0 \propto$ const, and $R_1/R_0 \approx \eta$ and $R_2/R_0 \approx P_2(\eta)$, which gives the flat dependences clearly seen in Figures 1.9 and 1.10, and $\epsilon(\boldsymbol{x}) \propto f_{\rm e}(\gamma,\eta)\,x/x_1$.

1.6 Sunyaev–Zeldovich effect

Let consider a cloud of isotropic Maxwellian electrons of temperature $\Theta \equiv kT_{\rm e}/m_{\rm e}c^2$, which moves with velocity $c\beta_{\rm b}$ (corresponding Lorentz factor $\Gamma_{\rm b}$) through the isotropic cosmic microwave background of temperature $\Theta_{\rm cmb} \equiv kT_{\rm cmb}/m_{\rm e}c^2$. We compute the thermal and kinematic Sunyaev–Zeldovich effects (Zeldovich & Sunyaev 1969; Sunyaev & Zeldovich 1972), i.e. the spectrum of the scattered radiation (and resulting deviations from the black body) as a function of Θ and the angle between the line of sight and the direction of motion.

One approach would be to make a Lorentz transformation of the incident radiation to the comoving frame, compute the Compton scattered radiation using the kernel corresponding to isotropic electron distribution, and then to Lorentz transform it back to the observer frame. Another way is to compute the electron distribution in the observer frame, approximate it by expansion (1.8) and compute directly the Compton scattered radiation in the observer frame. The second approach might be favorable from numerical point of view if the object velocity is variable in space and/or time, as allows to pre-compute redistribution functions at a fixed grid of angles and photon energies.

1.6.1 Scattering in the comoving frame

Let us first compute the scattered radiation by a standard method considering scattering in the comoving frame. The relativistic Maxwellian distribution of electrons in the comoving frame (quantities with primes) is given by

$$f'_{\rm e}(\boldsymbol{p}') = N'_{\rm e}\frac{\exp(-\gamma'/\Theta)}{4\pi\,\Theta\,K_2(1/\Theta)}, \tag{1.164}$$

where K_2 is the modified Bessel function and $N'_{\rm e}$ is the electron density in that frame. The incident black body radiation occupation number is

$$n_{\rm bb}(\boldsymbol{x}) = \frac{1}{\exp(x_t)-1}, \tag{1.165}$$

where $x_t = x/\Theta_{\rm cmb} = h\nu/kT_{\rm cmb}$. From the radiative transfer equation (1.5), in the limit of small optical depth, we get the correction to the black body spectrum:

$$\Delta n(x,\eta) = n(x,\eta) - n_{\rm bb}(x) = -\tau_{\rm T}\overline{s}_0(x')n_{\rm bb}(x) + S(x,\eta), \tag{1.166}$$

where $\tau_{\rm T}$ is the Lorentz invariant optical depth for Thomson scattering,

$$S(x,\eta) = \tau_{\rm T}\frac{1}{x'}\int_0^\infty x'_1 dx'_1 \int d^2\omega'_1\, R^{\rm iso}(\boldsymbol{x}'_1 \to \boldsymbol{x}')n_{\rm bb}(x_1) \tag{1.167}$$

is the source function, and we used here the fact that the photon occupation number is Lorentz invariant. The energy transformation is given by Doppler shift

$x = x'\mathcal{D}$ and $x_1 = x_1'\mathcal{D}_1$ with the Doppler factors

$$\mathcal{D} = \frac{1}{\Gamma_\mathrm{b}(1-\beta_\mathrm{b}\eta)}, \quad \mathcal{D}_1 = \Gamma_\mathrm{b}(1+\beta_\mathrm{b}\eta_1'). \tag{1.168}$$

The relation between the angles is given by the aberration formula:

$$\eta' = \frac{\eta - \beta_\mathrm{b}}{1-\beta_\mathrm{b}\eta}. \tag{1.169}$$

We note here that $\overline{s}_0$ is equal to unity with high accuracy, because scattering is in deep Thomson regime. The calculation of the redistribution function R^{iso} involves numerical integration over the Maxwellian distribution (see equation (1.133); note that $f_1 = f_2 = 0$) $f_0 = f_\mathrm{e}'(\gamma) = f_\mathrm{e}'(\boldsymbol{p})/N_\mathrm{e}'$ given by equation (1.164). Thus the source function (1.167) involves 4-dimensional integral to be taken numerically, which is rather time-consuming.

1.6.2 Scattering in the external frame

We can also compute the same effect directly in the external frame. The electron Lorentz factor in the comoving frame is related to the electron four-momentum in the external frame as

$$\gamma' = \Gamma_\mathrm{b}(\gamma - p\beta_\mathrm{b}\eta_\mathrm{e}), \tag{1.170}$$

where η_e is the cosine of the angle between the electron momentum and the direction of cloud motion. Because the distribution function is Lorentz invariant, we easily get the electron distribution in the external frame:

$$\begin{aligned} f_\mathrm{e}(\boldsymbol{p}) = f_\mathrm{e}'(\boldsymbol{p}') &= N_\mathrm{e}' \frac{\exp(-\gamma\Gamma_\mathrm{b}/\Theta)}{4\pi\,\Theta\,K_2(1/\Theta)}\ \exp(p\,\Gamma_\mathrm{b}\,\beta_\mathrm{b}\,\eta_\mathrm{e}/\Theta) \\ &\approx N_\mathrm{e}' \frac{\exp(-\gamma/\Theta)}{4\pi\,\Theta\,K_2(1/\Theta)} \left[1 + \frac{\beta_t^2}{6}(p^2 - 3\gamma\Theta) + \beta_t p\eta_\mathrm{e} + \frac{\beta_t^2 p^2}{3} P_2(\eta_\mathrm{e})\right], \end{aligned} \tag{1.171}$$

where $\beta_t = \beta_\mathrm{b}/\Theta$ and we expanded the expression up to the second order in β_b. The electron density in that frame is:

$$N_\mathrm{e} = \int f_\mathrm{e}(\boldsymbol{p}) d^3\boldsymbol{p} = \Gamma_\mathrm{b} N_\mathrm{e}'. \tag{1.172}$$

The corresponding terms f_k of the electron distribution can be obtained from equation (1.171) noting that $f_\mathrm{e}(\gamma, \eta_\mathrm{e}) = f_\mathrm{e}(\boldsymbol{p})/\Gamma_\mathrm{b} N_\mathrm{e}'$. The change to the occupation number is:

$$\Delta n(x,\eta) = -\tau_\mathrm{T}\overline{s}_0(x,\eta) n_\mathrm{bb}(x) + S(x,\eta). \tag{1.173}$$

The scattering cross-section is given by equation (1.26) and in the Thomson limit it is just $\overline{s}_0(x,\eta) \approx 1 - \beta_\mathrm{b}\eta$. The source function is now

$$S(x,\eta) = \tau_\mathrm{T}\frac{1}{x}\int_0^\infty x_1\, n_\mathrm{bb}(x_1)\, dx_1 \int d^2\omega_1\, R(\boldsymbol{x}_1 \to \boldsymbol{x}), \tag{1.174}$$

where the redistribution function R given by equation (1.133) is averaged over directions of incident photons, but still depends on the scattered photon direction η. This form of the source function is more favorable compared to equation (1.167) from numerical point of view, as it can be tabulated in advance at a given grid of photon energies and angles. Computed directly it still involves numerical calculations of 4-dimensional integrals.

1.6.3 Isotropic scattering in the Thomson regime in the electron rest frame

In the Thomson limit (as in the case of the Sunyaev-Zeldovich effect), the calculations in the external frame can be dramatically simplified. We can use the azimuthally averaged approximate expression (1.145), (1.161), and (1.162) for the redistribution functions:

$$\int d^2\omega_1\, R(\boldsymbol{x}_1 \to \boldsymbol{x}) = 2\pi \int_{-1}^{1} d\mu\, \frac{3}{8} \int\limits_{\gamma_*(x,x_1,\mu)}^{\infty} d\gamma \left[f_0 R_0 + f_1 \overline{R}_1 + f_2 \overline{R}_2 \right]. \qquad (1.175)$$

Interestingly, R_0 does not depend on γ and in expressions for $\overline{R}_1$ and $\overline{R}_2$ it comes only through $\cos\theta \approx (x_1 - x)\gamma/Qp$ (because $q \ll x, x_1$, see equation (1.107)). For the electron distribution given by equation (1.171), the integrals over γ thus can be taken analytically:

$$\begin{aligned}
\int d\gamma\, f_0 R_0 &= C \frac{1}{\Gamma_\mathrm{b}} \left[1 - \frac{\beta_\mathrm{b}^2}{6} \left(\frac{1}{\Theta^2} + 1 + \frac{\gamma_*}{\Theta} - \left(\frac{\gamma_*}{\Theta} \right)^2 \right) \right], \\
\int d\gamma\, f_1 R_1 &= C\, \beta_\mathrm{b}\, \eta\, \frac{x_1\mu - x}{Q}\, \frac{x_1 - x}{Q} \left(1 + \frac{\gamma_*}{\Theta} \right), \qquad (1.176) \\
\int d\gamma\, f_2 R_2 &= C\, \frac{\beta_\mathrm{b}^2}{3}\, P_2(\eta)\, \frac{x_1^2 P_2(\mu) - 2x x_1 \mu + x^2}{Q^2} \\
&\times \left[P_2\left(\frac{x_1 - x}{Q} \right) \left(2 + 2\frac{\gamma_*}{\Theta} + \left(\frac{\gamma_*}{\Theta} \right)^2 \right) + \frac{1}{2\Theta^2} \right],
\end{aligned}$$

where the proportionality coefficient $C = R_0 \exp(-\gamma_*/\Theta)/\ [4\pi K_2(1/\Theta)]$. The zeroth order term in β_b was derived by Poutanen (1994), see also Poutanen & Svensson (1996).

Evaluation of the source function (1.174) now involves only two numerical integrations over the photon energy x_1 and cosine of the scattering angle μ, reducing the computational time by 2-3 orders of magnitude.

For all three methods we numerically compute the correction function for the black body intensity

$$\Delta I(x) = \frac{1}{\tau_\mathrm{T}} x_t^3 \Delta n(x, \eta), \qquad (1.177)$$

and compare the results of calculations in Figure 1.11. The three different methods give nearly identical results.

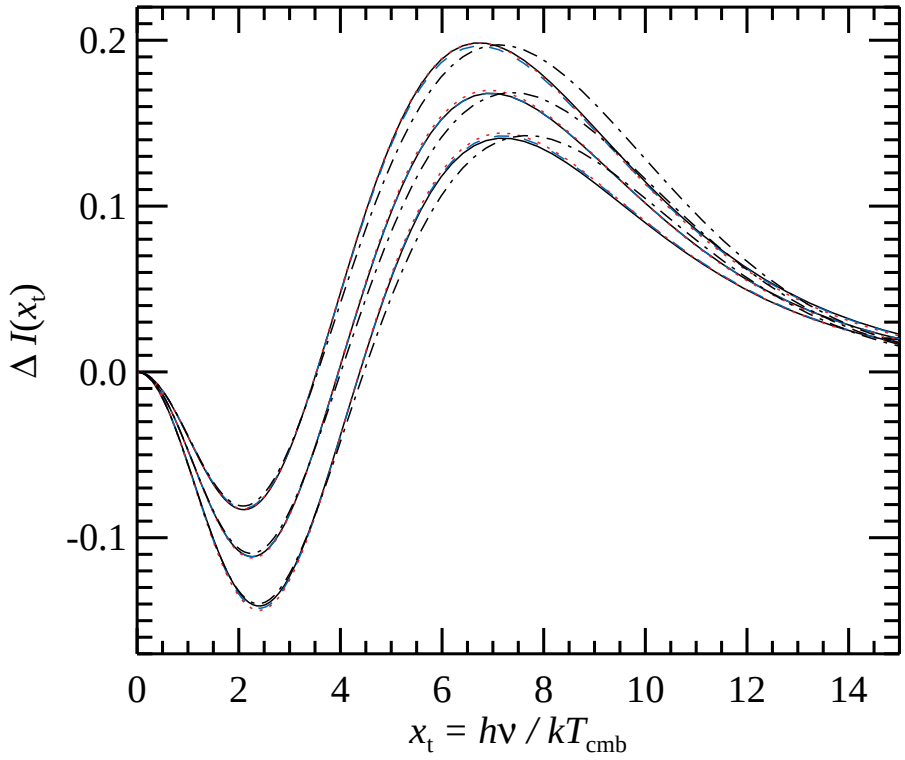

Figure 1.11: Deviation from the black body spectrum of cosmic microwave background radiation with $T_{\rm cmb} = 2.7$ K resulting from the Compton scattering in a moving cloud of isotropic hot electrons (thermal and kinematic Sunyaev-Zeldovich effects). The electron temperature is $\Theta = 0.03$ and the cloud velocity $\beta_{\rm b} = 0.01$. The solid curves are computed using equations (1.166)–(1.167), considering scattering in the cloud frame, where electrons are isotropic. The dashed curves show the results using the formalism developed in this chapter for anisotropic electrons, given by equations (1.173)–(1.174). The dotted curves correspond to the semi-analytical approximation of the angle-averaged redistribution function given by equations (1.175)–(1.176). The three different methods give nearly identical results. The three curves from bottom to the top correspond to the three viewing angles with $\eta = -0.98, 0, +0.98$. The dash-dotted curves show the analytical approximation of Sazonov & Sunyaev (1998), which includes terms up to second order in $\beta_{\rm b}$ and Θ, as well as a cross-term $\beta_{\rm b}\Theta$. It works reasonably well up to the temperatures $\Theta < 0.02$, but fails at higher temperatures in Wien tail.

1.7 Conclusions

We have developed the exact analytical theory of Compton scattering by anisotropic distribution of electrons that can be represented by a second order polynomial over cosine of some angle (dipole and quadrupole anisotropies). For the total cross-section, we reduce the 9-dimensional integral to a single integral over the electron energy. Analogous expressions have been derived for the mean energy of the scattered photons and its dispersion. We also obtained analytical expressions for the radiation pressure force acting on the electron gas. These moments can be used for analytical estimations as well as for the numerical solutions of the kinetic equations in the Fokker-Planck approximation (see e.g. Vurm & Poutanen 2009).

Furthermore, the expression for the redistribution function describing angle-dependent Compton scattering by anisotropic electrons is reduced to a single integral over the electron energy. Exact analytical formulae valid for any photon and electron energy are derived in the case of monoenergetic electrons. We have also derived approximate expressions for the redistribution function, assuming isotropic scattering in the electron rest frame, which are very accurate in the case of relativistic electrons interacting with soft photons in the Thomson regime.

We applied the developed formalism to the accurate calculations of the thermal and kinematic Sunyaev-Zeldovich effects for arbitrary electron distributions. A very similar problem arises in outflowing coronae around accreting black holes and neutron stars, where the bulk motion causes electron anisotropy. Another application could be a computation of the radiative transport in the synchrotron self-Compton sources with ordered magnetic field, where the electron distribution can have strong deviations from the isotropy because of pitch angle-dependent cooling. These problems will be considered in future publications.

Chapter 2

Photon–photon pair production and pair annihilation

2.1 Introduction

A large number of astrophysical sources such as jets from active galactic nuclei, gamma-ray bursts, pulsars as well as some X-ray binaries are capable of producing high-energy gamma-ray emission. Radiative modeling of such sources has to include the treatment of an additional physical process not relevant at lower energies: photon–photon pair production, by which two photons can annihilate to produce an electron–positron pair. The process can take place if $xx_1 \geq 1$, where x and x_1 are the photon energies in $m_\mathrm{e}c^2$ units, meaning that at least one of the interacting photons must have $x \geq 1$.

Pair production can have a profound effect on the shape of high-energy spectra. First, absorption of energetic photons on lower-energy radiation can attenuate the radiative power above $m_\mathrm{e}c^2$. Secondly, the produced electron–positron pairs can further modify the spectrum through inverse-Compton scattering and synchrotron emission. Also, if the inverse-Compton emission produced by the secondary pairs extends above $m_\mathrm{e}c^2$, the scattered photons can produce another generation of electron–positron pairs, which can upscatter further photons etc., leading to a so-called pair-cascade (see e.g. Bonometto & Rees 1971; Zdziarski & Lightman 1985; Svensson 1987). Furthermore, in high compactness sources such as gamma-ray bursts the secondary pairs can dominate the Thomson opacity of the source over the electrons associated with protons. It is therefore obvious that the pair production process can influence the spectrum over a wide range of photon energies not limited to high-energy gamma-rays.

To accurately model the effects of pair production and annihilation processes on both the electron and photon distributions without limitations on energies, we need to know the exact cross-sections for both processes as well as the spectra of injected pairs/photons. The exact pair annihilation cross-section was first derived already by Dirac (1930). A fully general analytic expression for the injected pho-

ton spectrum from annihilating pairs was derived by Svensson (1982), a similar expression for the injected pair spectrum due to photon–photon annihilation was found in Boettcher & Schlickeiser (1997). Although correct, their expressions suffer from cancellations in some regions of parameter space. In this chapter we will instead follow the framework laid out in Nagirner & Loskutov (1999) to derive all the relevant quantities, and will obtain expressions that are free of cancellations. The treatment is widely analogous to the treatment of Compton scattering in Chapter 1.

2.2 Relativistic kinetic equations

The relativistic kinetic equation for electrons accounting for photon–photon pair production and pair annihilation processes takes the form (ignoring induced terms as well as electron/positron degeneracy)

$$\underline{p}_- \cdot \underline{\nabla}\tilde{n}_-(\boldsymbol{p}_-) = \frac{r_\mathrm{e}^2}{4}\frac{2}{\lambda_\mathrm{C}^3}\int \frac{d^3p_+}{\gamma_+}\frac{d^3x_1}{x_1}\frac{d^3x}{x}\,\delta(\underline{p}_- + \underline{p}_+ - \underline{x}_1 - \underline{x})\,F_{\gamma\gamma} \times \left[\tilde{n}_\mathrm{ph}(\boldsymbol{x}_1)\tilde{n}_\mathrm{ph}(\boldsymbol{x}) - \tilde{n}_-(\boldsymbol{p}_-)\tilde{n}_+(\boldsymbol{p}_+)\right]. \tag{2.1}$$

Here we have used similar definitions used for the treatment of Compton scattering: dimensionless photon four-momentum $\underline{x} = \{x, \boldsymbol{x}\} = x\{1, \boldsymbol{\omega}\}$, where $x = h\nu/m_\mathrm{e}c^2$, dimensionless electron/positron four-momentum $\underline{p} = \{\gamma, \boldsymbol{p}\} = \{\gamma, p\boldsymbol{\Omega}\} = \gamma\{1, \beta\boldsymbol{\Omega}\}$, where $p = \sqrt{\gamma^2 - 1}$ and $\beta = p/\gamma$, the four-gradient $\underline{\nabla} = \{\partial/c\partial t, \boldsymbol{\nabla}\}$ and the occupation numbers $\tilde{n}_\pm$ and $\tilde{n}_\mathrm{ph}$ for pairs and photons, respectively. The invariant reaction rate $F_{\gamma\gamma}$ is (Berestetskii et al. 1982)

$$F_{\gamma\gamma} = \frac{\xi}{\xi_1} + \frac{\xi_1}{\xi} + 2\left(\frac{1}{\xi} + \frac{1}{\xi_1}\right) - \left(\frac{1}{\xi} + \frac{1}{\xi_1}\right)^2, \tag{2.2}$$

where we have defined the four-products between the particles' momenta as

$$\xi = \underline{p}_- \cdot \underline{x} = \underline{p}_+ \cdot \underline{x}_1, \qquad \xi_1 = \underline{p}_- \cdot \underline{x}_1 = \underline{p}_+ \cdot \underline{x}. \tag{2.3}$$

Later we will also need the invariant four-product of the photon momenta defined as

$$q = \underline{x} \cdot \underline{x}_1 = xx_1(1 - \boldsymbol{\omega}\cdot\boldsymbol{\omega}_1) = xx_1(1 - \mu) = \xi + \xi_1, \tag{2.4}$$

where the last equality arises from conservation laws for energy and momentum.

The kinetic equation can also be written in the form of a transfer equation

$$\left(\frac{1}{c}\frac{\partial}{\partial t} + \beta\,\boldsymbol{\Omega}\cdot\boldsymbol{\nabla}\right)\tilde{n}_-(\boldsymbol{p}_-) = -\sigma_\mathrm{T}\,N_+\,\overline{s}_\mathrm{pa}(\boldsymbol{p}_-)\,\tilde{n}_-(\boldsymbol{p}_-) + \sigma_\mathrm{T}\,N_\mathrm{ph}^2\,\frac{\lambda_\mathrm{C}^3}{2}\,j_\mathrm{pp}(\boldsymbol{p}_-), \tag{2.5}$$

where the pair annihilation cross-section (in units of $\sigma_{\rm T}$) is given by

$$\overline{s}_{\rm pa}(\boldsymbol{p}_-) = \frac{3}{32\pi}\frac{2}{\lambda_{\rm C}^3 N_+}\frac{1}{\gamma_-}\int \frac{d^3p_+}{\gamma_+}\frac{d^3x_1}{x_1}\frac{d^3x}{x}\,\tilde{n}_+(\boldsymbol{p}_+)\,F_{\gamma\gamma}\,\delta(\underline{p}_- + \underline{p}_+ - \underline{x}_1 - \underline{x}) \quad (2.6)$$

and the pair production rate by

$$j_{\rm pp}(\boldsymbol{p}_-) = \frac{3}{32\pi}\left(\frac{2}{\lambda_{\rm C}^3 N_{\rm ph}}\right)^2\frac{1}{\gamma_-}\int \frac{d^3p_+}{\gamma_+}\frac{d^3x_1}{x_1}\frac{d^3x}{x}\,\tilde{n}_{\rm ph}(\boldsymbol{x})\tilde{n}_{\rm ph}(\boldsymbol{x}_1)F_{\gamma\gamma}\delta(\underline{p}_- + \underline{p}_+ - \underline{x}_1 - \underline{x}). \quad (2.7)$$

Although no longer manifestly covariant, equation (2.5) is still relativistically correct and can be written in any frame.

The kinetic equation for photons can be written as

$$\underline{x}\cdot\underline{\nabla}\tilde{n}_{\rm ph}(\boldsymbol{x}) = \frac{r_{\rm e}^2}{2}\frac{2}{\lambda_{\rm C}^3}\int \frac{d^3x_1}{x_1}\frac{d^3p_-}{\gamma_-}\frac{d^3p_+}{\gamma_+}\,\delta(\underline{p}_- + \underline{p}_+ - \underline{x}_1 - \underline{x})\,F_{\gamma\gamma} \times\left[\tilde{n}_-(\boldsymbol{p}_-)\tilde{n}_+(\boldsymbol{p}_+) - \tilde{n}_{\rm ph}(\boldsymbol{x}_1)\tilde{n}_{\rm ph}(\boldsymbol{x})\right]. \quad (2.8)$$

Note that the extra factor $1/2$ on the right-hand side of equation (2.1) compared to equation (2.8) arises due to double counting of the photon states. In the form of the radiative transfer equation we have

$$\left(\frac{1}{c}\frac{\partial}{\partial t} + \boldsymbol{\omega}\cdot\boldsymbol{\nabla}\right)\tilde{n}_{\rm ph}(\boldsymbol{x}) = -\sigma_{\rm T}\,N_{\rm ph}\,\overline{s}_{\rm pp}(\boldsymbol{x})\,\tilde{n}_{\rm ph}(\boldsymbol{x}) + \sigma_{\rm T}\,N_-\,N_+\,\frac{\lambda_{\rm C}^3}{2}\,j_{\rm pa}(\boldsymbol{x}), \quad (2.9)$$

where the pair production cross-section is

$$\overline{s}_{\rm pp}(\boldsymbol{x}) = \frac{3}{16\pi}\frac{2}{\lambda_{\rm C}^3 N_{\rm ph}}\frac{1}{x}\int \frac{d^3x_1}{x_1}\frac{d^3p_-}{\gamma_-}\frac{d^3p_+}{\gamma_+}\,\tilde{n}_{\rm ph}(\boldsymbol{x}_1)\,F_{\gamma\gamma}\,\delta(\underline{p}_- + \underline{p}_+ - \underline{x}_1 - \underline{x}) \quad (2.10)$$

and the emissivity due to pair annihilation

$$j_{\rm pa}(\boldsymbol{x}) = \frac{3}{16\pi}\left(\frac{2}{\lambda_{\rm C}^3}\right)^2\frac{1}{N_-N_+}\frac{1}{x}\int \frac{d^3x_1}{x_1}\frac{d^3p_-}{\gamma_-}\frac{d^3p_+}{\gamma_+}\,\tilde{n}_-(\boldsymbol{p}_-)\tilde{n}_+(\boldsymbol{p}_+)F_{\gamma\gamma}\delta(\underline{p}_- + \underline{p}_+ - \underline{x}_1 - \underline{x}). \quad (2.11)$$

2.3 Pair production and annihilation rates

We will now turn to the calculation of the injection rates of pairs and photons given by equations (2.7) and (2.11) respectively. In what follows we will assume isotropic particle and photon distributions.

The isotropic pair injection rate (2.7) can be written in the form

$$j_{\rm pp}(p_-) = 3\pi\left(\frac{2}{\lambda_{\rm C}^3 N_{\rm ph}}\right)^2\frac{1}{\gamma_- p_-}\int_{x^{(L)}}^{\infty}\tilde{n}_{\rm ph}(x)\,dx\int_{x_1^{(L)}}^{\infty}\tilde{n}_{\rm ph}(x_1)\,dx_1\,R_{\gamma\gamma}(\gamma_-, x, x_1), \quad (2.12)$$

where we have defined

$$R_{\gamma\gamma}(\gamma_-, x, x_1) = \frac{1}{2}\frac{1}{(4\pi)^2} x x_1 p_- \int \frac{d^3 p_+}{\gamma_+} d^2\omega\, d^2\omega_1\, F_{\gamma\gamma}\, \delta(\underline{p}_- + \underline{p}_+ - \underline{x}_1 - \underline{x}). \quad (2.13)$$

Similarly, the photon emissivity due to pair annihilation is

$$j_{\rm pa}(x) = 6\pi \left(\frac{2}{\lambda_{\rm C}^3}\right)^2 \frac{1}{N_- N_+}\frac{1}{x^2} \int_{\gamma_+^{(L)}}^{\infty} \tilde{n}_+(p_+) d\gamma_+ \int_{\gamma_-^{(L)}}^{\infty} \tilde{n}_-(p_-) d\gamma_- R^\star_{\gamma\gamma}(x, \gamma_-, \gamma_+), \quad (2.14)$$

where

$$R^\star_{\gamma\gamma}(x, \gamma_-, \gamma_+) = \frac{1}{2}\frac{1}{(4\pi)^2} x p_- p_+ \int \frac{d^3 x_1}{x_1} d^2\Omega_-\, d^2\Omega_+\, F_{\gamma\gamma}\, \delta(\underline{p}_- + \underline{p}_+ - \underline{x}_1 - \underline{x}). \quad (2.15)$$

Before proceeding, let's compare the quantities $R_{\gamma\gamma}$ and $R^\star_{\gamma\gamma}$ defined by equations (2.13) and (2.15). Both of them contain integrals over the directions of three particles' momenta and an integral over one particle's energy. Due to rotational symmetry, there are no angles left in the problem after integrations over three solid angles, and the result does not depend on our choice of these three particles, over the directions of which we are integrating [1]. After the angular integrals we are left with integrals of type

$$\int d\gamma_+ \delta(\gamma_+ + \gamma_- - x_1 - x) \cdot ... \quad \text{and} \quad \int dx_1 \delta(\gamma_+ + \gamma_- - x_1 - x) \cdot ..., \quad (2.16)$$

which are equivalent. We can therefore see that $R_{\gamma\gamma}$ and $R^\star_{\gamma\gamma}$ are related simply as

$$R^\star_{\gamma\gamma}(x, \gamma_-, \gamma_+) = R_{\gamma\gamma}(\gamma_-, x, \gamma_- + \gamma_+ - x). \quad (2.17)$$

The problem of finding $j_{\rm pp}(p_-)$ and $j_{\rm pa}(x)$ thus reduces to the calculation of a single function $R_{\gamma\gamma}(\gamma_-, x, x_1)$.

The calculation of $R_{\gamma\gamma}$ will proceed in two steps. Following Nagirner & Loskutov (1999), we will first calculate the quanity

$$\overline{F}_{\gamma\gamma}(\gamma_-, x, x_1, \mu) = \frac{1}{2\pi} p_- \int \frac{d^3 p_+}{\gamma_+} d^2\Omega_-\, F_{\gamma\gamma}\, \delta(\underline{p}_- + \underline{p}_+ - \underline{x}_1 - \underline{x}), \quad (2.18)$$

which has the physical meaning of angle-averaged pair production rate from photons 'colliding' with a given angle of incidence. Once $\overline{F}_{\gamma\gamma}$ is known, we can calculate $R_{\gamma\gamma}$ from

$$R_{\gamma\gamma}(\gamma_-, x, x_1) = \frac{1}{8} x x_1 \int_{\mu_{\rm m}}^{\mu_+} \overline{F}_{\gamma\gamma}(\gamma_-, x, x_1, \mu)\, d\mu. \quad (2.19)$$

The integration limits for μ will be given below.

[1] To see that this is true we can formally add an integration over the directions of the remaining particle, which amounts to multiplication by 4π. We can then change the order of integration and remove an integral over the directions of another particle, which is equivalent to division by 4π.

2.3.1 Integration over electron directions

After using the three-dimensional delta-function to take the integral over d^3p_+, we can cast equation (2.18) in the form

$$\overline{F}_{\gamma\gamma}(\gamma_-, x, x_1, \mu) = \frac{1}{2\pi} p_- \int d^2\Omega_-\, F_{\gamma\gamma}\, \delta(\xi + \xi_1 - q), \tag{2.20}$$

where we have used the identity

$$\delta(\gamma_+ + \gamma_- - x_1 - x) = \gamma_+\, \delta(\xi + \xi_1 - q). \tag{2.21}$$

Writing the quantities ξ and ξ_1 as

$$\xi = x(\gamma - p\,\boldsymbol{\Omega}\cdot\boldsymbol{\omega}), \quad \xi_1 = x_1(\gamma - p\,\boldsymbol{\Omega}\cdot\boldsymbol{\omega}_1), \tag{2.22}$$

the argument of the delta-function becomes (hereafter dropping the '$-$' for electron quantities)

$$\xi + \xi_1 - q = \gamma_-(x + x_1) - p\,\boldsymbol{\Omega}\cdot(x\boldsymbol{\omega} + x_1\boldsymbol{\omega}_1) - xx_1(1 - \mu). \tag{2.23}$$

In analogy with the treatment of Compton scattering, it is easiest to perform the angular integration in a coordinate system where the polar axis is in the direction of $x\boldsymbol{\omega} + x_1\boldsymbol{\omega}_1$. The corresponding unit vector is defined as

$$\boldsymbol{n} = \frac{x\boldsymbol{\omega} + x_1\boldsymbol{\omega}_1}{Q}, \tag{2.24}$$

where

$$Q^2 = x^2 + x_1^2 + 2xx_1\mu = (x + x_1)^2 - 2q. \tag{2.25}$$

In this system

$$d^2\Omega = d\phi\, d\cos\theta, \quad \text{where} \quad \cos\theta = \boldsymbol{\Omega}\cdot\boldsymbol{n}. \tag{2.26}$$

Using this in equation (2.20), we can immediately take the integral over the polar angle θ, giving

$$\begin{aligned}\overline{F}_{\gamma\gamma}(\gamma, x, x_1, \mu) &= \frac{1}{2\pi} p \int d\phi \int d\cos\theta\, F_{\gamma\gamma}\, \delta[\gamma(x + x_1) - pQ\cos\theta - q] \\ &= \frac{1}{2\pi Q} \int d\phi\, F_{\gamma\gamma}.\end{aligned} \tag{2.27}$$

The invariant reaction rate $F_{\gamma\gamma}$ depends on the polar angle θ through ξ and ξ_1, which we have to substitute from

$$\cos\theta = \frac{\gamma(x + x_1) - q}{pQ}. \tag{2.28}$$

To integrate equation (2.27) over the azimuth, we need to specify the reference direction from which ϕ is measured, which we choose to be the projection of the photon direction $\boldsymbol{\omega}$ to the plane perpendicular to $\boldsymbol{n}$. Defining

$$\cos\kappa = \boldsymbol{\omega}\cdot\boldsymbol{n} = \frac{x + x_1\mu}{Q}, \qquad \sin\kappa = \frac{x_1\sqrt{1-\mu^2}}{Q}, \tag{2.29}$$

we then have

$$\boldsymbol{\omega} = (\sin\kappa, 0, \cos\kappa), \qquad \boldsymbol{\Omega} = (\sin\theta\cos\phi, \sin\theta\sin\phi, \cos\theta). \tag{2.30}$$

The dependence of $F_{\gamma\gamma}(\xi, \xi_1)$ on the azimuthal angle comes in through the scalar product

$$\boldsymbol{\omega}\cdot\boldsymbol{\Omega} = \cos\kappa\cos\theta + \sin\kappa\sin\theta\cos\phi, \tag{2.31}$$

which enters ξ and ξ_1 linearly through

$$\xi = x(\gamma - p\,\boldsymbol{\omega}\cdot\boldsymbol{\Omega}) \quad \text{and} \quad \xi_1 = q - \xi. \tag{2.32}$$

Therefore we can write ξ and ξ_1 in the form

$$\xi = \frac{q}{Q}\left(d_+ - b\cos\phi\right), \qquad \xi_1 = \frac{q}{Q}\left(d_- + b\cos\phi\right), \tag{2.33}$$

where, using equations (2.28), (2.29) and (2.31), we have

$$\begin{aligned} d_+ &= \gamma(x_1 - x) + x(x + x_1\mu), \\ d_- &= \gamma(x - x_1) + x_1(x_1 + x\mu) = Q^2 - d_+ \end{aligned} \tag{2.34}$$

and

$$b = \sqrt{r}\sqrt{p^2Q^2 - \left[\gamma(x + x_1) - q\right]^2}, \quad r = \sqrt{\frac{1+\mu}{1-\mu}}. \tag{2.35}$$

Writing the rate $F_{\gamma\gamma}$ in the form

$$F_{\gamma\gamma} = \frac{q^2 + 2q - 2}{q}\left(\frac{1}{\xi} + \frac{1}{\xi_1}\right) - \frac{1}{\xi^2} - \frac{1}{\xi_1^2} - 2, \tag{2.36}$$

we can see from equations (2.27), (2.33) and (2.36) that we need to calculate integrals of the following types:

$$\int_0^{2\pi}\frac{d\phi}{d_\pm \mp b\cos\theta} = \frac{2\pi}{\sqrt{d_\pm^2 - b^2}}, \quad \int_0^{2\pi}\frac{d\phi}{(d_\pm \mp b\cos\theta)^2} = \frac{2\pi d_\pm}{(d_\pm^2 - b^2)^{3/2}}. \tag{2.37}$$

The pair production rate $\overline{F}_{\gamma\gamma}$ thus becomes (Nagirner & Loskutov 1999)

$$\overline{F}_{\gamma\gamma}(\gamma_-, x, x_1, \mu) = \frac{q^2+2q-2}{q^2}\left(\frac{1}{a_+}+\frac{1}{a_-}\right) - \frac{1}{q^2}\left(\frac{d_+}{a_+^3}+\frac{d_-}{a_-^3}\right) - \frac{2}{Q}, \tag{2.38}$$

where we have defined

$$\begin{aligned} a_+^2 &= \frac{d_+^2 - b^2}{Q^2} = r + (\gamma - x)^2, \\ a_-^2 &= \frac{d_-^2 - b^2}{Q^2} = r + (\gamma - x_1)^2. \end{aligned} \tag{2.39}$$

2.3.2 Integration over photon directions

To calculate the angular integral in equation (2.19), it is convenient to first change the integration variable from μ to q, making use of the relation $q = xx_1(1-\mu)$. This gives

$$R_{\gamma\gamma}(\gamma_-, x, x_1) = \frac{1}{8}\int_{q^{(L)}}^{q^{(U)}} \overline{F}_{\gamma\gamma}(\gamma_-, x, x_1, \mu)\, dq. \tag{2.40}$$

Now all quantities appearing in $\overline{F}_{\gamma\gamma}$ have to be expressed in terms of q rather than μ. Looking at equation (2.38), we see that we need

$$d_\pm = s_\pm - q, \qquad a_\pm^2 = \frac{2xx_1}{q}(1 + w_\pm q), \tag{2.41}$$

where

$$s_+ = x(x+x_1) + \gamma(x_1 - x), \qquad s_- = x_1(x+x_1) + \gamma(x - x_1) \tag{2.42}$$

and

$$w_+ = \frac{(\gamma - x)^2 - 1}{2xx_1}, \qquad w_- = \frac{(\gamma - x_1)^2 - 1}{2xx_1}. \tag{2.43}$$

The integrand in equation (2.40) now takes the form

$$\begin{aligned} \overline{F}_{\gamma\gamma}(\gamma_-, x, x_1, \mu) = {} & \frac{1}{\sqrt{2xx_1}}\frac{q^2+2q-2}{q^{3/2}}\left(\frac{1}{\sqrt{1+w_+q}}+\frac{1}{\sqrt{1+w_-q}}\right) \\ & - \frac{1}{(2xx_1)^{3/2}\sqrt{q}}\left[\frac{s_+ - q}{(1+w_+q)^{3/2}} + \frac{s_- - q}{(1+w_-q)^{3/2}}\right] - \frac{2}{Q}, \end{aligned} \tag{2.44}$$

where $Q^2 = (x + x_1)^2 - 2q$. The required integrals are

$$\begin{aligned}
&\int \frac{\sqrt{q}\,dq}{\sqrt{1+wq}} = \frac{q^{3/2}}{h}\,[A(h) - A_0(h)]\,,\\
&\int \frac{dq}{\sqrt{q}\,\sqrt{1+wq}} = 2\,\sqrt{q}\,A_0(h),\\
&\int \frac{dq}{q^{3/2}\,\sqrt{1+wq}} = -\frac{2}{\sqrt{q}}\,A(h),\\
&\int \frac{\sqrt{q}\,dq}{(1+wq)^{3/2}} = \frac{2q^{3/2}}{h}\left[A_0(h) - \frac{1}{A(h)}\right],\\
&\int \frac{dq}{\sqrt{q}(1+wq)^{3/2}} = \frac{2\,\sqrt{q}}{A(h)},\\
&\int \frac{dq}{Q} = -Q,
\end{aligned} \tag{2.45}$$

where $h = wq$ and

$$A_0(h) = \begin{cases} \ln(\sqrt{h} + \sqrt{1+h})/\sqrt{h} & \text{if } h \geq 0,\\ \arcsin(\sqrt{-h})/\sqrt{-h} & \text{if } h \leq 0, \end{cases} \tag{2.46}$$

$$A(h) = \sqrt{1+h}. \tag{2.47}$$

After a little rearrangement, the angle-averaged pair production rate (2.40) finally becomes

$$R_{\gamma\gamma}(\gamma, x, x_1) = \frac{1}{4}\left[\,\sqrt{(x+x_1)^2 - 2q} + T_+(\gamma, x, x_1, q) + T_-(\gamma, x, x_1, q)\right]\Big|_{q^{(L)}}^{q^{(U)}}, \tag{2.48}$$

where the primitive functions are (Nagirner & Loskutov 1999)

$$\begin{aligned}
T_\pm(\gamma, x, x_1, q) = {}& \frac{q^{3/2}}{(2xx_1)^{3/2}}\,(xx_1 - 1)\,\frac{A(h_\pm) - A_0(h_\pm)}{h_\pm} + \sqrt{\frac{2}{q}}\,\frac{A(h_\pm)}{\sqrt{xx_1}}\\
&- \frac{\sqrt{q}}{(2xx_1)^{3/2}}\left[\frac{s_\pm - q}{A(h_\pm)} - 4xx_1A_0(h_\pm)\right],
\end{aligned} \tag{2.49}$$

while $s_\pm$ and $h_\pm = qw_\pm$ are determined by equations (2.42) and (2.43), respectively. The integration limits $q^{(L)}$ and $q^{(U)}$ in equations (2.40) and (2.48) are given in Section 2.6 below. Expressions similar to (2.48) and (2.49) have been derived by Svensson (1982) and Boettcher & Schlickeiser (1997). However, their formulae suffer from cancellations when h approaches zero, while in equation (2.49) cancellation appears only in the term $[A_0(h) - A(h)]/h$, which can easily be computed via Taylor series for small h.

2.4 Total pair production cross-section

Let's write the pair production cross-section given by equation (2.10) in the following form

$$\overline{s}_{\rm pp}(\boldsymbol{x}) = \frac{2}{\lambda_{\rm C}^3 N_{\rm ph}} \frac{1}{x} \int \frac{d^3x_1}{x_1}\, \tilde{n}_{\rm ph}(\boldsymbol{x}_1)\, s_0(q)\, q, \tag{2.50}$$

where

$$s_0(q) = \frac{3}{16\pi} \frac{1}{q} \int \frac{d^3p_-}{\gamma_-} \frac{d^3p_+}{\gamma_+}\, F_{\gamma\gamma}\, \delta(\underline{p}_- + \underline{p}_+ - \underline{x}_1 - \underline{x}). \tag{2.51}$$

To calculate $s_0(q)$, we first take the integral over d^3p_+ by making use of the three-dimensional delta-function, leaving us with

$$s_0(q) = \frac{3}{16\pi} \frac{1}{q} \int \frac{d^3p_-}{\gamma_-}\, F_{\gamma\gamma}\, \delta(\xi + \xi_1 - q), \tag{2.52}$$

where we have used the identity (2.21). The subsequent integral over d^3p_- is most easily taken in the centre-of-momentum (CM) frame of the interaction. In this frame we have

$$\boldsymbol{x}_{\rm cm} + \boldsymbol{x}_{1,\rm cm} = 0, \qquad q = xx_1(1-\mu) = 2x_{\rm cm}^2. \tag{2.53}$$

The delta-function in equation (2.52) thus becomes (dropping '$-$' from p)

$$\delta(\xi + \xi_1 - q) = \delta(\underline{p} \cdot (\underline{x} + \underline{x}_1) - \underline{x} \cdot \underline{x}_1) = \frac{\delta(\gamma_{\rm cm} - x_{\rm cm})}{2x_{\rm cm}}, \tag{2.54}$$

giving

$$s_0(x_{\rm cm}) = \frac{3}{64\pi} \frac{p_{\rm cm}}{x_{\rm cm}^3} \int F_{\gamma\gamma}\, d^2\Omega_{\rm cm} \tag{2.55}$$

after taking the integral over $\gamma_{\rm cm}$. Here we have defined $p_{\rm cm} = \sqrt{x_{\rm cm}^2 - 1}$ and have made use of the Lorentz invariance of d^3p/γ. Hereafter we write s_0 as a function of $x_{\rm cm}$ instead of q, the two designations are equivalent owing to the relation $q = 2x_{\rm cm}^2$.

In the CM-frame the invariant four-products ξ and ξ_1 entering $F_{\gamma\gamma}$ become

$$\begin{aligned} \xi &= x_{\rm cm}(\gamma_{\rm cm} - p_{\rm cm}\, \zeta_{\rm cm}), \\ \xi_1 &= x_{\rm cm}(\gamma_{\rm cm} - p_{\rm cm}\, \zeta_{1,\rm cm}) = x_{\rm cm}(\gamma_{\rm cm} + p_{\rm cm}\, \zeta_{\rm cm}), \end{aligned} \tag{2.56}$$

where we have introduced cosines of the angles between the electron and photon momenta in the CM-frame as

$$\zeta_{\rm cm} = \boldsymbol{\Omega}_{\rm cm} \cdot \boldsymbol{\omega}_{\rm cm} \qquad \zeta_{1,\rm cm} = -\zeta_{\rm cm} = \boldsymbol{\Omega}_{\rm cm} \cdot \boldsymbol{\omega}_{1,\rm cm}. \tag{2.57}$$

Writing the differential solid angle in (2.55) as $d^2\mathbf{\Omega}_{\rm cm} = d\zeta_{\rm cm} d\phi_{\rm cm}$, we can see that the azimuthal integral can be taken trivially since the integrand has no dependence on $\phi_{\rm cm}$. Making use of relations (2.56), the remaining integral can be written as

$$s_0(x_{\rm cm}) = \frac{3}{32}\frac{1}{x_{\rm cm}^4}\int_{\xi^{(L)}}^{\xi^{(U)}} F_{\gamma\gamma}\, d\xi = \frac{3}{32}\frac{1}{x_{\rm cm}^4}\int_{\xi^{(L)}}^{\xi^{(U)}} F_{\gamma\gamma}\, d\xi_1 \tag{2.58}$$

where the integration limits are given by

$$\xi^{(L)} = x_{\rm cm}(x_{\rm cm} - p_{\rm cm}), \qquad \xi^{(U)} = x_{\rm cm}(x_{\rm cm} + p_{\rm cm}). \tag{2.59}$$

Inserting the invariant cross-section (2.36) into (2.58) and integrating, we get

$$s_0(x_{\rm cm}) = \frac{3}{8}\frac{p_{\rm cm}}{x_{\rm cm}^3}\left[\frac{1}{\beta_{cm}}\left(1 + \frac{1}{x_{\rm cm}^2} - \frac{1}{2x_{\rm cm}^4}\right)\ln\left(\frac{1+\beta_{cm}}{1-\beta_{cm}}\right) - \frac{1}{x_{\rm cm}^2} - 1\right], \tag{2.60}$$

where $\beta_{cm} \equiv p_{\rm cm}/\gamma_{\rm cm} = p_{\rm cm}/x_{\rm cm}$. The quantity s_0 has the physical meaning of the centre-of-momentum frame cross-section for pair production.

For isotropic target photon distribution we can write the cross-section (2.50) in the following form

$$\overline{s}_{\rm pp}(x) = 4\pi\frac{2}{\lambda_{\rm C}^3 N_{\rm ph}}\int x_1^2\, dx_1\, \sigma_{\rm pp}(x, x_1)\, \tilde{n}_{\rm ph}(x_1), \tag{2.61}$$

where

$$\sigma_{\rm pp}(x, x_1) = \frac{1}{2\pi}\frac{1}{xx_1}\int d\mu d\phi\; x_{\rm cm}^2\, s_0(x_{\rm cm}) \tag{2.62}$$

and we have used the relation $q = 2x_{\rm cm}^2$. Since $x_{\rm cm}$ does not depend on ϕ, the azimuthal integral is again trivial. To take the last integral it is natural to change the integration variable from μ to $x_{\rm cm}$, using the second relation in (2.53),

$$d\mu = -\frac{4x_{\rm cm}dx_{\rm cm}}{xx_1}, \tag{2.63}$$

so that

$$\sigma_{\rm pp}(x, x_1) = \frac{4}{(xx_1)^2}\int_1^{\sqrt{xx_1}} x_{\rm cm}^3\, dx_{\rm cm}\, s_0(x_{\rm cm}). \tag{2.64}$$

The lower integration limit in equation (2.64) reflects the requirement that in the CM-frame the energies of the pair producing photons need to be at least equal to the electron/positron rest energy, whereas the upper limit is simply the maximum attainable CM-frame energy of photons with energies x and x_1 in the lab frame (i.e. a head-on collision).

Inserting the CM-frame cross-section (2.60) into equation (2.64) and performing the integrals, we arrive at the final expression for the photon–photon pair production cross-section (Gould & Schréder 1967; Zdziarski 1988):

$$\sigma_{\rm pp}(x,x_1) = \frac{3}{8}\frac{1}{x^2x_1^2}\left\{\frac{2v^2+2v+1}{v+1}\ln w - \frac{2(2v+1)\sqrt{v}}{\sqrt{v+1}} - \ln^2 w + 2\ln^2(w+1) + 4{\rm Li}_2\left(\frac{1}{w+1}\right) - \frac{\pi^2}{3}\right\}, \tag{2.65}$$

where

$$v = xx_1 - 1 \quad \text{and} \quad w = \frac{\sqrt{v+1}+\sqrt{v}}{\sqrt{v+1}-\sqrt{v}} \tag{2.66}$$

and Li_2 is the dilogarithm defined by

$$\mathrm{Li}_2(r) = -\int_0^r \frac{\ln(1-s)}{s}ds. \tag{2.67}$$

2.5 Total pair annihilation cross-section

The derivation of the pair annihilation cross-section follows along the same lines as the derivation of the pair production cross-section. The cross-section (2.6) is written as

$$\overline{s}_{\rm pa}(\boldsymbol{p}_-) = \frac{2}{\lambda_{\rm C}^3 N_+}\frac{1}{\gamma_-}\int \frac{d^3p_+}{\gamma_+}\,\tilde{n}_+(\boldsymbol{p}_+)\,s_0(q_e)\,(q_e+1), \tag{2.68}$$

where

$$s_0(q_e) = \frac{3}{32\pi}\frac{1}{(q_e+1)}\int \frac{d^3x}{x}\frac{d^3x_1}{x_1}\,F_{\gamma\gamma}\,\delta(\underline{p}_- + \underline{p}_+ - \underline{x}_1 - \underline{x}) \tag{2.69}$$

and

$$q_e = \underline{p}_+\cdot\underline{p}_- = \gamma_+\gamma_-(1-\beta_+\beta_-\boldsymbol{\Omega}_+\cdot\boldsymbol{\Omega}_-) = \gamma_+\gamma_-(1-\beta_+\beta_-\mu_e) = \xi+\xi_1-1. \tag{2.70}$$

After using the delta-function to take the integral over d^3x_1 in equation (2.69), we get

$$s_0(q_e) = \frac{3}{32\pi}\frac{1}{(q_e+1)}\int \frac{d^3x}{x}\,F_{\gamma\gamma}\,\delta(\xi+\xi_1-q_e-1), \tag{2.71}$$

where we have used the identity

$$\delta(\gamma_+ + \gamma_- - x_1 - x) = x_1\,\delta(\xi+\xi_1-q_e-1). \tag{2.72}$$

Passing into the CM-frame and using

$$\boldsymbol{p}_{+,\rm cm} + \boldsymbol{p}_{-,\rm cm} = 0, \qquad q_e = \gamma_+\gamma_-(1-\beta_+\beta_-\mu_e) = \gamma_{\rm cm}^2 + p_{\rm cm}^2 = 2\gamma_{\rm cm}^2 - 1 \tag{2.73}$$

and

$$\delta(\xi + \xi_1 - q_e - 1) = \delta(\underline{x} \cdot (\underline{p}_+ + \underline{p}_-) - \underline{p}_+ \cdot \underline{p}_- - 1) = \frac{\delta(\gamma_{\rm cm} - x_{\rm cm})}{2\gamma_{\rm cm}}, \quad (2.74)$$

the cross-section (2.71) becomes

$$s_0(\gamma_{\rm cm}) = \frac{3}{128\pi}\frac{1}{\gamma_{\rm cm}^2}\int F_{\gamma\gamma}\, d^2\omega_{\rm cm}. \quad (2.75)$$

Here we have again written s_0 as a function of $\gamma_{\rm cm}$ instead of q_e, using the second relation in (2.73).

In the CM-frame the invariant four-products ξ and ξ_1 entering $F_{\gamma\gamma}$ are

$$\begin{aligned}\xi &= \underline{p}_- \cdot \underline{x} = x_{\rm cm}(\gamma_{\rm cm} - p_{\rm cm}\,\zeta_{-,{\rm cm}}),\\ \xi_1 &= \underline{p}_+ \cdot \underline{x} = x_{\rm cm}(\gamma_{\rm cm} - p_{\rm cm}\,\zeta_{+,{\rm cm}}) = x_{\rm cm}(\gamma_{\rm cm} + p_{\rm cm}\,\zeta_{-,{\rm cm}}),\end{aligned} \quad (2.76)$$

where

$$\zeta_{-,{\rm cm}} = \boldsymbol{\Omega}_{-,{\rm cm}} \cdot \boldsymbol{\omega}_{\rm cm} \qquad \zeta_{+,{\rm cm}} = -\zeta_{\rm cm} = \boldsymbol{\Omega}_{+,{\rm cm}} \cdot \boldsymbol{\omega}_{\rm cm}. \quad (2.77)$$

The differential solid angle in (2.75) can be written as $d^2\boldsymbol{\omega}_{\rm cm} = d\zeta_{-,{\rm cm}} d\phi_{\rm cm}$, allowing the azimuthal integral to be taken trivially. Using the relations (2.76), we can write the remaining integral as

$$s_0(\gamma_{\rm cm}) = \frac{3}{64}\frac{1}{\gamma_{\rm cm}^3 p_{\rm cm}}\int_{\xi^{(L)}}^{\xi^{(U)}} F_{\gamma\gamma}\, d\xi = \frac{3}{64}\frac{1}{\gamma_{\rm cm}^3 p_{\rm cm}}\int_{\xi^{(L)}}^{\xi^{(U)}} F_{\gamma\gamma}\, d\xi_1, \quad (2.78)$$

where the integration limits are given by (2.59), with $x_{\rm cm} = \gamma_{\rm cm}$. Upon integration we get

$$s_0(\gamma_{\rm cm}) = \frac{3}{16}\frac{1}{\gamma_{\rm cm}^2}\left[\frac{1}{\beta_{cm}}\left(1 + \frac{1}{\gamma_{\rm cm}^2} - \frac{1}{2\gamma_{\rm cm}^4}\right)\ln\left(\frac{1+\beta_{cm}}{1-\beta_{cm}}\right) - \frac{1}{\gamma_{\rm cm}^2} - 1\right], \quad (2.79)$$

which can be regarded as the centre-of-momentum frame cross-section for pair annihilation.

For isotropic target electron/positron distribution the cross-section (2.68) can be written as

$$\overline{s}_{\rm pa}(p_-) = 4\pi\frac{2}{\lambda_{\rm C}^3 N_+}\int_0^\infty p_+^2 dp_+\, \sigma_{\rm pa}(\gamma_+, \gamma_-)\, \tilde{n}_+(p_+), \quad (2.80)$$

where

$$\sigma_{\rm pa}(\gamma_+, \gamma_-) = \frac{1}{2\pi}\frac{1}{\gamma_+\gamma_-}\int d\mu_e d\phi\; \gamma_{\rm cm}^2\, s_0(\gamma_{\rm cm}). \quad (2.81)$$

The CM-frame energy $\gamma_{\rm cm}$ depends only on the relative angle μ_e between the annihilating particles, making the azimuthal integral in (2.81) trivial. For the remaining integral we use the second relation in (2.73) to change the integration variable from μ to $\gamma_{\rm cm}$ through

$$d\mu = -\frac{4\gamma_{\rm cm} d\gamma_{\rm cm}}{p_+ p_-}. \tag{2.82}$$

This gives

$$\sigma_{\rm pa}(\gamma_+, \gamma_-) = \frac{4}{\gamma_+\gamma_- p_+ p_-} \int_{\gamma_{\rm cm}^-}^{\gamma_{\rm cm}^+} \gamma_{\rm cm}^3 \, d\gamma_{\rm cm} \, s_0(\gamma_{\rm cm}). \tag{2.83}$$

The integration limits in equation (2.83) can be read from (2.73) by setting $\mu_e = -1$ and 1, giving

$$\gamma_{\rm cm}^{\pm} = \sqrt{(\gamma_+\gamma_- + 1 \pm p_+ p_-)/2}. \tag{2.84}$$

All the integrals in (2.83) are elementary, the final result for the total pair annihilation cross-section is found to be (e.g. Svensson 1982)

$$\sigma_{\rm pa}(\gamma_+, \gamma_-) = \frac{3}{8} \frac{1}{\gamma_+\gamma_- p_+ p_-} \left[\beta_{cm}^3 \gamma_{\rm cm}^2 L(\beta_{cm}) - 2\gamma_{\rm cm}^2 + \frac{3}{4} L^2(\beta_{cm}) \right]_{\gamma_{\rm cm}^-}^{\gamma_{\rm cm}^+}, \tag{2.85}$$

where we have defined $L(\beta) = \ln[(1+\beta)/(1-\beta)]$.

2.6 Boundaries

The limits of integration in equations (2.19) and (2.40) arise from the requirement that $|\cos\theta| \le 1$ in equation (2.28), which constrains the allowed region in the parameter space of x, x_1, γ_- and μ. Expressing μ from the inequality

$$-1 \le \frac{\gamma_-(x + x_1) - q}{pQ} \le 1, \tag{2.86}$$

we get the condition $\mu_{\rm m} \le \mu \le \mu_+$, where

$$\mu_{\rm m} = \begin{cases} \mu_- & \text{if } 1 < \gamma_- < \gamma^{(-)}(x, x_1, -1), \\ \mu_- & \text{if } \gamma^{(+)}(x, x_1, -1) < \gamma_- < \gamma_{\rm m}, \\ -1 & \text{if } \gamma^{(-)}(x, x_1, -1) \le \gamma_- \le \gamma^{(+)}(x, x_1, -1) \end{cases} \tag{2.87}$$

and

$$\mu_\pm = 1 - \frac{q_\mp}{x x_1}. \tag{2.88}$$

Here we have defined

$$q_\pm = \gamma_+\gamma_- + 1 \pm p_+ p_-, \tag{2.89}$$

where $\gamma_+ = x + x_1 - \gamma_-$ and $p_\pm = \sqrt{\gamma_\pm^2 - 1}$, as well as

$$\gamma^{(\pm)}(x, x_1, -1) = \frac{1}{2}\left(x + x_1 \pm |x - x_1|\sqrt{1 - \frac{1}{x x_1}}\right), \quad \gamma_\mathrm{m} = x + x_1 - 1. \tag{2.90}$$

The corresponding limits for q in equation (2.40) read

$$q^{(U)} = \begin{cases} q_+ & \text{if } 1 < \gamma_- < \gamma^{(-)}(x, x_1, -1), \\ q_+ & \text{if } \gamma^{(+)}(x, x_1, -1) < \gamma_- < \gamma_\mathrm{m}, \\ 2xx_1 & \text{if } \gamma^{(-)}(x, x_1, -1) \le \gamma_- \le \gamma^{(+)}(x, x_1, -1) \end{cases} \tag{2.91}$$

and $q^{(L)} = q_-$.

Demanding that $\mu_\mathrm{m} \le \mu_+$, i.e. that the integral in equation (2.19) exist, will give us a constraint on the allowed region in energy space of the particles/photons. In fact, since $\mu_\mathrm{m} = \max\{-1, \mu_-\}$ and we always have $\mu_- \le \mu_+$, we only need to require that $\mu_+ \ge -1$. Given the energies of the annihilating photons, this determines the allowed range of electron/positron energies that can be produced. We find

$$\begin{array}{ll} \gamma^{(-)}(x, x_1, -1) \le \gamma_- \le \gamma^{(+)}(x, x_1, -1) & \text{if } x + x_1 > 2xx_1, \\ 1 \le \gamma_- \le \gamma_\mathrm{m} & \text{if } x + x_1 \le 2xx_1. \end{array} \tag{2.92}$$

The integration limits in equations (2.12) and (2.14) are obtained by expressing the necessary variables from conditions (2.92) in terms of the rest. For equation (2.12) we need constraints on the x, x_1 plane in terms of γ_-. After a lengthy but straightforward derivation we find the lower limits of the allowed region to be

$$x^{(L)} = \frac{1}{2}\gamma_-(1 - \beta_-), \qquad x_1^{(L)} = \begin{cases} x/\{[2x - \gamma_-(1 + \beta_-)]\gamma_-(1 + \beta_-)\} & \text{if } x > x_+, \\ x/\{[2x - \gamma_-(1 - \beta_-)]\gamma_-(1 - \beta_-)\} & \text{if } x < x_-, \\ \gamma_- + 1 - x & \text{if } x_- \le x \le x_+, \end{cases} \tag{2.93}$$

where we have defined

$$x_\pm = \frac{1}{2}\left[1 + \gamma_-(1 \pm \beta_-)\right]. \tag{2.94}$$

Because we always have $x_1^{(L)} \ge x^{(L)}$, the latter sets a lower limit for the energy of either photon for producing an electron (or positron) of energy γ_-.

For equation (2.14) we need constraints on the γ_+, γ_- plane in terms of x, which yield the lower limits

$$\gamma_-^{(L)} = \begin{cases} \gamma^{(-)} & \text{if } x \le 1/2, \\ \gamma^{(-)} & \text{if } 1/2 < x < 1 \text{ and } \gamma_+ < \gamma_\mathrm{B}, \\ \gamma^{(+)} & \text{if } x \ge 1 \text{ and } \gamma_+ < \gamma_\mathrm{B}, \\ 1 & \text{in all other cases,} \end{cases} \qquad \gamma_+^{(L)} = \begin{cases} \gamma_\mathrm{A} & \text{if } x < 1/2, \\ 1 & \text{if } x \ge 1/2, \end{cases} \tag{2.95}$$

where

$$\gamma^{(\pm)} = \frac{1}{2}\left(F_\pm + \frac{1}{F_\pm}\right), \quad F_\pm = 2x - \gamma_+(1 \pm \beta_+), \tag{2.96}$$

and

$$\gamma_{\rm A} = \frac{4x^2+1}{4x}, \quad \gamma_{\rm B} = \frac{2x^2-2x+1}{2x-1}. \tag{2.97}$$

Chapter 3

Synchrotron radiation

3.1 Introduction

Along with Compton scattering, sychrotron radiation can be regarded as one of the most important radiative processes in high-energy astrophysics. One of the reasons for this is that the emission from virtually all sources capable of producing high-energy radiation originates from highly conductive plasma, in which it is natural to expect a certain amount of magnetization. Also, the environments in the vicinity of compact objects tend to be strongly magnetized, the field can be generated in the accretion flow by dynamo action or can be anchored to the central object (neutron stars). In sources like blazars and gamma-ray bursts where outflows are produced, the plasma can carry the generated field to large distances from the central object into regions where the flow energy gets dissipated (e.g. through shocks), with profound effects on the produced emission.

The theory of synchrotron emission is well established (for reviews, see e.g. Ginzburg & Syrovatskii 1965, 1969; Pacholczyk 1970). The basic formula for the radiation spectrum from an electron moving with arbitrary Lorentz factor in a (macroscopic) circular orbit was given already by Schott (1907), albeit in a different context. Thereafter nearly forgotten for 40 years, its importance became apparent only in the late forties when emission from energetic charged particles in a magnetic field was discovered. In a weak magnetic field where classical theory is applicable, Schott's formula is exact. However, its direct application to relativistic particles is not feasible, since it involves summation over a large number of closely packed harmonics. In the ultrarelativistic limit the synchrotron emissivity of electrons moving with a given pitch angle is well known (Westfold 1959; Le Roux 1961; see also Scheuer 1968; Ginzburg et al. 1968), the expression for randomly oriented magnetic fields was derived by Crusius & Schlickeiser (1986) (see also Ghisellini & Svensson 1991). The trans-relativistic regime is least straightforward. One possible approach is to calculate the first couple of (tens of) harmonics separately and substitute the summation over harmonics by integration for the rest.

In this chapter we will derive the kinetic equations that describe the evolution of particle and photon distributions due to synchrotron emission and absorption. The electron equation will then be written in the form of the Fokker-Planck equation to facilitate practical application. Finally, we will give the formulae for single electron emissivities in different limits, in terms of which we can express all the coefficients entering the kinetic equations.

3.2 Kinetic equations

Writing down the kinetic equations for particles and photons interacting through synchrotron processes is somewhat less straightforward than in the case of processes involving binary particle collisions like e.g. Compton scattering and pair-production. The reason for this is that the interaction takes place in and through a field that in is 'external' and prescribed. This means that the conservation laws of the total four-momentum no longer hold as they do for binary collisions. More specifically, the conservation of three-momentum breaks down, while the total energy is still conserved. Furthermore, since we are considering a tangled magnetic field with no electric field, we are bound to a particular frame of reference. Therefore the kinetic equations cannot be written in a manifestly covariant form valid in any frame as they were for Compton scattering and pair-production.

To deduce the form of the kinetic equations for synchrotron processes, it is simplest to consider generic discrete energy levels of electrons in a magnetic field and study the transitions between these levels due to synchrotron emission and absorption (see e.g Twiss 1958; McCray 1969; Ghisellini & Svensson 1991). We will look at these transitions from the point of view of electrons and photons in turn.

3.2.1 Electron equation

Let's consider an isotropic distribution of electrons and photons in a volume ΔV in a tangled magnetic field. In such case we can label the electron quantum states by their energy $E_i \equiv m_e c^2 \gamma_i$ (which we regard as doubly degenerate due to spin, neglecting spin-field interaction). The occupation numbers for electrons and photons are defined as $\tilde{n}_i$ and $\tilde{n}_{\rm ph}$, respectively. The transition probabilities/rates between states i and j are described by Einstein coefficient A_{ij}. Note that since we are going to write all the rates in terms of occupation numbers, the Einstein coefficients describing spontaneous and stimulated emission as well as absorption all coincide.

Let's consider an electron state i and write down the rates for all transitions from and to this level. The rate of spontaneous downward transitions from level i, resulting in the emission of a photon with energy in the interval $(x, x + dx)$, can

be written as

$$\left.\frac{dN_i^-}{dt\,dx}\right|_{\rm sp.em.} = \sum_{E_j<E_i} \tilde{n}_i\, A_{ij}\, \delta(\gamma_i - \gamma_j - x), \tag{3.1}$$

where $x = h\nu/m_e c^2$, N_i^- denotes the number of transitions and the delta-function plays the role of the line 'profile' ϕ_{ij} and enforces energy conservation. The sum is to be taken over all states j that have $E_j < E_i$. The total transition rate is obtained simply by integrating over x, giving

$$\left.\frac{dN_i^-}{dt}\right|_{\rm sp.em.} = \sum_{E_j<E_i} \tilde{n}_i\, A_{ij}. \tag{3.2}$$

Similarly, the transition rate from level i due to stimulated emission is

$$\left.\frac{dN_i^-}{dt\,dx}\right|_{\rm st.em.} = \sum_{E_j<E_i} \tilde{n}_{\rm ph}(x)\; \tilde{n}_i\, A_{ij}\, \delta(\gamma_i - \gamma_j - x), \tag{3.3}$$

whereas the rate of transitions to upper levels resulting from absorption of a photon from energy range $(x, x + dx)$ is

$$\left.\frac{dN_i^-}{dt\,dx}\right|_{\rm abs.} = \sum_{E_j>E_i} \tilde{n}_{\rm ph}(x)\; \tilde{n}_i\, A_{ij}\, \delta(\gamma_j - \gamma_i - x). \tag{3.4}$$

The total rates are again obtained by integrating equations (3.3) and (3.4) over x.

Analogously, let us write the rates for all the transitions *to* level i. Due to spontaneous and stimulated emission from upper energy levels we have

$$\left.\frac{dN_i^+}{dt\,dx}\right|_{\rm em.} = \sum_{E_j>E_i} [1 + \tilde{n}_{\rm ph}(x)]\; \tilde{n}_j\, A_{ij}\, \delta(\gamma_j - \gamma_i - x), \tag{3.5}$$

while the upward transitions from lower levels due to absorption give

$$\left.\frac{dN_i^+}{dt\,dx}\right|_{\rm abs.} = \sum_{E_j<E_i} \tilde{n}_{\rm ph}(x)\; \tilde{n}_j\, A_{ij}\, \delta(\gamma_i - \gamma_j - x). \tag{3.6}$$

Our aim is to write all the above rates in terms of a single emissivity $P_{\rm n}(x, \gamma_i)$, which we define as the number of photons emitted in unit volume and unit time into interval $(x, x + dx)$ due to spontaneous emission, normalized to one electron:

$$P_{\rm n}(x, \gamma_i) \equiv \left.\frac{dN_{\rm ph}}{dt\,dx}\right|_{\rm sp.em.} = \sum_{E_j<E_i} A_{ij}\, \delta(\gamma_i - \gamma_j - x). \tag{3.7}$$

Passing into the continuous limit of electron states using

$$\sum_j \to \frac{2}{\lambda_{\rm C}^3}\, \Delta V \int d^3 p_j, \tag{3.8}$$

where $p_j = \sqrt{\gamma_j^2 - 1}$, we get

$$P_{\rm n}(x,\gamma_i) = \frac{2}{\lambda_{\rm C}^3}\,\Delta V \int d^3p_j\, A_{ij}\,\delta(\gamma_i - \gamma_j - x) = \frac{2}{\lambda_{\rm C}^3}\,4\pi\,\gamma_j p_j\, A_{ij}\,\Delta V, \qquad \gamma_j = \gamma_i - x. \tag{3.9}$$

We will also need an expression for sums over 'upper' energy levels, i.e.

$$\begin{aligned}\sum_{E_j>E_i} A_{ij}\,\delta(\gamma_j - \gamma_i - x) &\to \frac{2}{\lambda_{\rm C}^3}\,\Delta V \int d^3p_j\, A_{ij}\,\delta(\gamma_j - \gamma_i - x)\\ &= \frac{2}{\lambda_{\rm C}^3}\,4\pi\,\gamma_j p_j\, A_{ij}\,\Delta V, \quad \text{where} \quad \gamma_j = \gamma_i + x,\end{aligned} \tag{3.10}$$

which together with equation (3.9) gives

$$\sum_{E_j>E_i} A_{ij}\,\delta(\gamma_j - \gamma_i - x) = \frac{\gamma_i^+ p_i^+}{\gamma_i p_i} P_{\rm n}(x,\gamma_i^+), \quad \text{where} \quad \gamma_i^+ = \gamma_i + x. \tag{3.11}$$

Using equations (3.7) and (3.11), the transition rates (3.1), (3.3), (3.4), (3.5) and (3.6) from and to level i take the form

$$\left.\frac{dN_i^-}{dt\,dx}\right|_{\rm em.} = [1 + \tilde{n}_{\rm ph}(x)]\;\tilde{n}_{\rm e}(\gamma_i)\,P_{\rm n}(x,\gamma_i), \tag{3.12}$$

$$\left.\frac{dN_i^-}{dt\,dx}\right|_{\rm abs.} = \tilde{n}_{\rm ph}(x)\;\tilde{n}_{\rm e}(\gamma_i)\,\frac{\gamma_i^+ p_i^+}{\gamma_i p_i}\,P_{\rm n}(x,\gamma_i^+), \tag{3.13}$$

$$\left.\frac{dN_i^+}{dt\,dx}\right|_{\rm em.} = [1 + \tilde{n}_{\rm ph}(x)]\;\tilde{n}_{\rm e}(\gamma_i^+)\,\frac{\gamma_i^+ p_i^+}{\gamma_i p_i}\,P_{\rm n}(x,\gamma_i^+), \tag{3.14}$$

$$\left.\frac{dN_i^+}{dt\,dx}\right|_{\rm abs.} = \tilde{n}_{\rm ph}(x)\;\tilde{n}_{\rm e}(\gamma_i^-)\,P_{\rm n}(x,\gamma_i), \tag{3.15}$$

where $\gamma_i^- = \gamma_i - x$ and $\tilde{n}_{\rm e}(\gamma_i) \equiv \tilde{n}_i$. The total rate of change of the electron occupation number on level i is obtained by subtracting equations (3.12) and (3.13) from the sum of equations (3.14) and (3.15) and integrating over the photon energy

$$\begin{aligned}\frac{d\tilde{n}_{\rm e}(\gamma_i)}{dt} = &\int_0^\infty dx\,\frac{\gamma_i^+ p_i^+}{\gamma_i p_i}\,P_{\rm n}(x,\gamma_i^+)\,\left\{\tilde{n}_{\rm e}(\gamma_i^+)\,[1+\tilde{n}_{\rm ph}(x)] - \tilde{n}_{\rm e}(\gamma_i)\,\tilde{n}_{\rm ph}(x)\right\}\\ &- \int_0^\infty dx\,P_{\rm n}(x,\gamma_i)\,\left\{\tilde{n}_{\rm e}(\gamma_i)\,[1+\tilde{n}_{\rm ph}(x)] - \tilde{n}_{\rm e}(\gamma_i^-)\,\tilde{n}_{\rm ph}(x)\right\}.\end{aligned} \tag{3.16}$$

Going to the continuous limit and dropping the indices from electron quantities,

we can write this as

$$\frac{d}{dt}[\gamma p\,\tilde{n}_{\rm e}(\gamma)] = \int_0^\infty dx \int_\gamma^\infty d\gamma_1\,\gamma_1 p_1\,\frac{P(x,\gamma_1)}{x}\,\delta(\gamma_1-\gamma-x) \times\left\{\tilde{n}_{\rm e}(\gamma_1)\,[1+\tilde{n}_{\rm ph}(x)] - \tilde{n}_{\rm e}(\gamma)\,\tilde{n}_{\rm ph}(x)\right\} - \int_0^\infty dx \int_1^\gamma d\gamma_1\,\gamma p\,\frac{P(x,\gamma)}{x}\,\delta(\gamma-\gamma_1-x) \left\{\tilde{n}_{\rm e}(\gamma)\,[1+\tilde{n}_{\rm ph}(x)] - \tilde{n}_{\rm e}(\gamma_1)\,\tilde{n}_{\rm ph}(x)\right\}, \tag{3.17}$$

where we have formally reintroduced the energy-conservation delta-function together with integration over γ_1. We have also introduced the (energy) emissivity $P(x,\gamma) \equiv x\,P_{\rm n}(x,\gamma)$, explicit expressions for which will be given below for both cyclotron and sychrotron regimes. Equation (3.17) represents the final form of the kinetic equation for non-degenerate electrons in a magnetic field, accounting for spontaneous and stimulated cyclo-synchrotron emission as well as absorption.

3.2.2 Photon equation

The number of photons emitted into an energy interval $(x, x+dx)$ in unit time due to spontaneous as well as stimulated emission is

$$\frac{dN^+_{\rm ph}}{dt\,dx} = \sum_{E_i}\sum_{E_j<E_i}[1+\tilde{n}_{\rm ph}(x)]\,\tilde{n}_i\,A_{ij}\,\delta(\gamma_i-\gamma_j-x), \tag{3.18}$$

the rate of photon absorption from the same interval is

$$\frac{dN^-_{\rm ph}}{dt\,dx} = \sum_{E_i}\sum_{E_j<E_i}\tilde{n}_{\rm ph}(x)\,\tilde{n}_j\,A_{ij}\,\delta(\gamma_i-\gamma_j-x). \tag{3.19}$$

Recalling the definition of $P_{\rm n}(x,\gamma_i)$, equation (3.7), we can write the rates (3.18) and (3.19) as

$$\frac{dN^+_{\rm ph}}{dt\,dx} = \sum_{E_i}[1+\tilde{n}_{\rm ph}(x)]\,\tilde{n}_{\rm e}(\gamma_i)\,P_{\rm n}(x,\gamma_i), \tag{3.20}$$

and

$$\frac{dN^-_{\rm ph}}{dt\,dx} = \sum_{E_i}\tilde{n}_{\rm ph}(x)\,\tilde{n}_{\rm e}(\gamma_i^-)\,P_{\rm n}(x,\gamma_i). \tag{3.21}$$

Thus the total change of the number of photons in interval $(x, x+dx)$ is

$$\frac{dN_{\rm ph}}{dt\,dx} = \frac{2}{\lambda_{\rm C}^3}\,4\pi\Delta V\int_1^\infty d\gamma\,\gamma p\,P_{\rm n}(x,\gamma)\left\{\tilde{n}_{\rm e}(\gamma)\,[1+\tilde{n}_{\rm ph}(x)] - \tilde{n}_{\rm e}(\gamma^-)\,\tilde{n}_{\rm ph}(x)\right\}, \tag{3.22}$$

where we have used the relation (3.8) to pass to the continuous limit and defined $\gamma^- = \gamma - x$. The differential number of photons can be written in terms of the occupation number as

$$dN_{\rm ph} = \frac{2}{\lambda_{\rm C}^3}\, 4\pi\, x^2 dx\, \Delta V\, \tilde{n}_{\rm ph}(x). \tag{3.23}$$

Using this on the left hand side of equation (3.22) and reintroducing $\delta(\gamma - \gamma_1 - x)\, d\gamma_1$, we obtain the final form of the photon kinetic equation:

$$\begin{aligned}\frac{d}{dt}[x^2\, \tilde{n}_{\rm ph}(x)] = \int_1^\infty d\gamma \int_1^\gamma d\gamma_1\, \gamma p\, \frac{P(x,\gamma_1)}{x}\, \delta(\gamma - \gamma_1 - x) \\ \times \left\{ \tilde{n}_{\rm e}(\gamma)\, [1 + \tilde{n}_{\rm ph}(x)] - \tilde{n}_{\rm e}(\gamma_1)\, \tilde{n}_{\rm ph}(x) \right\}. \end{aligned} \tag{3.24}$$

3.3 Fokker-Planck equation for electrons

In its present form the electron kinetic equation (3.17) is not very useful for astrophysical calculations. The reason for this is that the magnetic field strengths are typically much below the critical field strength $B_{\rm cr} = m_{\rm e}^2 c^3/(e\hbar) = 4.41 \times 10^{13}$ G (although there are exceptions like e.g. magnetars). Therefore the typical energy of a synchrotron photon is much lower than the energy of the electron that emits or absorbs it. Thus at each event the electron gains or loses a tiny fraction of its initial energy, making it natural to regard the exchange as a continuous process rather than discrete. In such case the evolution of the energy distribution is described by a Fokker-Planck differential equation. To deduce its form in this particular case let's look at equation (3.16) and rearrange it in the form

$$\begin{aligned}\frac{d}{dt}[\gamma_i p_i\, \tilde{n}(\gamma_i)] = &\int_0^\infty dx\, \gamma_i^+ p_i^+\, P_{\rm n}(x,\gamma_i^+)\, \tilde{n}_{\rm ph}(x)\, [\tilde{n}_{\rm e}(\gamma_i^+) - \tilde{n}_{\rm e}(\gamma_i)] \\ &- \int_0^\infty dx\, \gamma_i p_i\, P_{\rm n}(x,\gamma_i)\, \tilde{n}_{\rm ph}(x)\, [\tilde{n}_{\rm e}(\gamma_i) - \tilde{n}_{\rm e}(\gamma_i^-)] \\ &+ \int_0^\infty dx\, \left[\gamma_i^+ p_i^+\, P_{\rm n}(x,\gamma_i^+)\, \tilde{n}_{\rm e}(\gamma_i^+) - \gamma_i p_i\, P_{\rm n}(x,\gamma_i)\, \tilde{n}_{\rm e}(\gamma_i)\right]. \end{aligned} \tag{3.25}$$

The next step is to expand quantities like $\tilde{n}_{\rm e}(\gamma_i^+)$, $\tilde{n}_{\rm e}(\gamma_i^-)$, $\gamma_i^+ p_i^+\, P_{\rm n}(x,\gamma_i^+)$ and $\gamma_i^+ p_i^+\, P_{\rm n}(x,\gamma_i^+)\, \tilde{n}(\gamma_i^+)$ to the second order in 'parameter' $x = \gamma_i^+ - \gamma_i = \gamma_i - \gamma_i^-$. Inserting the expansions into equation (3.25) and collecting terms, we get

$$\begin{aligned}\frac{d}{dt}[\gamma p\, \tilde{n}_{\rm e}(\gamma)] = &\int_0^\infty dx\, x\, \frac{\partial}{\partial\gamma}\, [\gamma p\, P_{\rm n}(x,\gamma)\, \tilde{n}_{\rm e}(\gamma)] \\ &+ \int_0^\infty dx\, x^2\, \tilde{n}_{\rm ph}(x)\, \frac{\partial}{\partial\gamma}\left[\gamma p\, P_{\rm n}(x,\gamma)\, \frac{\partial \tilde{n}_{\rm e}(\gamma)}{\partial\gamma}\right] \\ &+ \frac{1}{2}\int_0^\infty dx\, x^2\, \frac{\partial^2}{\partial\gamma^2}\, [\gamma p\, P_{\rm n}(x,\gamma)\, \tilde{n}_{\rm e}(\gamma)], \end{aligned} \tag{3.26}$$

where we have kept only terms up to second order in x. Introducing the functions

$$H(\gamma) = \int_0^\infty P_{\rm n}(x,\gamma)\,\tilde{n}_{\rm ph}(x)\,x^2\,dx, \qquad H_0(\gamma) = \int_0^\infty P_{\rm n}(x,\gamma)\,x^2\,dx, \tag{3.27}$$

as well as the electron cooling rate

$$\dot{\gamma}_{\rm s} = -\frac{4}{3}\frac{\sigma_{\rm T} U_{\rm B}\gamma^2}{m_{\rm e}c} = -\int_0^\infty P(x,\gamma)\,dx = -\int_0^\infty P_{\rm n}(x,\gamma)\,x\,dx, \tag{3.28}$$

we arrive at the Fokker-Planck type diffusion equation for electrons (McCray 1969; Ghisellini et al. 1988):

$$\frac{d}{dt}[\gamma p\,\tilde{n}_{\rm e}(\gamma)] = -\frac{\partial}{\partial\gamma}\left[\dot{\gamma}_{\rm s}\,\gamma p\,\tilde{n}_{\rm e}(\gamma) - H(\gamma)\,\gamma p\,\frac{\partial\tilde{n}_{\rm e}(\gamma)}{\partial\gamma}\right] + \frac{1}{2}\frac{\partial^2}{\partial\gamma^2}\left[H_0(\gamma)\,\gamma p\,\tilde{n}_{\rm e}(\gamma)\right]. \tag{3.29}$$

The term containing $\dot{\gamma}_{\rm s}$ on the right-hand side of equation (3.29) is responsible for electron cooling due to synchrotron emission, the term containing H accounts for heating as well as diffusion in energy space due to self-absorption. The latter term also enables us to treat electron thermalization in strongly self-absorbed regimes.

Note that the last term in equation (3.29) is missing in similar equations derived previously (McCray 1969; Ghisellini et al. 1988). It corresponds to the diffusion due to spontaneous emission, but does not contribute to the electron cooling/heating. However, in most cases we expect its contribution to be negligible compared to the other terms. It is of the order x/γ smaller than the cooling term with $|\dot{\gamma}_{\rm s}|$ and, when electrons are mildly-relativistic, self-absorption becomes important, $\tilde{n}_{\rm ph} \gg 1$ and the term containing H dominates. Therefore the term with H_0 can be neglected in most applications.

In the context of thermalization it is worth mentioning that a Maxwellian electron distribution $\tilde{n}_{\rm e,M}$ together with a Rayleigh-Jeans radiation field is a steady-state solution of equation (3.29) (neglecting the last term). To see this we simply observe that $\tilde{n}_{\rm ph,RJ}(x) = \Theta/x$, where $\Theta = kT/m_e c^2$, as well as $\partial\tilde{n}_{\rm e,M}/\partial\gamma = -\tilde{n}_{\rm e,M}/\Theta$. Thus $H(\gamma) = -\Theta\dot{\gamma}_{\rm s}$ and the expression in the first square brackets in equation (3.29) vanishes.

3.4 Cyclo-synchrotron emissivities

As we have seen, in order to calculate all the necessary rates in the electron and photon equations, it is sufficient to determine a single quantity: the emissivity $P(x,\gamma)$. The cyclo-synchrotron emissivity (here in units $\mathrm{s}^{-1}\,\mathrm{str}^{-1}$) at photon energy x in the direction given by angle θ to the magnetic field for an electron moving at

a pitch-angle α with velocity $\beta = p/\gamma$ is (Pacholczyk 1970)

$$\eta(x,\theta,\alpha) = \frac{c}{\lambda_{\rm C}}\alpha_{\rm f}\, x^2 \sum_{l=1}^{\infty}\left[\left(\frac{\cos\theta - \beta\cos\alpha}{\sin\theta}\right)^2 J_l^2(z) + \beta^2\sin^2\alpha\; J_l'^2(z)\right] \times \delta\left(l\frac{b}{\gamma} - x[1-\beta\;\cos\alpha\;\cos\theta]\right), \quad (3.30)$$

where $\alpha_{\rm f} = e^2/c\hbar$ is the fine-structure constant, $b = B/B_{\rm cr}$ is magnetic field in units of the critical field, J_l and J_l' are the Bessel function and its derivative, and their argument $z = xp\sin\alpha\;\sin\theta\;/b$. Averaging over pitch-angle and integrating over θ, we get the angle-averaged cyclo-synchrotron spectrum

$$P(x,\gamma) = \frac{1}{2}\int_{-1}^{1} d\cos\alpha\; 2\pi \int_{-1}^{1} d\cos\theta\; \eta(x,\theta,\alpha). \quad (3.31)$$

Direct summation over harmonics works fine for mildly relativistic electrons $\gamma < 3$. In this case, we first use the δ-function to integrate over the energy bin, and then integrate numerically over the angles (see e.g. Marcowith & Malzac 2003) and sum over harmonics contributing to a given bin. The same procedure is used for any larger γ at photon energies x corresponding to the first 30 harmonics (i.e. $x < 30\; b/\gamma$). At higher x, we use two different methods. In the ultra-relativistic regime $\gamma > 10$ we use the angle-averaged relativistic synchrotron spectrum (Crusius & Schlickeiser 1986; Ghisellini et al. 1988):

$$P(x,\gamma) = \frac{3\sqrt{3}}{\pi}\frac{\sigma_{\rm T}U_{\rm B}}{m_{\rm e}c}\frac{1}{b}\overline{x}^2\left\{K_{4/3}(\overline{x})K_{1/3}(\overline{x}) - \frac{3}{5}\overline{x}\left[K_{4/3}^2(\overline{x}) - K_{1/3}^2(\overline{x})\right]\right\}, \quad (3.32)$$

where $\overline{x} = x/(3\gamma^2 b)$ and K_y is the modified Bessel function. For $3 < \gamma < 10$, we substitute the sum over harmonics in equation (3.30) by the integral over l and use the δ-function to take it. The angular integrals are then taken numerically. Alternatively we can use the approximate formulae proposed by Katarzyński et al. (2006), which ignore harmonics. These give identical results for the simulations presented in this thesis, because low harmonics are self-absorbed.

For numerical calculations we renormalize all the emissivities $P(x,\gamma)$ to guarantee the correct cooling rate given by equation (3.28). As an example, in Figure 3.1 we plot the cyclo-synchrotron emissivities from a single electron for different relativistic momenta p.

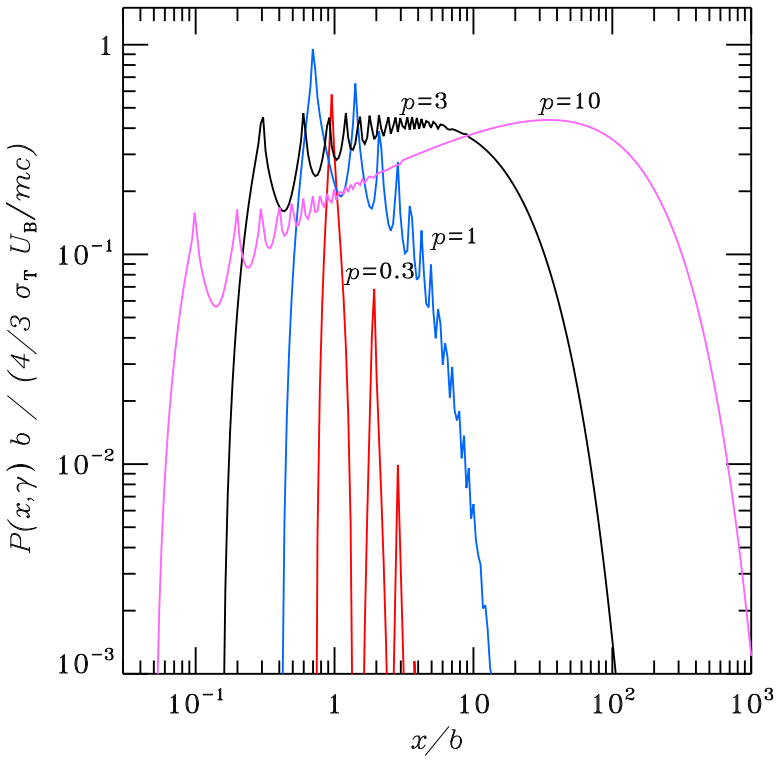

Figure 3.1: Single-electron synchrotron emissivities for different momenta p.

Chapter 4

Coulomb collisions

4.1 Introduction

Although the process of Coulomb scattering between electrons/positrons does not involve radiation, it can have a significant impact on the spectra that emerge from hot plasmas through its influence on the particle distributions. If one considers particles of a single species (e.g. electrons), the main effect of Coulomb collisions is relaxation of the distribution into a Maxwellian (i.e. thermal distribution). In high-energy astrophysics one frequently encounters processes that are capable of accelerating particles into relativistic non-thermal distributions, which subsequently cool by inverse-Compton scattering and/or synchrotron radiation. Typically, at transrelativistic energies thermalization processes such as Coulomb scattering and synchrotron self-absorption begin to compete with these cooling mechanisms, which can lead to a so-called "hybrid" distribution of particles: lower-energy Maxwellian with a high-energy non-thermal tail. As a well-known example, such hybrid distributions are expected to be responsible for the hard-state spectra of accreting black-hole binaries which exhibit a cut-off near 100 keV, followed by a MeV tail.

To properly account for the effects of Coulomb scattering on the particle distributions, we need an appropriate kinetic equation, which can be written down in a similar relativistic invariant form as was done for Compton scattering and pair-production. However, its direct application is prevented by the well-known divergence property of the Coulomb cross-section. A different approach is therefore needed. The birth of the kinetic theory of fully ionized gases can be associated with the paper by Landau (1937). In this work the kinetic equation for particle-particle interactions was written in terms of what is now known as the Landau collision integral. This approach treats energy exchange between particles as a continuous rather that discrete process and characterizes the evolution of the distribution in terms of a flux in momentum space. The treatment in Landau (1937) was non-relativistic, a generalization of the collision integral to arbitrary particle energies was done in Belyaev & Budker (1956).

The Landau collision integral formalism can treat distributions with arbitrary shape in momentum and physical space. If the problem is isotropic, however, the kinetic equation simplifies to a standard 1-dimensional Fokker-Planck equation in energy space. Determining the collision integral in this case reduces to calculating the average rate of change of γ (energy gain/loss) and γ^2 (diffusion) of a test particle interacting with the distribution, where γ is the particle's Lorentz factor. In the non-relativistic case, the energy exchange rate of a particle in a fully ionized plasma was calculated in the original paper by Landau (1937), its generalization to relativistic energies was done in Frankel et al. (1979). The diffusion coefficient in general case was found in Nayakshin & Melia (1998).

We will start with the relativistic kinetic equation and derive the Landau collision integral by assuming that the energy/momentum transfer is small in a single scattering event. Thereafter we will proceed to the isotropic case, which enables us to perform the angular integrals in the collision integral and obtain a second order differential equation for evolution of the distribution in energy space.

4.2 Relativistic kinetic equation

Let's consider a distribution of electrons and positrons with phase space densities $\tilde{n}_-(\boldsymbol{p})$ and $\tilde{n}_+(\boldsymbol{p})$, where $\boldsymbol{p}$ is the dimensionless momentum. The relativistic kinetic equation describing the evolution of either species interacting with both electrons and positrons via Coulomb collisions is

$$\underline{p}\cdot\underline{\nabla}\tilde{n}_\pm(\boldsymbol{p}) = r_\mathrm{e}^2\frac{2}{\lambda_\mathrm{C}^3}\int\frac{d^3p_1}{\gamma_1}\frac{d^3p_1'}{\gamma_1'}\frac{d^3p'}{\gamma'}\,\delta(\underline{p}_1+\underline{p}-\underline{p}_1'-\underline{p}')\,F_\mathrm{Coul} \times\left[\tilde{n}_\mathrm{e}(\boldsymbol{p}_1')\tilde{n}_\pm(\boldsymbol{p}')-\tilde{n}_\mathrm{e}(\boldsymbol{p}_1)\tilde{n}_\pm(\boldsymbol{p})\right], \tag{4.1}$$

where $\tilde{n}_\mathrm{e}=\tilde{n}_-+\tilde{n}_+$ and the four-momenta are defined in the usual way as $\underline{p}=\{\gamma,\boldsymbol{p}\}=\{\gamma,p\boldsymbol{\Omega}\}=\gamma\{1,\beta\boldsymbol{\Omega}\}$. The invariant reaction rate for Møller scattering (i.e. e^-e^- and e^+e^+) is (Berestetskii et al. 1982)

$$F_\mathrm{Coul}=\left(\frac{\xi_1}{\xi-1}+\frac{\xi}{\xi_1-1}+1\right)^2+\frac{1-4\xi\xi_1}{(\xi-1)(\xi_1-1)}+4, \tag{4.2}$$

where the scalar products of particles' four-momenta are defined as

$$\xi=\underline{p}\cdot\underline{p}'=\underline{p}_1\cdot\underline{p}_1', \qquad \xi_1=\underline{p}_1\cdot\underline{p}'=\underline{p}\cdot\underline{p}_1'. \tag{4.3}$$

The corresponding rates for Bhabha $e^\pm e^\mp$ scattering are nearly the same in the small-angle scattering approximation (see e.g. Baring 1987; Coppi & Blandford 1990), therefore we make no distinction between electrons and positrons in this chapter.

What immediately stands out in the reaction rate (4.2) is the divergence when ξ or ξ_1 approaches unity, which corresponds to the case where the particles' momenta change very little upon scattering. This is a manifestation of the well-known divergence of the Coulomb scattering cross-section for small-angle scatterings. Since $F_{\rm Coul}$ is not integrable, we cannot use the kinetic equation (4.1) as it stands. Instead, we can make use of the fact that very little energy gets exchanged upon each small-angle scattering which nevertheless dominate the total exchange rate over large-angle scatterings. Therefore the change of a particle's energy can be treated as a continuous process in which case the evolution of the distribution is described by a Fokker-Planck equation. Thus the simplest approach to the problem would be to take the Fokker-Planck equation as given and determine the coefficients in the equation from comparison with the moments of the kinetic equation (4.1). This has been done in several works (e.g. Dermer & Liang 1989; Nayakshin & Melia 1998). Another more elaborate approach involves exploiting the symmetry properties of the reaction rate as well as the fact that the momentum transfer is small to *derive* a differential (Fokker-Planck) equation directly from the kinetic equation. In this case the energy exchange as well as momentum space diffusion are described by the so-called Landau collision integral.

4.3 Landau collision integral

Let us start by writing the kinetic equation (4.1) in the form

$$\left(\frac{\partial}{\partial t} + c\beta\,\mathbf{\Omega}\cdot\boldsymbol{\nabla}\right)\tilde{n}_{\pm}(\boldsymbol{p}) = \frac{2}{\lambda_{\rm C}^3}\int d^3p_1 \int d^3q\; w(\boldsymbol{p},\boldsymbol{p}_1 \rightarrow \boldsymbol{p}+\boldsymbol{q},\boldsymbol{p}_1-\boldsymbol{q}) \times \left[\tilde{n}_{\rm e}(\boldsymbol{p}_1')\tilde{n}_{\pm}(\boldsymbol{p}') - \tilde{n}_{\rm e}(\boldsymbol{p}_1)\tilde{n}_{\pm}(\boldsymbol{p})\right], \tag{4.4}$$

where $\boldsymbol{q} = \boldsymbol{p}' - \boldsymbol{p} = \boldsymbol{p}_1 - \boldsymbol{p}_1'$ is the transferred momentum. The scattering rate is defined as

$$w(\boldsymbol{p},\boldsymbol{p}_1 \rightarrow \boldsymbol{p}+\boldsymbol{q},\boldsymbol{p}_1-\boldsymbol{q}) = c\,r_{\rm e}^2\frac{1}{\gamma\gamma_1\gamma'}\int\frac{d^3p_1'}{\gamma_1'}\,\delta(\underline{p}_1+\underline{p}-\underline{p}_1'-\underline{p}')\,F_{\rm Coul}$$
$$= \frac{c\,r_{\rm e}^2}{\gamma\gamma_1\gamma'\gamma_1'}\,\delta(\gamma+\gamma_1-\gamma'-\gamma_1')\,F_{\rm Coul} = \frac{c\,r_{\rm e}^2}{\gamma\gamma_1\gamma'}\,\delta(\xi+\xi_1-q_e-1)\,F_{\rm Coul}, \tag{4.5}$$

where we have defined

$$q_e = \underline{p}\cdot\underline{p}_1 = \underline{p}'\cdot\underline{p}_1' \tag{4.6}$$

and used the identity

$$\delta(\gamma+\gamma_1-\gamma'-\gamma_1') = \gamma_1'\,\delta(\xi+\xi_1-q_e-1) \tag{4.7}$$

After performing the three-dimensional integral in equation (4.5), we have to substitute $\gamma_1' = \sqrt{\boldsymbol{p}_1'^2+1}$, where $\boldsymbol{p}_1' = \boldsymbol{p}_1+\boldsymbol{p}-\boldsymbol{p}' = \boldsymbol{p}_1-\boldsymbol{q}$. Also, we have $\gamma' = \sqrt{\boldsymbol{p}'^2+1}$, where $\boldsymbol{p}' = \boldsymbol{p}+\boldsymbol{q}$.

The scattering rate w has the following symmetries

$$\begin{aligned} &w(\boldsymbol{p}, \boldsymbol{p}_1 \to \boldsymbol{p}+\boldsymbol{q}, \boldsymbol{p}_1-\boldsymbol{q}) = w(\boldsymbol{p}+\boldsymbol{q}, \boldsymbol{p}_1-\boldsymbol{q} \to \boldsymbol{p}, \boldsymbol{p}_1) \\ &= w(\boldsymbol{p}_1, \boldsymbol{p} \to \boldsymbol{p}+\boldsymbol{q}, \boldsymbol{p}_1-\boldsymbol{q}) = w(\boldsymbol{p}, \boldsymbol{p}_1 \to \boldsymbol{p}_1-\boldsymbol{q}, \boldsymbol{p}+\boldsymbol{q}). \end{aligned} \tag{4.8}$$

The last two equalities in equation (4.8) are applicable only if the interacting particles are identical. The first equality represents microscopic reversibility, i.e. the symmetry upon the interchange of initial and final particle states. This allows us to write w as

$$w\left(\boldsymbol{p}+\frac{\boldsymbol{q}}{2}, \boldsymbol{p}_1-\frac{\boldsymbol{q}}{2}, \boldsymbol{q}\right), \tag{4.9}$$

in which case the symmetry property reads

$$w\left(\boldsymbol{p}+\frac{\boldsymbol{q}}{2}, \boldsymbol{p}_1-\frac{\boldsymbol{q}}{2}, \boldsymbol{q}\right) = w\left(\boldsymbol{p}+\frac{\boldsymbol{q}}{2}, \boldsymbol{p}_1-\frac{\boldsymbol{q}}{2}, -\boldsymbol{q}\right). \tag{4.10}$$

To derive the Fokker-Planck equation from the kinetic equation (4.4), we will regard the transferred momentum as a small parameter and will expand w, $\tilde{n}_\mathrm{e}$ and $\tilde{n}_\pm$ in Taylor series in $\boldsymbol{q}$ around $\boldsymbol{p}$ and $\boldsymbol{p}_1$. We have

$$\begin{aligned} [\tilde{n}_\mathrm{e}(\boldsymbol{p}_1')\tilde{n}_\pm(\boldsymbol{p}') - \tilde{n}_\mathrm{e}(\boldsymbol{p}_1)\tilde{n}_\pm(\boldsymbol{p})] &\approx q^i \left[\tilde{n}_\mathrm{e}(\boldsymbol{p}_1)\frac{\partial \tilde{n}_\pm(\boldsymbol{p})}{\partial p^i} - \tilde{n}_\pm(\boldsymbol{p})\frac{\partial \tilde{n}_\mathrm{e}(\boldsymbol{p}_1)}{\partial p_1^i}\right] \\ &+\frac{1}{2}q^i q^j \left[\tilde{n}_\mathrm{e}(\boldsymbol{p}_1)\frac{\partial^2 \tilde{n}_\pm(\boldsymbol{p})}{\partial p^i \partial p^j} + \tilde{n}_\pm(\boldsymbol{p})\frac{\partial^2 \tilde{n}_\mathrm{e}(\boldsymbol{p}_1)}{\partial p_1^i \partial p_1^j} - 2\frac{\partial \tilde{n}_\pm(\boldsymbol{p})}{\partial p^i}\frac{\partial \tilde{n}_\mathrm{e}(\boldsymbol{p}_1)}{\partial p_1^j}\right] \end{aligned} \tag{4.11}$$

and

$$w\left(\boldsymbol{p}+\frac{\boldsymbol{q}}{2}, \boldsymbol{p}_1-\frac{\boldsymbol{q}}{2}, \boldsymbol{q}\right) \approx w(\boldsymbol{p}, \boldsymbol{p}_1, \boldsymbol{q}) + \frac{1}{2}q^i\left[\frac{\partial w(\boldsymbol{p}, \boldsymbol{p}_1, \boldsymbol{q})}{\partial p^i} - \frac{\partial w(\boldsymbol{p}, \boldsymbol{p}_1, \boldsymbol{q})}{\partial p_1^i}\right]. \tag{4.12}$$

Inserting the expansions (4.11) and (4.12) into equation (4.4), we see that the first order term vanishes upon integration over d^3q since $q^i w(\boldsymbol{p}, \boldsymbol{p}_1, \boldsymbol{q})$ is antisymmetric in $\boldsymbol{q}$. The second order terms give

$$\begin{aligned} &\left(\frac{\partial}{\partial t} + c\beta\,\boldsymbol{\Omega}\cdot\boldsymbol{\nabla}\right)\tilde{n}_\pm(\boldsymbol{p}) = \frac{2}{\lambda_\mathrm{C}^3}\int d^3p_1 \int d^3q\, \frac{1}{2}q^i q^j \\ &\times\left\{w(\boldsymbol{p}, \boldsymbol{p}_1, \boldsymbol{q})\left[\tilde{n}_\mathrm{e}(\boldsymbol{p}_1)\frac{\partial^2 \tilde{n}_\pm(\boldsymbol{p})}{\partial p^i \partial p^j} + \tilde{n}_\pm(\boldsymbol{p})\frac{\partial^2 \tilde{n}_\mathrm{e}(\boldsymbol{p}_1)}{\partial p_1^i \partial p_1^j} - 2\frac{\partial \tilde{n}_\pm(\boldsymbol{p})}{\partial p^i}\frac{\partial \tilde{n}_\mathrm{e}(\boldsymbol{p}_1)}{\partial p_1^j}\right]\right. \\ &\left.+\left[\frac{\partial w(\boldsymbol{p}, \boldsymbol{p}_1, \boldsymbol{q})}{\partial p^i} - \frac{\partial w(\boldsymbol{p}, \boldsymbol{p}_1, \boldsymbol{q})}{\partial p_1^i}\right]\left[\tilde{n}_\mathrm{e}(\boldsymbol{p}_1)\frac{\partial \tilde{n}_\pm(\boldsymbol{p})}{\partial p^j} - \tilde{n}_\pm(\boldsymbol{p})\frac{\partial \tilde{n}_\mathrm{e}(\boldsymbol{p}_1)}{\partial p_1^j}\right]\right\} \\ &= \frac{2}{\lambda_\mathrm{C}^3}\int d^3p_1 \int d^3q\, \frac{1}{2}q^i q^j \\ &\times\left(\frac{\partial}{\partial p^i} - \frac{\partial}{\partial p_1^i}\right)\left\{w(\boldsymbol{p}, \boldsymbol{p}_1, \boldsymbol{q})\left[\tilde{n}_\mathrm{e}(\boldsymbol{p}_1)\frac{\partial \tilde{n}_\pm(\boldsymbol{p})}{\partial p^j} - \tilde{n}_\pm(\boldsymbol{p})\frac{\partial \tilde{n}_\mathrm{e}(\boldsymbol{p}_1)}{\partial p_1^j}\right]\right\}. \end{aligned} \tag{4.13}$$

Note that the integral over d^3p_1 of the derivative $\partial/\partial p_1^i$ vanishes and we have finally

$$\left(\frac{\partial}{\partial t} + c\beta\,\mathbf{\Omega}\cdot\boldsymbol{\nabla}\right)\tilde{n}_\pm(\boldsymbol{p}) = -\frac{\partial s^i}{\partial p^i}, \tag{4.14}$$

where we have defined the so-called Landau collision integral (Landau 1937; see also Lifshitz & Pitaevskii 1981)

$$s^i = \frac{2}{\lambda_\mathrm{C}^3}\int\left[\tilde{n}_\pm(\boldsymbol{p})\,\frac{\partial\tilde{n}_\mathrm{e}(\boldsymbol{p}_1)}{\partial p_1^j} - \tilde{n}_\mathrm{e}(\boldsymbol{p}_1)\,\frac{\partial\tilde{n}_\pm(\boldsymbol{p})}{\partial p^j}\right] B^{ij}(\boldsymbol{p},\boldsymbol{p}_1)\,d^3p_1, \tag{4.15}$$

where

$$B^{ij}(\boldsymbol{p},\boldsymbol{p}_1) = \frac{1}{2}\int q^i q^j\,w(\boldsymbol{p},\boldsymbol{p}_1,\boldsymbol{q})\,d^3q \tag{4.16}$$

is a spatial tensor that is symmetric in $i \leftrightarrow j$ as well as $\boldsymbol{p} \leftrightarrow \boldsymbol{p}_1$. The collision integral s^i can be regarded as the particle flux in momentum space, giving equation (4.14) the meaning of a continuity equation in 6-dimensional phase space. Together with equations (4.15) and (4.16) the second order differential equation (4.14) describes the evolution of the particle distribution in phase space due to interactions with an arbitrary target distribution. In this form it is quite general and is not limited to Coulomb collisions, the only requirement for its validity is that the energy/momentum exchange can be regarded as a continuous process. All the physics in contained in the quantity B^{ij}, which we will evaluate separately for non-relativistic and relativistic (general) cases.

4.3.1 Non-relativistic treatment

Rewriting the scattering rate as

$$w\,d^3q = |\boldsymbol{v}-\boldsymbol{v}_1|\,d\sigma, \tag{4.17}$$

where $\boldsymbol{v}$ and $\boldsymbol{v}_1$ are the velocities of the interacting particles, equation (4.16) becomes

$$B^{ij} = \frac{1}{2}\int q^i q^j\,|\boldsymbol{v}-\boldsymbol{v}_1|\,d\sigma. \tag{4.18}$$

Assuming the scattering angle is small, the transferred momentum $\boldsymbol{q}$ is approximately perpendicular to the relative velocity of the particles before collision, therefore [1]

$$B^{ij}(v^j - v_1^j) = 0. \tag{4.19}$$

[1] Since in this subsection we are working in Cartesian three-space, we make no distinction between covariant and contravariant vector components. The summation convention therefore applies for repeated upper or lower indices.

A tensor satisfying this condition has to be of the form

$$B^{ij} = \frac{1}{2} B \left[\delta^{ij} - \frac{(v^i - v_1^i)(v^j - v_1^j)}{(\boldsymbol{v} - \boldsymbol{v}_1)^2} \right], \tag{4.20}$$

where B is the trace

$$B = B_{ij} = \frac{1}{2} \int q^2 |\boldsymbol{v} - \boldsymbol{v}_1| \, d\sigma. \tag{4.21}$$

For small scattering angles one can write $mcq \approx \mu |\boldsymbol{v} - \boldsymbol{v}_1| \theta$, where θ is the scattering angle in the centre-of-momentum frame and μ is the reduced mass. Therefore B becomes

$$B = \frac{\mu^2}{(mc)^2} |\boldsymbol{v} - \boldsymbol{v}_1|^3 \sigma_t, \quad \text{where} \quad \sigma_t = \frac{1}{2} \int \theta^2 \, d\sigma. \tag{4.22}$$

The differential cross-section is approximated by the Rutherford formula

$$d\sigma \approx \frac{4e^4 d\Omega}{\mu^2 (\boldsymbol{v} - \boldsymbol{v}_1)^4 \, \theta^4} = \frac{8\pi e^4 d\theta}{\mu^2 (\boldsymbol{v} - \boldsymbol{v}_1)^4 \, \theta^3}, \tag{4.23}$$

whereby the quantity σ_t becomes

$$\sigma_t = \frac{4\pi e^4}{\mu^2 (\boldsymbol{v} - \boldsymbol{v}_1)^4} \ln \Lambda, \quad \text{where} \quad \ln \Lambda = \int \frac{d\theta}{\theta} \tag{4.24}$$

is the Coulomb logarithm. For the tensor B^{ij} we get

$$B^{ij} = \frac{2\pi e^4}{(mc)^2} \frac{1}{|\boldsymbol{v} - \boldsymbol{v}_1|} \ln \Lambda \left[\delta^{ij} - \frac{(v^i - v_1^i)(v^j - v_1^j)}{(\boldsymbol{v} - \boldsymbol{v}_1)^2} \right]. \tag{4.25}$$

4.3.2 Relativistic treatment

Although not manifestly covariant, the analysis of the preceding section up to equation (4.16) is not limited by the particles' energies and is therefore valid also in relativistic case, provided that the correct relativistic rate w is used. It is possible, in principle, to calculate the components of the tensor B^{ij} entering the collision integral directly from equations (4.16) and (4.5). However, it is much simpler to employ the properties of B^{ij} to make an educated guess what form it should take. Let's start by noting that $\gamma\gamma_1 \, w \, d^3q$ is a Lorentz-invariant quantity. Indeed, from equation (4.5) we have [2]

$$\gamma\gamma_1 \, w(\boldsymbol{p}, \boldsymbol{p}_1, \boldsymbol{q}) \, d^3q = c \, r_e^2 \, \frac{d^3p'}{\gamma'} \int \frac{d^3p_1'}{\gamma_1'} \, \delta(\underline{p}_1 + \underline{p} - \underline{p}_1' - \underline{p}') \, F_{\text{Coul}}, \tag{4.26}$$

[2] Here we are approximating $w(\boldsymbol{p}, \boldsymbol{p}_1, \boldsymbol{q}) \approx w(\boldsymbol{p} + \boldsymbol{q}/2, \boldsymbol{p}_1 - \boldsymbol{q}/2, \boldsymbol{q})$, which we can do if we are interested in only second order terms in B^{ij}.

where $d^3p'/\gamma' = d^3q/\gamma'$, d^3p_1'/γ_1', $F_{\rm Coul}$ as well as the four-dimensional delta-function are all Lorentz-invariant. We can now define a Lorentz tensor

$$W^{\alpha\beta} = \frac{1}{2}\gamma\gamma_1 \int q^\alpha q^\beta\, w(\boldsymbol{p}, \boldsymbol{p}_1, \boldsymbol{q})\, d^3q, \tag{4.27}$$

where q^α and q^β are the components of the *four*-momentum transferred in a scattering event. Obviously, the components of the 3-tensor B^{ij} are related to the spatial components of $W^{\alpha\beta}$ as

$$B^{ij} = \frac{W^{ij}}{\gamma\gamma_1}. \tag{4.28}$$

Let's proceed by calculating the quantity W^α_α. Using equations (4.27) and (4.5), we get

$$W^\alpha_\alpha \equiv W = \frac{1}{2}\, c\, r_{\rm e}^2 \int \frac{d^3p'}{\gamma'}\, q^\alpha q_\alpha\, \delta(\xi + \xi_1 - q_e - 1)\, F_{\rm Coul}. \tag{4.29}$$

Note that as an invariant scalar it can be evaluated in any frame, which we choose to be the centre-of-momentum frame. Using the identities

$$\gamma_{\rm cm} = \gamma_{1,\rm cm}, \qquad \boldsymbol{p}_{\rm cm} + \boldsymbol{p}_{1,\rm cm} = 0, \qquad q_e = \gamma\gamma_1 - \boldsymbol{p}\cdot\boldsymbol{p}_1 = 2\gamma_{\rm cm}^2 - 1, \tag{4.30}$$

we find

$$\delta(\xi + \xi_1 - q_e - 1) = \delta(\underline{p}' \cdot (\underline{p} + \underline{p}_1) - \underline{p}\cdot\underline{p}_1 - 1) = \frac{\delta(\gamma'_{\rm cm} - \gamma_{\rm cm})}{2\gamma_{\rm cm}}. \tag{4.31}$$

Putting this in equation (4.29) and noting that $d^3p'/\gamma' = p'_{\rm cm}\, d\gamma'_{\rm cm}\, d\boldsymbol{\Omega}'_{\rm cm}$, we get after taking the $d\gamma'_{\rm cm}$ integral

$$W = \frac{1}{4}\, c\, r_{\rm e}^2\, \frac{p_{\rm cm}}{\gamma_{\rm cm}} \int q^\alpha q_\alpha\, F_{\rm Coul}\, d\boldsymbol{\Omega}'_{\rm cm}. \tag{4.32}$$

With $\gamma'_{\rm cm} = \gamma_{\rm cm}$, the scalar products ξ and ξ_1 entering $F_{\rm Coul}$ become

$$\xi = \gamma_{\rm cm}^2(1 - p_{\rm cm}^2\, \cos\theta_{\rm cm}), \qquad \xi_1 = \gamma_{\rm cm}^2(1 + p_{\rm cm}^2\, \cos\theta_{\rm cm}), \tag{4.33}$$

where $\theta_{\rm cm}$ is the scattering angle in the CM-frame. We also find

$$\begin{aligned} q^\alpha q_\alpha &= (p'^{\,\alpha} - p^\alpha)(p'_\alpha - p_\alpha) = 2\,(1 - \xi) \\ &= -2p_{\rm cm}^2(1 - \cos\theta_{\rm cm}) = -\frac{2p_{\rm cm}^2 \sin^2\theta_{\rm cm}}{(1 + \cos\theta_{\rm cm})}. \end{aligned} \tag{4.34}$$

In terms of CM-frame quantities the invariant reaction rate $F_{\rm Coul}$ given by equation (4.2) takes the form (Møller 1932; Jauch & Rohrlich 1976)

$$F_{\rm Coul} = \frac{4\,(\gamma_{\rm cm}^2 + p_{\rm cm}^2)^2}{p_{\rm cm}^4 \sin^4\theta_{\rm cm}} + \frac{1 - 4\gamma_{\rm cm}^2(\gamma_{\rm cm}^2 + p_{\rm cm}^2)}{p_{\rm cm}^4 \sin^2\theta_{\rm cm}} + 1. \tag{4.35}$$

In the small-angle scattering approximation, it is the leading term on the right-hand side of equation (4.35) that makes the dominant contribution to the scattering rate. It is therefore common practice to neglect the other terms altogether. The error that one makes by doing this is small compared to uncertainties arising from evaluating the Coulomb logarithm.

Inserting equations (4.34) and (4.35) into (4.32) and writing $d\mathbf{\Omega}'_{\rm cm} = d\cos\theta_{\rm cm}\, d\phi_{\rm cm}$, we get

$$W = -2\pi\, c\, r_{\rm e}^2\, \ln\Lambda\, \frac{(\gamma_{\rm cm}^2 + p_{\rm cm}^2)^2}{\gamma_{\rm cm} p_{\rm cm}}, \tag{4.36}$$

where

$$\ln\Lambda = \int \frac{2}{1+\cos\theta_{\rm cm}}\, \frac{d\cos\theta_{\rm cm}}{\sin^2\theta_{\rm cm}} \approx \int \frac{d\theta_{\rm cm}}{\theta_{\rm cm}}. \tag{4.37}$$

This can be written in terms of the Lorentz-invariant quantity q_e as

$$W = -4\pi c\, r_{\rm e}^2\, \ln\Lambda\, \frac{q_e^2}{(q_e^2-1)^{1/2}} \tag{4.38}$$

if we observe that

$$\gamma_{\rm cm}^2 + p_{\rm cm}^2 = \underline{p}\cdot\underline{p}_1 = q_e \quad \text{and} \quad \gamma_{\rm cm} p_{\rm cm} = \frac{1}{2}\left[(\underline{p}\cdot\underline{p}_1)^2 - 1\right]^{1/2} = (q_e^2-1)^{1/2}. \tag{4.39}$$

Owing to the fact that $q^0_{\rm cm} = 0$, the time components of tensor $W^{\alpha\beta}$ vanish in the CM-frame:

$$W^{\alpha 0}_{\rm cm} = W^{0\alpha}_{\rm cm} = 0. \tag{4.40}$$

Using this and also the fact that $\boldsymbol{p}_{\rm cm}$ is nearly perpendicular to $\boldsymbol{q}_{\rm cm}$ for small-angle scattering, we find that

$$W^{\alpha\beta} p_\beta = W^{\alpha\beta} p_{1,\beta} = 0, \tag{4.41}$$

since these scalar products vanish in the CM frame and if a Lorentz 4-vector is zero in one frame it is zero in all frames.

Let us now try to determine the form of the tensor $W^{\alpha\beta}$. In addition to being symmetric in the two indices, $W^{\alpha\beta}$ also has to be symmetric with respect to switching the particles' momenta. The most general form of such tensor, depending only on 4-vectors $\underline{p}$ and $\underline{p}_1$, is (Belyaev & Budker 1956; Lifshitz & Pitaevskii 1981)

$$W^{\alpha\beta} = A\,\eta^{\alpha\beta} + B\,(p^\alpha p^\beta + p_1^\alpha p_1^\beta) + C\,(p^\alpha p_1^\beta + p_1^\alpha p^\beta), \tag{4.42}$$

where $\eta^{\alpha\beta}$ is the Minkowski tensor. The scalar coefficients A, B and C can be determined from conditions (4.38) and (4.41), giving

$$A = \frac{W}{2}, \qquad B = \frac{W}{2(q_e^2 - 1)}, \qquad C = -\frac{q_e W}{2(q_e^2 - 1)}, \tag{4.43}$$

whereby equation (4.42) becomes

$$W^{\alpha\beta} = 2\pi c\, r_{\rm e}^2\, \ln\Lambda\, \frac{q_e^2}{(q_e^2 - 1)^{3/2}} \times \left\{-(q_e^2 - 1)\,\eta^{\alpha\beta} - (p^\alpha p^\beta + p_1^\alpha p_1^\beta) + q_e\,(p^\alpha p_1^\beta + p_1^\alpha p^\beta)\right\}. \tag{4.44}$$

The 3-tensor B^{ij} is now simply

$$B^{ij} = 2\pi c\, r_{\rm e}^2\, \ln\Lambda\, \frac{1}{\gamma\gamma_1}\frac{q_e^2}{(q_e^2 - 1)^{3/2}} \times \left\{(q_e^2 - 1)\,\delta^{ij} - (p^i p^j + p_1^i p_1^j) + q_e\,(p^i p_1^j + p_1^i p^j)\right\}. \tag{4.45}$$

It can be shown that B^{ij} defined by the preceding equation satisfies the condition

$$B^{ij}\, v^j = B^{ij}\, v_1^j, \tag{4.46}$$

where $v^j = cp^j/\gamma$ and $v_1^j = cp_1^j/\gamma_1$ are three-velocities. Equation (4.46) is identical to condition (4.19) obtained in the non-relativistic case. Also, it is easy to verify that B^{ij} given by equation (4.45) reduces to equation (4.25) in the non-relativistic limit.

4.3.3 Collision integral in the isotropic case

The evolution of the electron distribution due to Coulomb scattering in general case is determined by equations (4.14), (4.15) and (4.45). However, let's now assume that the distributions of the interacting particles are isotropic. In this case the kinetic equation (4.14) reduces to a scalar second-order differential equation.

Consider the collision integral given by equation (4.15). For isotropic particle distribution functions the gradients of the occupation numbers become [3]

$$\frac{\partial\tilde{n}_\pm(p)}{\partial p^j} = \hat{p}^j\,\frac{\partial\tilde{n}_\pm(p)}{\partial p} \quad \text{and} \quad \frac{\partial\tilde{n}_{\rm e}(p_1)}{\partial p_1^j} = \hat{p}_1^j\,\frac{\partial\tilde{n}_{\rm e}(p_1)}{\partial p_1}, \tag{4.47}$$

where $\hat{p}^j$ and $\hat{p}_1^j$ are unit vectors pointing in the directions of p^j and p_1^j, respectively. Thus using the identities $d^3p_1 = p_1^2 dp_1\, d\Omega_1$ and $pdp = \gamma d\gamma$ we can write

[3] As before, we do not distinguish between covariant and contravariant indices in Cartesian three-space.

the momentum space flux (4.15) as

$$s^i = \frac{2}{\lambda_{\rm C}^3}\left[\tilde{n}_\pm(p)\int\frac{\partial\tilde{n}_{\rm e}(p_1)}{\partial\gamma_1}\,p_1^2dp_1\int\frac{p_1}{\gamma_1}\,\hat{p}_1^jB^{ij}\,d\Omega_1 - \frac{\partial\tilde{n}_\pm(p)}{\partial\gamma}\int\tilde{n}_{\rm e}(p_1)\,p_1^2dp_1\int\frac{p}{\gamma}\,\hat{p}^jB^{ij}\,d\Omega_1\right]. \tag{4.48}$$

By virtue of relation (4.46) the last integrals in both terms in (4.48) are equal, i.e.

$$K^i \equiv \int\frac{p_1}{\gamma_1}\,\hat{p}_1^jB^{ij}\,d\Omega_1 = \int\frac{p}{\gamma}\,\hat{p}^jB^{ij}\,d\Omega_1, \tag{4.49}$$

so we only need to calculate one of them.

As a sidenote, observe that for Maxwellian energy distributions $\partial\tilde{n}_{\rm e,M}/\partial\gamma = -\tilde{n}_{\rm e,M}/\Theta$, where $\Theta = kT/mc^2$, and therefore $s^i = 0$ as one would expect in equilibrium.

In order to determine K^i we first need to evaluate $\hat{p}^jB^{ij}$. To simplify the notation equation (4.45) for B^{ij}, we identify

$$\gamma_{\rm rel} = \gamma\gamma_1 - \boldsymbol{p}\cdot\boldsymbol{p}_1 = q_e, \qquad p_{\rm rel} = \sqrt{q_e^2-1} \tag{4.50}$$

as the Lorentz factor and momentum of one particle in the rest frame of the other. The scalar product $\hat{p}_\beta B_{\alpha\beta}$ now becomes

$$\hat{p}^jB^{ij} = 2\pi c\,r_{\rm e}^2\,\ln\Lambda\,\frac{1}{\gamma\gamma_1}\frac{\gamma_{\rm rel}^2}{p_{\rm rel}^3} \times\left\{p_{\rm rel}^2\,\hat{p}^i - p^2\,\hat{p}^i - \frac{p_1}{p}\,(\boldsymbol{p}\cdot\boldsymbol{p}_1)\,\hat{p}_1^i + \gamma_{\rm rel}\left[(\boldsymbol{p}\cdot\boldsymbol{p}_1)\,\hat{p}^i + pp_1\,\hat{p}_1^i\right]\right\}. \tag{4.51}$$

The relation (4.51) describes a three-vector, which we can rotate into the frame where it is most convenient to take the angular integral ($d\Omega_1$ is rotational invariant). After taking the integral we can perform a rotation back to the lab frame. Let's choose this frame in such way that the three-axis points to the direction of (fixed) $\hat{p}^i$. In this frame we have

$$\boldsymbol{p} = \{0,0,p\}, \qquad \boldsymbol{p}_1 = p_1\,\{\sin\theta\cos\phi, \sin\theta\sin\phi, \cos\theta\}, \tag{4.52}$$

where θ is the angle between $\boldsymbol{p}$ and $\boldsymbol{p}_1$, and ϕ is the azimuthal angle defined on a plane perpendicular to $\boldsymbol{p}$ and measured from an arbitrary reference direction (say, from the projection of the lab-frame 3-axis onto this plane). The solid angle element is $d\Omega_1 = d\cos\theta\,d\phi$.

We now notice that upon taking the integral in this frame the first two components ($i = 1, 2$) of K^i vanish. Indeed, inserting equation (4.51) into (4.49) we see that in the terms proportional to $\hat{p}_1^i$ we encounter integrals like $\int_0^{2\pi}\sin\phi\,d\phi = 0$

and $\int_0^{2\pi} \cos\phi \, d\phi = 0$ in the first two components. Of course, in terms proportional to $\hat{p}^i$ these components are equal to zero by definition. We are therefore concerned only with the third component of the vector $\hat{p}^j B^{ij}$, which becomes

$$\hat{p}^j B^{3j} = 2\pi c \, r_e^2 \, \ln\Lambda \, \frac{1}{\gamma\gamma_1} \frac{\gamma_{\rm rel}^2}{p_{\rm rel}^3} \left(p_{\rm rel}^2 - p^2 - p_1^2\mu^2 + 2\gamma_{\rm rel} \, p p_1 \mu \right), \tag{4.53}$$

where $\mu = \cos\theta$. For taking the integral it is more convenient to write equation (4.53) in terms of the relative Lorentz factor $\gamma_{\rm rel}$ instead of μ. To do this we write equation (4.50) as $\gamma_{\rm rel} = \gamma\gamma_1 - p p_1 \mu$. Expressing μ and substituting into equation (4.53) gives

$$\hat{p}^j B^{3j} = 2\pi c \, r_e^2 \, \ln\Lambda \, \frac{1}{\gamma\gamma_1} \frac{\gamma_{\rm rel}^2}{p_{\rm rel}^3} \left[p_{\rm rel}^2 - p^2 - \frac{(\gamma\gamma_1 - \gamma_{\rm rel})^2}{p^2} + 2\gamma_{\rm rel} \, (\gamma\gamma_1 - \gamma_{\rm rel}) \right], \tag{4.54}$$

which, after some manipulation, can be written as

$$\hat{p}^j B^{3j} = 2\pi c \, r_e^2 \, \ln\Lambda \, \frac{1}{\gamma\gamma_1} \frac{\gamma^2}{p^2} \frac{\gamma_{\rm rel}^2}{p_{\rm rel}^3} \, (\gamma_{\rm rel}^+ - \gamma_{\rm rel}) \, (\gamma_{\rm rel} - \gamma_{\rm rel}^-), \tag{4.55}$$

where we have defined

$$\gamma_{\rm rel}^+ = \gamma\gamma_1 + p p_1 \quad \text{and} \quad \gamma_{\rm rel}^- = \gamma\gamma_1 - p p_1. \tag{4.56}$$

The differential solid angle in the expression (4.49) for K^i can be written as

$$d\Omega_1 = -\frac{d\gamma_{\rm rel} \, d\phi}{p p_1}, \tag{4.57}$$

where we have used the relation $d\gamma_{\rm rel} = -p p_1 \, d\mu$. The three-component of K^i now becomes

$$K^3(\gamma, \gamma_1) = 2\pi \, \frac{p}{\gamma} \int_{\gamma_{\rm rel}^-}^{\gamma_{\rm rel}^+} \frac{d\gamma_{\rm rel}}{p p_1} \, \hat{p}^j B^{3j} \equiv K(\gamma, \gamma_1), \tag{4.58}$$

the azimuthal integral contributing 2π since the integrand does not depend on ϕ. Inserting expression (4.55) into (4.58) and defining

$$\Delta(\gamma, \gamma_1) = \int_{\gamma_{\rm rel}^-}^{\gamma_{\rm rel}^+} \frac{\gamma_{\rm rel}^2}{p_{\rm rel}^3} \, (\gamma_{\rm rel}^+ - \gamma_{\rm rel}) \, (\gamma_{\rm rel} - \gamma_{\rm rel}^-) \, d\gamma_{\rm rel}, \tag{4.59}$$

we will have

$$K(\gamma, \gamma_1) = 4\pi^2 c \, r_e^2 \, \ln\Lambda \, \frac{1}{\gamma\gamma_1 p p_1} \frac{\gamma}{p} \, \Delta(\gamma, \gamma_1). \tag{4.60}$$

The integral in equation (4.59) is elementary and gives

$$\Delta(\gamma,\gamma_1) = \left\{ -\left(\gamma^2+\gamma_1^2+\frac{1}{2}\right)\ln(\gamma_{\rm rel}+p_{\rm rel}) + \frac{1}{p_{\rm rel}}\left[\gamma_{\rm rel}\,(\gamma^2+\gamma_1^2) - 2\gamma\gamma_1\right] + p_{\rm rel}\left(2\gamma\gamma_1 - \frac{\gamma_{\rm rel}}{2}\right)\right\}\Bigg|_{\gamma_{\rm rel}^-}^{\gamma_{\rm rel}^+}. \tag{4.61}$$

The next step in our derivation is to note that the vector K^i points in the same direction as p^i, since for both of these only the third component has a nonzero value in the frame we are working in. Therefore, rotation into an arbitrary frame gives

$$K^i = \hat{p}^i\, K(\gamma,\gamma'). \tag{4.62}$$

The momentum space flux (4.48) is proportional to K^i and can be written in a similar manner

$$s^i = \hat{p}^i\, s(p), \tag{4.63}$$

where

$$s(p) = \frac{2}{\lambda_{\rm C}^3}\left[\tilde{n}_\pm(p)\int \frac{\partial\tilde{n}_{\rm e}(p_1)}{\partial\gamma_1}\,K(\gamma,\gamma_1)\;p_1^2 dp_1 - \frac{\partial\tilde{n}_\pm(p)}{\partial\gamma}\int \tilde{n}_{\rm e}(p_1)\,K(\gamma,\gamma_1)\;p_1^2 dp_1\right]. \tag{4.64}$$

For later use let's rewrite the last equation as

$$s(p) = \frac{2}{\lambda_{\rm C}^3}\left\{\tilde{n}_\pm(p)\int \tilde{n}_{\rm e}(p_1)\frac{\partial}{\partial\gamma_1}\left[\gamma_1 p_1\,K(\gamma,\gamma_1)\right]\,d\gamma_1 - \frac{\partial\tilde{n}_\pm(p)}{\partial\gamma}\int \tilde{n}_{\rm e}(p_1)\;\gamma_1 p_1\,K(\gamma,\gamma_1)\,d\gamma_1\right\}. \tag{4.65}$$

The divergence of the momentum space flux on the right-hand side of the evolution equation (4.14) takes the form

$$\frac{\partial s^i}{\partial p^i} = \frac{\partial}{\partial p^i}\left[\frac{p^i}{p}s(p)\right] = 3\,\frac{s(p)}{p} + p\,\frac{\partial}{\partial p}\left[\frac{s(p)}{p}\right] = \frac{1}{p^2}\frac{\partial}{\partial p}\left[p^2\,s(p)\right]. \tag{4.66}$$

The isotropic evolution equation is

$$\frac{\partial\tilde{n}_\pm(p)}{\partial t} = -\frac{1}{p^2}\frac{\partial}{\partial p}\left[p^2\,s(p)\right], \tag{4.67}$$

where spatial homogeneity has been assumed.

Let's now try to write equation (4.67) in the standard form of the diffusion equation in energy space, namely

$$\frac{\partial N_{\pm}(\gamma)}{\partial t} = -\frac{\partial}{\partial \gamma}\left\{\dot{\gamma}\, N_{\pm}(\gamma) - \frac{1}{2}\frac{\partial}{\partial \gamma}\left[D(\gamma)\, N_{\pm}(\gamma)\right]\right\}, \tag{4.68}$$

where $\dot{\gamma}$ and $D(\gamma)$ are the energy exchange and diffusion coefficients, respectively. For isotropic distributions the particle density $N(\gamma)$ is related to the occupation number as

$$N(\gamma) = \frac{2}{\lambda_{\rm C}^3}\, 4\pi\gamma p\, \tilde{n}(p). \tag{4.69}$$

Using the expression (4.65), the quantity in square brackets on the right-hand side of equation (4.67) can be written in the following form

$$\begin{aligned} p^2\, s(p) = {} & \frac{1}{(4\pi)^2}\left(\frac{2}{\lambda_{\rm C}^3}\right)^{-1} \frac{N_{\pm}(\gamma)}{\gamma p}\int \frac{N_{\rm e}(\gamma_1)\, d\gamma_1}{\gamma_1 p_1} \\ & \times\left\{\frac{\partial\left[p^2 p_1 \gamma_1 K(\gamma,\gamma_1)\right]}{\partial\gamma} - \frac{\partial\left[p^2 p_1 \gamma_1 K(\gamma,\gamma_1)\right]}{\partial\gamma_1}\right\} \\ & - \frac{1}{(4\pi)^2}\left(\frac{2}{\lambda_{\rm C}^3}\right)^{-1} \frac{\partial}{\partial\gamma}\left\{\frac{N_{\pm}(\gamma)}{\gamma p}\int \frac{N_{\rm e}(\gamma_1)\, d\gamma_1}{\gamma_1 p_1}\, p^2 p_1 \gamma_1 K(\gamma,\gamma_1)\right\}. \end{aligned} \tag{4.70}$$

Substituting $K(\gamma,\gamma_1)$ from equation (4.60), this becomes

$$\begin{aligned} p^2\, s(p) = \frac{1}{4} c\, r_{\rm e}^2 \left(\frac{2}{\lambda_{\rm C}^3}\right)^{-1} \ln\Lambda \Bigg\{ & \frac{N_{\pm}(\gamma)}{\gamma p}\int \frac{N_{\rm e}(\gamma_1)\, d\gamma_1}{\gamma_1 p_1}\left[\frac{\partial\Delta(\gamma,\gamma_1)}{\partial\gamma} - \frac{\partial\Delta(\gamma,\gamma_1)}{\partial\gamma_1}\right] \\ & - \frac{\partial}{\partial\gamma}\left[\frac{N_{\pm}(\gamma)}{\gamma p}\int \frac{N_{\rm e}(\gamma_1)\, d\gamma_1}{\gamma_1 p_1}\,\Delta(\gamma,\gamma_1)\right]\Bigg\}. \end{aligned} \tag{4.71}$$

Putting this into equation (4.67) and substituting $\tilde{n}_{\pm}(p)$ from equation (4.69), we find

$$\begin{aligned} \frac{\partial N_{\pm}(\gamma)}{\partial t} = -\frac{\partial}{\partial\gamma}\Bigg\{ & N_{\pm}(\gamma)\int a(\gamma,\gamma_1)\, N_{\rm e}(\gamma_1)\, d\gamma_1 \\ & - \frac{1}{2}\frac{\partial}{\partial\gamma}\left[N_{\pm}(\gamma)\int d(\gamma,\gamma_1)\, N_{\rm e}(\gamma_1)\, d\gamma_1\right]\Bigg\}, \end{aligned} \tag{4.72}$$

where we have defined

$$d(\gamma,\gamma_1) = \frac{3}{4}\frac{c\sigma_T \ln\Lambda}{\gamma\gamma_1 p p_1}\,\Delta(\gamma,\gamma_1) \tag{4.73}$$

and

$$a(\gamma,\gamma_1) = \frac{3}{8}\frac{c\sigma_T \ln\Lambda}{\gamma\gamma_1 p p_1}\left[\frac{\partial\Delta(\gamma,\gamma_1)}{\partial\gamma} - \frac{\partial\Delta(\gamma,\gamma_1)}{\partial\gamma_1}\right]. \tag{4.74}$$

Equation (4.72) has the same form as (4.68) if we identify

$$\dot{\gamma} = \int a(\gamma, \gamma_1)\, N_e(\gamma_1)\, d\gamma_1 \quad \text{and} \quad D(\gamma) = \int d(\gamma, \gamma_1)\, N_e(\gamma_1)\, d\gamma_1. \tag{4.75}$$

Together with equation (4.61), we have an explicit expression for the diffusion coefficient $d(\gamma, \gamma_1)$. To find an explicit expression for the energy exchange coefficient $a(\gamma, \gamma_1)$, let's calculate the expression in the square brackets in equation (4.74), using the definition (4.59). Since the integrand in equation (4.59) is zero in both the upper and lower integration limits, the derivative over γ can be written as

$$\frac{\partial \Delta(\gamma, \gamma_1)}{\partial \gamma} = \int_{\gamma_{\rm rel}^-}^{\gamma_{\rm rel}^+} \frac{\gamma_{\rm rel}^2}{p_{\rm rel}^3} \frac{\partial}{\partial \gamma} \left[(\gamma_{\rm rel}^+ - \gamma_{\rm rel})\, (\gamma_{\rm rel} - \gamma_{\rm rel}^-) \right] d\gamma_{\rm rel}. \tag{4.76}$$

The derivative under the integral is

$$\begin{aligned} \frac{\partial}{\partial \gamma} \left[(\gamma_{\rm rel}^+ - \gamma_{\rm rel})\, (\gamma_{\rm rel} - \gamma_{\rm rel}^-) \right] &= \frac{\partial \gamma_{\rm rel}^+}{\partial \gamma} (\gamma_{\rm rel} - \gamma_{\rm rel}^-) - \frac{\partial \gamma_{\rm rel}^-}{\partial \gamma} (\gamma_{\rm rel}^+ - \gamma_{\rm rel}) \\ &= 2(\gamma_1 \gamma_{\rm rel} - \gamma). \end{aligned} \tag{4.77}$$

Because $\Delta(\gamma, \gamma_1)$ is symmetric, its derivative with respect to γ_1 is given by expressions (4.76) and (4.77) with the arguments γ and γ_1 reversed. The coefficient $a(\gamma, \gamma_1)$ now becomes

$$a(\gamma, \gamma_1) = \frac{3}{4} \frac{c \sigma_T \ln \Lambda}{\gamma \gamma_1 p p_1} (\gamma_1 - \gamma)\, \chi(\gamma, \gamma_1), \tag{4.78}$$

where

$$\chi(\gamma, \gamma_1) = \int_{\gamma_{\rm rel}^-}^{\gamma_{\rm rel}^+} \frac{\gamma_{\rm rel}^2 (\gamma_{\rm rel} + 1)}{p_{\rm rel}^3}\, d\gamma_{\rm rel} = \left[p_{\rm rel} - \frac{\gamma_{\rm rel} + 1}{p_{\rm rel}} + \ln(\gamma_{\rm rel} + p_{\rm rel}) \right] \Bigg|_{\gamma_{\rm rel}^-}^{\gamma_{\rm rel}^+}. \tag{4.79}$$

The interpretation of $\dot{\gamma}$ and $D(\gamma)$ as energy exchange and diffusion coefficients can be made clear by directly calculating the average rate of change of $\gamma' - \gamma$ and $(\gamma' - \gamma)^2$ for a test-particle interacting with a given target distribution. This was done by Frankel et al. (1979) and Nayakshin & Melia (1998) for the energy exchange and diffusion coefficients, respectively. The expressions obtained in these works are identical to the ones derived here. On physical grounds this result should be expected, however mathematically it seems quite remarkable due to the different approximations made along the way. On the other hand, all those approximations boil down to the assumption of the dominance of small-angle scatterings and simply lead to slightly different definitions of the Coulomb logarithm.

Simple approximate expressions for the energy exchange and diffusion coefficients can be obtained by using the one-point trapezoidal rule to approximate

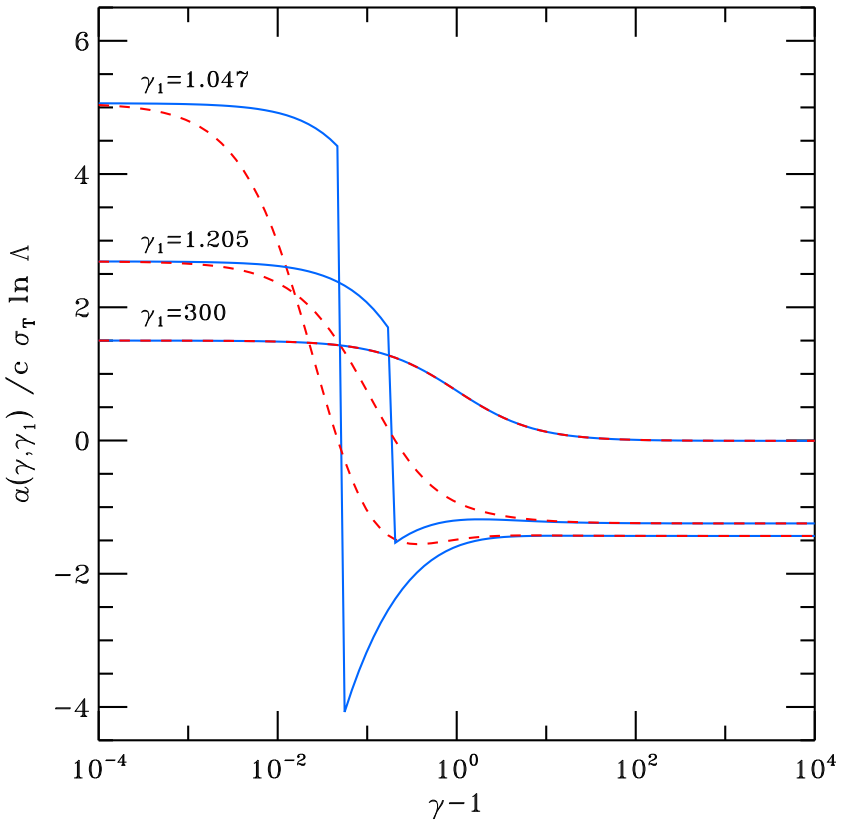

Figure 4.1: Energy exchange rate of a test particle interacting with a mono-energetic background distribution with different Lorentz factors γ_1. Solid lines correspond to the exact expression (4.78), dashed lines correspond to the approximation (4.80). Note that for $\gamma_1 = 300$ the curves corresponding to the approximate and exact expressions are indistinguishable.

the integral in equation (4.79) and the 3-point Simpson's rule to approximate the integral in equation (4.59):

$$a(\gamma,\gamma_1) \approx \frac{3}{2} c\sigma_T \ln\Lambda \frac{(\gamma_1-\gamma)\,\gamma\gamma_1}{(\gamma\gamma_1-1)\sqrt{(\gamma\gamma_1)^2-1}} \tag{4.80}$$

and

$$d(\gamma,\gamma_1) \approx c\sigma_T \ln\Lambda \frac{\gamma\gamma_1 p^2 p_1^2}{[(\gamma\gamma_1)^2-1]^{3/2}}\,, \tag{4.81}$$

which agree with the exact coefficients reasonably well, except in the region $\gamma \approx \gamma_1$. In Figures 4.1 and 4.2 we plot the energy exchange and diffusion coefficients given by equations (4.78) and (4.73) for different target photon energies, together with the approximate expressions (4.80) and (4.81).

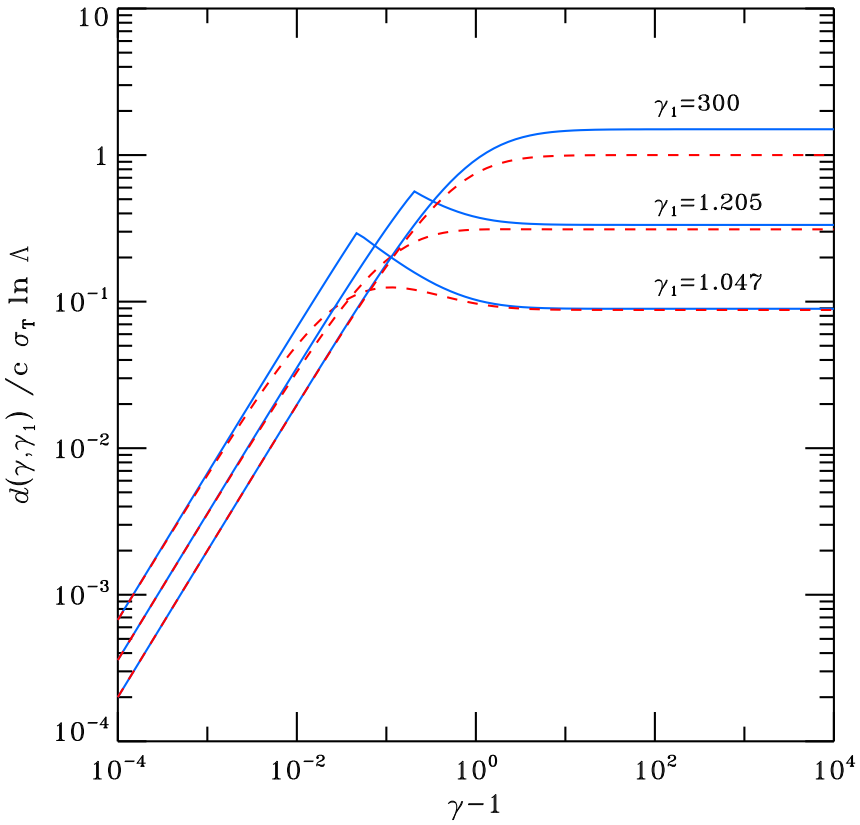

Figure 4.2: The diffusion coefficient for a particle interacting with a mono-energetic background distribution with different Lorentz factors γ_1. Solid and dashed lines correspond to the exact and approximate expressions (4.73) and (4.81), respectively. Note that both axes are in logarithmic units.

Part II

The kinetic code

Chapter 5

Kinetic equations

We are considering a region of relativistic plasma of charged particles (electrons and positrons, which we call "electrons" below if the relevant processes, e.g. Compton scattering and synchrotron, operate identically on both types of particles) permeated by radiation and tangled magnetic fields. We study the evolution of lepton and photon distributions by solving the time-dependent coupled kinetic equations accounting for synchrotron emission and absorption, Compton scattering, Coulomb scattering, and electron-positron pair production and annihilation. To do this we first need to collect the kinetic equations describing different processes discussed in the preceding sections and rewrite them in form that is most suitable for numerical calculations. We make a simplifying assumption of homogeneity and isotropy of the particle distributions. The escape of radiation (and also electrons) from the region is modeled by a simple escape probability formalism. The energization of electrons is modeled either through injection of high-energy electrons or diffusive acceleration within the active region, which allows us to accommodate different physical mechanisms through which energy transfer to electrons can be realized.

5.1 Distribution functions

The dimensionless four-momentum of a photon is $\underline{x} = \{x, \boldsymbol{x}\} = x\{1, \boldsymbol{\omega}\}$, where $\boldsymbol{\omega}$ is the unit vector in the photon propagation direction and $x \equiv h\nu/m_e c^2$. The photon distribution can be described by the occupation number $\tilde{n}_{\rm ph}$ or by the photon number density per linear and logarithmic interval of photon energy:

$$N_{\rm ph} = \int N_{\rm ph}(x)\, dx = \int n_{\rm ph}(x)\, d\ln x = \frac{2}{\lambda_{\rm C}^3} \int d^2\omega \int \tilde{n}_{\rm ph}(\boldsymbol{x})\, x^2\, dx, \qquad (5.1)$$

where $\lambda_{\rm C} = h/m_e c$ is the Compton wavelength. Functions $N_{\rm ph}(x)$ and $\tilde{n}_{\rm ph}$ are used in general forms of kinetic equations and $n_{\rm ph}(x)$ is convenient for numerical work.

The dimensionless electron (positron) four-momentum is defined as $\underline{p} = \{\gamma, \boldsymbol{p}\}$ $= \{\gamma, p\boldsymbol{\Omega}\} = \gamma\{1, \beta\boldsymbol{\Omega}\}$, where $\boldsymbol{\Omega}$ is the unit vector in the electron propagation di-

rection, γ, β, and $p = \beta\gamma = \sqrt{\gamma^2 - 1}$ are the electron Lorentz factor, dimensionless velocity and momentum, respectively. We can use subscripts + and − to distinguish between positrons and electrons. The electron/positron distributions can be defined in a number of alternative ways (normalized to their number density):

$$N_\pm = \int N_\pm(\gamma) d\gamma = \int n_\pm(p)\, d\ln p = \frac{2}{\lambda_{\rm C}^3} \int d^2\Omega \int \tilde{n}_\pm(\boldsymbol{p})\, p^2 dp. \tag{5.2}$$

The occupation number $\tilde{n}_\pm(p)$ and the density per unit Lorentz factor are useful quantities used in general kinetic equations, while the electron density per logarithmic momentum interval $n_\pm(p)$ is more appropriate for numerical work. For the processes, where the distinction between electrons and positrons is unnecessary, we use the sum of the distributions, for example, $n_{\rm e} = n_- + n_+$.

5.2 General form of the kinetic equations

The relativistic kinetic equation (RKE) describing the evolution of the occupation number $\tilde{n}_1(\boldsymbol{p}_1)$ of species 1 (electron or photon) as a result of binary collisions can be written in the covariant form (de Groot et al. 1980)

$$\begin{aligned} \underline{p}_1 \cdot \underline{\nabla}\tilde{n}_1(\boldsymbol{p}_1) = \int \frac{d^3p_2}{\epsilon_2}\frac{d^3p_3}{\epsilon_3}\frac{d^3p_4}{\epsilon_4}\delta(\underline{p}_1 + \underline{p}_2 - \underline{p}_3 - \underline{p}_4) W_{12\to34} \\ \times \left[\tilde{n}_3(\boldsymbol{p}_3)\tilde{n}_4(\boldsymbol{p}_4) - \tilde{n}_1(\boldsymbol{p}_1)\tilde{n}_2(\boldsymbol{p}_2)\right], \end{aligned} \tag{5.3}$$

where $\underline{\nabla} = \{\partial/c\partial t, \boldsymbol{\nabla}\}$ is the four-gradient, ϵ_i is the zeroth component of the corresponding four-momentum, and $W_{12\to34} = W_{34\to12}$ is a Lorentz scalar transition rate, which possesses the obvious symmetry. In this equation, the non-linear terms related to fermion degeneracy and induced photon scattering are omitted. As it stands, the right-hand side of equation (5.3) accounts for the rate of one particular process. To determine the full evolution of $\tilde{n}_1$ we should therefore sum up the collisional integrals accounting for all relevant processes.

In the frame where the particle distributions are isotropic (we call this frame E), the kinetic equation can be represented in the form (skipping subscript 1):

$$\frac{\partial\tilde{n}(p)}{\partial t} + \frac{1}{p^2}\frac{\partial}{\partial p}\left\{\dot{\epsilon}\,\epsilon\, p\,\tilde{n}(p) - \frac{1}{2}\frac{\partial}{\partial\epsilon}\left[D(\epsilon)\,\epsilon\, p\,\tilde{n}(p)\right]\right\} = \left.\frac{D\tilde{n}(p)}{Dt}\right|_{\rm coll}, \tag{5.4}$$

where the momentum derivative term accounts for continuous energy gain/loss processes, while the right-hand side contains all discontinuous processes such as scattering, emission, absorption and escape. The quantities $\dot{\epsilon}$ and $D(\epsilon)$ account for systematic particle heating/cooling and diffusion in energy space, respectively. Both are generally energy-dependent for the processes we are considering here. For the following discussion it is convenient to decompose the kinetic equations

in terms of the contributions from different physical processes as

$$\frac{\partial n_{\rm ph}(x)}{\partial t} = \dot{n}_{\rm ph,syn}(x) + \dot{n}_{\rm ph,cs}(x) + \dot{n}_{\rm ph,pp}(x) - \frac{n_{\rm ph}(x)}{t_{\rm esc}} + Q_{\rm ph}, \quad (5.5)$$

$$\frac{\partial n_{\pm}(p)}{\partial t} = \dot{n}_{\pm,\rm syn}(p) + \dot{n}_{\pm,\rm cs}(p) + \dot{n}_{\pm,\rm pp}(p) + \dot{n}_{\pm,\rm Coul}(p) - \frac{n_{\pm}(p)}{t_{\pm,\rm esc}} + Q_{\pm}, \quad (5.6)$$

where syn, cs, pp and Coul stand for synchrotron, Compton scattering, pair production (and annihilation), and Coulomb scattering, respectively. The terms describing physical processes can contain both differential and integral parts, depending on the nature of the process and the way we find most convenient to treat it. Thus the equation for photons has the form:

$$\frac{\partial n_{\rm ph}(x)}{\partial t} = -\frac{\partial}{\partial \ln x}\left[A_{\rm ph}(x) n_{\rm ph}(x) - B_{\rm ph}(x)\frac{\partial n_{\rm ph}(x)}{\partial \ln x}\right] + \int K_{\rm ph}(x, x_1) n_{\rm ph}(x_1)\, d\ln x_1 - \frac{n_{\rm ph}(x)}{t_{\rm ph}} + S_{\rm ph}. \quad (5.7)$$

Here the differential term is responsible for Compton scattering in diffusion approximation, while the integral term with kernel $K_{\rm ph}$ describes scattering that can be resolved on the grid. The sink term $\propto 1/t_{\rm ph}$ describes photon absorption (by synchrotron and pair-production) and scattering as well as the escape, while $S_{\rm ph}$ gives the contribution from pair annihilation, synchrotron emission and other (e.g. blackbody) photon injections.

Similarly, for electrons and positrons we write

$$\frac{\partial n_{\pm}(p)}{\partial t} = -\frac{\partial}{\partial \ln p}\left[A_{\rm e}(p) n_{\pm}(p) - B_{\rm e}(p)\frac{\partial n_{\pm}(p)}{\partial \ln p}\right] + \int K_{\rm e}(p, p_1) n_{\pm}(p_1)\, d\ln p_1 - \frac{n_{\pm}(p)}{t_{\pm}} + S_{\pm}, \quad (5.8)$$

where coefficients $A_{\rm e}$ and $B_{\rm e}$ describe electron cooling, heating and diffusion as a result of synchrotron emission and absorption, Compton scattering in Thomson limit, Coulomb scattering as well as possible diffusive particle acceleration. The integral term with kernel $K_{\rm e}$ describes Compton scattering in Klein-Nishina limit into the bin and the sink term $\propto 1/t_{\pm}$ gives the scattering from the bin as well as the electron escape and pair annihilation. The source term $S_{\pm}$ contains pair production as well as a possible electron injection term.

5.3 Escape probability formalism

As we are studying radiative processes in a simple one-zone framework neglecting the radiative transport effects, we must include an escape term in equation (5.5) to allow for the fact that photons can leave the emission region of finite size R and

produce the radiation flux that is actually observed. The typical escape timescale is usually estimated from random walk arguments resulting in $t_{\rm esc} \sim R(1+\tau_{\rm sc})/c$, where $\tau_{\rm sc}$ is the scattering opacity. Such form accounts for the fact that if multiple scatterings are important ($\tau_{\rm sc} > 1$), photons have to 'diffuse' out of the medium and the escape time is prolonged by a factor $\tau_{\rm sc}$. However, it does not account for the fact that if the medium is absorptive, a typical photon cannot diffuse further than the thermalization length $l_\star = [\alpha_{\rm a}(\alpha_{\rm a}+\alpha_{\rm sc})]^{-1/2}$ before it is destroyed ($\alpha_{\rm a}$ and $\alpha_{\rm sc}$ are extinction coefficients due to absorption and scattering, respectively). To incorporate both effects, we employ the solution of a simple radiative diffusion problem in a sphere of radius R with constant emissivity, absorptivity and monochromatic scattering. The escape timescale is estimated by comparing the emergent flux to the radiation density inside the source. While clearly an oversimplification, such estimation nevertheless has the desired properties mentioned above.

Defining the effective optical thickness of the medium as $\tau^\star = \sqrt{3\tau_{\rm a}(\tau_{\rm a}+\tau_{\rm sc})}$, where $\tau_{\rm a} = \alpha_{\rm a}R$ and $\tau_{\rm sc} = \alpha_{\rm sc}R$ are optical thicknesses due to absorption and scattering, respectively, we find

$$t_{\rm esc} = \frac{2R}{3c}\left\{1+\frac{\sqrt{3}}{2\sqrt{1-\lambda}}\left[\frac{\tau^\star\left(1-{\rm e}^{-2\tau^\star}\right)}{\tau^\star\left(1+{\rm e}^{-2\tau^\star}\right)-\left(1-{\rm e}^{-2\tau^\star}\right)}-\frac{3}{\tau^\star}\right]\right\}, \qquad (5.9)$$

where $\lambda = \alpha_{\rm sc}/(\alpha_{\rm a}+\alpha_{\rm sc})$ is the single-scattering albedo. If the medium is translucent ($\tau^\star \ll 1$), equation (5.9) reduces to a more familiar form

$$t_{\rm esc} = \frac{2R}{3c}\left(1+\frac{3}{10}\tau_{\rm sc}\right). \qquad (5.10)$$

In our simulations, $\alpha_{\rm a}$ includes cyclo-synchrotron absorption and photon-photon pair production, and $\alpha_{\rm sc}$ is the extinction coefficient for Compton scattering.

5.4 Compton scattering

5.4.1 Compton scattering of photons

The explicitly covariant form of RKE for Compton scattering of photons ignoring non-linear terms is (Pomraning 1973; Nagirner & Poutanen 1994)

$$\underline{x}\cdot\underline{\nabla}\tilde{n}_{\rm ph}(\boldsymbol{x}) = \frac{r_{\rm e}^2}{2}\frac{2}{\lambda_{\rm C}^3}\int\frac{d^3p}{\gamma}\frac{d^3p_1}{\gamma_1}\frac{d^3x_1}{x_1}\,\delta(\underline{p}_1+\underline{x}_1-\underline{p}-\underline{x})\,F \times\left[\tilde{n}_{\rm ph}(\boldsymbol{x}_1)\tilde{n}_{\rm e}(\boldsymbol{p}_1)-\tilde{n}_{\rm ph}(\boldsymbol{x})\tilde{n}_{\rm e}(\boldsymbol{p})\right], \qquad (5.11)$$

where $r_{\rm e}$ is the classical electron radius, F is the Klein-Nishina reaction rate (Berestetskii et al. 1982)

$$F = \left(\frac{1}{\xi}-\frac{1}{\xi_1}\right)^2 + 2\left(\frac{1}{\xi}-\frac{1}{\xi_1}\right)+\frac{\xi}{\xi_1}+\frac{\xi_1}{\xi}, \qquad (5.12)$$

and $\xi = \underline{p}_1 \cdot \underline{x}_1 = \underline{p} \cdot \underline{x}$ and $\xi_1 = \underline{p}_1 \cdot \underline{x} = \underline{p} \cdot \underline{x}_1$ are the scalar products of four-vectors.

We assume the existence of a reference frame where the particle and photon distributions are approximately homogeneous and isotropic. Under the spacial homogeneity assumption we can write equation (5.11) as

$$\left.\frac{D\tilde{n}_{\rm ph}(\boldsymbol{x})}{Dt}\right|_{\rm coll,cs} = -c\,\sigma_{\rm T}\,\overline{s}_0(\boldsymbol{x})\,N_{\rm e}\,\tilde{n}_{\rm ph}(\boldsymbol{x}) + c\sigma_{\rm T}N_{\rm e}\frac{1}{x}\int\frac{d^3x_1}{x_1}\,R_{\rm ph}(\boldsymbol{x}_1\to\boldsymbol{x})\,\tilde{n}_{\rm ph}(\boldsymbol{x}_1). \tag{5.13}$$

The scattering cross-section (in units of Thomson cross-section $\sigma_{\rm T}$) is given by

$$\overline{s}_0(\boldsymbol{x}) = \frac{3}{16\pi}\frac{2}{\lambda_{\rm C}^3 N_{\rm e}}\frac{1}{x}\int\frac{d^3p}{\gamma}\frac{d^3p_1}{\gamma_1}\frac{d^3x_1}{x_1}\,\tilde{n}_{\rm e}(\boldsymbol{p})\,F\,\delta(\underline{p}_1+\underline{x}_1-\underline{p}-\underline{x}) \tag{5.14}$$

and the redistribution function is

$$R_{\rm ph}(\boldsymbol{x}_1\to\boldsymbol{x}) = \frac{3}{16\pi}\frac{2}{\lambda_{\rm C}^3 N_{\rm e}}\int\frac{d^3p}{\gamma}\frac{d^3p_1}{\gamma_1}\,\tilde{n}_{\rm e}(\boldsymbol{p}_1)\,F\,\delta(\underline{p}_1+\underline{x}_1-\underline{p}-\underline{x}). \tag{5.15}$$

For isotropic particle distributions in frame E, equation (5.13) can be written as

$$\left.\frac{D\tilde{n}_{\rm ph}(x)}{Dt}\right|_{\rm coll,cs} = -c\,\sigma_{\rm T}\,\overline{s}_0(x)\,N_{\rm e}\,\tilde{n}_{\rm ph}(x) + c\sigma_{\rm T}N_{\rm e}\frac{4\pi}{x}\int x_1 dx_1\,\overline{R}_{\rm ph}(x,x_1)\,\tilde{n}_{\rm ph}(x_1), \tag{5.16}$$

where the redistribution function averaged over the cosine of the scattering angle $\mu = \boldsymbol{x}\cdot\boldsymbol{x}_1/(xx_1) = \boldsymbol{\omega}\cdot\boldsymbol{\omega}_1$ is expressed via an integral over the electron distribution (Nagirner & Poutanen 1994):

$$\overline{R}_{\rm ph}(x,x_1) = \frac{1}{2}\int_{-1}^{1}R_{\rm ph}(\boldsymbol{x}_1\to\boldsymbol{x})\,d\mu = \frac{3}{16}\frac{2}{\lambda_{\rm C}^3 N_{\rm e}}\int_{\gamma_\star(x,x_1)}^{\infty}\overline{R}_{\rm ph}(x,x_1,\gamma_1)\,\tilde{n}_{\rm e}(p_1)\,d\gamma_1. \tag{5.17}$$

Here

$$\overline{R}_{\rm ph}(x,x_1,\gamma_1) = \frac{1}{4\pi^2}\,p_1\int\frac{d^3p}{\gamma}d^2\Omega_1\,d^2\omega_1\,F\,\delta(\underline{p}_1+\underline{x}_1-\underline{p}-\underline{x}), \tag{5.18}$$

and the lower limit of the second integral in equation (5.17) comes from the condition of energy and momentum conservation and is given in Appendix A.6. The integrals in equation (5.18) can be calculated analytically (Brinkmann 1984; Nagirner & Poutanen 1994) to obtain a fully general expression for $\overline{R}_{\rm ph}(x,x_1,\gamma_1)$ valid in all regimes (see Appendix A.8). This is an alternative form of the function derived by Jones (1968).

Since the total number of particles is conserved in Compton scattering, multiplying the right-hand side of equation (5.16) by x^2 integrating over dx must give zero, implying a relation between the redistribution function and the extinction coefficient (Nagirner & Poutanen 1994)

$$\overline{s}_0(x) = \frac{4\pi}{x}\int_0^{\infty}\overline{R}_{\rm ph}(x_1,x)\,x_1\,dx_1\,. \tag{5.19}$$

This can also be inferred directly from the definitions (5.14) and (5.15).

In the kinetic equation (5.5) for the photon density $n_{\rm ph}(x)$ the Compton term is obtained by multiplying equation (5.16) by $8\pi\lambda_{\rm C}^{-3}x^3$.

5.4.2 Compton scattering of electrons and positrons

The description of Compton scattering for electrons and positrons is very similar to that for photons. In the linear approximation the RKE reads

$$\underline{p}\cdot\underline{\nabla}\tilde{n}_{\pm}(\boldsymbol{p}) = \frac{r_{\rm e}^2}{2}\frac{2}{\lambda_{\rm C}^3}\int\frac{d^3x}{x}\frac{d^3x_1}{x_1}\frac{d^3p_1}{\gamma_1}\,\delta(\underline{p}_1+\underline{x}_1-\underline{p}-\underline{x})\,F \times\left[\tilde{n}_{\rm ph}(\boldsymbol{x}_1)\tilde{n}_{\pm}(\boldsymbol{p}_1)-\tilde{n}_{\rm ph}(\boldsymbol{x})\tilde{n}_{\pm}(\boldsymbol{p})\right]. \tag{5.20}$$

Neglecting spatial gradients, equation (5.20) becomes

$$\left.\frac{D\tilde{n}_{\pm}(\boldsymbol{p})}{Dt}\right|_{\rm coll,cs} = -c\,\sigma_{\rm T}\,\overline{s}_0(\boldsymbol{p})\,N_{\rm ph}\,\tilde{n}_{\pm}(\boldsymbol{p}) + c\sigma_{\rm T}N_{\rm ph}\frac{1}{\gamma}\int\frac{d^3p_1}{\gamma_1}\,R_{\rm e}(\boldsymbol{p}_1\to\boldsymbol{p})\,\tilde{n}_{\pm}(\boldsymbol{p}_1), \tag{5.21}$$

where the scattering cross-section for electrons is

$$\overline{s}_0(\boldsymbol{p}) = \frac{3}{16\pi}\frac{2}{\lambda_{\rm C}^3N_{\rm ph}}\frac{1}{\gamma}\int\frac{d^3x}{x}\frac{d^3x_1}{x_1}\frac{d^3p_1}{\gamma_1}\tilde{n}_{\rm ph}(\boldsymbol{x})\,F\,\delta(\underline{p}_1+\underline{x}_1-\underline{p}-\underline{x}) \tag{5.22}$$

and the redistribution function

$$R_{\rm e}(\boldsymbol{p}_1\to\boldsymbol{p}) = \frac{3}{16\pi}\frac{2}{\lambda_{\rm C}^3N_{\rm ph}}\int\frac{d^3x}{x}\frac{d^3x_1}{x_1}\,\tilde{n}_{\rm ph}(\boldsymbol{x}_1)\,F\,\delta(\underline{p}_1+\underline{x}_1-\underline{p}-\underline{x}). \tag{5.23}$$

Making use of the isotropy of the problem, we can rewrite the kinetic equation in frame E for isotropic distribution $\tilde{n}_{\pm}(p)$:

$$\left.\frac{D\tilde{n}_{\pm}(p)}{Dt}\right|_{\rm coll,cs} = -c\,\sigma_{\rm T}\,\overline{s}_0(p)\,N_{\rm ph}\,\tilde{n}_{\pm}(p) + c\sigma_{\rm T}N_{\rm ph}\frac{4\pi}{\gamma}\int p_1 d\gamma_1\,\overline{R}_{\rm e}(p,p_1)\,\tilde{n}_{\pm}(p_1), \tag{5.24}$$

where the electron redistribution function averaged over cosine of the electron scattering angle μ_e is

$$\overline{R}_{\rm e}(p,p_1) = \frac{1}{2}\int_{-1}^{1}R_{\rm e}(\boldsymbol{p}_1\to\boldsymbol{p})\,d\mu_e = \frac{3}{16}\,\frac{2}{\lambda_{\rm C}^3N_{\rm ph}}\int_{x_\star(\gamma,\gamma_1)}^{\infty}\overline{R}_{\rm e}(\gamma,\gamma_1,x_1)\,\tilde{n}_{\rm ph}(x_1)\,dx_1, \tag{5.25}$$

where

$$\overline{R}_{\rm e}(\gamma,\gamma_1,x_1) = \frac{1}{4\pi^2}\,x_1\int\frac{d^3x}{x}d^2\omega_1\,d^2\Omega_1\,F\,\delta(\underline{p}_1+\underline{x}_1-\underline{p}-\underline{x}) \tag{5.26}$$

and

$$x_\star(\gamma,\gamma_1) = [\gamma - \gamma_1 + |p - p_1|]/2. \tag{5.27}$$

The relation between the redistribution function and the extinction coefficient is

$$\overline{s}_0(p) = \frac{4\pi}{\gamma}\int \overline{R}_{\rm e}(p_1, p)\, p_1\, d\gamma_1. \tag{5.28}$$

Not surprisingly, there turns out to be a relation between the quantities $\overline{R}_{\rm ph}$ and $\overline{R}_{\rm e}$ (proved in Appendix A.7), namely

$$pp_1\overline{R}_{\rm e}(\gamma,\gamma_1,x_1) = xx_1\overline{R}_{\rm ph}(x,x_1,\gamma_1), \tag{5.29}$$

together with the energy conservation condition $x + \gamma = x_1 + \gamma_1$. Through equations (5.29) and (5.18) we have a generally valid expression also for $\overline{R}_{\rm e}(\gamma,\gamma_1,x_1)$.

In the kinetic equation (5.6) for the electron and positron densities $n_\pm(p)$ the Compton terms can be obtained by multiplying equation (5.24) by $8\pi\lambda_{\rm C}^{-3}p^3$.

5.5 Photon–photon pair production and pair annihilation

The electron RKE accounting for pair production and annihilation processes can be written as (Nagirner & Loskutov 1999)

$$\begin{aligned}\underline{p}_- \cdot \underline{\nabla}\tilde{n}_-(\boldsymbol{p}_-) = \frac{r_{\rm e}^2}{4}\frac{2}{\lambda_{\rm C}^3}\int \frac{d^3p_+}{\gamma_+}\frac{d^3x_1}{x_1}\frac{d^3x}{x}\,\delta(\underline{p}_- + \underline{p}_+ - \underline{x}_1 - \underline{x})\,F_{\gamma\gamma}\\ \times\left[\tilde{n}_{\rm ph}(\boldsymbol{x}_1)\tilde{n}_{\rm ph}(\boldsymbol{x}) - \tilde{n}_-(\boldsymbol{p}_-)\tilde{n}_+(\boldsymbol{p}_+)\right],\end{aligned} \tag{5.30}$$

where we used subscripts $\mp$ to explicitly show the momenta and the occupation number of electrons and positrons. Assuming homogeneity, we get

$$\left.\frac{D\tilde{n}_-(\boldsymbol{p}_-)}{Dt}\right|_{\rm coll,pp} = -c\,\sigma_{\rm T}\,\overline{s}_{\rm pa}(\boldsymbol{p}_-)\,N_+\,\tilde{n}_-(\boldsymbol{p}_-) + c\,\sigma_{\rm T}\,N_{\rm ph}^2\,\frac{\lambda_{\rm C}^3}{2}\,j_{\rm pp}(\boldsymbol{p}_-), \tag{5.31}$$

where the pair annihilation cross-section (in units of $\sigma_{\rm T}$) is given by

$$\overline{s}_{\rm pa}(\boldsymbol{p}_-) = \frac{3}{32\pi}\frac{2}{\lambda_{\rm C}^3 N_+}\frac{1}{\gamma_-}\int \frac{d^3p_+}{\gamma_+}\frac{d^3x_1}{x_1}\frac{d^3x}{x}\,\tilde{n}_+(\boldsymbol{p}_+)\,F_{\gamma\gamma}\,\delta(\underline{p}_- + \underline{p}_+ - \underline{x}_1 - \underline{x}) \tag{5.32}$$

and the pair-production rate by

$$j_{\rm pp}(\boldsymbol{p}_-) = \frac{3}{32\pi}\left(\frac{2}{\lambda_{\rm C}^3 N_{\rm ph}}\right)^2\frac{1}{\gamma_-}\int \frac{d^3p_+}{\gamma_+}\frac{d^3x_1}{x_1}\frac{d^3x}{x}\,\tilde{n}_{\rm ph}(\boldsymbol{x})\tilde{n}_{\rm ph}(\boldsymbol{x}_1)F_{\gamma\gamma}\delta(\underline{p}_- + \underline{p}_+ - \underline{x}_1 - \underline{x}). \tag{5.33}$$

The relativistically invariant reaction rate $F_{\gamma\gamma}$ is (Berestetskii et al. 1982)

$$F_{\gamma\gamma} = \frac{\xi}{\xi_1} + \frac{\xi_1}{\xi} + 2\left(\frac{1}{\xi} + \frac{1}{\xi_1}\right) - \left(\frac{1}{\xi} + \frac{1}{\xi_1}\right)^2, \tag{5.34}$$

where $\xi = \underline{p}_- \cdot \underline{x} = \underline{p}_+ \cdot \underline{x}_1$ and $\xi_1 = \underline{p}_- \cdot \underline{x}_1 = \underline{p}_+ \cdot \underline{x}$.

Assuming again isotropic particle distributions in frame E, we can write equation (5.33) as

$$j_{\rm pp}(p_-) = 3\pi\left(\frac{2}{\lambda_{\rm C}^3 N_{\rm ph}}\right)^2 \frac{1}{\gamma_- p_-} \int_{x^{(L)}}^{\infty} \tilde{n}_{\rm ph}(x)\, dx \int_{x_1^{(L)}}^{\infty} \tilde{n}_{\rm ph}(x_1)\, dx_1\, R_{\gamma\gamma}(\gamma_-, x, x_1), \tag{5.35}$$

where we have defined

$$R_{\gamma\gamma}(\gamma_-, x, x_1) = \frac{1}{2}\frac{1}{(4\pi)^2} x x_1 p_- \int \frac{d^3p_+}{\gamma_+}\, d^2\omega\, d^2\omega_1\, F_{\gamma\gamma}\, \delta(\underline{p}_- + \underline{p}_+ - \underline{x}_1 - \underline{x}). \tag{5.36}$$

The cross-section becomes

$$\overline{s}_{\rm pa}(p_-) = 4\pi \frac{2}{\lambda_{\rm C}^3 N_+} \int_0^{\infty} p_+^2 dp_+\, \sigma_{\rm pa}(\gamma_+, \gamma_-)\, \tilde{n}_+(p_+), \tag{5.37}$$

where

$$\sigma_{\rm pa}(\gamma_+, \gamma_-) = \frac{3}{8}\frac{1}{(4\pi)^2}\frac{1}{\gamma_-\gamma_+} \int \frac{d^3x_1}{x_1}\frac{d^3x}{x}\, d^2\Omega_+\, F_{\gamma\gamma}\, \delta(\underline{p}_- + \underline{p}_+ - \underline{x}_1 - \underline{x}). \tag{5.38}$$

The treatment of positrons is identical if we switch the subscripts $-$ and $+$ in equations (5.30)–(5.38).

The photon kinetic equation accounting for pair production/annihilation processes is

$$\begin{aligned}\underline{x} \cdot \underline{\nabla}\tilde{n}_{\rm ph}(\boldsymbol{x}) = \frac{r_{\rm e}^2}{2}\frac{2}{\lambda_{\rm C}^3} \int \frac{d^3x_1}{x_1}\frac{d^3p_-}{\gamma_-}\frac{d^3p_+}{\gamma_+}\, \delta(\underline{p}_- + \underline{p}_+ - \underline{x}_1 - \underline{x})\, F_{\gamma\gamma} \\ \times \left[\tilde{n}_-(\boldsymbol{p}_-)\tilde{n}_+(\boldsymbol{p}_+) - \tilde{n}_{\rm ph}(\boldsymbol{x}_1)\tilde{n}_{\rm ph}(\boldsymbol{x})\right].\end{aligned} \tag{5.39}$$

Neglecting the spatial derivatives in the left hand side, this becomes

$$\left.\frac{D\tilde{n}_{\rm ph}(\boldsymbol{x})}{Dt}\right|_{\rm coll,pp} = -c\,\sigma_{\rm T}\,\overline{s}_{\rm pp}(\boldsymbol{x})\,N_{\rm ph}\,\tilde{n}_{\rm ph}(\boldsymbol{x}) + c\,\sigma_{\rm T}\,N_-\,N_+\,\frac{\lambda_{\rm C}^3}{2}\,j_{\rm pa}(\boldsymbol{x}), \tag{5.40}$$

where the pair-production cross-section is

$$\overline{s}_{\rm pp}(\boldsymbol{x}) = \frac{3}{16\pi}\frac{2}{\lambda_{\rm C}^3 N_{\rm ph}}\frac{1}{x} \int \frac{d^3x_1}{x_1}\frac{d^3p_-}{\gamma_-}\frac{d^3p_+}{\gamma_+}\, \tilde{n}_{\rm ph}(\boldsymbol{x}_1)\, F_{\gamma\gamma}\, \delta(\underline{p}_- + \underline{p}_+ - \underline{x}_1 - \underline{x}) \tag{5.41}$$

and the emissivity due to pair annihilation

$$j_{\rm pa}(\boldsymbol{x}) = \frac{3}{16\pi}\left(\frac{2}{\lambda_{\rm C}^3}\right)^2 \frac{1}{N_- N_+}\frac{1}{x}\int \frac{d^3x_1}{x_1}\frac{d^3p_-}{\gamma_-}\frac{d^3p_+}{\gamma_+}\,\tilde{n}_-(\boldsymbol{p}_-)\tilde{n}_+(\boldsymbol{p}_+)F_{\gamma\gamma}\delta(\underline{p}_- + \underline{p}_+ - \underline{x}_1 - \underline{x}). \tag{5.42}$$

Notice that unlike the electron equation, the photon equation is nonlinear owing to the fact that the cross-section (5.41) depends explicitly on the photon distribution.

Under the isotropy assumption equations (5.41) and (5.42) in frame E become

$$j_{\rm pa}(x) = 6\pi\left(\frac{2}{\lambda_{\rm C}^3}\right)^2 \frac{1}{N_- N_+}\frac{1}{x^2}\int_{\gamma_+^{(L)}}^{\infty}\tilde{n}_+(p_+)\,d\gamma_+ \int_{\gamma_-^{(L)}}^{\infty}\tilde{n}_-(p_-)\,d\gamma_- R_{\gamma\gamma}(\gamma_-, x, x_1), \tag{5.43}$$

where we have to substitute $x_1 = \gamma_- + \gamma_+ - x$ from the energy conservation condition, and

$$\overline{s}_{\rm pp}(x) = 4\pi\frac{2}{\lambda_{\rm C}^3 N_{\rm ph}}\int_{1/x}^{\infty} x_1^2 dx_1\,\sigma_{\rm pp}(x, x_1)\,\tilde{n}_{\rm ph}(x_1), \tag{5.44}$$

where

$$\sigma_{\rm pp}(x, x_1) = \frac{3}{4}\frac{1}{(4\pi)^2}\frac{1}{xx_1}\int \frac{d^3p_-}{\gamma_-}\frac{d^3p_+}{\gamma_+}\,d^2\omega_1\,F_{\gamma\gamma}\,\delta(\underline{p}_- + \underline{p}_+ - \underline{x}_1 - \underline{x}). \tag{5.45}$$

Explicit expressions for the rate $R_{\gamma\gamma}(\gamma_-, x, x_1)$ (derived by Svensson 1982, see also Boettcher & Schlickeiser 1997 and Nagirner & Loskutov 1999) and the cross-sections $\sigma_{\rm pa}(\gamma_+, \gamma_-)$, $\sigma_{\rm pp}(x, x_1)$ as well as the lower integration limits in equations (5.35) and (5.43) were given in Chapter 2.

The pair-production terms in equations (5.5) and (5.6) take the form

$$\dot{n}_{\rm ph,pp}(x) = -c\,\alpha_{\rm pp}(x)\,n_{\rm ph}(x) + \epsilon_{\rm pa}(x), \tag{5.46}$$

$$\dot{n}_{\pm,\rm pp}(p_\pm) = -c\,\alpha_{\rm pa}(p_\pm)\,n_\pm(p_\pm) + \epsilon_{\rm pp}(p_\pm). \tag{5.47}$$

By comparing with equations (5.31) and (5.40) we find the absorption coefficients and emissivities to be

$$\alpha_{\rm pp}(x) = \sigma_{\rm T}\,\overline{s}_{\rm pp}(x)\,N_{\rm ph}, \qquad \epsilon_{\rm pa}(x) = 4\pi\,c\,\sigma_{\rm T}\,N_-\,N_+\,x^3\,j_{\rm pa}(x), \tag{5.48}$$

$$\alpha_{\rm pa}(p_\pm) = \sigma_{\rm T}\,\overline{s}_{\rm pa}(p_\pm)\,N_\mp, \qquad \epsilon_{\rm pp}(p_\pm) = 4\pi\,c\,\sigma_{\rm T}\,N_{\rm ph}^2\,p_\pm^3\,j_{\rm pp}(p_\pm). \tag{5.49}$$

5.6 Synchrotron radiation

The kinetic equations describing synchrotron radiation need to be written in frame E, where we assume there is only tangled magnetic field (and no electric field). Using the Einstein coefficients and the cross-sections describing synchrotron emission and absorption (Ghisellini & Svensson 1991), we found in Chapter 3 that the

collision terms for these processes in the electron/positron and photon equations take the form (see also Ochelkov et al. 1979):

$$\left.\frac{D}{Dt}\left[\gamma p\,\tilde{n}_{\pm}(p)\right]\right|_{\rm coll,syn} = \int_0^\infty dx \int_\gamma^\infty d\gamma_1\,\gamma_1 p_1\,\frac{P(x,\gamma_1)}{x}\,\delta(\gamma_1-\gamma-x) \times\left\{\tilde{n}_{\pm}(p_1)\,[1+\tilde{n}_{\rm ph}(x)]-\tilde{n}_{\pm}(p)\,\tilde{n}_{\rm ph}(x)\right\} - \int_0^\infty dx \int_1^\gamma d\gamma_1\,\gamma p\,\frac{P(x,\gamma)}{x}\,\delta(\gamma-\gamma_1-x) \times\left\{\tilde{n}_{\pm}(p)\,[1+\tilde{n}_{\rm ph}(x)]-\tilde{n}_{\pm}(p_1)\,\tilde{n}_{\rm ph}(x)\right\}, \tag{5.50}$$

$$\left.\frac{D}{Dt}\left[x^2\tilde{n}_{\rm ph}(x)\right]\right|_{\rm coll,syn} = \int_1^\infty d\gamma \int_1^\gamma d\gamma_1\,\gamma p\,\frac{P(x,\gamma)}{x}\,\delta(\gamma-\gamma_1-x) \times\left\{\tilde{n}_{\rm e}(p)[1+\tilde{n}_{\rm ph}(x)]-\tilde{n}_{\rm e}(p_1)\tilde{n}_{\rm ph}(x)\right\}. \tag{5.51}$$

Here $P(x,\gamma)$ is the angle-integrated cyclo-synchrotron spectrum of a single electron, normalized to the electron cooling rate:

$$\int_0^\infty P(x,\gamma)\,dx = -\dot{\gamma}_{\rm s} = \frac{4}{3}\frac{\sigma_{\rm T}U_{\rm B}}{m_{\rm e}c}p^2, \tag{5.52}$$

where $U_{\rm B} = B^2/(8\pi)$ is the magnetic energy density. One can readily verify that equations (5.50) conserve the total number of electrons and positrons, and that the total energy is conserved by equations (5.50) and (5.51).

Under the physical conditions that we are interested in, the average energy (or momentum) of an emitted or absorbed photon is much lower than the energy (momentum) of the electron taking part in the process. The standard way is therefore to treat synchrotron processes as continuous cooling or heating for electrons and as an emission or absorption process for photons.

We write the photon terms in the form

$$\left.\frac{D\tilde{n}_{\rm ph}(x)}{Dt}\right|_{\rm coll,syn} = -c\,\alpha_{\rm s}(x)\,\tilde{n}_{\rm ph}(x) + \frac{\lambda_{\rm C}^3}{8\pi}\frac{\epsilon_{\rm s}(x)}{x^3}, \tag{5.53}$$

where $\alpha_{\rm s}$ and $\epsilon_{\rm s}$ are cyclo-synchrotron absorption and emission coefficients, respectively. In the kinetic equation (5.5) for the photon density $n_{\rm ph}(x)$ the corresponding term can be obtained by multiplying equation (5.53) by $8\pi\lambda_{\rm C}^{-3}x^3$:

$$\dot{n}_{\rm ph,syn}(x) = -c\,\alpha_{\rm s}(x)\,n_{\rm ph}(x) + \epsilon_{\rm s}(x). \tag{5.54}$$

The emissivity $\epsilon_{\rm s}$ gives the number of photons emitted per logarithmic dimensionless energy interval $d\ln x$, per unit volume and time and can be identified by comparing the corresponding terms in equations (5.51) and (5.53):

$$\epsilon_{\rm s}(x) = \frac{8\pi}{\lambda_{\rm C}^3}\int P(x,\gamma)\;p^2\tilde{n}_{\rm e}(p)\;dp = \int P(x,\gamma)\;n_{\rm e}(p)\;d\ln p. \tag{5.55}$$

Similarly, by comparing the terms proportional to $\tilde{n}_{\rm ph}$ we identify the absorption coefficient (e.g. Twiss 1958; Rybicki & Lightman 1979):

$$\alpha_{\rm s}(x) = \frac{1}{4\pi c x^3}\int d^3p\,[\tilde{n}_{\rm e}(p_1)-\tilde{n}_{\rm e}(p)]\,P(x,\gamma) = -\frac{1}{c\,x^2}\int \frac{d\tilde{n}_{\rm e}(p)}{dp}P(x,\gamma)\,\gamma p\,dp\,, \tag{5.56}$$

where $p_1 = \sqrt{(\gamma-x)^2-1}$ is the electron momentum corresponding to energy $\gamma_1 = \gamma - x$ and the second expression is obtained by expansion to the first order in $x \ll \gamma$.

In terms of the electron number density $n_{\rm e}(p)$ the absorption coefficient takes the form:

$$\alpha_{\rm s}(x) = \frac{\lambda_{\rm C}^3}{8\pi c}\frac{1}{x^2}\int \frac{\gamma P(x,\gamma)}{p^2}\left[3n_{\rm e}(p) - \frac{dn_{\rm e}(p)}{d\ln p}\right] d\ln p. \tag{5.57}$$

The synchrotron processes for electrons can be treated as continuous using the Fokker-Planck equation. It can be obtained from equation (5.50) employing the delta-function to take the integral over γ_1 and expanding $\gamma_1 p_1\ P(x,\gamma_1)$ and $n_\pm(p_1)$ near p to the second order in the small 'parameter' x. Collecting the terms and finally integrating over the photon energy x we get (see Chapter 3)

$$\frac{\partial}{\partial t}\left[\gamma p\,\tilde{n}_\pm(p)\right] = -\frac{\partial}{\partial\gamma}\left[\dot{\gamma}_{\rm s}\,\gamma p\,\tilde{n}_\pm(p) - H(p)\,\gamma p\,\frac{\partial\tilde{n}_\pm(p)}{\partial\gamma}\right] + \frac{1}{2}\frac{\partial^2}{\partial\gamma^2}\left[H_0(p)\,\gamma p\,\tilde{n}_\pm(p)\right], \tag{5.58}$$

where

$$\begin{aligned} H(p) &= \int P(x,\gamma)\,\tilde{n}_{\rm ph}(x)\,x\,dx = \frac{\lambda_{\rm C}^3}{8\pi}\int\frac{P(x,\gamma)}{x}\,n_{\rm ph}(x)\,d\ln x,\\ H_0(p) &= \int P(x,\gamma)\,x\,dx. \end{aligned} \tag{5.59}$$

To get the total electron energy gain/loss rate, one has to multiply equation (5.58) by $8\pi\lambda_{\rm C}^{-3}\gamma\,d\gamma$ and integrate. Multiplying equation (5.53) by $8\pi\lambda_{\rm C}^{-3}x^3dx$ and integrating gives the corresponding rate for photons. Using expressions (5.52), (5.55), (5.56) and (5.59), we can verify that energy conservation is maintained when switching from equation (5.50) to the continuous approximation (5.58).

The last term on the right-hand side of equation (5.58) corresponds to diffusion due to spontaneous emission. However, as was discussed in Chapter 3, it is expected to be negligible compared to the other terms in most cases. Therefore, we neglect the term with H_0 in our simulations. Thus, for the distributions $n_\pm(p)$, equation (5.58) takes the form

$$\dot{n}_{\pm,{\rm syn}}(p) = -\frac{\partial}{\partial\ln p}\left[A_{\rm e,syn}(p)n_\pm(p) - B_{\rm e,syn}(p)\frac{\partial n_\pm(p)}{\partial\ln p}\right], \tag{5.60}$$

where

$$A_{\rm e,syn}(p) = \left(\dot{\gamma}_{\rm s} + 3\frac{\gamma}{p^2}H(p)\right)\frac{\gamma}{p^2}, \qquad B_{\rm e,syn}(p) = H(p)\frac{\gamma^2}{p^4}. \tag{5.61}$$

It is worth mentioning here that other emission/absorption processes, e.g. bremsstrahlung, can be implemented analogously to the synchrotron radiation, once the emissivity function of a single electron $P(x, \gamma)$ (which now may depend on the particle distribution) is specified.

5.7 Coulomb collisions

The RKE accounting for electron (positron) evolution due to Coulomb scatterings is (see Chapter 4)

$$\underline{p} \cdot \underline{\nabla} \tilde{n}_{\pm}(\boldsymbol{p}) = r_{\rm e}^2 \frac{2}{\lambda_{\rm C}^3} \int \frac{d^3p_1}{\gamma_1} \frac{d^3p_1'}{\gamma_1'} \frac{d^3p'}{\gamma'} \, \delta(\underline{p}_1 + \underline{p} - \underline{p}_1' - \underline{p}') \, F_{\rm Coul} \times \left[\tilde{n}_{\rm e}(\boldsymbol{p}_1') \tilde{n}_{\pm}(\boldsymbol{p}') - \tilde{n}_{\rm e}(\boldsymbol{p}_1) \tilde{n}_{\pm}(\boldsymbol{p}) \right] . \tag{5.62}$$

The invariant reaction rate for Møller scattering (i.e. e^-e^- and e^+e^+) is given by (Berestetskii et al. 1982)

$$F_{\rm Coul} = \left(\frac{\xi_1}{\xi - 1} + \frac{\xi}{\xi_1 - 1} + 1 \right)^2 + \frac{1 - 4\xi\xi_1}{(\xi - 1)(\xi_1 - 1)} + 4 \tag{5.63}$$

and the scalar products of particles' four-momenta are defined as $\xi = \underline{p} \cdot \underline{p}'$ and $\xi_1 = \underline{p}_1 \cdot \underline{p}'$. As discussed by Baring (1987) and Coppi & Blandford (1990), the corresponding rates for Bhabha $e^{\pm}e^{\mp}$ scattering are nearly the same in the small-angle scattering approximation, we therefore do not distinguish between electrons and positrons in these equations.

We saw in Chapter 4 that although the Coulomb process is collisional in nature, it is necessary to treat it in the Fokker-Planck framework, i.e. as a continuous diffusive energy exchange mechanism. This is due to the well-known divergent nature of the Coulomb cross-section for small-angle scatterings with negligible energy exchange per event, while in the parameter regimes we are interested in, a large number of such scatterings dominates the energy gain or loss rate of a particle over a much smaller number of large-angle scatterings. In terms of $n_{\pm}(p)$ the Fokker-Planck equation (4.72) for isotropic particle distributions takes the form

$$\dot{n}_{\pm,\rm Coul}(p) = -\frac{\partial}{\partial \ln p} \left[A_{\rm e,Coul}(p) n_{\pm}(p) - B_{\rm e,Coul}(p) \frac{\partial n_{\pm}(p)}{\partial \ln p} \right] \tag{5.64}$$

with coefficients given by

$$A_{\rm e,Coul}(p) = \frac{\dot{\gamma}_{\rm Coul} \gamma}{p^2} - \frac{\partial}{\partial \gamma} \left(\frac{1}{2} \frac{\gamma D_{\rm Coul}}{p^2} \right), \qquad B_{\rm e,Coul}(p) = \frac{1}{2} \frac{\gamma^2 D_{\rm Coul}}{p^4}. \tag{5.65}$$

The energy exchange rate and the diffusion coefficient can be obtained by calculating the first and second moments of equation (5.62) keeping only small-angle

scatterings and are expressed as integrals over the particle distributions:

$$\dot{\gamma}_{\rm Coul} = \int a(\gamma,\gamma_1)\, n_{\rm e}(p_1)\, d\ln p_1, \qquad D_{\rm Coul}(p) = \int d(\gamma,\gamma_1)\, n_{\rm e}(p_1)\, d\ln p_1. \tag{5.66}$$

The rates $a(\gamma,\gamma_1)$ and $d(\gamma,\gamma_1)$ were given by equations (4.78) and (4.73) in Chapter 4.

Chapter 6

Numerical treatment

We numerically solve the set of coupled integro-differential equations of the general form (5.7)–(5.8). We first define an equally spaced grid in the logarithms of particles' momenta:

$$\ln p_i = \ln p_{\min} + (i-1)\cdot\Delta_p, \quad i \in [1, i_m], \tag{6.1}$$

$$\ln x_l = \ln x_{\min} + (l-1)\cdot\Delta_x, \quad l \in [1, l_m]. \tag{6.2}$$

Writing all differentials and integrals on the finite grids, we get three systems (for photons, electrons and positrons) of linear algebraic equations of the general form

$$\frac{n_i^{k+1} - n_i^k}{\Delta t_k} = \sum_{i'=1}^{i_m} M_{i,i'}^{k+1/2} \cdot \frac{1}{2}\left(n_{i'}^{k+1} + n_{i'}^k\right), \tag{6.3}$$

where Δt_k is the size of the k-th (variable) timestep. Such semi-implicit differencing scheme, where both sides of the equation are centered at timestep $k + 1/2$, is known as the Crank-Nicolson scheme (see e.g. Press et al. 1992). All physics is contained within the matrix $M_{i,i'}$, which can be explicitly calculated at each step. The systems of equations for all types of particles are solved stepwise, alternating between equations and requiring a matrix inversion at every step. After solving a set of equations for photons, the updated photon distribution is used to calculate matrix M for electron and positron equations. Then we solve for distributions of electrons/positrons and substitute it to the photon equation and so on.

6.1 The Chang and Cooper scheme

The matrix $M_{i,i'}$ of the linear system can be decomposed into two parts arising from the differential and integral terms in equations (5.7)–(5.8). The differential part contributes a tridiagonal matrix, the form of the equation (e.g. for electrons), giving rise to it, is

$$\frac{n_i^{k+1} - n_i^k}{\Delta t_k} = -\frac{1}{\Delta_p}\left[F_{i+1/2}^{k+1/2} - F_{i-1/2}^{k+1/2}\right], \tag{6.4}$$

where the momentum space flux is given by

$$F_{i+1/2}^{k+1/2} = A_{i+1/2}^{k+1/2}\, n_{i+1/2}^{k+1/2} - B_{i+1/2}^{k+1/2}\, \frac{n_{i+1}^{k+1/2} - n_i^{k+1/2}}{\Delta_p}. \tag{6.5}$$

The distribution function between time gridpoints is defined according to the Crank-Nicolson scheme as (omitting the momentum index)

$$n^{k+1/2} = \frac{1}{2}\left(n^{k+1} + n^k\right). \tag{6.6}$$

We also have to somehow define the distribution function between momentum gridpoints. Following Chang & Cooper (1970) we introduce a parameter δ_i so that (now omitting the time index)

$$n_{i+1/2} = (1-\delta_i) n_{i+1} + \delta_i n_i, \quad \delta_i \in [0,1]. \tag{6.7}$$

The basic idea of the Chang and Cooper scheme is to employ this parameter to ensure that the differencing scheme converges to the correct equilibrium solution independently of the size of the gridstep Δ_p. Assuming that the momentum space flux through the boundaries vanishes, the equilibrium solution tells us that it must vanish everywhere, i.e. $F = 0$. From equations (6.5) and (6.7) we then have

$$\frac{n_{i+1}}{n_i} = \frac{\delta_i\, A_{i+1/2}\, \Delta_p + B_{i+1/2}}{B_{i+1/2} - (1-\delta_i)\, A_{i+1/2}\, \Delta_p}, \tag{6.8}$$

while the exact solution gives (Chang & Cooper 1970)

$$\frac{n_{i+1}}{n_i} = \exp\left[\frac{A_{i+1/2}}{B_{i+1/2}}\Delta_p\right]. \tag{6.9}$$

We can see that using either centered-differencing ($\delta = 1/2$) or forward differencing $\delta = 0$, equations (6.8) and (6.9) agree only to the first order in $A\,\Delta_p/B$. To make the correspondence exact, one has to equate the two equations and solve for δ_i, to get

$$\delta_i = \frac{1}{w_i} - \frac{1}{\exp(w_i) - 1}, \qquad w_i = -\frac{A_{i+1/2}}{B_{i+1/2}}\,\Delta_p. \tag{6.10}$$

Aside from converging to the correct equilibrium solution, such choice of δ_i also guarantees positive spectra, as shown by Chang & Cooper (1970). Although this method applies to purely differential equations, we can still use it in our integro-differential equations to ensure that the differential part *tends* toward its own correct equilibrium solution, which would also be the correct solution for the full equation in the region where the differential terms happen to dominate.

6.2 Treatment of Compton scattering

Accurate numerical treatment of Compton scattering over a wide range of energies is not straightforward. This is caused by the well-known fact that at different energies the process takes place in different regimes. If the energy of a photon in electron rest frame is much smaller than the electron rest energy, the process takes place in the Thomson regime and the electron loses a very small amount of its energy in one scattering. Correspondingly, there is a sharp peak in the electron redistribution function R_e near $p = p_1$. We cannot therefore numerically resolve R_e on our finite grid and have to treat the energy loss process as continuous. On the other hand, for scattering in the Klein-Nishina regime the electron can lose a significant amount of its energy in one scattering. Wishing to include both regimes, we need a way to switch from the continuous approximation (implying a differential equation) to direct calculation of scattering through the integral terms. Similar treatment is required for photons, although the continuous approximation is only needed in the regime where the photon energy is much lower than the electron rest energy and the electron is non-relativistic.

6.2.1 Scattering of electrons: separation of regimes

Let us first look at the electron redistribution function (5.25). We wish to know what is the lowest incoming photon energy $x_\star^\pm(p_1)$ that can cause a shift in electron momentum p_1 by $|\Delta \ln p|$. This energy is related to the lower limit (5.27) of the integral in equation (5.25). If the shift is small enough, we can write

$$x_\star^\pm(p_1) \approx x_\star(\gamma, \gamma_1) = \frac{1}{2}\left(\pm|\Delta\gamma| + |\Delta p|\right) \approx \frac{1}{2} p_1 \,|\Delta \ln p_1| \left(1 \pm \frac{p_1}{\gamma_1}\right), \qquad (6.11)$$

where we have used $p\,dp = \gamma\,d\gamma$. The plus sign applies when the electron gains energy and the minus when it loses it. We see that for high energy electrons, the minimum energy of photons for which we can resolve up- or downscattering is vastly different. However, since the upscattering (energy increase) of relativistic electrons is extremely inefficient, we concern ourselves only with being able to resolve their downscattering (i.e. cooling) and so use the minus sign in equation (6.11). Choosing $|\Delta \ln p_1|$ comparable to our grid step (we use somewhat arbitrarily $3\Delta_p$) in the electron equation, we then state that scattering of electrons on photons with $x_1 < x_\star^-(p_1)$ cannot be resolved.

We now split the redistribution function into two parts according to whether we can or cannot resolve it on our grid

$$\overline{R}_\mathrm{e}(p, p_1) = \overline{R}_\mathrm{e}^{<}(p, p_1) + \overline{R}_\mathrm{e}^{>}(p, p_1), \qquad (6.12)$$

where for the first term the integral in equation (5.25) is taken over $x_1 < x_\star^-(p_1)$, and the second term is defined by integrating over the remaining x_1. To totally

isolate scatterings that undergo on photons with energies below and above $x_\star^-$, we have to write the extinction coefficient as an analogous sum, $\overline{s}_0(p) = \overline{s}_0^<(p) + \overline{s}_0^>(p)$, where

$$\overline{s}_0^{\lessgtr}(p) = \frac{4\pi}{\gamma} \int \overline{R}_\mathrm{e}^{\lessgtr}(p_1, p)\; p_1\, d\gamma_1 \;, \tag{6.13}$$

in accordance with equation (5.28). For the terms containing $\overline{R}_\mathrm{e}^>$ and $\overline{s}_0^>$ in the electron equation, we compute the integrals through the discrete sums, but the terms containing $\overline{R}_\mathrm{e}^<$ and $\overline{s}_0^<$ have to be accounted for by continuous energy exchange terms in the equation. Since we also want to treat thermalization by Compton scattering, these terms have to contain a second order derivative of the electron distribution (a diffusive term). Therefore, we take the standard form of the Fokker-Planck equation

$$\dot{N}_{\pm,\mathrm{diff,cs}}(\gamma) = -\frac{\partial}{\partial\gamma}\left\{\dot{\gamma}_\mathrm{c}\, N_\pm(\gamma) - \frac{1}{2}\frac{\partial}{\partial\gamma}\left[D_\mathrm{e}(\gamma)\, N_\pm(\gamma)\right]\right\}, \tag{6.14}$$

while the exact equation for the (<) terms comes from equation (5.24), written here for $N_\pm(\gamma)$

$$\dot{N}^<_{\pm,\mathrm{coll,cs}}(\gamma) = -c\,\sigma_\mathrm{T}\,\overline{s}_0^<(p)\; N_\mathrm{ph}\, N_\pm(\gamma) + 4\pi\, c\,\sigma_\mathrm{T} N_\mathrm{ph}\, p \int \frac{d\gamma_1}{\gamma_1}\,\overline{R}_\mathrm{e}^<(p, p_1)\, N_\pm(\gamma_1). \tag{6.15}$$

In order to make a physically sensible correspondence between these two representations, we demand that the first three moments of equations (6.14) and (6.15) were identical. Substituting equation (6.13) to (6.15) we find

$$\begin{aligned}
&\int \dot{N}^<_{\pm,\mathrm{coll,cs}}(\gamma)\gamma^i d\gamma \\
&= 4\pi\, c\,\sigma_\mathrm{T} N_\mathrm{ph} \int d\gamma \int d\gamma_1\, \gamma^i \left\{-\frac{p_1}{\gamma}\,\overline{R}_\mathrm{e}^<(p_1, p)\, N_\pm(\gamma) + \frac{p}{\gamma_1}\,\overline{R}_\mathrm{e}^<(p, p_1)\, N_\pm(\gamma_1)\right\} \\
&= 4\pi\, c\,\sigma_\mathrm{T} N_\mathrm{ph} \int d\gamma \int d\gamma_1 \frac{p_1}{\gamma}\left(\gamma_1^i - \gamma^i\right)\overline{R}_\mathrm{e}^<(p_1, p)\, N_\pm(\gamma) \\
&= c\,\sigma_\mathrm{T} N_\mathrm{ph} \int d\gamma\, \overline{(\gamma_1^i - \gamma^i)}\,\overline{s}_0^<(p)\, N_\pm(\gamma)\,,
\end{aligned} \tag{6.16}$$

where similarly to the moments of the photon redistribution function (Nagirner & Poutanen 1994), we defined the moments of the electron redistribution function

$$\overline{\gamma_1^i}\,\overline{s}_0^<(p) \equiv \frac{4\pi}{\gamma} \int p_1\gamma_1^i\, d\gamma_1\, \overline{R}_\mathrm{e}^<(p_1, p). \tag{6.17}$$

The zeroth moment (giving zero in the right-hand side of eq. [6.16]) is just a statement of particle number conservation, while the first moment gives the total rate at which the electrons gain (or lose) energy. The moments defined by equation (6.17) can be calculated analytically using the exact Klein-Nishina scattering

cross-section. For photons this was shown by Nagirner & Poutanen (1994), while the extension of these calculations to the electrons is given in Appendix A.9.

The moments of the continuous approximation (6.14) are

$$\int \dot{N}_{\pm,\mathrm{diff,cs}}(\gamma)\, d\gamma = 0, \tag{6.18}$$

$$\int \dot{N}_{\pm,\mathrm{diff,cs}}(\gamma)\, \gamma\, d\gamma = \int \dot{\gamma}_\mathrm{c}\, N_\pm(\gamma)\, d\gamma, \tag{6.19}$$

$$\int \dot{N}_{\pm,\mathrm{diff,cs}}(\gamma)\, \gamma^2\, d\gamma = \int \left[2\gamma\dot{\gamma}_\mathrm{c} + D_\mathrm{e}(\gamma)\right]\, N_\pm(\gamma)\, d\gamma. \tag{6.20}$$

Here we have assumed that the distribution function $N_\pm(\gamma)$ vanishes at the boundaries of integration. Exact correspondence with equation (6.16) can be made if we identify

$$\dot{\gamma}_\mathrm{c} = c\,\sigma_\mathrm{T} N_\mathrm{ph}\, \overline{(\gamma_1 - \gamma)}\, \overline{s}_0^<(p), \qquad D_\mathrm{e}(\gamma) = c\,\sigma_\mathrm{T} N_\mathrm{ph}\, \overline{(\gamma_1 - \gamma)^2}\, \overline{s}_0^<(p), \tag{6.21}$$

while for the zeroth moment the correspondence is automatic. These moments can be computed using equations (A.66) and (A.67) given in Appendix A.9. Finally, we write equation (6.14) through $n_\pm(p)$ and in the form that can be included in the Chang & Cooper differencing scheme together with other terms

$$\dot{n}_{\pm,\mathrm{diff,cs}}(p) = -\frac{\partial}{\partial \ln p}\left[A_\mathrm{e,cs}(p) n_\pm(p) - B_\mathrm{e,cs}(p)\frac{\partial n_\pm(p)}{\partial \ln p}\right], \tag{6.22}$$

where

$$A_\mathrm{e,cs}(p) = \frac{\dot{\gamma}_\mathrm{c}\gamma}{p^2} - \frac{\partial}{\partial\gamma}\left(\frac{1}{2}\frac{\gamma\, D_\mathrm{e}(\gamma)}{p^2}\right), \qquad B_\mathrm{e,cs}(p) = \frac{1}{2}\frac{\gamma^2 D_\mathrm{e}(\gamma)}{p^4}. \tag{6.23}$$

6.2.2 Scattering of photons and three-bin approximation

Insufficient resolution of numerical calculations can become an issue also for the scattering of photons if the electron energies are low enough. A photon will then exchange very little energy with an electron upon scattering and the redistribution function is strongly peaked near $x = x_1$. To overcome this we propose the following approach. We separate scatterings that take place within some narrow interval around the energy of the incoming photon from those invoking photon energy outside this interval. We then approximate the scatterings taking place within the central interval by a continuous process and account for this by differential terms calculated through the exact moments of the redistribution function.

To keep the correspondence to the electron equation, we rewrite the photon evolution equation (5.16) in terms of $N_\mathrm{ph}(x)$:

$$\dot{N}_\mathrm{ph,coll,cs}(x) = 4\pi\, c\,\sigma_\mathrm{T} N_\mathrm{e}\left\{\int_{\notin} dx_1 \left[N_\mathrm{ph}(x_1)\frac{x}{x_1}\overline{R}_\mathrm{ph}(x, x_1) - N_\mathrm{ph}(x)\frac{x_1}{x}\overline{R}_\mathrm{ph}(x_1, x)\right]\right.$$
$$\left. + \int_{\in} dx_1 \left[N_\mathrm{ph}(x_1)\frac{x}{x_1}\overline{R}_\mathrm{ph}(x, x_1) - N_\mathrm{ph}(x)\frac{x_1}{x}\overline{R}_\mathrm{ph}(x_1, x)\right]\right\}, \tag{6.24}$$

where the extinction coefficient is expressed explicitly through $\overline{R}_{\rm ph}$ using equation (5.19). Here $\in$ stands for the interval $[x\mathrm{e}^{-\delta_x}, x\mathrm{e}^{\delta_x}]$ and $\notin$ means integration from 0 to ∞ excluding that interval. The width of the central region ($2\delta_x$ in log units) is somewhat arbitrary, but should include at least a couple of bins, with our choice being three, i.e. $\delta_x = \frac{3}{2}\Delta_x$.

For the second integral in equation (6.24) we wish to write a continuous approximation similar to equation (6.14)

$$\dot{N}_{\rm ph,diff,cs}(x) = -\frac{\partial}{\partial x}\left\{\dot{x}_{\rm c}\, N_{\rm ph}(x) - \frac{1}{2}\frac{\partial}{\partial x}\left[D_{\rm ph}(x)\, N_{\rm ph}(x)\right]\right\}. \tag{6.25}$$

Similarly to what was done for electrons, the coefficients in equation (6.25) are determined from the requirement that the first three moments of the differential and integral equations coincide. The moments of the 'central' part of equation (6.24) (denoted by $\in$) are

$$\int_0^\infty \dot{N}^{\in}_{\rm ph,coll,cs}(x)\, x^i\, dx = 4\pi\, c\, \sigma_{\rm T} N_{\rm e} \int_0^\infty dx \int_\in dx_1\, \left(x_1^i - x^i\right)\, \frac{x_1}{x}\, \overline{R}_{\rm ph}(x_1, x)\, N_{\rm ph}(x), \tag{6.26}$$

where the integration limits for x and x_1 in the first term were switched, because for constant δ_x the area on the (x, x_1) plane is the same. The moments of the differential equation are similar to what were obtained for electrons

$$\int_0^\infty \dot{N}^{\in}_{\rm ph,diff,cs}(x)\, dx = 0, \tag{6.27}$$

$$\int_0^\infty \dot{N}^{\in}_{\rm ph,diff,cs}(x)\, x\, dx = \int_0^\infty \dot{x}_{\rm c}\, N_{\rm ph}(x)\, dx\,, \tag{6.28}$$

$$\int_0^\infty \dot{N}^{\in}_{\rm ph,diff,cs}(x)\, x^2\, dx = \int_0^\infty \left[2x\dot{x}_{\rm c} + D_{\rm ph}(x)\right]\, N_{\rm ph}(x)\, dx. \tag{6.29}$$

Equations (6.26) and (6.27)–(6.29) give identical expressions for the first three moments of the 'central' part of the equation if we identify

$$\begin{aligned} \dot{x}_{\rm c} &= 4\pi\, c\, \sigma_{\rm T} N_{\rm e} \int_\in dx_1\, (x_1 - x)\, \frac{x_1}{x}\, \overline{R}_{\rm ph}(x_1, x), \\ D_{\rm ph}(x) &= 4\pi\, c\, \sigma_{\rm T} N_{\rm e} \int_\in dx_1\, (x_1 - x)^2\, \frac{x_1}{x}\, \overline{R}_{\rm ph}(x_1, x). \end{aligned} \tag{6.30}$$

The 0-th moment is identically zero for both equations (6.26) and (6.27), implying particle conservation.

The integrals in equations (6.30) are computed numerically at a finer grid. At low photon energies, the redistribution function can be narrower than the whole integration interval, and integration can present a problem. In this case, however, we can extend the integration limits in equations (6.30) from 0 to ∞ and to calculate the moments of the redistribution function analytically (Nagirner & Poutanen

1994). Using the limits on $\gamma_\star$, given by equation (A.42) in Appendix A.6, one can show that scattering takes place entirely within the central interval $\in$ for incident photons and electrons satisfying the following relations:

$$x < \frac{\delta_x}{2}, \qquad p < p_\star^-(x) = \frac{\delta_x}{2} - x. \tag{6.31}$$

We can write the moments of the redistribution function in a way similar to equation (6.17):

$$\overline{x_1^i}\,\overline{s}_0^<(x) \equiv \frac{4\pi}{x}\int x_1^{i+1}\,dx_1\,\overline{R}_{\rm ph}^<(x_1,x), \tag{6.32}$$

where the $<$ superscript signifies that only electrons with $p < p_\star^-(x)$ are taken into account. Equations (6.30) then (for $x < \delta_x/2$) become

$$\dot{x}_{\rm c} = c\,\sigma_{\rm T} N_{\rm e}\,\overline{(x_1 - x)}\,\overline{s}_0^<(x), \qquad D_{\rm ph}(x) = c\,\sigma_{\rm T} N_{\rm e}\,\overline{(x_1 - x)^2}\,\overline{s}_0^<(x), \tag{6.33}$$

and can be computed using equations (A.60)–(A.61) in Appendix A.9.

For numerical differencing equation (6.25) has to be written in the form

$$\dot{n}_{\rm ph,diff,cs}(x) = -\frac{\partial}{\partial \ln x}\left[A_{\rm ph,cs}(x) n_{\rm ph}(x) - B_{\rm ph,cs}(x)\frac{\partial n_{\rm ph}(x)}{\partial \ln x}\right], \tag{6.34}$$

where

$$A_{\rm ph,cs}(x) = \frac{\dot{x}_{\rm c}}{x} - \frac{\partial}{\partial x}\left(\frac{1}{2}\frac{D_{\rm ph}(x)}{x}\right), \qquad B_{\rm ph,cs}(x) = \frac{1}{2}\frac{D_{\rm ph}(x)}{x^2}. \tag{6.35}$$

6.3 Pair production and annihilation

The numerical treatment of pair production and annihilation processes in our code is fairly straightforward. The only potential difficulty can arise from the non-linearity of the absorption term in the photon equation. To deal with this we have chosen the simplest possible approach: for calculating the pair-production opacity at each step we simply use the photon distribution from the previous step. The error caused by doing so is not expected to be significant in most cases. It is well-known that a photon of energy x will most efficiently interact with photons of energy $x_1 \approx 3/x$, thus if its energy is not very close to the electron/positron rest energy, the photon will most likely annihilate on another photon of a vastly different energy than its own. Therefore, we can visualize two separate populations of photons that pair-produce on each other, with the dividing energy at $m_{\rm e}c^2$. The photon distribution from the previous step is then taken to be the 'target' population on which the photons that are being evolved pair produce.

Since we wish the numerical scheme to treat electrons and positrons identically (particularly when we are dealing with pure pair plasma), while at each step

one of them has to be evolved first when the outcome of the other is yet unknown, we use a fully implicit scheme for the pair annihilation terms.

The quantities $R_{\gamma\gamma}(\gamma_-, x, x_1)$, $\sigma_{\rm pa}(\gamma_+, \gamma_-)$ and $\sigma_{\rm pp}(x, x_1)$ defined by equations (5.36), (5.38) and (5.45) are precalculated on a fine grid and thereafter averaged within the electron/positron and photon bins used by the code. The integrals in the expressions (5.35), (5.37), (5.43) and (5.44) for emissivities and absorption coefficients are calculated through discrete sums.

6.4 Treatment of synchrotron processes

One of the main difficulties in numerically treating synchrotron processes in compact sources is that the optical thickness of the medium due to self-absorption might become extremely large at low energies compared to, say, Thomson optical thickness. Almost all photons that are produced are immediately absorbed, so very few escape. But the energy which those few carry away comes from the small net energy exchange rate between electrons and photons, which we need to keep track of to maintain the energy balance. Near the equilibrium, in the photon equation we have two large terms describing emission and absorption, which nearly exactly cancel out. A small error in either of them produces a significant error in the total energy transfer rate. In the electron equation this transfer rate is given by the difference in the synchrotron cooling and heating rates. To maintain the energy balance between the two equations, we need to ensure that in our numerical scheme these rates are seen identically by both equations.

In discretized form, the synchrotron processes for electrons/positrons are described by equations (6.4)–(6.5), with $n = n_\pm$, $A = A_{\rm e,syn}$ and $B = B_{\rm e,syn}$. To obtain the total energy gain we have to multiply equation (6.4) by $\gamma_i\,\Delta_p$, sum over i and sum the corresponding terms in the electron and positron equations. Assuming vanishing boundary currents, we have

$$\frac{\Delta E_{\rm e}}{\Delta t_k\,\Delta V} = \sum_{i=1}^{i_m-1} \Delta\gamma_{i+1/2}\left[A_{i+1/2}\; n_{{\rm e},i+1/2} - B_{i+1/2}\frac{n_{{\rm e},i+1} - n_{{\rm e},i}}{\Delta_p}\right], \qquad (6.36)$$

where $\Delta\gamma_{i+1/2} \equiv \gamma_{i+1} - \gamma_i$ and we have omitted the time index $k + 1/2$ for brevity. The exchange rate as seen by the photon equation can be evaluated by writing the integrals in emissivity and absorptivity expressions (5.55) and (5.57) as sums over

the grid, multiplying equation (5.54) by $x_l\,\Delta_x$ and summing over l:

$$\begin{aligned}\frac{\Delta E_{\rm ph}}{\Delta t_k\,\Delta V} &= \sum_{l=1}^{l_m}\Big[-c\,x_l\,\alpha_l\,n_{{\rm ph},\,l}+x_l\,\epsilon_l\Big]\Delta_x\\ &= \frac{\lambda_{\rm C}^3}{8\pi}\sum_{l=1}^{l_m}\left[\frac{n_{{\rm ph},\,l}}{x_l}\,\Delta_x\sum_{i=1}^{i_m}\frac{\gamma_i P_{l,i}}{p_i^2}\Delta_p\left(-3n_{{\rm e},i}+\frac{n_{{\rm e},i+1}-n_{{\rm e},i}}{\Delta_p}\right)\right]\\ &+\sum_{l=1}^{l_m}\left[x_l\,\Delta_x\sum_{i=1}^{i_m}n_{{\rm e},i}\,P_{l,i}\,\Delta_p\right],\end{aligned}$$

where $P_{l,i}=P(x_l,\gamma_i)$. Changing the order of summation, identifying the sum over the photon distribution as the discretized version of the definition $H(p)$, and noticing that $\sum_l P_{l,i}x_l\Delta_x$ gives the electron cooling rate $-\dot\gamma_{{\rm s},i}$, we get:

$$\frac{\Delta E_{\rm ph}}{\Delta t_k\,\Delta V}=\sum_{i=1}^{i_m}\Delta_p\left[-\left(\dot\gamma_{{\rm s},i}+\frac{3\gamma_i H_i}{p_i^2}\right)n_{{\rm e},\,i}+\frac{\gamma_i H_i}{p_i^2}\frac{n_{{\rm e},\,i+1}-n_{{\rm e},\,i}}{\Delta_p}\right]. \tag{6.37}$$

To make equations (6.36) and (6.37) identical (except for the sign) we have to make subtle changes in the definition of coefficients and the way integrals are numerically calculated. In equation (6.37) we have to define the coefficients in between the electron momentum gridpoints, at $i+1/2$, substitute the electron distribution $n_{{\rm e},\,i}$ by $n_{{\rm e},\,i+1/2}$ (except in the derivative term), where the latter is calculated using the same Chang & Cooper coefficients δ_i as in the electron equation, and sum up to $i=i_m-1$ instead of i_m. This amounts to defining the emission and absorption coefficients as

$$\begin{aligned}\epsilon_l &= \sum_{i=1}^{i_m-1}P_{l,i+1/2}\,n_{{\rm e},\,i+1/2}\,\Delta_p,\\ \alpha_l &= \frac{\lambda_{\rm C}^3}{8\pi}\frac{1}{x_l^2}\sum_{i=1}^{i_m-1}\frac{\gamma_{i+1/2}\,P_{l,i+1/2}}{p_{i+1/2}^2}\left[3n_{{\rm e},i+1/2}-\frac{n_{{\rm e},i+1}-n_{{\rm e},i}}{\Delta_p}\right]\Delta_p.\end{aligned} \tag{6.38}$$

Also, the coefficients A and B entering the momentum space flux (6.5) and thus also the electron energy exchange rate (6.36) should be written as

$$A_{i+1/2}=\frac{\Delta_p}{\Delta\gamma_{i+1/2}}\left(\dot\gamma_{\rm s}+3\frac{\gamma}{p^2}H\right)_{i+1/2}\quad\text{and}\quad B_{i+1/2}=\frac{\Delta_p}{\Delta\gamma_{i+1/2}}\left(\frac{\gamma}{p^2}H\right)_{i+1/2}, \tag{6.39}$$

which become identical to (5.61) in the limit $\Delta_p\to 0$ and ensure that the energy exchange rates as seen by the electron and photon equations are the same.

The only discrepancy left is that we cannot use the same $n_{\rm ph}^{k+1/2}$ and $n_{\rm e}^{k+1/2}$ in both equations. This is because each of them contains a function n^{k+1}, which, in the equation that we evolve before, is not known for the other type of particle. The solution to this, at least in the average sense, is to regard the time-grids for each equation as shifted by a half timestep. Then n^{k+1} obtained from one equation can be used as $n^{k+1/2}$ in the other and vice versa.

6.5 Coulomb collisions

Coulomb scattering only redistributes the energy between different parts of the lepton population. It is easy to see that the total energy is conserved in the sum of two equations (5.64) for electrons and positrons, provided that $a(\gamma, \gamma_1)$ is antisymmetric, the latter simply reflects the energy conservation in two-body interactions. Similarly to synchrotron, our numerical treatment has to ensure that the conservation is exact, otherwise unphysical runaways can occur near the equilibrium.

The flux in momentum space in equation (6.4) for Coulomb scattering is given by equation (6.5) with coefficients expressed as (see eq. (5.65))

$$A_{i+1/2} = \left(\frac{\dot\gamma\gamma}{p^2}\right)_{i+1/2} - \frac{1}{2\Delta\gamma_{i+1/2}}\left[\left(\frac{\gamma D}{p^2}\right)_{i+1} - \left(\frac{\gamma D}{p^2}\right)_{i}\right], \qquad B_{i+1/2} = \frac{1}{2}\left(\frac{\gamma^2 D}{p^4}\right)_{i+1/2}. \tag{6.40}$$

The total energy exchange rate is identical to equation (6.36) for synchrotron.

Let us now look separately at terms containing $\dot\gamma$ and D. For $\dot\gamma$ we have

$$\left.\frac{\Delta E_\mathrm{e}}{\Delta t_k\,\Delta V}\right|_{\dot\gamma} = \sum_{i=1}^{i_m-1} \Delta\gamma_{i+1/2}\left(\frac{\dot\gamma\gamma}{p^2}\right)_{i+1/2} n_{\mathrm{e},i+1/2}. \tag{6.41}$$

It is now easy to see that this quantity can be made to vanish if we write

$$\dot\gamma_{i+1/2} = \sum_{l=1}^{i_m-1} a(\gamma_{i+1/2}, \gamma_{l+1/2})\, n_{\mathrm{e},l+1/2}\,\Delta_p \quad \text{and} \quad \left(\frac{\dot\gamma\gamma}{p^2}\right)_{i+1/2} \to \dot\gamma_{i+1/2}\frac{\Delta_p}{\Delta\gamma_{i+1/2}}, \tag{6.42}$$

provided that a is antisymmetric. The terms containing $D(\gamma)$ in the energy exchange rate are

$$\left.\frac{\Delta E_\mathrm{e}}{\Delta t_k\,\Delta V}\right|_{D} = -\frac{1}{2}\sum_{i=1}^{i_m-1}\left\{\left[\left(\frac{\gamma D}{p^2}\right)_{i+1} - \left(\frac{\gamma D}{p^2}\right)_{i}\right] n_{\mathrm{e},i+1/2} + \left(\frac{\gamma D}{p^2}\right)_{i+1/2}(n_{\mathrm{e},i+1} - n_{\mathrm{e},i})\right\}, \tag{6.43}$$

where we have redefined the coefficient B as

$$B_{i+1/2} \to \frac{1}{2}\frac{\Delta_p}{\Delta\gamma_{i+1/2}}\left(\frac{\gamma D}{p^2}\right)_{i+1/2}. \tag{6.44}$$

One can see that equation (6.43) has the form of an integral over a full differential and, as such, should vanish provided that $D = 0$ at the boundaries. To ensure this numerically for any electron distribution we write explicitly $n_{\mathrm{e},i+1/2} = (1 - \delta_i)n_{\mathrm{e},i+1} + \delta_i n_{\mathrm{e},i}$ and demand that the coefficient in front of $n_{\mathrm{e},i}$ in equation (6.43) is equal to zero for every i. Rearranging terms, we get

$$\left.\frac{\Delta E_\mathrm{e}}{\Delta t_k\,\Delta V}\right|_{D} = -\frac{1}{2}\sum_{i=2}^{i_m-1} n_{\mathrm{e},i}\left\{\delta_i\left[\left(\frac{\gamma D}{p^2}\right)_{i+1} - \left(\frac{\gamma D}{p^2}\right)_{i}\right] + (1-\delta_{i-1})\left[\left(\frac{\gamma D}{p^2}\right)_{i} - \left(\frac{\gamma D}{p^2}\right)_{i-1}\right] - \left(\frac{\gamma D}{p^2}\right)_{i+1/2} + \left(\frac{\gamma D}{p^2}\right)_{i-1/2}\right\} + n_{\mathrm{e},1}S^- + n_{\mathrm{e},i_m}S^+. \tag{6.45}$$

The expression in the curly brackets is identically zero if we set

$$\left(\frac{\gamma D}{p^2}\right)_{i+1/2} = \delta_i \left(\frac{\gamma D}{p^2}\right)_{i+1} + (1-\delta_i)\left(\frac{\gamma D}{p^2}\right)_i, \tag{6.46}$$

while the boundary terms S^- and S^+ vanish if

$$\left(\frac{\gamma D}{p^2}\right)_1 = 0 \quad \text{and} \quad \left(\frac{\gamma D}{p^2}\right)_{i_m} = 0. \tag{6.47}$$

Using expressions (6.42) in the first term in coefficient A and equations (6.46) and (6.47) in the definition (6.44), we ensure precise energy conservation in the numerical scheme.

Chapter 7

Numerical tests

Our careful treatment of the micro-physical processes makes the code applicable over a wide range of parameter regimes. The current version covers 15 orders of magnitude in photon energy (from 10^{-5} to 10^{10} eV) and 8 orders of magnitude in electron momentum, while there is no fundamental difficulty in extending this range further, e.g. to TeV energies for application to blazars. Energy conservation is achieved to within 1% in the majority of cases. All the rates and cross-sections of different processes have been precalculated once and for all and are read into memory as the code initializes. A typical simulation for 200 grid points in photon energy and electron momentum on a 3 GHz PC running Linux takes between a few minutes and half an hour.

In order to test the performance of our code in different parameter regimes, we have chosen three setups from earlier works and run the code with similar parameters for comparison.

7.1 Non-thermal pair model

As a first test we compare our code to the well-known pair plasma code EQPAIR by Coppi (1992, 1999). EQPAIR also considers an uniform emission region into which high-energy electrons/pairs are injected, mimicking an unspecified acceleration mechanism. Some low-energy photons are also injected, emulating a source of external soft radiation (e.g. accretion disk). The high-energy pairs cool by Compton scattering and Coulomb energy exchange with colder thermal pairs. The Compton upscattered photons can produce electron-positron pairs which then upscatter more photons etc., initiating a pair cascade. Once the pairs cool down to low enough energies, the timescale of the systematic energy losses becomes longer than that of diffusive processes, leading to relaxation into a low-energy thermal distribution. In EQPAIR, Coulomb collisions between particles are assumed to be the thermalizing mechanism. However, the thermalization process is not treated entirely consistently in this code in a sense that there exists only one thermal bin into which particles are put once they have cooled below a certain threshold energy,

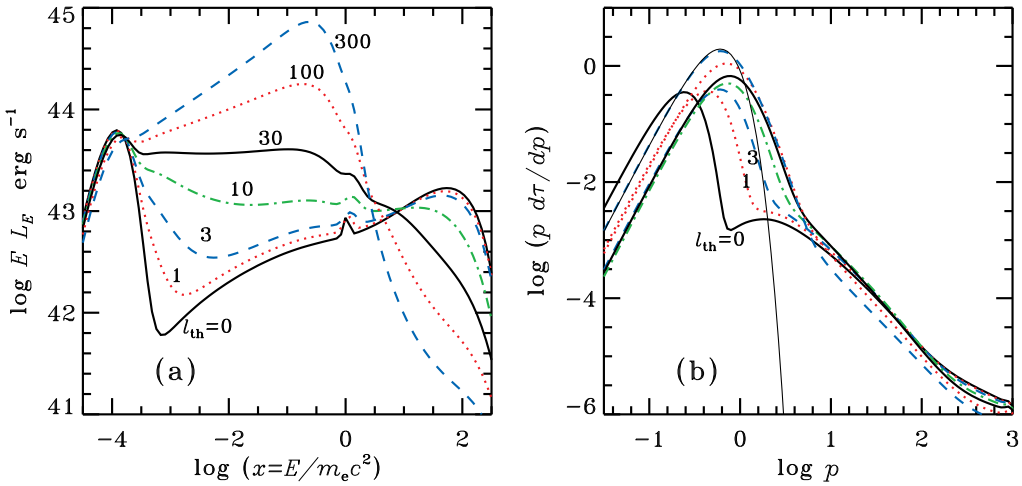

Figure 7.1: Equilibrium (*a*) photon spectra and (*b*) electron distributions (Thomson optical depth per ln p, i.e. $n_{\rm e}(p)\sigma_{\rm T}R$) for various stochastic heating compactnesses $l_{\rm th}$ as labeled. The size of the emission region is $R = 10^{14}$ cm, the soft input radiation has a compactness $l_{\rm s} = 10$ and a blackbody temperature $T_{\rm BB} = 15$ eV, the injection compactness is $l_{\rm nth} = 10$. The thin solid line on the right panel shows a Maxwellian fit of temperature $T_{\rm e} = 53$ keV. Compare to Figure 1 in Coppi (1999).

chosen to be $\gamma = 1.3$. The electron temperature associated with this thermal bin is nevertheless calculated self-consistently from energetic considerations. Furthermore, the code does not consider thermalization by synchrotron self-absorption, which can be an efficient mechanism if the medium is magnetized (Ghisellini et al. 1988, 1998).

The setup of this test run is similar to what was used for Figure 1 in Coppi (1999). We switched off synchrotron processes in our code and left other processes. We inject a Gaussian distribution of pairs centered at $\gamma_{\rm inj} = 10^3$ and a low-energy blackbody distribution of photons. In addition, there is a background electron plasma present with optical depth $\tau_{\rm p} = 0.1$. There is no escape term for pairs, meaning that all injected pairs eventually annihilate transferring their energy to the radiation field. The power injected as non-thermal pairs is parametrized by compactness

$$l_{\rm nth} = \frac{\sigma_{\rm T}}{m_{\rm e}c^3}\frac{L_{\rm nth}}{R}, \tag{7.1}$$

where $L_{\rm nth}$ is the injected luminosity (including rest mass) and R is the linear dimension of the emission region. Similarly, we define the compactness of the injected soft radiation as

$$l_{\rm s} = \frac{\sigma_{\rm T}}{m_{\rm e}c^3}\frac{L_{\rm s}}{R}, \tag{7.2}$$

where L_s is the relevant luminosity. To mimic acceleration with less than 100% efficiency, additional power is supplied to low-energy electrons in the form of continuous heating, parametrized by l_{th}. In Coppi (1999) this energy was just given to the thermal bin, but since we do not have such bin in our code, we need to explicitly specify the form of this heating. This is done by stochastic acceleration prescription of the form

$$\left.\frac{D\tilde{n}_{\pm}(p)}{Dt}\right|_{\text{stoch.}} = \frac{1}{p^2}\frac{\partial}{\partial p}\left[p^2 D_{\text{acc}}(p)\frac{\partial \tilde{n}_{\pm}(p)}{\partial p}\right]. \tag{7.3}$$

The momentum diffusion coefficient is assumed to take the form characteristic of stochastic acceleration by resonant interactions with plasma waves (Dermer et al. 1996), $D_{\text{acc}}(p) \propto p^q$. We have chosen $q = 2$ in our calculations. The mean energy gain rate of a particle resulting from equation (7.3) is

$$\left\langle\frac{d\gamma}{dt}\right\rangle\Bigg|_{\text{stoch.}} = \frac{1}{p^2}\frac{\partial}{\partial p}\left[\beta p^2 D_{\text{acc}}(p)\right], \tag{7.4}$$

where $\beta = p/\gamma$ is the particle speed. We can see that for a power-law diffusion coefficient the gain rate is proportional to p^{q-1} in the relativistic regime, while in the nonrelativistic regime it is proportional to p^q. Our choice $q = 2$ means that at high energies Compton losses always overcome gains by stochastic acceleration, the main effect of the latter process is therefore the heating of low-energy pairs.

The differential term given by equation (7.3) is included in the Chang & Cooper scheme on the same grounds with other continuous terms. Therefore before discretization it has to be written in the form compatible with equations (6.4) and (6.5):

$$\left.\frac{Dn_{\pm}(p)}{Dt}\right|_{\text{stoch.}} = -\frac{\partial}{\partial \ln p}\left\{D_{\text{acc}}(p)\frac{1}{p^2}\left[3n_{\pm}(p) - \frac{\partial n_{\pm}(p)}{\partial \ln p}\right]\right\}. \tag{7.5}$$

The results of the test are shown in Figure 7.1. Varying the amount of stochastic heating (l_{th}) keeping all other parameters constant, we see that we can well reproduce the behavior of the spectrum in Figure 1 in Coppi (1999). Just as expected by Coppi (1999), the equilibrium electron distribution is hybrid: Maxwellian at low energies with a nonthermal high-energy tail. Note that we get such shape even if we switch off Coulomb scattering. The thermal-looking distribution is produced by the stochastic heating itself, which gives a Maxwellian slope at low energies irrespective of the shape of $D_{\text{acc}}(p)$, while the location of the peak of the distribution is determined by the balance between heating and Compton cooling. The behavior of the spectrum in response to varying the power of stochastic heating seen in Figure 7.1(a) was analyzed in detail by Coppi (1999), we are not going to repeat it here.

7.2 Thermalization by synchrotron self-absorption

For the second test, we compared our results with these of Ghisellini et al. (1998) They studied electron thermalization by synchrotron self-absorption in the presence of Compton cooling. The electron cooling, heating and diffusion due to the synchrotron were described by equation (5.58) (without the last term), while Compton scattering was assumed to take place in the Thomson regime and contribute only to systematic cooling. Furthermore, the treatment was not fully self-consistent since only the electron equation was actually solved. While the equilibrium synchrotron spectrum was self-consistently calculated at each timestep from the formal solution of the radiative transfer equation, the Comptonized spectrum was not. Thus only the synchrotron spectrum entered the electron heating rate by self-absorption, while the radiation energy density needed to account for Compton cooling was estimated from energetic considerations.

We ran our code with the same parameters used to obtain the results in Figures 1 and 2 in Ghisellini et al. (1998). The pair production/annihilation and Coulomb scattering have been switched off for this test. High-energy electrons are injected into the emission region, with the total power (including rest mass) parametrized by the injection compactness $l_{\rm nth}$. The magnetic compactness is defined by

$$l_{\rm B} = \frac{\sigma_{\rm T}}{m_{\rm e}c^2} R U_{\rm B}, \tag{7.6}$$

where $U_{\rm B}$ is the magnetic energy density. In addition there is an external source of soft blackbody photons assumed to arise from reprocessing half of the hard radiation by cold matter in the vicinity of the emission region. The electron escape timescale is fixed at $t_{\rm esc} = R/c$.

In the first case the injected electrons have a Gaussian distribution peaking at $\gamma = 10$. The evolution of this distribution is followed in time as it cools and thermalizes by Compton and synchrotron processes. We can see that our results shown in Figure 7.2 are almost identical to those presented in Figure 1 in Ghisellini et al. (1998). However, we would like to stress that we also compute self-consistently the photon spectrum. We see the partially self-absorbed synchrotron bump at small energies, then the blackbody photons and two Compton scattering orders at higher energies.

In the second case we calculated the steady-state particle distributions for different injection compactnesses. The injected electron distribution (per unit $\ln p$) is

$$Q_{\rm e} = Q_0 \frac{p^3}{\gamma^2} \exp\left(-\frac{\gamma}{\gamma_{\rm c}}\right), \tag{7.7}$$

where $\gamma_{\rm c} = 3.33$. The resulting equilibrium electron distributions plotted in Figure 7.3(b) are again very similar to the ones obtained by Ghisellini et al. (1998) in their Figure 2. The corresponding radiation spectra shown in Figure 7.3(a) are computed self-consistently and simultaneously with the electron distribution

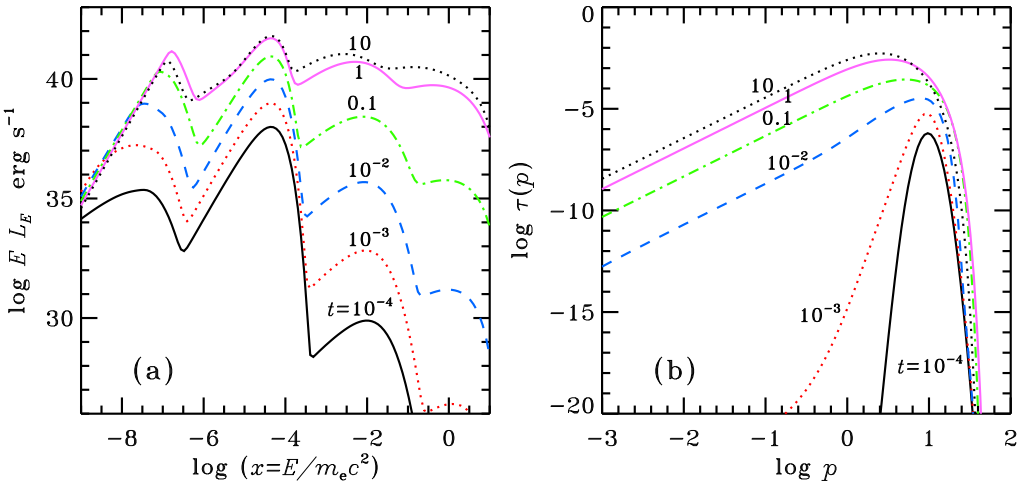

Figure 7.2: Evolving (*a*) photon spectra and (*b*) electron distributions ($\tau(p) = \sigma_{\rm T} R n_{\rm e}(p)/p$) for Gaussian electron injection under action of Compton and synchrotron processes at different times (in R/c units) as labeled. The source size is $R = 10^{13}$ cm, the magnetic compactness is $l_{\rm B} = 10$ and the injection compactness $l_{\rm nth} = 1$. Compare to Figure 1 in Ghisellini et al. (1998).

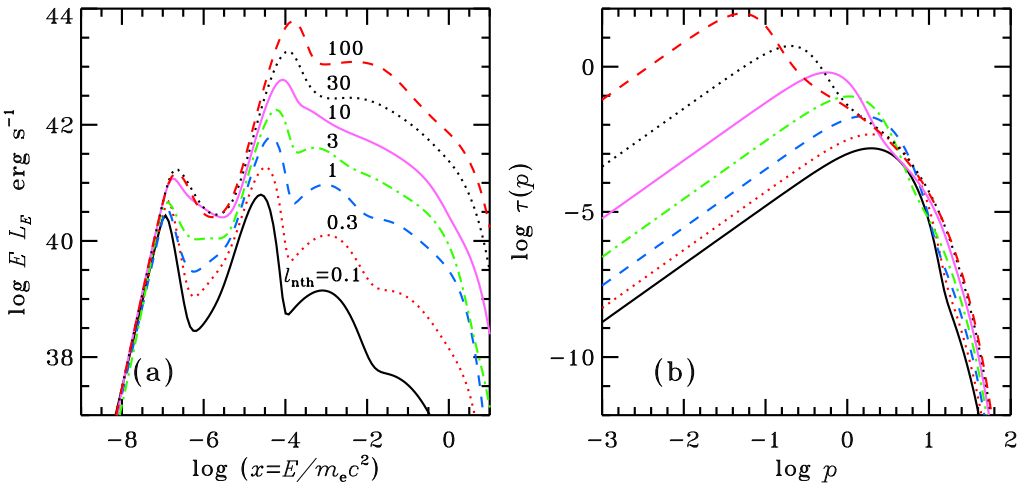

Figure 7.3: Equilibrium (*a*) photon spectra and (*b*) electron distributions for injection (7.7) for various injection compactnesses $l_{\rm nth}$ as labeled. Parameters: $R = 10^{13}$ cm, $l_{\rm B} = 30$. Compare to Figure 2 in Ghisellini et al. (1998).

(while the spectra in Figure 4 of Ghisellini et al. (1998) are calculated a posteriori, i.e. after the equilibrium electron distribution has been determined). As discussed in Ghisellini et al. (1998), if the source is strongly magnetically dominated, the equilibrium distribution is almost purely Maxwellian. When the injection compactness increases, Compton losses become non-negligible and the electrons cool down to lower energies before they have time to thermalize. Notice that at the highest compactness ($l_{\rm nth} = 100$) the temperature of the Maxwellian part of the distribution inferred from Figure 7.3(b) deviates appreciably from the one obtained by Ghisellini et al. (1998). This is caused by the fact that at high compactness a significant fraction of the soft radiation is Compton upscattered to energies comparable to the energies of the Maxwellian electrons. These photons are therefore not effective in cooling the electrons any further. However, in Ghisellini et al. (1998) Compton cooling is accounted for through a term proportional to the radiation energy density, which includes all photons, and therefore overestimates the cooling rate. Overall, the simple prescription for Compton cooling without actually solving the photon equation appears to work well in the parameter regimes considered here.

7.3 Gamma-ray bursts from stochastically heated pairs

Finally, we compare our code to the Large Particle Monte Carlo code by Stern et al. (1995a), with all the processes operating now. The setup is similar to the one used in Stern & Poutanen (2004) for simulating the spectral evolution of gamma-ray bursts. They consider an initially optically thin distribution of electrons in a cylinder-shaped emission region. Arguing that impulsive first-order Fermi acceleration would result in cooling spectra that are too soft to be consistent with observations, energy is instead supplied to the electrons continuously, mimicking dissipation by plasma instabilities behind the shock front. As electrons are heated to relativistic energies in the prescribed background magnetic field, they emit synchrotron radiation, providing seed photons for Compton upscattering. The high-energy upscattered photons then initiate pair-production.

In our simulation we consider a spherical region permeated by magnetic field and start by heating a cold electron distribution (with initial Thomson optical depth $\tau_0 = 6 \times 10^{-4}$) according to the stochastic acceleration prescription (7.5). No pair escape is allowed. The results of simulations are shown in Figure 7.4 and can be compared to a similar Figure 2 in Stern & Poutanen (2004). In both cases the electrons are rapidly heated to about $\gamma \sim 100$, as determined by the balance between stochastic heating and synchrotron cooling. As the photon field builds up, additional cooling by Compton scattering causes the electron 'temperature' to start dropping. After about 1/3 of the light crossing time, the number of photons upscattered to the MeV range becomes large enough to start significant

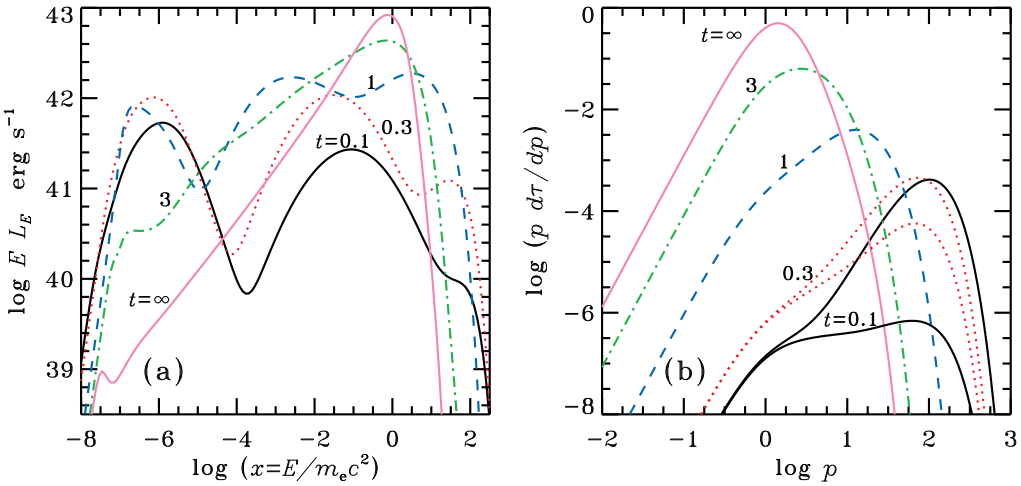

Figure 7.4: Evolving (*a*) photon spectra and (*b*) Thomson optical depth per ln p for stochastically heated pairs at different times (in units R/c) as labeled. Parameters: the source size $R = 10^{13}$ cm, the magnetic compactness $l_{\rm B} = 0.3$, the stochastic heating compactness $l_{\rm th} = 30$, the initial Thomson optical depth of electrons is $\tau_0 = 6 \times 10^{-4}$. For $t = 0.1, 0.3$ we also plot positrons, at later times only the electrons as their opacities are nearly identical. Compare to Figure 2 in Stern & Poutanen (2004).

pair-production. With the increasing pair density (at $t = 1$, opacity has grown by a factor of 20) the available energy per particle decreases, causing a further drop in the temperature of the now almost pure pair plasma. After about ten light-crossing times the Thomson opacity is $\tau_{\rm T} = 1.3$ and the pair density reaches the value where the pair annihilation and creation rates are balanced and a steady state is attained.

The spectral behavior seen in Figure 7.4(a) is similar to what was obtained by Stern & Poutanen (2004). The synchrotron peak rises first, being initially in the optically thin regime and thus following the evolution of the peak of the electron distribution according to $x \propto \gamma^2$. The first Compton scattering order lags slightly behind synchrotron, while the second scattering order is initially in Klein-Nishina regime and thus hardly visible at all. As the electron temperature drops and the peak of the first scattering order evolves to lower energies, the second order shifts to the Thomson regime and becomes comparable to and eventually dominant over the first order. At the same time the decreasing temperature and increasing pair opacity causes the synchrotron emission to switch to optically thick regime and the synchrotron luminosity to drop dramatically. The plasma becomes photon starved and the Comptonized spectrum hardens.

Part III

Astrophysical applications

Chapter 8

Gamma-ray bursts from neutron-loaded flows

Gamma-ray bursts (GRB) are short-lived and extremely powerful events associated with the birth of a compact object that undergoes a brief episode of hyper-accretion and is capable of launching ultra-relativistic jets. If such jet happens to point towards the observer, an intense flash of soft gamma-rays is seen, followed by longer-lasting emission at longer wavelengths (the afterglow).

Apart from the jet launching itself, one of the primary questions in GRB science concerns the way the energy deposited into the flow by the central engine is converted into observable radiation. When the jet is launched, its internal energy strongly dominates over its rest mass energy, which allows it to accelerate to relativistic velocities. If the magnetic field is not dynamically dominant, this energy is in the form of radiation. It is generally assumed that in such case most of the radiation energy is converted to the bulk kinetic energy of the outflow before the latter becomes optically thin and allows the radiation to escape. The question then is how to recover this energy to produce the observed non-thermal emission.

One way of converting ordered bulk motion to random (thermal) motions is through shocks, which take place when the flow encounters slower-moving material. This can occur within the flow itself when a faster-moving shell catches up a slower one (so-called internal shocks) or when the ejecta plough into the interstellar medium (external shocks) (for a review, see Piran 2004). The former is usually thought to be responsible for the prompt emission and the latter for the afterglow. Significant advances have recently been made in simulating the dynamics of relativistic shocks. The latest ab initio particle-in-cell (PIC) simulations now begin to provide answers to long-standing questions like the nature of particle acceleration, generation of the magnetic field, energy exchange between electrons and ions etc. (Spitkovsky 2008a,b).

In spite of these developments, the internal shock model faces several difficulties in trying to explain prompt GRB emission. First is the well-known efficiency problem: since bulk of the GRB energy appears to be released in the prompt phase

(as opposed to the afterglow), a significant fraction of the flow kinetic energy has to be dissipated at this stage. This however requires a large variation of shell Lorentz factors (Beloborodov 2000; Kobayashi & Sari 2001). Another problem concerns the spectra produced in such shocks. It is conventionally assumed that the timescales associated with plasma processes responsible for particle energization near the shock front are significantly shorter than the timescales for radiative losses. It would therefore seem natural to visualize instantaneous injection of high-energy particles into the emission region. However, this approach leads to the problem that the produced spectra (so-called cooling spectra, $F_\nu \propto \nu^{-1/2}$) will be too soft to account for the majority of GRB spectral hardnesses (Preece et al. 2000). Alternatively, hard spectra could be produced if the electrons emit in the slow cooling regime (Panaitescu & Mészáros 2000) which, however, leads to very low radiative efficiency. As another alternative the energy could be shared among a large number of particles and doled out continuously throughout the lifetime of the source. Depending on the optical depth, hard spectra could then be produced by quasi-thermal Comptonization (Ghisellini & Celotti 1999; Stern 1999) or the synchrotron self-Compton mechanism (Stern & Poutanen 2004; Vurm & Poutanen 2009; see also Section 7.3 in the previous chapter).

Problems with spectral hardnesses as well as efficiency can be alleviated by invoking a contribution from an additional thermal radiation component to the observed spectrum (Mészáros & Rees 2000b; Daigne & Mochkovitch 2002). Indeed, such component is a natural ingredient since at the base of the flow the radiation is in thermal equilibrium with matter, in weakly magnetized outflows it also initially carries most of the energy. Although in the majority of cases most of this energy is converted to the kinetic energy of the outflow, some fraction is always left in the radiation field and can be released at the photosphere. Such thermal spectral components have been identified in several bursts (see e.g. Ghirlanda et al. 2003; Ryde 2004, 2005). The inclusion of a photospheric component has two significant advantages: it can accommodate the observed hard slopes below the spectral peak, and it can alleviate the efficiency problem encountered in internal shock models. Furthermore, it can be shown that in case a significant fraction of the flow energy is released as photospheric emission, the spectrum will peak at ~ 1 MeV in the observer frame and is a weak function of the outflow luminosity. If the peak of the gamma-ray spectrum is attributed to the photospheric component, this provides a natural explanation to the observed clustering of GRB peak energies (Preece et al. 2000).

Despite these advantages, it is obvious that the photospheric emission alone is not capable of explaining the prompt GRB emission. The reason is that being a blackbody, it cuts off exponentially above the peak, which is clearly not what is observed in GRB-s whose spectra extend to energies $E \gg E_{peak}$. This extended high-energy emission requires additional dissipation to take place in the flow. Examples of dissipation mechanisms considered in the literature in the context of photospheric models include the aforementioned internal shocks (e.g. Pe'er et al.

2006) and dissipation of magnetic energy (Giannios 2008).

An alternative mechanism of flow enery dissipation was recently proposed by Beloborodov (2010) which does not rely on internal shocks or the poorly understood magnetic dissipation mechanisms. It was argued in Beloborodov (2003b) that when the outflow is launched from the central compact object, it necessarily contains a significant neutron component. If the flow has sufficiently low baryon loading, the protons decouple from neutrons before the jet reaches its terminal Lorentz factor (Derishev et al. 1999b). This happens in jets that get accelerated to $\Gamma \geq 400$ and leads to the formation of a *compound* flow: a slower neutron component embedded in a faster proton flow. It was shown in Beloborodov (2010) that nuclear collisions in such compound flows constitute an efficient mechanism of dissipating the flow energy, capable of reaching a sizable fraction of the total flow luminosity. This occurs through two main branches: (1) inelastic collisions between neutrons and protons can result in pion production, which upon decay ultimately leads to the injection of high-energy electron-positron pairs with Lorentz factor $\gamma \sim 300$, and (2) elastic collisions heat the proton component to relativistic temperatures leading to continuous Coulomb heating of the electron/positron component, which is kept at a much lower temperature by Compton cooling. The energy dissipated by these branches turns out to be about equal. The main advantage of this mechanism lies in the fact that it relies only on well-understood collisional processes, which greatly contributes to the predictive power of the model. This is in contrast with collisionless mechanisms such as shock acceleration and magnetic dissipation, which involve collective plasma interactions and are much less understood.

Regardless of the dissipation mechanism, accurate modeling of the spectral formation in the flow requires a self-consistent solution for the evolution of particle and photon distributions in the dissipation region, which can span several orders of magnitude in radii from the central source. Two basic approaches are available: Monte-Carlo methods (used in e.g. Stern & Poutanen 2004; Beloborodov 2010) in which a sample of interacting particles/photons is followed along the flow, and kinetic treatment where a set of coupled time-dependent integro-differential equations is solved for photon and particle distributions (used in e.g. Pe'er et al. 2006). We will take the kinetic theory approach and will calculate the emission from both non-magnetized and magnetized neutron-loaded flows.

This chapter is organized as follows: In section 8.1 we will give a summary of the physics of relativistic hydrodynamical outflows where the magnetic field is not strong enough to influence the flow dynamics. The model for energy dissipation as well as the simulation setup are described in section 8.2. In section 8.3 we present the results of numerical modeling of non-magnetized and magnetized flows. We will summarize in section 8.4.

8.1 Relativistic fireballs

When the outflow is launched from the central object, its internal energy must strongly dominate over its rest mass energy in order to allow its acceleration to relativistic velocities. If the magnetic field is not strong enough to influence the dynamics of the flow, this internal energy is in the form of radiation, which is strongly coupled to matter due to the huge optical depths involved. Matter and radiation therefore behave like a single fluid, allowing the flow properties to be determined from fluid-dynamical considerations (see e.g. Goodman 1986; Paczynski 1986; Piran et al. 1993). This regime extends out to the radius where the flow becomes optically thin and radiation decouples from matter.

To lay the groundwork for our simulations we will therefore start with an overview of the hydrodynamics of relativistic spherical outflows and derive the scaling laws for comoving energy and number densities. This can be done most elegantly by employing the covariant tensor formalism and writing down conservation laws for the energy-momentum tensor that is valid irrespective of our choice of coordinate system. In what follows we assume that the magnetic field, if present, is not strong enough to significantly influence the dynamics of the flow.

Consider a fluid element moving with a four-velocity U^μ in some freely chosen frame of reference. Its energy-momentum tensor takes the form (Weinberg 1973)

$$T^{\mu\nu} = pg^{\mu\nu} + (p + \rho)\, U^\mu U^\nu, \tag{8.1}$$

where p and ρ are the pressure and total energy density (including the rest mass) of matter and radiation *in the comoving frame* of the fluid element and $g^{\mu\nu}$ is the metric tensor. We adopt a convention where the indices run from 0 to 3 and 0 refers to the temporal coordinate. The energy-momentum tensor satisfies the conservation law (for proof see Weinberg 1973)

$$\frac{DT^{\mu\nu}}{Dx^\nu} \equiv \frac{\partial T^{\mu\nu}}{\partial x^\nu} + \Gamma^\mu_{\lambda\nu} T^{\lambda\nu} + \Gamma^\nu_{\nu\lambda} T^{\mu\lambda} = 0, \tag{8.2}$$

where D/Dx^ν denotes covariant differentiation with respect to the space-time coordinate x^ν and the Christoffel symbols are defined as

$$\Gamma^\mu_{\lambda\nu} = \frac{1}{2} g^{\alpha\mu} \left(\frac{\partial g_{\nu\alpha}}{\partial x^\lambda} + \frac{\partial g_{\lambda\alpha}}{\partial x^\nu} - \frac{\partial g_{\lambda\nu}}{\partial x^\alpha} \right). \tag{8.3}$$

In other words, equation (8.2) states that the covariant divergence of $T^{\mu\nu}$ vanishes.

We can also write down the covariant form of the continuity equation,

$$\frac{D}{Dx^\nu}(nU^\nu) = \frac{\partial}{\partial x^\nu}(nU^\nu) + \Gamma^\nu_{\nu\lambda}\, nU^\lambda = 0, \tag{8.4}$$

where n is the comoving particle number density.

By noting that (Weinberg 1973)

$$\Gamma^{\nu}_{\nu\lambda} = \frac{1}{\sqrt{g}} \frac{\partial}{\partial x^{\lambda}} \sqrt{g}, \tag{8.5}$$

where

$$g \equiv -\text{Det}\, g_{\mu\nu}, \tag{8.6}$$

we can cast the conservation laws given by equations (8.2) and (8.4) in a simpler form

$$\frac{DT^{\mu\nu}}{Dx^{\nu}} = \frac{1}{\sqrt{g}} \frac{\partial}{\partial x^{\nu}} (\sqrt{g}\, T^{\mu\nu}) + \Gamma^{\mu}_{\lambda\nu} T^{\lambda\nu} = 0, \tag{8.7}$$

$$\frac{D}{Dx^{\nu}} (nU^{\nu}) = \frac{1}{\sqrt{g}} \frac{\partial}{\partial x^{\nu}} (\sqrt{g}\, n\, U^{\nu}) = 0. \tag{8.8}$$

Equations (8.7) and (8.8) are the fundamental equations governing the evolution of relativistic non-dissipative hydrodynamic flows and represent the conservation of energy, momentum and particle (in our case baryon) number. In this form they are valid in any coordinate system, rectilinear or curvilinear, and as such, are able to accommodate the effects of curved space-time and thus also General Relativity. We, however, are interested only in special relativistic effects in flat spacetime. The reason for employing such general formalism lies in our desire to determine the relativistically correct scaling laws in a spherically symmetric outflow for which we need to write the conservation laws in a curvilinear (spherical) coordinate system.

Using the usual transformation between the spherical and Cartesian coordinates,

$$\begin{aligned} ct &= ct, \\ x &= r \sin\theta \cos\phi, \\ y &= r \sin\theta \sin\phi, \\ z &= r \cos\theta, \end{aligned} \tag{8.9}$$

we find the covariant metric tensor to be

$$g_{\mu\nu} = \frac{\partial x^{\alpha}}{\partial x'^{\mu}} \frac{\partial x^{\beta}}{\partial x'^{\nu}} \eta_{\alpha\beta} = \begin{pmatrix} -1 & 0 & 0 & 0 \\ 0 & 1 & 0 & 0 \\ 0 & 0 & r^2 & 0 \\ 0 & 0 & 0 & r^2 \sin^2\theta \end{pmatrix}, \tag{8.10}$$

where x'^{μ} refers to the coordinates ct, r, θ and ϕ, and $\eta_{\mu\nu}$ is the Minkowski tensor. In contravariant components the metric becomes

$$g^{\mu\nu} = \begin{pmatrix} -1 & 0 & 0 & 0 \\ 0 & 1 & 0 & 0 \\ 0 & 0 & 1/r^2 & 0 \\ 0 & 0 & 0 & 1/r^2 \sin^2\theta \end{pmatrix}. \tag{8.11}$$

In spherical symmetry the four-velocity of the outflow is $U^{\mu} = \Gamma(1, \overline{\beta}, 0, 0)$, where $\overline{\beta}$ is the radial outflow speed in units of c and Γ is the Lorentz factor. Using this and the contravariant components of the metric tensor given by (8.11), the energy-momentum tensor (8.1) becomes

$$T^{\mu\nu} = \begin{pmatrix} -p + (p+\rho)\Gamma^2 & (p+\rho)\Gamma^2\overline{\beta} & 0 & 0 \\ (p+\rho)\Gamma^2\overline{\beta} & p + (p+\rho)\Gamma^2\overline{\beta}^2 & 0 & 0 \\ 0 & 0 & p/r^2 & 0 \\ 0 & 0 & 0 & p/r^2 \sin^2\theta \end{pmatrix} \tag{8.12}$$

In order to write out the dynamical equations, we need to calculate the Christoffel symbols. The only relevant non-zero components turn out to be

$$\Gamma^1_{22} = -r, \qquad \Gamma^1_{33} = -r\sin^2\theta \quad \text{and} \quad \Gamma^2_{33} = -\sin\theta\cos\theta. \tag{8.13}$$

As one would expect in spherical symmetry, the θ and ϕ ($\mu = 2, 3$) components of the conservation law (8.7) yield trivial results and thus contain no information about the dynamical evolution. The temporal and radial components give

$$\frac{\partial}{c\,\partial t}\left[(p+\rho)\Gamma^2\right] + \frac{1}{r^2}\frac{\partial}{\partial r}\left[r^2(p+\rho)\Gamma^2\overline{\beta}\right] - \frac{\partial p}{c\,\partial t} = 0, \tag{8.14}$$

$$\frac{\partial}{c\,\partial t}\left[(p+\rho)\Gamma^2\overline{\beta}\right] + \frac{1}{r^2}\frac{\partial}{\partial r}\left[r^2(p+\rho)\Gamma^2\overline{\beta}^2\right] + \frac{\partial p}{\partial r} = 0, \tag{8.15}$$

while the continuity equation reads

$$\frac{\partial}{c\,\partial t}(n\Gamma) + \frac{1}{r^2}\frac{\partial}{\partial r}\left(r^2 n\Gamma\overline{\beta}\right) = 0, \tag{8.16}$$

where we have used $g = -\mathrm{Det}\, g_{\mu\nu} = r^4\sin^2\theta$.

To make further progress, we make the assumption that the flow is highly relativistic and each fluid element propagates (nearly) along characteristic world lines described by $ct - r = \text{const}$. Therefore it is natural to make a change of variables $r, t \to r, s = ct - r$ (Piran et al. 1993). The derivatives with respect to ct and r become

$$\frac{\partial}{c\,\partial t} \to \frac{\partial}{\partial s} \quad \text{and} \quad \frac{\partial}{\partial r} \to \frac{\partial}{\partial r} - \frac{\partial}{\partial s}, \tag{8.17}$$

where now the r derivative has to be taken at constant s (along the characteristic). The conservation laws (8.14)-(8.16) take the form

$$\frac{1}{r^2}\frac{\partial}{\partial r}\left[r^2(p+\rho)\,\Gamma^2\overline{\beta}\right] = -\frac{\partial}{\partial s}\left[(p+\rho)\,\frac{\Gamma}{\Gamma+\Gamma\overline{\beta}}\right] + \frac{\partial p}{\partial s}, \tag{8.18}$$

$$\frac{1}{r^2}\frac{\partial}{\partial r}\left[r^2(p+\rho)\,\Gamma^2\overline{\beta}^2\right] = -\frac{\partial}{\partial s}\left[(p+\rho)\,\frac{\Gamma\overline{\beta}}{\Gamma+\Gamma\overline{\beta}}\right] + \frac{\partial p}{\partial s} - \frac{\partial p}{\partial r}, \tag{8.19}$$

$$\frac{1}{r^2}\frac{\partial}{\partial r}\left(r^2 n\,\Gamma\overline{\beta}\right) = -\frac{\partial}{\partial s}\left(\frac{n}{\Gamma+\Gamma\overline{\beta}}\right). \tag{8.20}$$

If $\Gamma \gg 1$ and the flow is not strongly variable, the terms under the differentials on the left hand sides of the equations (8.18)–(8.20) are much larger than those on the right-hand sides. Therefore we can immediately see that the following scalings hold for each fluid element along its trajectory:

$$r^2 n\,\Gamma = \text{constant} \quad \text{and} \quad r^2(p+\rho)\,\Gamma^2 = \text{constant}, \tag{8.21}$$

corresponding to number and momentum conservation, respectively.

Under the assumptions we have made, equations (8.18) and (8.19) seem redundant. To see that this is not true and that equations (8.18)–(8.20) yield another scaling law for internal energy, let us go back to the original conservation law (8.2) for the energy-momentum tensor (8.1) and contract it with U_μ:

$$U_\mu\frac{DT^{\mu\nu}}{Dx^\nu} = U^\nu\frac{Dp}{Dx^\nu} - \frac{D}{Dx^\nu}\left[U^\nu(p+\rho)\right] + (p+\rho)\,U_\mu U^\nu\,\frac{DU^\mu}{Dx^\nu} = 0, \tag{8.22}$$

where we have used the fact that the covariant divergence of the metric tensor vanishes and that $U_\mu U^\mu = -1$. The last term in equation (8.22) vanishes owing to the fact that

$$U_\mu\,\frac{DU^\mu}{Dx^\nu} = \frac{1}{2}\frac{D}{Dx^\nu}\left(U_\mu U^\mu\right) = 0. \tag{8.23}$$

At this point it is convenient to separate the contributions to $p+\rho$ from the rest mass of the matter and the internal energy:

$$p + \rho = p + \rho_{\rm kin} + m_{\rm p}c^2 n, \tag{8.24}$$

where $\rho_{\rm kin}$ refers to the sum of the comoving internal kinetic energy densities of matter and radiation, and the bulk of the rest energy is assumed to be carried by baryons. Inserting (8.24) into equation (8.22) and using the continuity equation (8.8), we immediately see that the term containing n vanishes and we get

$$U_\mu\frac{DT^{\mu\nu}}{Dx^\nu} = U^\nu\frac{\partial p}{\partial x^\nu} - \frac{1}{r^2\sin\theta}\,\frac{\partial}{\partial x^\nu}\left[r^2\sin\theta\;U^\nu(p+\rho_{\rm kin})\right] = 0, \tag{8.25}$$

where x^μ now refer to ct, r, θ and ϕ and we have used equations (8.5) and (8.6) to explicitly write the covariant divergence in spherical coordinates.

To go further we have to specify the equation of state of the fluid. In the typical GRB outflows that we are interested in, by far most of the internal energy is carried by radiation (this statement can be checked a posteriori, i.e. after we have determined all the scaling laws). We therefore have $p = \rho_{\rm kin}/3$ and equation (8.25) becomes

$$U^\nu \frac{\partial \rho_{\rm kin}}{\partial x^\nu} + \frac{4}{3}\rho_{\rm kin} \frac{1}{r^2} \frac{\partial}{\partial x^\nu}\left(r^2 U^\nu\right) = 0, \tag{8.26}$$

which can also be written as

$$\frac{\partial}{\partial x^\nu}\left(r^2 \rho_{\rm kin}^{3/4} U^\nu\right) = 0. \tag{8.27}$$

Note that by cancelling $\sin\theta$ in equation (8.26) we have already implicitly assumed that the poloidal component of U^μ vanishes. Making the transformation $r, ct \rightarrow r, s = ct - r$, the energy equation (8.27) for a radial outflow becomes (Piran et al. 1993)

$$\frac{1}{r^2}\frac{\partial}{\partial r}\left(r^2 \rho_{\rm kin}^{3/4} \Gamma\overline{\beta}\right) = -\frac{\partial}{\partial s}\left(\frac{\rho_{\rm kin}^{3/4}}{\Gamma + \Gamma\overline{\beta}}\right). \tag{8.28}$$

As before, we argue that the term under the differential is significantly larger on the left-hand side than that on the right-hand side for $\Gamma \gg 1$, and we find that the following scaling holds for the internal energy:

$$r^2 \rho_{\rm kin}^{3/4} \Gamma = \text{constant}. \tag{8.29}$$

Looking at the scalings (8.21) and (8.29) we can identify two distinct regimes. If the comoving radiation energy density exceeds the rest energy density of matter, the flow is in the radiation-dominated regime and the scalings become

$$\Gamma \propto r, \quad n \propto r^{-3}, \quad \rho_{\rm kin} \propto r^{-4}, \tag{8.30}$$

while in the opposite case we are in the matter-dominated phase and the scalings read

$$\Gamma = \text{const}, \quad n \propto r^{-2}, \quad \rho_{\rm kin} \propto r^{-8/3}. \tag{8.31}$$

We will use these scaling laws to determine the initial conditions at the start of our simulations, as well as for determining the additional terms in the kinetic equations that need to be included to account for the energy losses due to adiabatic cooling and the decrease of comoving densities in a diverging outflow.

8.2 Physical model and simulation setup

The simulations are set up using the following simple picture: a neutron-loaded fireball is launched from the central source and is accelerated to ultrarelativistic velocities at the expense of its internal energy. As the flow accelerates and expands, its rest mass energy eventually becomes comparable to and then exceeds the internal energy of the fireball, the flow enters a matter-dominated regime and thereafter coasts with a constant Lorentz factor Γ. At some radius $r_{\rm n}$ (to be determined below) the proton and neutron components of the flow decouple from each other, allowing a compound flow to develop (Beloborodov 2010): a slower neutron component inside a faster proton flow. The kinetic energy of the relative motion of the two flows can then be dissipated through elastic and inelastic nuclear collisions. The dissipation is assumed to begin at $r_{\rm n}$, at which point the simulation is started. The simulation is run in the frame comoving with the outflow. We choose and follow a 'representative' element of the flow, self-consistently solving the time-dependent kinetic equations for particles and photons inside this element as it propagates outward along its characteristic world-line. The included physical processes are Compton scattering, cyclo-synchrotron emission and absorption, photon-photon pair production and annihilation and Coulomb collisions. No approximations have been made regarding the relevant rates and cross-sections.

Since we are working with a one-zone kinetic code, the treatment is essentially local. Such simplified approach can be justified by noting that the collisional mechanism described above operates relatively close to the central source, in the range $R_{\rm diss} \sim 10^{11} - 10^{13}$ cm, while for typical burst durations Δt the radiation remains embedded in the flow out to radii $c\,\Delta t\,\Gamma^2 \sim 10^{16}$ cm. This implies that the flow and radiation are essentially moving together throughout the dissipation episode, therefore radius and time can be viewed as equivalent independent variables for describing the problem. It also means that portions of the flow emitted earlier are causally disconnected from those emitted later. Therefore radiative transfer can be regarded as the evolution of the local photon field in the comoving time. Other elements of the flow are expected to undergo the same evolution as a function of their own comoving lifetimes.

The assumption of isotropy of the material and photon fields in the comoving frame (inherent in one-zone treatment) is strictly justified only as long as the flow remains optically thick. After transition to the optically thin regime, the radiation gradually becomes collimated along the radial direction. This is a geometric effect associated with the fact that most of the photons originate from close to the photosphere, which subtends a decreasing angle when viewed from increasing radii. Although this presents a problem to our simulations, we generally do not have to follow the flow to very large radii, owing to the fact that the emerging spectrum is shaped predominantly close to the photosphere where the deviation from isotropy in the comoving frame is not large.

To set up the simulations we will proceed as follows:

(1) Since we are simulating diverging outflows, the code needs to be able to handle expansion related effects such as adiabatic cooling. The additional terms that have to be included in the kinetic equations will be determined in the following subsection.
(2) We will then determine the rates at which energy is dissipated in the flow through heating and injection, using a physical model detailed in Beloborodov (2010).
(3) The initial conditions at the start of the simulations are determined in the framework of the fireball model described above, using the scaling laws (8.30) and (8.31).
(4) Finally, we will describe a simple method to account for the fact that at any given moment the observer will see a superposition of emission originating from different parts of the flow that propagate at various angles to the line of sight, resulting in different Doppler shifts and opacities along different rays.

8.2.1 Implementation of expansion effects

The fluid dynamical treatment described in section (8.1) deals with integrated quantities such as energy density, energy flux and pressure. Furthermore, it assumes that all the components making up the flow are strongly coupled to each other so that matter and radiation behave like a single fluid in local thermodynamical equilibrium. In contrast, we are interested in the *distributions* of particles and photons in energy space, which do not need to take the shape of equilibrium distributions (i.e. Maxwellian and Planck/Bose-Einstein). Also, the spectrum that the observer will see is predominantly shaped close to the photosphere ($\tau \sim 1$), where, by definition, matter and radiation start to decouple from each other. In fact, energy dissipation such as the collisional heating we are discussing here can force matter and radiation out equilibrium already at much higher optical depths than unity. Therefore, the question we need to answer is how to implement the effects like adiabatic losses and dilution of matter and photon number densities obtained from general fluid-dynamical considerations in our kinetic treatment, in a way that would recover the correct scalings for the integrated quantities as well as account for the decoupling of radiation from matter near the photosphere. In what follows we will assume that the flow has reached a matter-dominated stage by the time we start our simulations, so that $\Gamma = \text{const}$.

Let us first consider adiabatic losses. Since we are dealing with arbitrary energy distributions we need to determine the average energy loss rate of particles and photons *of each particular energy*, rather than that of the whole distribution. To do this let's consider a monoenergetic population of N_e electrons with energy γ (in units of $m_\mathrm{e}c^2$) inside a volume V. The total kinetic energy of the electrons is $U = N_\mathrm{e}(\gamma - 1)$, while the pressure is

$$p = \frac{1}{3}\frac{N_\mathrm{e}}{V}\gamma\beta^2 \tag{8.32}$$

The first law of thermodynamics $dU = -p\,dV$ reads

$$N_\mathrm{e}\,d\gamma = -\frac{1}{3}\frac{N_\mathrm{e}}{V}\,\gamma\beta^2\,dV, \tag{8.33}$$

or

$$d\gamma = -\frac{1}{3}\,\gamma\beta^2\,d\ln V. \tag{8.34}$$

Depending on whether the expansion is in 2D or 3D we have $V \propto l^2$ or $V \propto l^3$, respectively, where l is a linear dimension. If the expansion proceeds at a rate dl/dt', where t' is the comoving time, we can define a characteristic expansion timescale

$$t_\mathrm{adiab} \equiv \frac{l}{dl/dt'} = \left(\frac{d\ln l}{dt'}\right)^{-1}. \tag{8.35}$$

Dividing equation (8.34) by dt' and using the definition (8.35), we find

$$\dot\gamma_\mathrm{2D} = -\frac{2}{3}\,\frac{\gamma\beta^2}{t_\mathrm{adiab}} \quad \text{and} \quad \dot\gamma_\mathrm{3D} = -\frac{\gamma\beta^2}{t_\mathrm{adiab}} \tag{8.36}$$

for expansion into 2 or 3 dimensions, respectively. Note that the scaling laws (8.31) imply that the expansion in matter-dominated regime proceeds in two dimensions (since $n \propto r^{-2}$), so we will appropriately use the cooling rate $\dot\gamma_\mathrm{2D}$ in our simulations.

Similar reasoning holds for the photon field, provided that the source is optically thick and the photon gas thus behaves like a fluid. Instead of equation (8.32) we now have

$$p = \frac{1}{3}\frac{N_\mathrm{e}}{V}\,x, \tag{8.37}$$

where x is the photon energy in $m_\mathrm{e}c^2$ units. This leads to cooling rates

$$\dot x_\mathrm{2D} = -\frac{2}{3}\,\frac{x}{t_\mathrm{adiab}} \quad \text{and} \quad \dot x_\mathrm{3D} = -\frac{x}{t_\mathrm{adiab}}. \tag{8.38}$$

In the spherical outflow the comoving linear dimension scales as $l \propto r$, while in matter-dominated regime $r \propto t'$ (since $\Gamma = \text{const.}$) and we can write for adiabatic cooling timescale

$$t_\mathrm{adiab} = \left(\frac{d\ln r}{dt'}\right)^{-1} = \left(\frac{d\ln t'}{dt'}\right)^{-1} = t', \tag{8.39}$$

that is, the adiabatic cooling timescale is equal to the comoving lifetime of the shell element.

Another effect in the expanding flow that we need to account for is the decrease of particle and photon densities over time. As the operating physical processes can create and destroy both photons and particles one cannot just prescribe the dependence of the number densities with radius (i.e. $n \propto r^{-2}$). Instead one can introduce a *rate* at which particles are lost from a unit volume, which we parametrize by "escape" timescale. This is done simply by differentiating the relation $n \propto t'^{-2}$ (2D expansion) to give

$$\frac{dn}{dt'} = -\frac{2n}{t'} \equiv -\frac{n}{t_{\rm esc}}, \tag{8.40}$$

where we have defined $t_{\rm esc} \equiv t'/2$. Here n denotes the comoving number density of either particles or photons. For 3D expansion we have $t_{\rm esc} = t'/3$.

As a consistency check, we note here that if we write the evolution equation of pure adiabatic expansion (say, for photons)

$$\frac{dn(x)}{dt'} = -\frac{\partial}{\partial x}\left[\dot{x}\, n(x)\right] - \frac{n}{t_{\rm esc}}, \tag{8.41}$$

multiply it by particle energy and integrate over all energies, we will recover the proper adiabatic scaling laws given by equations (8.30) and (8.31) for 3D and 2D expansion, $\rho_{\rm kin} \approx u_{\rm rad} \propto r^{-4}$ and $u_{\rm rad} \propto r^{-8/3}$, appropriate for radiation and matter dominated phases, respectively.

The remaining question concerns the criterion to determine whether the photon field is coupled to the electron gas strongly enough to participate in adiabatic cooling. The simplest way of doing this is to consider the number of interactions a photon undergoes during $t_{\rm adiab}$, given by

$$\tau^\star(x) = c\,\alpha\, t_{\rm adiab}, \tag{8.42}$$

where $\alpha(x)$ is the (energy-dependent) extinction coefficient. We then assume that if $\tau^\star > 1$, i.e. a typical photon interacts several times during the typical expansion timescale, the radiation field behaves like a fluid and one has to include cooling rate (8.38) in the kinetic equations. Conversely, if $\tau^\star < 1$, photons are not assumed to be coupled to matter and do not cool upon expansion. A simple prescription to incorporate both regimes in the cooling rate would be

$$\dot{x}_{\rm 2D} = -\frac{2}{3}\,\frac{x}{t_{\rm adiab}}\,\frac{\tau^\star(x)}{1+\tau^\star(x)}. \tag{8.43}$$

8.2.2 Energy dissipation in neutron-loaded flows

We will now give a summary of the mechanisms by which energy can be dissipated in a neutron-loaded flow, following a model by Beloborodov (2010). It was shown in Paczynski (1986) that releasing $\sim 10^{52}$ ergs of energy into a small volume within a couple of seconds leads to a temperature of several MeV at the

central source. At such temperatures ($kT \gtrsim (m_{\rm n} - m_{\rm p})c^2 \approx 1.3\,{\rm MeV}$) neutrons and protons can be converted to each other via $e^{\pm}$ capture reactions

$$e^- + p \rightarrow n + \nu \quad \text{and} \quad e^+ + n \rightarrow p + \overline{\nu}, \tag{8.44}$$

leading to the establishment of a nuclear statistical equilibrium between the two species (Beloborodov 2003b). The flow therefore inevitably carries a significant neutron component. As has been discussed in several works (Derishev et al. 1999a,b; Pruet & Dalal 2002; Beloborodov 2003a), this can have profound observable effects on both prompt and afterglow phases of GRB emission. Here we are focusing on the former, and will see that a significant fraction of the bulk energy can be dissipated in a neutron-loaded flow at the stages when the outflow is still collisional.

The obvious main requirement for collisional dissipation to occur is a non-zero relative velocity between the proton and neutron components of the flow. This can be realized in two ways (Beloborodov 2010): First, internal shocks that develop if the flow is variable do not involve the neutron component, which can penetrate through the shocked gas into the region propagating with a different Lorentz factor (Mészáros & Rees 2000a). Secondly, it was shown in Derishev et al. (1999b) that protons and neutrons in the outflow can decouple before the flow reaches its terminal Lorentz factor if the latter is sufficiently high. Both cases lead to volume dissipation of energy by nuclear collisions in the interpenetrating proton and neutron flows. To keep our model simple and avoid dealing with simulating flows that are still accelerating, we will assume that the decoupling of proton and neutron flows takes place in the matter-dominated phase. We will also not concern ourselves with the details of the development of compound flows and will simply assume that such flow has already been set up at some radius $r_{\rm n}$ where we start the simulation.

It is natural to expect most of the collisional dissipation to take place near the radius where the neutron flow becomes "optically thin" to protons, i.e. $\tau_{\rm n} \lesssim 1$, where

$$\tau_{\rm n} = \int_r^\infty \frac{n_{\rm n}\sigma dr'}{\Gamma_{\rm n}} = \frac{L_{\rm n}\sigma}{4\pi m_{\rm n} c^3 r \Gamma_{\rm n}^3}. \tag{8.45}$$

Here we have defined $\Gamma_{\rm n}$ and $n_{\rm n}$ as the Lorentz factor and comoving number density of the neutron component of the flow, as well as its kinetic luminosity $L_{\rm n} = 4\pi m_{\rm n} c^3 r^2 \Gamma_{\rm n}^2 n_{\rm n}$. The quantity $\sigma \sim 3 \times 10^{-26}\,{\rm cm}^2$ is the effective cross-section for nuclear collisions. At smaller radii (higher optical depths) the neutron and proton flows are still coupled to each other, whereas at larger radii nuclear collisions between neutrons and protons become too infrequent to dissipate significant amount of energy. The number of collisions per unit time between radii r_1 and r_2 is given by

$$4\pi \int_{r_1}^{r_2} \dot{n}_{\rm coll}\, r^2 dr \approx \int_{\tau_{\rm n}(r_1)}^{\tau_{\rm n}(r_2)} \frac{1}{2}\dot{N}_{\rm p} d\tau_{\rm n}, \tag{8.46}$$

where we have introduced the Lorentz invariant collision rate

$$\dot{n}_{\rm coll} \equiv \frac{dN_{\rm coll}}{dVdt} = c\sigma n_{\rm p} n_{\rm n} \Gamma_{\rm rel}, \tag{8.47}$$

where $\Gamma_{\rm rel} \approx \Gamma/2\Gamma_{\rm n}$ is the relative Lorentz factor between the proton and neutron components of the flow. In the last equality in (8.46) we have defined the proton number flux $\dot{N}_{\rm p} = 4\pi c\, r^2 \Gamma n_{\rm p}$ and used equation (8.45). Since dissipated energy is proportional to the number of collisions and $\dot{N}_{\rm p}$ is approximately constant, equation (8.46) confirms the expected result that bulk of the dissipation occurs in regions of the highest $\tau_{\rm n}$ (lowest r) that permits the compound flow to exist, i.e. $\tau_{\rm n} \sim 1$. Therefore we will choose

$$r_{\rm n} = \frac{L_{\rm n}\sigma}{4\pi m_{\rm n} c^3 \Gamma_{\rm n}^3} \tag{8.48}$$

as the starting radius of our simulations.

A collisional encounter between a neutron and a proton can be either elastic or inelastic. Upon an elastic collision the energy gained by a proton is quickly shared with the rest of the flow by Coulomb collisions with other protons. As a result, the proton flow is heated to mildly relativistic temperatures. This thermal energy is then continuously transferred to the lepton component by Coulomb interactions and thereafter to the radiation field by inverse-Compton scattering. The corresponding (volume) dissipation rate in the frame comoving with the proton flow is

$$\dot{Q}_{\rm ep} = \sqrt{\frac{2}{\pi}} \ln\Lambda \, \frac{\sigma_{\rm T}\, m_{\rm e} c^3\, n_{\pm} n_{\rm p} \Theta_{\rm p}}{(\hat{\gamma}-1)(\Theta_{\rm e}+\Theta_{\rm p})^{3/2}}, \tag{8.49}$$

where $n_{\pm}$ is the number density of positrons/electrons, $\Theta_{\rm p} = kT_{\rm p}/m_{\rm p}c^2$, $\Theta_{\rm e} = kT_{\rm e}/m_{\rm e}c^2$, $\ln\Lambda$ is the Coulomb logarithm and $\hat{\gamma}$ if the adiabatic index of the (presumably thermal) proton gas.

In order to assess the amount of energy that is dissipated by Coulomb heating it is more instructive to rewrite equation (8.49) in terms of dissipated energy per baryon (in units of $m_{\rm p}c^2$) over one dynamical timescale $t_{\rm dyn} = r/c\Gamma$

$$\frac{1}{n_{\rm p} m_{\rm p} c^2} \frac{r\dot{Q}_{\rm ep}}{c\Gamma} = \sqrt{\frac{2}{\pi}} \ln\Lambda \, \frac{m_{\rm e}}{m_{\rm p}} \frac{\Theta_{\rm p}\, \tau_{\rm T}}{(\hat{\gamma}-1)(\Theta_{\rm e}+\Theta_{\rm p})^{3/2}}, \tag{8.50}$$

where $\tau_{\rm T} = n_{\pm}\sigma_{\rm T} r/\Gamma$. Plugging in the typical values $\Theta_{\rm p} \sim 1$, $\ln\Lambda \approx 15$, $\hat{\gamma} \approx 1.4$ – 1.5 and assuming $\Theta_{\rm e} \ll \Theta_{\rm p}$ due to strong Compton cooling of electrons/positrons, we find

$$\frac{1}{n_{\rm p} m_{\rm p} c^2} \frac{r\dot{Q}_{\rm ep}}{c\Gamma} \approx 0.015\, \tau_{\rm T}. \tag{8.51}$$

Equation (8.51) tells us the fraction of the flow energy that is dissipated over the timescale of expansion from r to $2r$. Since $\tau_{\rm T} \propto n_{\pm} r \propto r^{-1}$, this once again confirms that most of the collisional heating takes place at small radii.

It was shown by Beloborodov (2010) that shortly after the dissipation starts, the Thomson opacity of the flow is dominated by electrons and positrons generated by non-thermal pair cascades (see below) in pair creation-annihilation balance, rather than by the electrons associated with protons. The typical optical depth at $r_{\rm n}$ is about 20. Using this in equation (8.51) we can see that a significant fraction of the kinetic energy of the flow can be dissipated by collisional heating. One has to keep in mind, however, that the energy dissipated while the flow is still optically thick tends to be converted back to the bulk motion of the flow by adiabatic cooling. To obtain the actual energy in the radiation field at the point when the photons decouple from the flow one has to write the equation accounting for heating as well as adiabatic losses and integrate it from $r_{\rm n}$ to the photospheric radius $r_\star$.

About half of the encounters between protons and neutrons are inelastic (Amsler et al. 2008). In such case the proton and neutron are converted to mildly relativistic pions π^+, π^- and π^0, which promptly decay: $\pi^+ \rightarrow \mu^+ + \nu_\mu$, $\pi^- \rightarrow \mu^- + \overline{\nu}_\mu$ and $\pi^0 \rightarrow \gamma + \gamma$. The muons, in turn, decay through $\mu^+ \rightarrow e^+ + \nu_{\rm e} + \overline{\nu}_\mu$ and $\mu^- \rightarrow e^- + \overline{\nu}_{\rm e} + \nu_\mu$. Altogether, about half of the energy of the inelastic proton-neutron collision is carried away by neutrinos. The other half is converted to several relativistic electrons and positrons with Lorentz factors $\gamma_0 \sim m_\pi/m_{\rm e} \approx 300$. Thus, taking into account both elastic and inelastic collisions, on average about $1/4$ of the collision energy $\Gamma_{\rm rel} m_{\rm p} c^2$ is given to the injected $e^\pm$. The rate of dissipation is therefore

$$\dot{Q}_{\rm inj} = \frac{1}{4} \Gamma_{\rm rel} m_{\rm p} c^2 \dot{n}_{\rm coll}, \tag{8.52}$$

where $\dot{n}_{\rm coll}$ is given by equation (8.47), while the fraction of the flow energy dissipated over one dynamical time becomes

$$\frac{1}{n_{\rm p} m_{\rm p} c^2} \frac{r \dot{Q}_{\rm inj}}{c\Gamma} = \frac{1}{16} \frac{\Gamma}{\Gamma_{\rm n}} \tau_{\rm n}, \tag{8.53}$$

where $\tau_{\rm n} = r_{\rm n}/r$. Equation (8.53) confirms what one would expect intuitively: the rate of energy injection in non-thermal pairs increases with $\tau_{\rm n}$ (larger number of collisions per proton) and $\Gamma/\Gamma_{\rm n}$ (higher relative Lorentz factor between neutrons and protons, i.e. higher collision energy). The non-thermal energy injection rate exhibits the same r^{-1} dependence on radius as the thermal heating rate (8.51), making their ratio fairly constant along the flow.

8.2.3 Initial conditions

In order to use the hydrodynamic scaling laws for determining the initial conditions at the start of simulations, we must first determine the constants of motion

on the right-hand sides of equations (8.21) and (8.29), i.e. we must find C_1, C_2, C_3 in

$$r^2 n\,\Gamma = C_1, \quad r^2\left(\frac{4}{3}\rho_{\rm kin} + m_{\rm p}c^2 n\right)\Gamma^2 = C_2 \quad \text{and} \quad r^{8/3}\rho_{\rm kin}\,\Gamma^{4/3} = C_3. \quad (8.54)$$

The first two are obtained by noticing that they are proportional to the baryon number and total energy fluxes of the flow, respectively. Defining $\dot{N}$ and L as the total (spherical equivalent) number flux and luminosity of the flow and noting that at large radii $m_{\rm p}c^2 n \gg \rho_{\rm kin}$, we have

$$C_1 = \frac{\dot{N}}{4\pi c} \quad \text{and} \quad C_2 = \frac{L}{4\pi c}. \quad (8.55)$$

For determining C_3 we also need to specify the initial size r_0 of the fireball. Assuming that $m_{\rm p}c^2 n \ll \rho_{\rm kin}$ and $\Gamma \sim 1$ at $r = r_0$, we find from the second and third equations in (8.54)

$$C_3 = \frac{3Lr_0^{2/3}}{16\pi c}. \quad (8.56)$$

Note that C_1 can equivalently be expressed in terms of the so-called baryon loading of the flow, $\eta = L/m_{\rm p}c^2\dot{N}$, whereby the scaling laws become

$$r^2 n\,\Gamma = \frac{L}{4\pi m_{\rm p}c^3\eta}, \quad r^2\left(\frac{4}{3}\rho_{\rm kin} + m_{\rm p}c^2 n\right)\Gamma^2 = \frac{L}{4\pi c},$$
$$r^{8/3}\rho_{\rm kin}\,\Gamma^{4/3} = \frac{3Lr_0^{2/3}}{16\pi c}. \quad (8.57)$$

The evolution of the flow can be summarized as follows: a radiation-dominated fireball of initial dimension r_0 accelerates as $\Gamma(r) = r/r_0$ until the radiation energy density of the flow becomes comparable to rest energy density. This occurs at the so-called saturation radius $r_s \approx \eta r_0$, where $\Gamma \approx \eta/2$. The expansion at larger radii proceeds in a matter dominated coasting phase with a constant Lorentz factor $\Gamma = \eta$, However, bulk of the *internal* energy at this stage is still carried by radiation, so that $\rho_{\rm kin} \approx u_{\rm rad}$. The whole history of the fireball evolution is determined by just three parameters: luminosity L, baryon loading η and radius r_0 at the base of the flow.

The conditions at the start of the simulations ($r = r_{\rm n}$) can now be simply read from equations (8.57). The required quantities are the (comoving) proton number density, radiation energy density as well as radiation temperature. Assuming that the proton and neutron flows decouple at $r_{\rm n} > r_{\rm s}$, the proton number density at $r_{\rm n}$ is [1]

$$n = \frac{L}{4\pi m_{\rm p}c^3 r_{\rm n}^2\eta^2}. \quad (8.58)$$

[1]Here we have assumed that the energy carried by protons significantly exceeds the energy carried by neutrons.

The radiation energy density and temperature can be written as

$$u_{\rm rad}(r_{\rm n}) = u_{\rm rad,s}\left(\frac{r_{\rm n}}{r_{\rm s}}\right)^{-8/3}, \quad \theta(r_{\rm n}) = \theta_s\left(\frac{r_{\rm n}}{r_{\rm s}}\right)^{-2/3}, \tag{8.59}$$

where

$$u_{\rm rad,s} \approx \frac{3L}{16\pi c r_{\rm s}^2 \eta^2}, \quad \text{and} \quad \theta_{\rm s} = \frac{kT_{\rm s}}{m_{\rm e}c^2} \approx \frac{k}{m_{\rm e}c^2}\left(\frac{3L}{16\pi ac\, r_{\rm s}^2\eta^2}\right)^{1/4} \tag{8.60}$$

are the radiation energy density and temperature at the saturation radius (a is the radiation density constant).

Note that if the flow becomes optically thin before $r_{\rm n}$, the scaling laws (8.59) only hold out to the radius where the optically thick/thin transition takes place. After that the scalings become $u_{\rm rad} \propto r^{-2}$ and $\theta = {\rm const}$.

We are now in a position to verify our earlier claim that most of the internal energy of the flow is carried by radiation. Assuming a common temperature, we simply need to show that the number of photons far exceeds the number of protons and their associated electrons. First note that the photon number density is $n_{\rm ph} = u_{\rm rad}/3kT \propto u_{\rm rad}^{3/4}$, which, by virtue of (8.29), confirms the well-known result that the total number of photons (in our case, the total number flux) is a conserved quantity in adiabatic cooling. This statement holds regardless of whether the flow is in radiation- or matter-dominated regime. From the first and third equations in (8.57) we then get

$$\frac{n_{\rm ph}}{n} \approx \frac{a^{1/4}\,u_{\rm rad}^{3/4}}{3kn} \approx 2\times 10^4\,\frac{r_{0,7}^{1/2}\,\eta_2}{L_{52}^{1/4}}, \tag{8.61}$$

where we have used the notation $A = 10^x A_x$ (in cgs units). Equation (8.61) confirms that for any plausible GRB parameters the internal energy of the flow is indeed dominated by radiation and we are thus justified in using the equation of state $p = \rho_{\rm kin}/3$ in section 8.1.

We should mention here that the above reasoning does not hold at the very early stages of the expansion when the lepton component is dominated by electron-positron pairs, which can carry a significant fraction of the internal energy if the comoving temperature is not much below 1 MeV (Paczynski 1986). However, employing the relativistic equation of state in section 8.1 is still justified in this case since the pairs are relativistic (albeit marginally) at such temperatures.

8.2.4 Calculation of the observed spectrum

As the simulation is run, we obtain the history of comoving photon and pair distributions on a characteristic world line $ct - r = {\rm const}$. In a steady flow (which we are considering here) all such world lines are equivalent and we simply get

the distributions as a function of distance r from the central source. To find the spectrum seen by the observer, one could then choose some large r where $\tau \ll 1$ and simply Lorentz transform the comoving radiation field at this radius into the external frame, assuming that no further spectral evolution takes place at larger radii. However, there are some problems with this simple approach. First, the radius where the flow becomes optically thin is not a well-defined quantity, since the optical depth is a function of viewing angle. Second, the one-zone treatment becomes less accurate when the flow is optically thin. The reason for this is that our simulations deal with only local (comoving) distributions and neglect the fact that each point in the flow is in causal contact with other parts of the flow that have different (relative) Doppler factors, therefore the photons arriving at a given point at a given time have undergone different Doppler shifts. While our local treatment is still correct energetically, it misses the effect of such superposition of relative Doppler shifts on the spectral shape. A related problem is that the radiation field becomes increasingly beamed in the radial direction as the optical depth decreases, and is no longer isotropic in the frame comoving with the flow. This is a geometric effect caused by the fact that bulk of the radiation originates from close to the photosphere ($\tau \approx 1$), which subtends an increasingly small angle when viewed from $r \gg r_\star$.

To overcome these problems we propose an alternative method of calculating the observed spectrum that takes into account the effects arising from the non-locality of the radiative transfer problem. The idea is simple: having found the photon and particle distributions at all radii from the simulation, we can use them to calculate the emissivities and extinction coefficients for all processes everywhere in the flow. The emerging spectrum can then be found by simply employing the formal solution to the radiative transfer equation in the external frame. This way the distributions obtained from the simulation are regarded as a 0-th order approximation, while using the formal solution provides the next order in accuracy.

During a simulation the code outputs the comoving emissivities j' and absorption coefficients κ' as a function of radius r, both of which are isotropic in the flow frame. The corresponding quantities j and κ in the external frame are found using the Lorentz invariants

$$\frac{j}{\nu^2} = \text{invariant} \quad \text{and} \quad \kappa\nu = \text{invariant}, \tag{8.62}$$

where ν is the photon frequency. Defining the Doppler factor as

$$\mathcal{D} = [\Gamma(1 - \overline{\beta}\mu)]^{-1}, \tag{8.63}$$

where μ is the angle between the radial direction and the line of sight, we find

$$j(r, \nu, \mu) = j'(r, \nu/\mathcal{D})\, \mathcal{D}^2 \quad \text{and} \quad \kappa(r, \nu, \mu) = \frac{\kappa'(r, \nu/\mathcal{D})}{\mathcal{D}}, \tag{8.64}$$

where we have used the relation $\nu = \nu'\mathcal{D}$ between the frequency in the external and the comoving frames.

Let's now use the quantities defined by equation (8.64) to write the formal solution of the radiative transfer equation in cylindrical coordinates, with the z-axis pointing towards the observer. The intensity along a ray with an impact parameter h propagating along the z-axis to the distant observer can be written as

$$I(z \to \infty, \nu) = I'(r_{\rm n}, \nu/\mathcal{D}_n)\, \mathcal{D}_n^3\, e^{-\tau(z_n,\nu)} + \int_{z_n}^{\infty} e^{-\tau(z,\nu)}\, j'(r, \nu/\mathcal{D})\, \mathcal{D}^2\, dz, \quad (8.65)$$

where $r = \sqrt{z^2 + h^2}$, $\mathcal{D}_n = \mathcal{D}(r_{\rm n})$, $z_n = \sqrt{r_{\rm n}^2 - h^2}$ and we have used $I(\nu)/\nu^3 =$ invariant. The comoving intensity I' at the starting radius $r_{\rm n}$ is obtained from fluid-dynamical considerations and is given by

$$I'(r_{\rm n}, \nu') = B[\nu', \theta(r_{\rm n})], \quad (8.66)$$

where B is the blackbody intensity and $\theta(r_{\rm n})$ is given by equation (8.59). The optical depth along the ray from z to infinity (observer) is

$$\tau(z, \nu) = \int_z^{\infty} \frac{\kappa'(r, \nu/\mathcal{D})}{\mathcal{D}}\, dz. \quad (8.67)$$

Note that the Doppler factor $\mathcal{D}$ in equations (8.65) and (8.67) is a function of z through $\mu = z/\sqrt{z^2 + h^2}$.

Once the intensity is known for all impact parameters h, the flux at the observer can be calculated simply as

$$F(\nu) = \frac{2\pi}{d^2} \int_0^{\infty} I(z \to \infty, \nu)\, h\, dh. \quad (8.68)$$

Compared to simple boosting of the comoving spectrum into the external frame, the described method of calculating the observed spectrum has the following advantages:
(1) It automatically includes contributions from different parts of the flow moving at different angles to the line of sight, resulting in different Doppler boosts from the local comoving frames.
(2) It correctly accounts for the dependence of the photospheric radius on the viewing angle, which varies within a factor of ~ 2 inside the cone of opening angle $1/\Gamma$ where bulk of the emission originates from.

In this form the preceding calculation assumes a steady outflow. However, the method can be extended also to variable flows. In this case the emission and absorption coefficients become functions of time as well as the distance from the central source and one needs to employ the formal solution for time-dependent radiative transfer problem. The characteristic world lines $ct - r =$ constant are obviously no longer equivalent and several simulation runs are required to obtain j' and κ' on a two-dimensional grid (t, r).

8.3 Numerical results

8.3.1 Non-magnetized flows

Let us now consider some particular realizations of gamma-ray bursts outflows, using the framework described in the preceding sections. Starting with non-magnetized flows we will describe the evolution of particle and photon fields inside the flow as well as the formation of the observed spectrum, paying particular attention to high-energy emission. To demonstrate the viability of the kinetic theory approach we have adopted here to model GRB emission and allow direct comparison with Monte-Carlo simulations by Beloborodov (2010), we have chosen to study a similar region in parameter space.

For our simulations we choose the following fiducial model: proton flow luminosity $L = 10^{52}$ erg s^{-1}, neutron flow luminosity $L_{\rm n} = 10^{51}$ erg s^{-1}, Lorentz factor of the proton flow (baryon loading) $\Gamma = 600$, Lorentz factor of the neutron flow $\Gamma_{\rm n} = 100$, initial radius of the flow $r_0 = 10^7$ cm. The starting radius of the simulations is determined from equation (8.48), which gives $r_{\rm n} = 5 \times 10^{10}$ cm. The comoving radiation temperature is found from equation (8.59) to be about 0.5 keV.

The formation of the spectrum within the flow as we follow a characteristic $ct - r =$ constant from $r_{\rm n}$ to the photosphere can be summarized as follows: After the dissipation starts, most of the energy is initially delivered in the form of high-energy pairs, which can be seen by comparing equations (8.51) and (8.53) and noting that the initial Thomson optical depth is of the order of unity. As the pairs cool, they upscatter photons from the thermal pool to start forming a tail to the Planck distribution with a slope characteristic of a cooling spectrum (photon index $\alpha = 1.5$). Due to the low blackbody temperature, the source is initially optically thin to pair production for photons with (comoving) energies below $x' = E/m_{\rm e}c^2 \approx 100$. However, this soon changes as more and more photons are upscattered from the thermal distribution. The source becomes optically thick to pair production and a cascade develops. The pairs produced by the cascade will quickly (within about 1/2 of the dynamical time) increase the Thomson optical depth to about 20. By that time the continuous heating rate, being proportional to $\tau_{\rm T}$, has increased to deliver about the same power as the non-thermal injection. As a result of the pair cascade, the high-energy slope of the pair distribution becomes steeper than that of the cooling distribution ($N(\gamma) \propto \gamma^{-2}$).The Compton upscattered spectrum will soften accordingly.[2]

Due to the high compactnesses involved, the pair cascade takes place in the saturated regime, i.e. all high-energy upscattered photons will produce further pairs. An important parameter characterizing the cascade can be defined as $z_T =$

[2]We must stress here that the preceding description merely illustrates the history of spectral formation as we follow an element of the flow along a characteristic world line, and is *not* the spectral evolution seen by the observer.

$(2/3)\gamma_0 x'_0$ (Svensson 1987), where γ_0 is the injection energy of primary non-thermal pairs and x'_0 is the typical energy of soft photons. The quantity z_T determines whether the cascade takes place in the Thomson or Klein-Nishina regime ($z_T \leq 1$ or > 1, respectively), also how many generations of secondary pairs are created etc. In our case $x'_0 \sim 1/200$ (comoving) and $\gamma_0 = 300$, so $z_T \sim 1$. Most of the cascade is in Thomson regime (only scatterings on the highest energy primary pairs take place in the Klein-Nishina regime) and there are several generations of secondary pairs and photons, leading to a smooth overall spectrum. If we consider the non-thermal cascade alone, it can be classified as being of type II according to Svensson (1987), i.e. partly non-linear. In this case the soft target photons for pair production are provided by the cascade itself, while pair cooling is still dominated by the original pool of soft photons. Saturated type II cascade lends itself to an analytic solution and is determined by just two parameters: z_T and the minimum photon energy $x'_{\rm min}$ where saturated pair production takes place. Most importantly, such cascade is independent of the soft photon luminosity (Zdziarski & Lightman 1985), whereas pair-production opacity enters only through the parameter $x'_{\rm min}$. However, if we include thermal heating, the preceding classification is no longer strictly valid. The reason is that it introduces an additional non-linearity to the problem through Comptonizing photons into the range where they can contribute to the pair-production opacity, as well as producing additional cooling for the high-energy pairs. At the same time, the power in thermal heating depends on the optical depth of thermalized pairs, which is determined by the pair-cascade itself. Despite this, the robustness of saturated cascades still allows us to make reasonable estimates using the analytic solution together with the appropriate values for x'_0 and $x'_{\rm min}$.

In Figure 8.1 we plot the observed spectrum for the fiducial model. It bears a strong resemblance with the Band-type spectrum usually seen in GRB-s, consisting of two smoothly joined power-law segments and peaking close to MeV. The spectrum below the peak is made up of blackbody photons advected from the central source and released at the photosphere. However, the photon index deviates appreciably from the Rayleigh-Jeans slope. This can be attributed to the fact that the observed spectrum is a superposition of emission from different parts of the photosphere having different Doppler factors, leading to softening of the low-energy power-law. Just above the peak the dominant contribution to the spectrum comes from thermal Comptonization by Coulomb-heated pairs. The Comptonization takes place in unsaturated regime, leading to a power-law spectral segment starting from the thermal peak. The thermally Comptonized spectrum cuts off above a few 10 MeV, corresponding to the electron temperature of around 15 keV in the comoving frame. Above this energy, inverse-Compton scattering on non-thermal pairs starts to contribute. Note, however, that there is no easily discernible break between the two components. One of the reasons for that is the fact that comparable amount of energy is dissipated by collisional heating and high-energy pair injection (see equations (8.51) and (8.53)). Also, most of the photons in this

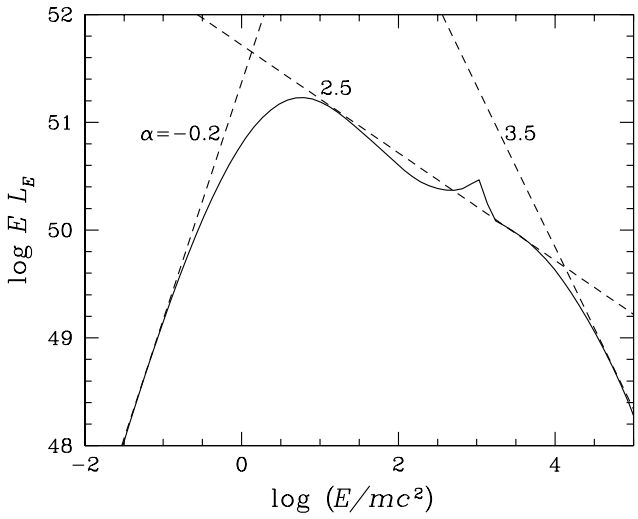

Figure 8.1: Spectrum from a collisionally heated outflow. Model parameters: proton flow luminosity $L = 10^{52}$ erg/s, neutron flow luminosity $L_{\rm n} = 10^{51}$ erg/s, Lorentz factor of the proton flow $\Gamma = 600$, Lorentz factor of the neutron flow $\Gamma_{\rm n} = 100$. The dashed straight lines correspond to photon indices −0.2, 2.5 and 3.5.

energy range undergo several scattering events on cold pairs before being able to escape, losing a significant fraction of their energy in the process. This Compton downscattering has an overall smoothing effect on the spectrum. A distinct feature of the model is a broad annihilation line on top of the otherwise smooth spectrum, due to cooled-down electron-positron pairs. Overall, the spectrum in Figure 8.1 is remarkably consistent with the spectrum obtained by Beloborodov (2010) for similar parameters using Monte-Carlo methods.

As discussed before, the spectrum at the highest energies (above GeV in the external frame) is shaped by saturated pair cascades. The parameter z_T is close to unity, for which the analytic solution predicts an almost flat injection spectrum $x' j_{\rm pa}(x')$ of cascade photons in terms of injected energy per logarithmic photon energy interval. The $x'^2 n'(x')$ photon distribution in the optically thick regime is simply proportional to $x' j_{\rm pa}(x')/\kappa_{\rm pp}(x')$. Here $n'(x')$ is the comoving photon number density per dimensionless energy interval (the primes signify that we are dealing with comoving frame quantities). The absorption coefficient $\kappa_{\rm pp}(x') \propto x'^{\alpha-1}$, where α is the photon index of the target photon population (see below). This leads to $x'^2 n'(x') \propto x'^{-\alpha+1}$, which is steeper by unity compared to the target spectrum at $x' < m_e c^2$. This steepening can be seen starting at $x \sim 3000$ in Figure 8.1,

which corresponds to $x' \equiv x'_{\rm min} \sim 5$ in the comoving frame. Below this energy the saturated pair-cascade is quenched, since the timescale for Compton downscattering becomes shorter than that for $\gamma\gamma$ absorption. Downscattering flattens the spectrum below $x'_{\rm min}$ and leads to a smooth break connecting the high- and low-energy power-laws.

In view of the relatively small distances of the dissipation region from the central source, it seems rather remarkable that significant GeV emission is able to emerge from the flow. The pair-production opacity constraints on the flow Lorentz factor and the dissipation radius have been discussed in several works (e.g. Woods & Loeb 1995; Baring & Harding 1997; Lithwick & Sari 2001). Recently, the observed GeV emission together with the typical variability timescale in different sources like e.g. GRB 080916C and GRB 090902B has been used to place stringent lower limits on Γ (Abdo et al. 2009b,a). We argue here that such argument is strictly valid only if the dissipation process ceases while the flow is still optically thick to pair production, in which case high-energy emission is quenched exponentially ($F \propto F_0 \exp(-\tau_{\gamma\gamma})$). In the model considered here the dissipation operates over a range of radii, including those where $\tau_{\gamma\gamma} < 1$. In such case we can see the photons that are produced within unit optical depth inside the source, which merely leads to a steepening of the spectrum at higher energies instead of a cut-off. The variability timescales deduced from soft gamma-ray lightcurves characterize emission from smaller radii compared to where the high-energy emission originates from, despite the fact that both MeV and GeV emission are produced by the same mechanism. We have already shown how the steepening of the spectrum comes about for the comoving photon distribution as a result of saturated pair-cascades. In what follows we will show that the same holds for the spectrum seen by the distant observer.

We can make a simple analytic estimate of the pair-production opacity and the photospheric radius as a function of photon energy by using the delta-function approximation to the pair-production cross-section (Gould & Schréder 1967)

$$\sigma_{\rm pp}(x', x'_1) \approx \eta(\alpha)\, \sigma_{\rm T} x'_1 \delta\left(x'_1 - \frac{1}{x'}\right) \tag{8.69}$$

to write the optical depth for a photon of energy x' propagating over distance ds' in the flow frame

$$d\tau_{\gamma\gamma}(x') = ds' \int \sigma_{\rm pp}(x', x'_1)\, n'(x'_1)\, dx'_1 \approx ds'\, \eta(\alpha)\, \sigma_{\rm T}\, x'_1\, n'(x'_1)\Big|_{x'_1 = 1/x'}\,, \tag{8.70}$$

where $\eta(\alpha)$ is a numerical factor that depends on the power-law index of the target photon distribution. To write this in terms of external frame quantities we assume an isotropic comoving radiation field with a power-law energy distribution $n'(x') \propto x'^{-\alpha}$, in which case the external and comoving frame distributions are related as

$$x'\, n'(x') = \frac{\alpha + 1}{\Gamma(1 + \overline{\beta})}\; x\, n(x)\big|_{x = x'\,\Gamma(1+\overline{\beta})}\,. \tag{8.71}$$

The photon propagation distances in the two frames are related by $ds' = ds/\mathcal{D}$. The optical depth for a radially propagating photon can therefore be written as

$$d\tau_{\gamma\gamma}(x') \approx dr\,\eta(\alpha)\,\sigma_{\rm T}\,\frac{\alpha+1}{\left[\Gamma(1+\overline{\beta})\right]^2}\,x_1\,n(x_1)|_{x_1=\Gamma(1+\overline{\beta})/x'}\,. \tag{8.72}$$

The total pair-production optical depth at radius r can be obtained by defining $L(x) = 4\pi r^2 c\,x\,n(x)$ and using it to integrate equation (8.72) from r to infinity. Setting $\tau_{\gamma\gamma} = 1$ and expressing r we then find the photospheric radius

$$r^{\star}_{\gamma\gamma}(x) = \eta(\alpha)\,\sigma_{\rm T}\,\frac{\alpha+1}{\left[\Gamma(1+\overline{\beta})\right]^2}\,\frac{L(x_1)}{4\pi c}\bigg|_{x_1=\frac{\left[\Gamma(1+\overline{\beta})\right]^2}{x}}\,, \tag{8.73}$$

where we have used the relation $x' = x/\Gamma(1+\overline{\beta})$ between the comoving and external frame energy of a radially moving photon.

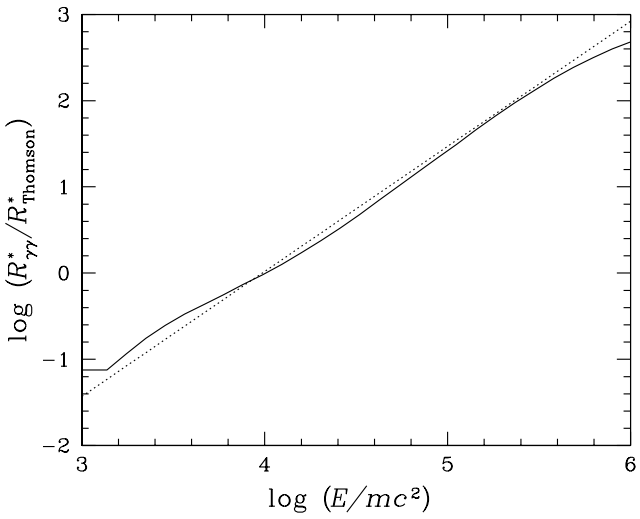

Figure 8.2: Radius of the pair-production photosphere relative to the Thomson photosphere as a function of photon energy for the fiducial model. Solid curve represents the numerically calculated radius, the dashed line corresponds to the analytical estimate given by equation (8.73).

In Figure 8.2 we plot the photospheric radius for the model spectrum shown in Figure 8.1, calculated by using the exact pair-production cross-section as well as the actual photon distributions at all radii, together with the analytic estimate (8.73) calculated for power-law target spectrum (the line with photon index 2.5 in

Figure 8.1). We can see that the agreement between our rough estimate and exact calculations is rather good. For these particular parameters the pair-production photosphere is outside the Thomson photosphere only for photon energies above ~ 5 GeV.

To make an estimation of the expected luminosity as well as the spectral shape at high energies one can follow the argument made in Beloborodov (2010) and assume that all energy injected as high energy pairs will be reprocessed to lower energy photons by pair cascades and released at $r^{\star}_{\gamma\gamma}(x)$. This implies that all photons emerging from the source above a given energy x are the result of energy injection at radii larger than $r^{\star}_{\gamma\gamma}(x)$. Defining the fraction of the flow energy carried by radiation (per dimensionless energy interval) as

$$\varepsilon_{\rm rad}(x) = \frac{m_{\rm e}}{m_{\rm p}} \frac{L(x)}{4\pi c\, r^2 n_{\rm p} \Gamma^2}, \tag{8.74}$$

we can thus write

$$\int_x^{\infty} \varepsilon_{\rm rad}(x)\, dx = \int_{r^{\star}_{\gamma\gamma}(x)}^{\infty} \frac{1}{n_{\rm p} m_{\rm p} c^2} \frac{r\dot{Q}_{\rm inj}}{c\Gamma}\, d\ln r = \frac{1}{16} \frac{\Gamma}{\Gamma_{\rm n}} \frac{r_{\rm n}}{r^{\star}_{\gamma\gamma}(x)}, \tag{8.75}$$

where we have used the collisional dissipation rate given by (8.53), noting that energy dissipated over one dynamical time equals the energy dissipated per $d\ln r$. Differentiating both sides of equation (8.75) with respect to x and using (8.73) we obtain

$$\varepsilon_{\rm rad}(x) = \frac{\pi c\, r_{\rm n}\, \Gamma}{4\eta(\alpha)\, \sigma_{\rm T} (\alpha+1)\, \Gamma_{\rm n}} \left[\Gamma(1+\overline{\beta})\right]^2 \frac{1}{x} \left.\frac{dL^{-1}(x_1)}{d\ln x_1}\right|_{x_1 = \frac{\left[\Gamma(1+\overline{\beta})\right]^2}{x}}. \tag{8.76}$$

By noticing that $L(x_1) \propto x_1^{-\alpha+1}$ we can take the derivative in (8.76) and cast the equation in a more transparent form

$$\varepsilon_{\rm rad}(x) = \frac{1}{16\,\eta(\alpha)} \frac{\sigma}{\sigma_{\rm T}} \frac{m_{\rm e}}{m_{\rm p}} \frac{L_{\rm n}}{L} \frac{(\alpha-1)}{(\alpha+1)} \frac{\Gamma\left[\Gamma(1+\overline{\beta})\right]^{2\alpha}}{\Gamma_{\rm n}^4} \frac{x^{-2\alpha+1}}{\varepsilon_{\rm rad,0}(x)}, \tag{8.77}$$

where we have used the definitions (8.48) and (8.74) for $r_{\rm n}$ and $\varepsilon_{\rm rad,0}(x)$, respectively, as well as $L = 4\pi m_{\rm p} c^3 r^2 n_{\rm p} \Gamma^2$. The quantity $\varepsilon_{\rm rad,0}(x)$ denotes the extension of the low-energy (target) photon distribution to the observed energy, allowing direct comparison between the expected power in the high energy spectrum versus a simple extrapolation of the lower-energy power-law. For $\varepsilon_{\rm rad,0}(x) \propto x^{-\alpha+1}$ we find from equation (8.77) that $\varepsilon_{\rm rad}(x) \propto x^{-\alpha}$, i.e. we should observe a steepening of the spectrum by $\Delta\alpha = 1$ at high energies. This is consistent with the earlier discussion in terms of pair-cascades in the comoving frame.

8.3.2 Magnetized flows

In most plausible scenarios the GRB outflow is expected to carry at least a moderate magnetic field. Magnetization will provide an additional mechanism of cooling electron-positron pairs in addition to Compton and will therefore affect the spectral formation at all energies: directly through synchrotron radiation in the hard X-ray range as well as indirectly through suppressing the pair-cascades at high energies.

Magnetization is parametrized as the fraction ϵ_B of the bulk kinetic energy carried by the magnetic field, leading to compactness

$$l_B = \frac{\sigma_{\rm T}}{m_{\rm e}c^2}\,\frac{r}{\Gamma}\,U_{\rm B} = \frac{\epsilon_B\,\sigma_{\rm T}L}{4\pi m_{\rm e}c^3 r\Gamma^3}. \tag{8.78}$$

The case with $\Gamma = 600$ and $\Gamma_n = 100$ has been taken as the basis and the simulation was run for $\epsilon_B = 0$, 10^{-3}, 10^{-2}, 0.1 and 0.5. The corresponding ratios of magnetic and radiation compactnesses at the start of simulations are $l_B(r_{\rm n})/l_{\rm rad}(r_{\rm n}) = 0$, 0.0043, 0.043, 0.43 and 2.2. Here the compactness $l_{\rm rad}(r_{\rm n})$ is defined as

$$l_{\rm rad}(r_{\rm n}) = \frac{\sigma_{\rm T}L_\gamma(r_{\rm n})}{4\pi m_{\rm e}c^3 r_{\rm n}\Gamma^3}, \tag{8.79}$$

where $L_\gamma(r_{\rm n}) = 16\pi c r_{\rm n}^2\Gamma^2 u_{\rm rad}(r_{\rm n})/3$ is the luminosity carried by radiation and $u_{\rm rad}(r_{\rm n})$ is given by equation (8.59). Figure 8.3 shows the effect of the magnetic field on the spectrum. The effects on different quantities characterizing the flow are summarized in Table 8.1.

The synchrotron radiation from the thermal component of the pair distribution is strongly self-absorbed and makes no contribution to the observed spectrum. The relativistic non-thermal pairs (above $\gamma \sim$ a few) on the other hand radiate synchrotron in the optically thin regime. It was shown in Beloborodov (2010) that for typical parameters their synchrotron radiation peaks in the same domain as the blackbody component and is therefore buried under the latter for sub-dominant magnetizations. Just below the thermal peak the addition of synchrotron photons has the effect of softening the spectral slope (see Table 8.1), to values more compatible with those typically observed (Preece et al. 2000). At lower energies the softer synchrotron spectrum will emerge from under the hard thermal spectrum, and can be seen as a separate component. This might provide an explanation for the X-ray excesses that have been observed in several bursts (Preece et al. 1996), a prominent recent example being GRB 090902B (Abdo et al. 2009a).

Low-energy emission

Below 5 – 10 keV the synchrotron emission switches to a partially self-absorbed regime. At any given stage of the flow expansion there exists a well-defined self-absorption energy $x_{\rm s}$, below which the source is optically thick to synchrotron

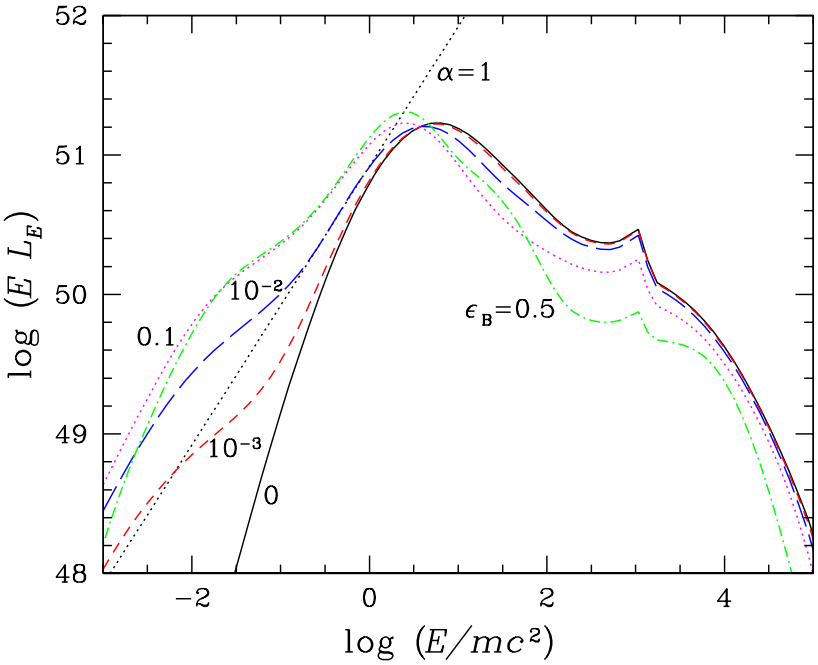

Figure 8.3: Spectra from a magnetized flow. The solid, short-dashed, long-dashed, dotted and dash-dotted lines correspond to magnetizations $\epsilon_B = 0$, 10^{-3}, 10^{-2}, 0.1 and 0.5, respectively. The straight dotted line shows a power-law spectrum with $\alpha = 1$.

radiation. The *intrinsic* spectrum at $x < x_s$ has a photon index $\alpha = -1.5$, characteristic of a power-law electron distribution producing the self-absorbed emission. However, as the flow expands, the self-absorption frequency decreases, as does the synchrotron emissivity above x_s. The *observed* low-energy spectrum is therefore formed as a superposition of emission produced right above the self-absorption frequency at different radii. To see this and also give a rough estimate for the expected spectral shape, let's write the emission and absorption coefficients as [3] (see e.g. Ghisellini & Svensson 1991)

$$j_s(x) = \int P(x,\gamma)\, n_e(\gamma)\, d\gamma, \tag{8.80}$$

$$\kappa_s(x) = \frac{\lambda_C^3}{8\pi c}\frac{1}{x^2}\int P(x,\gamma)\,\gamma p\,\frac{d}{d\gamma}\left[\frac{n_e(\gamma)}{\gamma p}\right] d\gamma, \tag{8.81}$$

[3] We are temporarily omitting the primes from all quantities for simplicity even though we are working in the comoving frame.

Table 8.1: Results of simulations

ϵ_B[a]	$E_{\rm peak}$[b] (MeV)	α[c]	$\varepsilon_{\rm rad}$[d]	$r_\star/r_{\rm n}$[e]	Y[f]	$\dot{Q}_{\rm ep}/\dot{Q}_{\rm inj}$[g]	$kT_{\rm e}$[h] (keV)
0	3.2		0.30	25.6	0.20	1.03	9.7
10^{-3}	2.8	0.60	0.30	25.0	0.20	1.01	9.6
10^{-2}	2.1	0.98	0.30	23.0	0.17	0.93	9.1
0.1	1.3	1.17	0.31	16.9	0.08	0.68	7.9
0.5	1.2	1.10	0.36	8.9	0.03	0.36	6.8

Notes.
[a] Magnetization
[b] Spectral peak energy.
[c] Photon index in the 100 – 500 keV range.
[d] Radiative efficiency $\varepsilon_{\rm rad} = L_\gamma/L$.
[e] Radius of the Thomson photosphere relative to the radius $r_{\rm n} = 5.3\times10^{10}$ cm where the dissipation starts.
[f] Pair yield $Y = \mathcal{M}/\gamma_0$, where $\mathcal{M}$ is the secondary pair multiplicity and $\gamma_0 = 300$ is the Lorenz factor of injected electrons.
[g] Ratio of thermal and non-thermal dissipation rates at $r_\star$.
[h] Pair temperature at $r_\star$.

where $n_{\rm e}(\gamma)$ is the pair number density per $d\gamma$. For our purposes it is sufficient to use a simple delta-function approximation for the isotropic single-particle synchrotron emissivity, i.e.

$$P(x,\gamma) = \frac{4}{3}\frac{\sigma_{\rm T}U_{\rm B}}{m_{\rm e}c}\,p^2\,\delta\left(x-\gamma^2 x_{\rm L}\right), \tag{8.82}$$

where $x_{\rm L} = B/B_{\rm cr}$ is the Larmor energy in $m_{\rm e}c^2$ units and $B_{\rm cr} = m_{\rm e}^2c^3/\hbar e \approx 4.4\times10^{13}$ G is the critical magnetic field strength. The electrons/positrons responsible for the partially self-absorbed emission are in the power-law tail of the distribution, thus we may write $n_{\rm e}(\gamma) = A\gamma^{-\delta}$. The emission and absorption coefficients now take the form

$$j_{\rm s}(x) = \frac{2}{3}A\,\frac{\sigma_{\rm T}U_{\rm B}}{m_{\rm e}c}\,\frac{1}{x_{\rm L}}\,\left(\frac{x}{x_{\rm L}}\right)^{-(\delta-1)/2} \tag{8.83}$$

and

$$\kappa_{\rm s}(x) = \frac{2\pi^2}{9}\,(\delta+2)\,A\,\frac{e}{B}\left(\frac{x}{x_{\rm L}}\right)^{-(\delta+4)/2}. \tag{8.84}$$

In the comoving frame the following scalings hold as a function radius from the central source (or, equivalently, comoving time)

$$B = \sqrt{8\pi\epsilon_B n_{\rm p} m_{\rm p}c^2} \propto r^{-1}, \qquad x_{\rm L}\propto r^{-1}, \qquad A\propto r^{-2}. \tag{8.85}$$

The characteristic optical depth at a given photon energy is thus

$$\tau_{\rm s}(x) = \frac{2}{\delta+4}\,\frac{r}{\Gamma}\,\kappa_{\rm s}(x) \propto (x\,r)^{-(\delta+4)/2}. \tag{8.86}$$

Setting $\tau_{\rm s}(x) = 1$ we find that the self-absorption frequency scales as

$$x_{\rm s} \propto r^{-1}. \tag{8.87}$$

From Equations (8.84), (8.85) and (8.86) we also find that

$$\frac{x_{\rm s}}{x_{\rm L}} = \gamma_{\rm s}^2 = \text{constant}, \tag{8.88}$$

thus the energy $\gamma_{\rm s}$ of the pairs emitting near the self-absorption frequency remains the same along the flow. The value of $\gamma_{\rm s}$ is a weak function of the magnetic field strength and takes on values between 10 and 15 for the cases considered here.

The emissivity near the self-absorption frequency can be read from Equation (8.83), setting $x = x_{\rm s}$. Using (8.85) and (8.88) we find that

$$j_{\rm s}(x_{\rm s}) \propto r^{-3}. \tag{8.89}$$

For the optically thin synchrotron emissivity we may write

$$j_{\rm s}(x) = j_{\rm s}(x_{\rm s})\left(\frac{x}{x_{\rm s}}\right)^{-(\delta-1)/2}. \tag{8.90}$$

The radiation energy per dx in the external frame normalized to the total flow energy is expressed as (reintroducing primes for comoving frame quantities)

$$\varepsilon_{\rm rad}(x) = \int_{r_s^\star(x)}^{\infty} \frac{1}{n_{\rm p} m_{\rm p} c^2}\,\frac{r\,j_{\rm s}'(x')}{c\Gamma^2}\,d\ln r, \tag{8.91}$$

where $r_s^\star(x) \propto 1/x$ is the photospheric radius. The integral is performed over the optically thin domain for a given photon energy. Inserting Equation (8.90) into (8.91), using the scalings (8.87), (8.89) and $n_{\rm p} \propto r^{-2}$, and finally observing that $x_{\rm s} = x$ at the photospheric radius, we arrive at the result

$$\varepsilon_{\rm rad}(x) \propto x^0, \tag{8.92}$$

with the corresponding photon index for the partially self-absorbed emission $\alpha = 1$.

Note that the low-energy emission is delayed relative to the gamma-rays, owing to $x_{\rm s} \propto r^{-1} = (c\Gamma^2 t_{\rm obs})^{-1}$. In principle, this emission can extend all the way down to the optical band, with a typical delay of the order of 1 sec. However, it is not strong enough to explain the bright optical flashes seen in some bursts (e.g. GRB 080319B).

High-energy emission and pair cascades

Increasing the magnetization has strong effect on the high-energy emission since synchrotron cooling of the non-thermal pairs starts competing with the inverse-Compton process. A direct consequence of this is the decrease of the high-energy flux. Magnetization also has a suppressing effect on the pair-cascade as a fraction of the particles' energy is given to low-energy synchrotron radiation which cannot participate in the creation of secondary pairs and is thus lost to the cascade process. One can show that the multiplicity of each subsequent pair generation in a saturated cascade is suppressed by a factor $f_{\rm B} \approx 1 + \epsilon_B/\varepsilon_{\rm rad}$. For magnetic fields approaching equipartition with radiation (i.e. $\epsilon_B/\varepsilon_{\rm rad} \sim 1$), only two generations of secondary pairs can make a significant contribution to the total pair multiplicity. As a result, the total pair yield decreases from $Y = 0.20$ to about 0.025 as the magnetization parameter increases from 0 to 0.5 (Table 8.1).

The decrease of the pair yield leads to the decline of the Thomson optical depth in pair creation-annihilation balance, as the two are related by $\tau_{\rm T} \propto Y^{1/2}$ (see Equation (23) in Beloborodov 2010). As a consequence, the radius of the Thomson photosphere also decreases as magetization is increased. Most importantly, however, it results in the decrease of the thermal heating rate, since the latter proportional to $\tau_{\rm T}$ (see Equation (8.51)), and thus also the ratio $\dot{Q}_{\rm ep}/\dot{Q}_{\rm inj}$, as the non-thermal injection rate is unaffected. Interestingly enough, the total radiative efficiency $\varepsilon_{\rm rad}$ remains almost unchanged (or even increases moderately). The diminished total dissipated energy is more than compensated by the decrease in adiabatic losses of the photon field due to the lower optical depth, which allows an earlier decoupling of radiation from matter.

On the other hand, the mean photon energy, which is roughly correlated with the spectral peak, does decrease. This is the result of the increased *number* of photons due to synchrotron radiation, which have to share the available energy. In the absence of magnetization, the number of photons is approximately conserved: it is unchanged by adiabatic cooling and Compton scattering, and the amount produced by the annihilation of injected pairs is negligible. Therefore given the flow energy per photon at launch, the average observed photon energy simply tracks the radiative efficiency. Instead, with increasing magnetization, the average energy approximately follows the number of introduced photons, since the radiative efficiency does not change significantly.

Looking at Table 8.1, we can see that the temperature $\Theta_{\rm e}$ of the thermal component of the pair distribution decreases by about 30 % as magnetization is increased to $\epsilon_B = 0.5$. This is a sole consequence of the decreasing Compton temperature $\Theta_{\rm C}$ of the radiation field, brought about mainly by the introduction of soft synchrotron radiation from non-thermal pairs. Note that even though the thermal (volume) heating rate of pairs decreases with increasing magnetization, the heating rate *per particle* does not. Also, the thermal pairs are unable to cool by synchrotron radiation because they emit in a strongly self-absorbed regime.

As $\Theta_e - \Theta_C \approx$ constant, the decrease of the Kompaneets y-parameter defined as $y = 4\tau_T(\Theta_e - \Theta_C)$ is mainly the result of the smaller Thomson optical depth of the pairs. This leads to a steeper slope of the thermal-Comptonized spectrum above the peak. At high magnetization, however, the synchrotron emission from the highest energy electrons will start distorting the high-energy power-law, as evidenced by a subtle bump near 15 MeV in the $\epsilon_B = 0.5$ spectrum in Figure 8.3.

8.4 Conclusions

Nuclear collisions between protons and neutrons can dissipate a significant fraction of the kinetic energy of a GRB outflow by heating the proton component as well as via non-thermal injection of high-energy pairs resulting from inelastic p-n collisions (Beloborodov 2010). The dissipation operates relatively close to the central source and over a range of radii ($\sim 10^{11} - 10^{13}$ cm).

We have modeled the emission from such an outflow by self-consistently solving the time-dependent kinetic equations describing the evolution of particle and photon distributions inside the flow. The simulations are run in the comoving frame, following a 'representative' fluid element along its world-line as it propagates through the dissipation region, expecting all other elements of the outflow to undergo similar evolution. Although our treatment of radiative processes is local (in a sense that different elements of the flow are assumed to be causally disconnected), we have proposed a simple method of taking into account the effects of emission from different flow elements propagating at various angles to the line of sight on the observed spectrum.

Owing to the relatively small distances from the central engine, the thermal photon field advected from the centre still carries a sizable fraction of the total flow energy when the dissipation begins and has a significant influence of the spectral formation. Most importantly, it provides the seed photons for Comptonization, leading to a Band-type spectral shape peaking in the MeV range. The hard low-energy slope of the thermal component also makes it easy to accommodate even the hardest observed GRB spectra.

An important feature of the model is the significant amount of (multi-)GeV emission it predicts. It is a direct consequence of the fact that collisional heating operates over a range of radii. Thus, even though the flow is optically thick to GeV photons at the beginning of the dissipation episode, it becomes transparent to photons at progressively higher energies as the flow expands, but while the dissipation is still operating. As a result, the high-energy spectrum exhibits a steepening relative to the slope at lower energies, instead of a cutoff.

A subdominant magnetization will lead to softening of the spectral slope below the peak due to the additional contribution from soft synchrotron radiation of non-thermal pairs. A separate soft component at lower energies is also produced. The additional cooling of the high-energy pair distribution due to synchrotron has

a throttling effect on the pair-cascades. The multiplicity of secondary pairs will decline, as will the thermal heating rate since it depends on the Thomson optical depth. The resulting spectra will peak at lower energies compared to the non-magnetized case. All in all, the low-energy slopes as well as spectral peaks from magnetized flows are in better agreement with those typically observed in GRB-s (Preece et al. 2000; Nava et al. 2010), relative to case with no magnetic field.

Chapter 9

Spectral states of accreting black holes

The physical processes giving rise to the X-ray/gamma-ray emission of accreting black-hole binaries (BHBs) have been a matter of debates over the last four decades. The hard-state spectra, showing a strong cut-off around 100 keV, are well described by thermal Comptonization (e.g. Poutanen 1998; Zdziarski & Gierliński 2004), while a weak MeV tail requires the presence of nonthermal particles (McConnell et al. 1994; Ling et al. 1997). The origin of seed soft photons for Comptonization is, however, much less clear. An apparent correlation between the spectral slope and the amount of Compton reflection (Zdziarski et al. 1999) argues in favor of the accretion disk, while the observed optical/X-ray correlation (Motch et al. 1982; Kanbach et al. 2001) leans toward the synchrotron hypothesis (e.g. Fabian et al. 1982; Wardziński & Zdziarski 2001). Interesting questions are then: what stabilizes the X-ray spectral slope at $\alpha \sim 0.6$–0.8, and what fixes the temperature of the emitting plasma at $kT_{\rm e} \sim 50$–100 keV (Zdziarski et al. 1997; Poutanen 1998; Zdziarski & Gierliński 2004)? Do the feedback from the cool accretion disk and the thermostatic properties of electron-positron pairs (Haardt & Maraschi 1993; Haardt et al. 1994; Stern et al. 1995b; Malzac et al. 2001) play a role here? Or does the cooling by synchrotron radiation (Narayan & Yi 1995) act as a stabilizer?

In the soft state, BHB spectra are dominated by thermal disk emission of temperature $kT_{\rm BB} \sim 0.4$–1.5 keV. At higher energies the spectrum is power-law-like and shows no signatures of the cut-off (Grove et al. 1998), extending possibly up to 10 MeV (McConnell et al. 2002). This emission is well described by Comptonization in almost purely nonthermal plasmas (Poutanen & Coppi 1998; Gierliński et al. 1999; Coppi 1999; Zdziarski et al. 2001; Zdziarski & Gierliński 2004). We can then ask why the electrons are nearly thermal in the hard state, and what causes such a dramatic change in the electron distribution when transition to the soft state happens. Poutanen & Coppi (1998) proposed that the two states are distinguished by the way the energy is supplied to the electrons: by thermal heating,

dominating during the hard state, and by nonthermal acceleration, operating in the soft state. However, their treatment of Coulomb collisions (using EQPAIR code by Coppi 1992, 1999) was approximate, and they have neglected the effect of synchrotron boiler, involving the emission and absorption of synchrotron photons, which can act as an efficient particle thermalizer (Ghisellini et al. 1988).

Ghisellini et al. (1998) studied for the first time the combined effect of the synchrotron boiler and Compton cooling on the electron distribution and photon spectra (but neglected Coulomb scattering). They considered a two-phase corona model (Haardt & Maraschi 1993; Haardt et al. 1994; Stern et al. 1995b), where half of the high-energy radiation was assumed to be reprocessed by the disk to soft photons. As the actual geometry of the emitting region is not known, we start from pure synchrotron self-Compton models (i.e. with no external soft photons) and compute self-consistently the electron (positron) and photon distributions. We then investigate how the additional soft photons (e.g., associated with the inner radius of the cool accretion disk) affect the equilibrium distributions and compare the results of simulations with the data on Cyg X-1. The preliminary results of this study were presented by Vurm & Poutanen (2008).

9.1 Model setup

We consider a black hole of mass 10 $M_\odot$, typical for stellar-mass BHBs. We assume that the inner accretion flow is hot and almost spherical, corresponding to the advection-dominated (Narayan & Yi 1995; Abramowicz et al. 1995; Esin et al. 1997) or to the recently discovered luminous hot accretion flow solutions (Yuan 2003; Yuan & Zdziarski 2004). One expects that most of the gravitational energy release happens within about $R = 10R_\mathrm{S} = 3\times10^7$ cm (where $R_\mathrm{S} = 2GM/c^2$ is the Schwarzschild radius) from the black hole, and we thus fix the size of the active region at this value in most of the simulations. The released energy needs to be transferred to electrons via, e.g., Coulomb collisions with hot protons, collective plasma effects, magnetic reconnection, or shocks. We assume that the energy transfer to the electrons is given by a power-law-injection function $dN_\mathrm{e}/(dt\,d\gamma) \propto \gamma^{-\Gamma_\mathrm{inj}}$ extending in the Lorentz factor from $\gamma = 1$ to 10^3. To keep the Thomson optical depth of the electrons associated with protons τ_p constant,[1] the same number of electrons from the equilibrium distribution is removed from the system. In this case, the net power is $L_\mathrm{inj}{=}\frac{4\pi}{3}R^3\dot{N}_\mathrm{e}(\langle\gamma\rangle_\mathrm{inj} - \langle\gamma\rangle_\mathrm{eq})m_\mathrm{e}c^2$, where $\langle\gamma\rangle_\mathrm{inj}$ and $\langle\gamma\rangle_\mathrm{eq}$ are the mean Lorentz factors of the injection function and of the equilibrium distribution, respectively, and $\dot{N}_\mathrm{e}$ is uniquely determined by the model parameters and $\langle\gamma\rangle_\mathrm{eq}$.

The injected electrons are cooled by synchrotron emission and Compton scattering at timescales much shorter than the accretion time. The synchrotron ra-

[1]The total optical depth might be larger due to the produced pairs, but for parameters considered here, the amount of pairs is negligible.

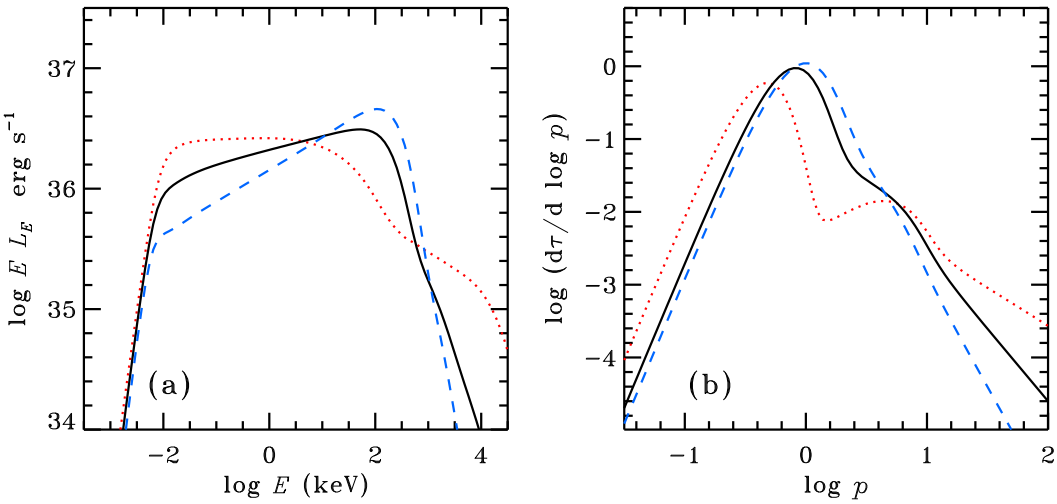

Figure 9.1: Equilibrium photon spectra (left panel) and electron distributions (right panel) $p^2 d\tau/dp$ (i.e., momentum per log p, where τ is the Thomson optical depth and $p = \sqrt{\gamma^2 - 1}$ is the dimensionless electron momentum) for different electron injection slopes: $\Gamma_{\rm inj} = 2$ (dotted curve), 3 (solid) and 4 (dashed). The results for the fiducial parameter set $L = L_{\rm inj} = 10^{37}$ erg s^{-1}, $\Gamma_{\rm inj} = 3$, $\tau_{\rm p} = 1.5$, $\eta_{\rm B} = 1$, $f = 0$, are shown by solid curves in both panels. The electron temperatures and photon spectral indices are given in Table 9.1.

diation is strongly self-absorbed up to hundreds of harmonics, and therefore the cooling depends strongly on the high-energy tail of the electron distribution (see e.g. Wardziński & Zdziarski 2001). The importance of synchrotron processes is determined by the ratio $\eta_{\rm B} = U_{\rm B} R^2 c/L_{\rm inj}$, where $U_{\rm B} = B^2/(8\pi)$ is the magnetic energy density and $L_{\rm inj} \approx \frac{4\pi}{3} R^2 c U_{\rm rad}$ (so that $\eta_{\rm B} \approx 3/4\pi \approx 0.25$ corresponds to an equipartition of the magnetic and radiation energy densities, $U_{\rm B} = U_{\rm rad}$). The seed photons for Compton upscattering can be provided by the synchrotron as well as by the external sources, the cool accretion disk being the most natural one. The external soft photons are modeled as a blackbody of temperature $T_{\rm BB}$ determined from the Stefan-Boltzmann law $L_{\rm disk} = 4\pi R^2 \sigma_{\rm SB} T_{\rm BB}^4$. The cooling by external photons depends on the ratio $f = L_{\rm disk}/L_{\rm inj}$. The total escaping photon luminosity is $L = L_{\rm disk} + L_{\rm inj} = (1 + f) L_{\rm inj}$.

9.2 Synchrotron self-Compton models

We first assume that the cool disk is sufficiently far away and does not supply any seed soft photons to the inner hot flow. Thus we consider pure synchrotron self-Compton (SSC) models (f=0). We choose the fiducial parameter set $L = L_{\rm inj} = 10^{37}$ erg s^{-1} and $\tau_{\rm p}$=1.5 (typical for the hard state of BHBs, Zdziarski et al. 1997), $R = 3{\times}10^7$ cm, $\Gamma_{\rm inj} = 3$ (ad hoc), and $\eta_{\rm B}$ =1. The equilibrium electron

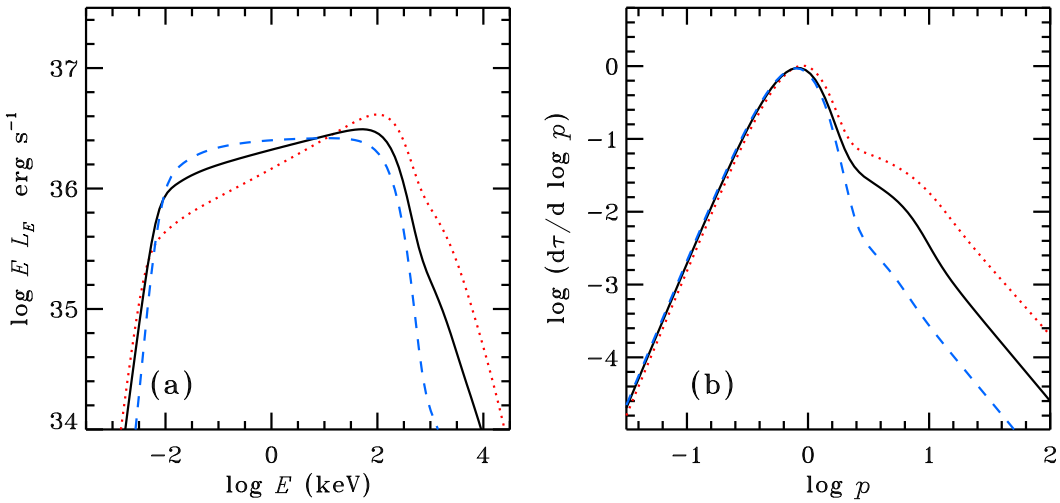

Figure 9.2: Equilibrium photon spectra (left panel) and electron distributions (right panel) $p^2 d\tau/dp$ for different magnetization $\eta_{\rm B} = 0.1$ (dotted), 1 (solid), 10 (dashed). The results for the fiducial parameter set are shown by solid curves.

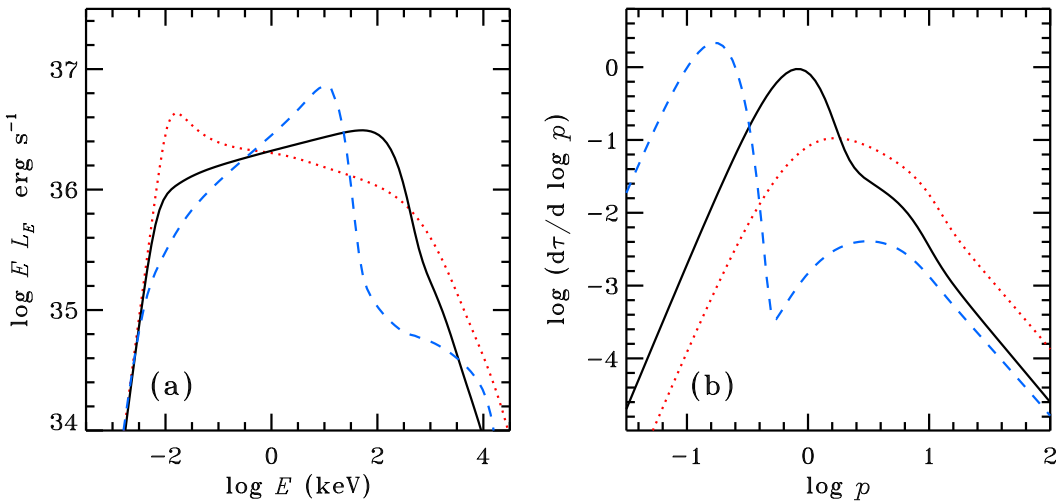

Figure 9.3: Equilibrium photon spectra (left panel) and electron distributions (right panel) $p^2 d\tau/dp$ for different optical depth $\tau_{\rm p} = 0.15$ (dotted), 1.5 (solid), 15 (dashed). The results for the fiducial parameter set are shown by solid curves.

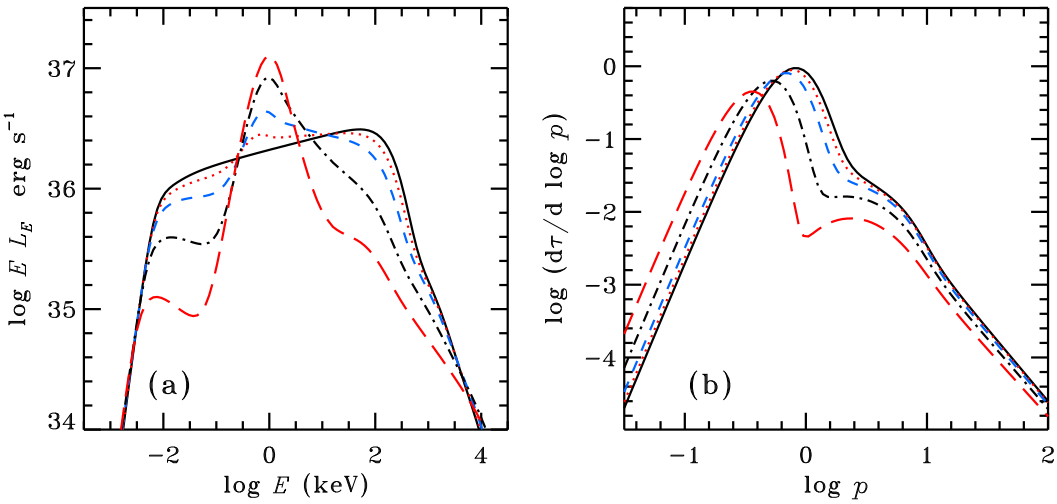

Figure 9.4: Equilibrium photon spectra (left panel) and electron distributions (right panel) $p^2 d\tau/dp$ for different ratios of the external disk photons to the injected power $f = 0, 0.1, 0.3, 1, 3$ (solid, dotted, dashed, dot-dashed, long-dashed curves, respectively) for constant total luminosity L. The results for the fiducial parameter set are shown by solid curves.

distribution consists of a Maxwellian part with kT_e =66 keV and a power-law-like tail with the slope modified by cooling $\Gamma_e = \Gamma_{inj} + 1 = 4$ (where $dN_e/d\gamma \propto \gamma^{-\Gamma_e}$; see the solid curve in Figure 9.1(b)). The synchrotron emission is strongly self-absorbed with only the nonthermal tail above $\gamma \gtrsim 20$ contributing to emission above the self-absorption energy at $\gtrsim 10$ eV. As the amount of seed soft (synchrotron) photons is low, the Comptonization spectrum (produced predominantly by the thermal electron population) is hard with the photon energy index $\alpha \approx 0.9$ and a cut-off at ~ 100 keV, which is similar to the hard state of BHBs. A tail produced by single-Compton scattering off the power-law electron tail is clearly visible above MeV.

Variation of the slope of the injected electrons leads to a large change in the tail of the electron distribution and dramatic difference in the synchrotron emission. A soft electron injection with $\Gamma_{inj} \gtrsim 4$ leads to efficient thermalization and a small amount of soft photons resulting in rather hard radiation spectra, with the photon energy index $\alpha \lesssim 0.7$ (see dashed curves in Figure 9.1). A hard injection gives more power to the nonthermal tail and more seed photons for Comptonization (see also Ghisellini et al. 1998; Wardziński & Zdziarski 2001), which causes a drop in the electron temperature (see the dotted curves in Figure 9.1). A strong 'bump' also develops in the tail of the electron distribution at $\gamma \sim 3$. The synchrotron emission produced by these electrons is still strongly self-absorbed, while the energy losses and gains stay close to each other for an extended energy interval (Katarzyński et al. 2006). In this regime, the ratio of synchrotron heating and cooling rates for a power-law distribution of relativistic electrons is

Table 9.1: Results of simulations

P[a]		α[b]	T_e[c] (keV)
Fiducial[d]		0.89	66
Γ_{inj}	2	1.07	27
	4	0.73	90
η_B	0.1	0.75	77
	10	0.98	64
τ_p	0.15	1.12	160
	15	0.58	4
f	0.1	0.97	61
	0.3	1.13	49
	1	1.61	31
	3	2.46	16

Notes.
[a] Varying parameter and its value.
[b] Photon spectral index in the 2–10 keV range.
[c] Temperature of the Maxwellian part of the electron distribution.
[d] Fiducial set of parameters $L = 10^{37}$ erg s^{-1}, $R = 3 \times 10^7$ cm, $f = 0$, $\Gamma_{inj} = 3$, $\tau_p = 1.5$, $\eta_B = 1$.

$\dot{\gamma}_h/\dot{\gamma}_c \approx 5/(\Gamma_e + 2)$.[2] Observe that for $\Gamma_e = 3$ (i.e. for $\Gamma_{inj} = 2$) the heating and cooling rates are balanced, however, such an equilibrium is unstable (Rees 1967). The Comptonized spectrum for hard injection $\Gamma_{inj} = 2$ (see Figure 9.1(a)) is much softer than the hard-state spectra of BHBs, even without any contribution to the cooling from the disk, strongly constraining the electron injection mechanism in BHBs.

The efficiency of synchrotron cooling depends on the magnetic field strength parametrized here via magnetization η_B. At small η_B (see Figure 9.2(b)), synchrotron is inefficient and cooling is dominated by thermal Comptonization. A higher normalization of the power-law part of the equilibrium electron distribution leads to a stronger MeV tail. For $\eta_B \lesssim 1$ (and $\Gamma_{inj} > 3$), the thermal Comptonization spectrum is very stable with $\alpha \sim 0.7$–0.9. At large $\eta_B > 1$, the synchrotron thermalization operates more efficiently and the thermal part of the distribution persists to higher energies. The increasing B-field compensates for the decrease in the power-law tail leading to a higher synchrotron emission, which results in softening of the Comptonized spectrum.

[2]This expression can be derived by employing the delta-function approximation for synchrotron emissivity to calculate the source function and using it in the expression for heating by self-absorption (see e.g. Ghisellini et al. 1988; Katarzyński et al. 2006).

Consider now variations of $\tau_{\rm p}$ for the fixed $L_{\rm inj}$. At high $\tau_{\rm p}$, the equilibrium electron temperature drops, leaving fewer energetic electrons for synchrotron emission and, therefore, reducing the number of seed photons for Comptonization (Figure 9.3). This, in turn, results in the harder photon spectra produced by saturated Comptonization (by thermal electrons) and a weak high-energy tail (produced by nonthermal electrons), very similar to the ultrasoft spectra of BHBs (see Figures 8 and 9 in Zdziarski & Gierliński 2004). At smaller $\tau_{\rm p}$, the higher electron temperature leads to a stronger synchrotron cooling and to a lower Comptonized luminosity and, therefore, softer Comptonized spectra.

Let us now apply the developed model to the hard state of Cyg X-1. The MeV tail observed there with $\alpha_{\rm MeV} \approx 2$ (McConnell et al. 2002) constrains the injection slope to be $\Gamma_{\rm inj} < 2\alpha_{\rm MeV} = 4$. Then the hard X-ray spectra with $\alpha \lesssim 0.7$ and a high-energy cutoff at ~ 100 keV (see Figure 9.5) require $\tau_{\rm p} \sim 1$ and low $\eta_{\rm B} \lesssim 0.1$ (see also Wardziński & Zdziarski 2001; McConnell et al. 2002). Any additional soft photons from the disk will make the spectrum softer, reducing $\eta_{\rm B}$ even more. The low magnetic field rules out magnetic reconnection as the energy dissipation mechanism. This also implies that electrons cannot be thermalized by the synchrotron self-absorption. On the other hand, if the size of the active region is $R \sim 60R_{\rm S}$, Coulomb scattering becomes important (as its influence grows linearly with size for constant L, see, e.g., Coppi 1999; Svensson 1999), and it can thermalize electrons at a rather high temperature of $kT_{\rm e} \sim 100$ keV as observed in Cyg X-1 (Gierlinski et al. 1997; Poutanen 1998).

We reiterate that the whole spectrum here is produced by the SSC mechanism.[3] Its thermostatic properties fix the electron temperature at 50–100 keV (for $\tau_{\rm p} \sim 1$) and stabilize the spectral slope at $\alpha \sim 0.7$–0.9. The feedback from the disk (Haardt & Maraschi 1993; Haardt et al. 1994; Stern et al. 1995b; Malzac et al. 2001) does not seem to be needed.

9.3 Spectral transitions and the role of disk photons

The spectral transitions observed in BHBs are most probably accompanied by a change in the geometry of the accretion disk. The cool outer disk moves toward the central black hole causing an increasing flux of the soft photons to the central hot flow (Esin et al. 1997; Poutanen et al. 1997; Poutanen & Coppi 1998), which we simulate here by increasing f (see Figure 9.4). Higher soft photon flux leads to faster Compton cooling and lower equilibrium electron temperature, making the nonthermal part more pronounced. The resulting photon distribution changes from the hard, thermal Comptonization dominated, spectrum to the one dominated by the disk blackbody, with a nonthermal tail extending to tens of MeV, which becomes harder at higher f. The spectral changes triggered by varying f are

[3] ADAF-based models also consider SSC as the main cooling mechanism; see Narayan et al. (1998) for the review.

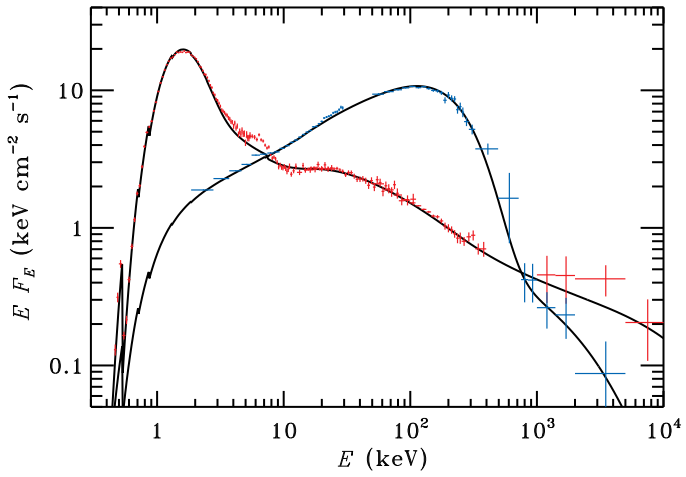

Figure 9.5: Spectral states of Cyg X-1. Crosses show the unfolded spectral data presented by Zdziarski et al. (2002). The model spectra with interstellar absorption (described by the column density $N_{\rm H}$) and Compton reflection (described by the solid angle Ω and ionization parameter ξ, Magdziarz & Zdziarski 1995) taken into account are shown by the solid curves. The parameters for the hard-state model are: $L = 2.7\times10^{37}$ erg s^{-1}, $R = 1.8\times10^8$ cm, $f = 0$, $\Gamma_{\rm inj} = 3.8$, $\tau_{\rm p} = 2.5$, $\eta_{\rm B} = 0.083$, $N_{\rm H} = 3\times10^{21}$ cm^{-2}, $\Omega/(2\pi) = 0.2$, $\xi = 0$. The soft state can be described by $L = 4.85\times10^{37}$ erg s^{-1}, $R = 3.85\times10^7$ cm, $f = 2.13$, $\Gamma_{\rm inj} = 2.2$, $\tau_{\rm p} = 0.3$, $\eta_{\rm B} = 1.5$, $N_{\rm H} = 5\times10^{21}$ cm^{-2}, $\Omega/(2\pi) = 0.7$, $\xi = 100$.

similar to the one observed in Cyg X-1 (see Figure 9.5). A detailed comparison with Cyg X-1 spectra shows, however, that other parameters change too.

Compared to the hard state, the soft state corresponds to a higher total luminosity. The MeV tail is harder $\alpha_{\rm MeV} \approx 1.6$ (McConnell et al. 2002), and therefore $\Gamma_{\rm inj} < 3.2$. If the tail of the blackbody at 3–10 keV (see Figure 9.5) is produced in the same emission region, it requires a rather hot thermal population of electrons, which needs high $\eta_{\rm B}$ for the synchrotron thermalization to operate (because Coulomb thermalization is not efficient under the conditions of strong Compton cooling). This would be consistent with the magnetically dominated emission region. Alternatively, there may be additional heating mechanisms operating. Also the tail might be a result of Comptonization in the hot ionized skin of the disk, not directly related to the emission we discuss here, but this interpretation might not be easily reconciled with the fact that the disk is stable, while the tail varies (Churazov et al. 2001). While the dramatic changes in the electron and photon distributions between the states are mainly caused by variations of the disk luminosity, it is obvious that other parameters do change during the transition. We stress that none of the presented models requires any additional thermal heating, which is different from the models of Poutanen & Coppi (1998) and Gierliński et al. (1999).

9.4 Conclusions

The hard state of BHBs can well be described by the quasi-thermal SSC mechanism. The feedback from the cool disk is not needed to stabilize the spectral slope and the electron temperature. Electrons can be injected to the active region with the power-law spectrum, but Coulomb scattering and synchrotron self-absorption thermalize them efficiently. This reduces the need for mysterious 'thermal heating' that was invoked previously to explain thermal Comptonization spectra of BHBs. The MeV tail together with the hard X-ray spectra of BHBs with photon indices $\alpha \lesssim 0.7$ and a cutoff at 100 keV require rather low magnetization $\eta_{\rm B} < 0.1$ and a large size of $R \gtrsim 60 R_{\rm S}$. In that case, magnetic reconnection can be ruled out as a source of energy. Similar results we obtained independently by Malzac & Belmont (2009).

At high optical depth of the emitting region $\tau_{\rm p} \gtrsim 10$, in the absence of disk radiation, the spectrum is close to saturated Comptonization, peaking at a few keV. This Wien-type spectrum might be associated with the ultrasoft state of BHBs. At low $\tau_{\rm p}$, the electrons are hotter and the spectra are softer due to the efficient synchrotron cooling.

A behavior similar to what is observed during the spectral state transitions in BHBs can be reproduced by varying the ratio of injected soft luminosity and the power dissipated in the hot phase, which could be caused by varying the radius of the inner cool disk. The increasing Compton cooling causes dramatic changes in the electron distribution from almost purely thermal to nearly nonthermal. The photon distribution also changes from quasi-thermal SSC to the nonthermal Comptonization of the disk photons. In the soft state of Cyg X-1, a strong magnetic field can thermalize electrons at sufficiently high temperature, which is consistent with a magnetically dominated corona being responsible for the high-energy emission.

Summary

Understanding the physical conditions as well as the radiative mechanisms giving rise to the broad-band spectra in various astrophysical sources like accreting black holes, relativistic jets in active galaxies and gamma-ray bursts requires detailed modeling of particle–photon interactions taking place via different processes. This is a formidable task for several reasons. First, both the particle and photon energies can span many orders of magnitude. Aside from different processes behaving differently, a given process can also exhibit significantly different behaviour depending of the energy regime. Compton scattering is the most prominent example: depending on the particle/photon energies, either the particle or the photon can gain or lose a negligible or significant fraction of its energy in one scattering, each case requiring different numerical treatment. Secondly, the wide energy range also means that we have vastly different timescales in the problem, which has implications for the stability of the numerical scheme. Finally, the kinetic equations describing the evolution of particle and photon distributions are coupled, making the problem non-linear.

We have developed a new computer code for simulations of radiative processes in magnetized rarefied plasmas that is able handle the aforementioned difficulties. The included processes Compton scattering, pair production and annihilation, synchrotron processes and Coulomb scattering. All the relevant rates are calculated without approximations and are therefore valid irrespective of the particle/photon energies. The interaction terms in the kinetic equations are written in the form most suitable for the treatment of each process, resulting in both integral and up to second order differential terms in the equations. The resulting coupled integro-differential kinetic equations describing time evolution of the photon and electron/positron distributions are solved simultaneously. The inclusion of second order differential terms allows us to treat particle thermalization by Compton and Coulomb scattering as well as synchrotron self-absorption.

The employed numerical techniques guarantee energy (and particle, when relevant) conservation with high accuracy which is especially important when dealing with strongly self-absorbed synchrotron radiation. The implementation of the Chang and Cooper scheme gives the correct shape of the particle distribution at low energies. The area of application of the code is enormous as it can deal with photons and leptons covering many orders of magnitude in momentum space, with no potential difficulty of extending it to even lower/higher energies.

We present a number of test runs, where we consider problems previously solved by other methods. We compute non-thermal pair cascades, and study lepton thermalization by synchrotron self-absorption, as well as model the emission from the stochastically heated pairs that might have a relation to the prompt emission of gamma-ray bursts. We find a good agreement in the parameter space where comparison is feasible while the differences can be explained by our improved treatment of microphysics.

We have applied the code to study prompt gamma-ray burst emission from neutron-loaded flows, in which the relative kinetic energy of neutron and proton flows can be dissipated through nuclear collisions. The dissipation is in the form of thermal heating as well as high-energy injection of electron-positron pairs and takes place over a range of distances from the central source. We have described a method of simulating radiative processes in the relativistic diverging outflow with our one-zone code by considering the evolution of particle and photon distributions in the comoving frame of the fluid. Adiabatic losses of the particle as well as photon distributions (the latter only in the optically thick regime) are taken into account. A simple method is described to take into account the effects of variable Doppler boosting as well as opacity in flow elements propagating at different angles to the line of sight. Our results are in good agreement with those obtained by Monte Carlo methods by Beloborodov (2010).

The spectrum is formed by the combined effect of thermal and non-thermal Compton scattering, the seed photons for which are provided by the thermal radiation component advected from the central source. The overall spectral shape resembles the Band-type spectrum typically observed in gamma-ray bursts, peaking near 1 MeV. Below the peak, the spectrum is hard and is determined by the advected thermal component (in the non-magnetized case). Above the peak, the comparable amount of thermal and non-thermal dissipation leads to relatively smooth Comptonized spectrum. At the highest energies (above several GeV) the spectral shape is determined by saturated pair cascade, which leads to steepening by unity in photon index relative to lower energies. On top of the otherwise smooth spectrum, the model predicts a Lorentz boosted annihilation feature at a couple of 100 MeV. In principle, this constitutes a well-defined observational test. However, in reality the detection of such feature might prove difficult due to the limited photon statistics at these energies.

The introduction of a magnetic field has two main effects: it softens the spectrum below the peak, and it introduces an additional partially self-absorbed synchrotron component at lower energies. The softer spectra might be easier to reconcile with “typical” observed spectral hardnesses, whereas pure thermal emission tends to be too hard even when accounting for softening due to large-angle emission. The low-energy synchrotron component could account for the X-ray excesses that have been observed in some bursts. Further exploration of the magnetized model is currently underway.

We have also applied the code to study the radiative mechanisms responsible

for different spectral states of black hole X-ray binaries, using a simple two-phase disk-corona model. We find that that thermalizing processes like synchrotron self-absorption and Coulomb scattering can play an important role in determining the spectral shape. This especially applies to the hard state, where efficient Coulomb thermalization can lead to quasi-thermal Comptonized spectra even for purely non-thermal (power-law) electron injection. The whole spectrum in this state can be produced by the synchrotron self-Compton mechanism, without the need for soft photons from the accretion disk.

Increasing the amount of soft radiation that enters the active region leads to stronger cooling of the electrons and a transition to a power-law dominated (soft) state, which is consistent with the decreasing inner radius of the accretion disk bringing about the spectral state transition.

Appendix A

Compton scattering

A.1 Functions s_j and S_j

All functions s_j and S_j defined in Chapter 1 can be expanded to series, which converge in the region $\xi < 1/2$. It is easy to show that

$$s_j(\xi) = \sum_{n=0}^{\infty} a_{jn}\,(-2\,\xi)^n, \qquad S_j(\xi) = \sum_{n=0}^{\infty} A_{jn}\,(-2\,\xi)^n, \tag{A.1}$$

where

$$\begin{aligned} a_{0n} &= \frac{3}{8}\left[n+2+\frac{2}{n+1}+\frac{8}{n+2}-\frac{16}{n+3}\right], \\ a_{1n} &= \frac{1}{8}\left[n\,(n+5)+\frac{24}{n+3}\right], \quad a_{2n} = \frac{1}{32}\left(n^3+9\,n^2+22\,n+32\right). \end{aligned} \tag{A.2}$$

Using equations (1.48), one can obtain the expressions for the coefficients A

Table A.1: Coefficients a_{jn} and A_{jn}.

n	0	1	2
a_{0n}	1	1	13/10
a_{1n}	1	3/2	47/20
a_{2n}	1	2	15/4
A_{1n}	1	21/10	147/40
A_{2n}	6/5	53/20	159/35
A_{3n}	1	14/5	47/8
A_{4n}	7/5	22/5	341/35
A_{5n}	1/5	2	401/70
A_{6n}	1/10	1/5	207/280
A_{7n}	3/10	3/5	281/280

through a:

$$A_{1n} = 2\,(a_{1\,n+1} - a_{0\,n+1}), \quad A_{2n} = 2\,(A_{1\,n+1} - a_{1\,n+1}), \quad A_{3n} = 2\,(a_{2\,n+1} - a_{1\,n+1}),$$
$$A_{4n} = 2\,(A_{3\,n+1} - A_{1\,n+1}), \quad A_{5n} = 3\,A_{4n} - 4A_{3n}, \quad A_{7n} = A_{3n} - A_{4n}/2,$$
$$A_{6n} = a_{2n} - 3\,A_{7n}. \tag{A.3}$$

The coefficients for $n = 0, 1, 2$ are presented in Table A.1.

A.2 Auxiliary functions ψ_{ij} and Ψ_{ij}

The total cross-section and mean powers of energy of scattered photons are expressed through the functions of one variable

$$\psi_{ij}(\xi) = \frac{i+1}{\xi^{i+1}} \int_0^\xi x^i\, s_j(x)\, dx, \quad i > -1, \qquad \psi_{-1j}(\xi) = \frac{1}{\xi} \int_0^\xi [1 - s_j(x)] \frac{dx}{x},$$
$$\Psi_{ij}(\xi) = \frac{i+1}{\xi^{i+1}} \int_0^\xi x^i\, S_j(x)\, dx. \tag{A.4}$$

Calculations of functions ψ_{ij} involve integrals of the following types:

$$\int dx\, x^m \ln(1+2x), \quad \int dx\, \frac{x^n}{(1+2x)^l}, \quad g(\xi) = \int_0^\xi \ln(1+2x)\, \frac{dx}{x}, \tag{A.5}$$

where $m = -1, 0, 1, 2, 3$ and $n, l = 1, 2, 3, 4$. All integrals are elementary except $g(\xi)$, which is described in details in Appendix A.3.

The explicit expressions for the functions ψ_{ij} are the following:

$$\psi_{-10}(\xi) = \frac{1}{8\,\xi}\left[\frac{4}{\xi^2} + \frac{2}{\xi} + \left(8 + \frac{3}{\xi} - \frac{3}{\xi^2} - \frac{2}{\xi^3}\right) l_\xi - 3\,R_\xi - \frac{11}{3}\right],$$
$$\psi_{-11}(\xi) = \frac{1}{8\,\xi}\left[\frac{7}{3} + \frac{2}{\xi} - \frac{2}{\xi^2} + \left(8 + \frac{1}{\xi^3}\right) l_\xi - 4\,R_\xi - R_\xi^2\right],$$
$$\psi_{-12}(\xi) = \frac{1}{16\,\xi}\left[11 + 16\,l_\xi - 7\,R_\xi - 3\,R_\xi^2 - R_\xi^3\right],$$
$$\psi_{00}(\xi) = \frac{3}{8\,\xi}\left[g(\xi) - \frac{2}{\xi} + \left(\frac{1}{2} + \frac{2}{\xi} + \frac{1}{\xi^2}\right) l_\xi - \frac{1}{2}\,R_\xi - \frac{3}{2}\right],$$
$$\psi_{01}(\xi) = \frac{3}{8\,\xi}\left[\frac{1}{\xi} - \frac{1}{2} + \left(\frac{4}{3} - \frac{1}{2\,\xi^2}\right) l_\xi - \frac{1}{3}\,R_\xi - \frac{1}{6}\,R_\xi^2\right], \tag{A.6}$$
$$\psi_{02}(\xi) = \frac{1}{32\,\xi}\left[\frac{7}{2} + 9\,l_\xi - R_\xi - \frac{3}{2}\,R_\xi^2 - R_\xi^3\right],$$
$$\psi_{10}(\xi) = \frac{3}{4\,\xi^2}\left[\left(\xi + \frac{9}{2} + \frac{2}{\xi}\right) l_\xi - 4 - \xi + \xi^2\,R_\xi - 2\,g(\xi)\right],$$
$$\psi_{11}(\xi) = \frac{1}{4\,\xi^2}\left[6 + 4\,\xi - 3\left(\frac{3}{2} + \frac{1}{\xi}\right) l_\xi - \xi\,(1+\xi)\,R_\xi^2\right],$$

$$\psi_{12}(\xi) = \frac{1}{16\,\xi^2}\left[\frac{1}{2} + 9\,\xi - 4\,l_\xi - R_\xi + \frac{1}{2}\,R_\xi^3\right],$$
$$\psi_{20}(\xi) = \frac{9}{32\,\xi^3}\left[25\,\xi + \left(2\xi^2 - 8\,\xi - 5\right)\,l_\xi + \xi\,R_\xi - 8\,g(\xi)\right],$$
$$\psi_{21}(\xi) = \frac{9}{8\,\xi^3}\left[g(\xi) + \frac{2}{3}\,\xi^2 - \frac{3}{2}\,\xi - \frac{1}{4}\,l_\xi - \frac{\xi^2}{6}\,R_\xi^2\right],$$
$$\psi_{22}(\xi) = \frac{3}{64\,\xi^3}\left[9\,\xi^2 - 8\,\xi + 5\,l_\xi - \xi\,(2 + 11\xi + 10\,\xi^2)\,R_\xi^3\right], \qquad \text{(A.6)}$$
$$\psi_{30}(\xi) = \frac{3}{12\,\xi^4}\left[\frac{\xi^3}{3} + \frac{31}{2}\xi^2 + \frac{31}{4}\,\xi + \left(2\xi^3 - 6\xi^2 - 12\,\xi - \frac{7}{2}\right)\,l_\xi - \frac{3}{4}\xi\,R_\xi\right],$$
$$\psi_{31}(\xi) = \frac{1}{24\,\xi^4}\left[16\xi^3 - 27\xi^2 - 45\,\xi + 3(7 + 12\xi)\,l_\xi + 3\xi\,(1 + 3\xi)\,R_\xi^2\right],$$
$$\psi_{32}(\xi) = \frac{1}{16\,\xi^4}\left[6\xi^3 - 4\xi^2 + 5\,\xi - 3\,l_\xi + \xi\,(1 + 4\xi + 2\xi^2)\,R_\xi^3\right],$$
$$\psi_{40}(\xi) = \frac{15}{128\,\xi^5}\left[\xi^4 + \frac{230}{9}\xi^3 + \frac{23}{6}\xi^2 - \frac{17}{6}\,\xi + \left(4\xi^4 - \frac{32}{3}\xi^3 - 16\xi^2 + \frac{11}{12}\right)\,l_\xi + \xi\,R_\xi\right],$$
$$\psi_{41}(\xi) = \frac{5}{64\,\xi^5}\left[8\xi^4 - 12\xi^3 - 9\xi^2 + 8\,\xi + 3\left(4\xi^2 - 1\right)\,l_\xi - \xi(2 + 5\xi)\,R_\xi^2\right],$$
$$\psi_{42}(\xi) = \frac{5}{256\,\xi^5}\left[18\xi^4 - \frac{32}{3}\xi^3 + 10\xi^2 - 12\,\xi + \frac{11}{2}\,l_\xi + \xi\,(1 + 7\xi + 14\xi^2)\,R_\xi^3\right],$$

where $l_\xi = \ln(1 + 2\xi)$ and $R_\xi = 1/(1 + 2\xi)$.

The explicit expressions for Ψ_{ij} can be obtained using definitions (1.48) for S_j:

$$\begin{aligned}
&\Psi_{11} = 2\,(\psi_{00} - \psi_{01})/\xi, && \Psi_{13} = 2\,(\psi_{01} - \psi_{02})/\xi,\\
&\Psi_{14} = 2\,(2\psi_{-11} - \psi_{-10} - \psi_{-12})/\xi, && \Psi_{16} = \psi_{12} - 3\,\Psi_{13} + 3\,\Psi_{14}/2,\\
&\Psi_{21} = 3\,(\psi_{10} - \psi_{11})/2\xi, && \Psi_{22} = 3\,(\psi_{11} - \Psi_{11})/2\xi,\\
&\Psi_{23} = 3\,(\psi_{11} - \psi_{12})/2\xi, && \Psi_{24} = 3\,(\Psi_{11} - \Psi_{13})/2\xi,\\
&\Psi_{25} = 3\,\Psi_{24} - 4\,\Psi_{23}, && \Psi_{26} = \psi_{22} - 3\,\Psi_{23} + 3\,\Psi_{24}/2,\\
&\Psi_{31} = 4\,(\psi_{20} - \psi_{21})/3\xi, && \Psi_{32} = 4\,(\psi_{21} - \Psi_{21})/3\xi,\\
&\Psi_{33} = 4\,(\psi_{21} - \psi_{22})/3\xi, && \Psi_{34} = 4\,(\Psi_{21} - \Psi_{23})/3\xi,\\
&\Psi_{35} = 3\,\Psi_{34} - 4\,\Psi_{33}, && \Psi_{37} = \Psi_{33} - \Psi_{34}/2,\\
&\Psi_{36} = \psi_{32} - 3\Psi_{37}, && \Psi_{41} = 5\,(\psi_{30} - \psi_{31})/4\xi,\\
&\Psi_{42} = 5\,(\psi_{31} - \Psi_{31})/4\xi, && \Psi_{43} = 5\,(\psi_{31} - \psi_{32})/4\xi,\\
&\Psi_{44} = 5\,(\Psi_{31} - \Psi_{33})/4\xi, && \Psi_{45} = 3\,\Psi_{44} - 4\,\Psi_{43},\\
&\Psi_{47} = \Psi_{43} - \Psi_{44}/2, && \Psi_{51} = 6\,(\psi_{40} - \psi_{41})/5\xi,\\
&\Psi_{54} = 6\,(\Psi_{41} - \Psi_{43})/5\xi, && \Psi_{57} = 6\,(\psi_{41} - \psi_{42})/5\xi - \Psi_{54}/2. \qquad \text{(A.7)}
\end{aligned}$$

In these formulae the argument ξ is omitted. For complete evaluation of these functions we need to compute 18 different functions ψ_{ij} given above.

To prevent the loss of accuracy if ξ is very small, we can use the series expansions (see Nagirner & Poutanen 1994) that directly follow from the definitions (A.4) and Taylor expansions (A.1):

$$\psi_{ij}(\xi) = \sum_{n=0}^{\infty} a_{jn} (-2\,\xi)^n \frac{i+1}{i+n+1},\ i > -1, \quad \psi_{-1j}(\xi) = \sum_{n=0}^{\infty} a_{j\,n+1} (-2\,\xi)^n \frac{2}{n+1}, \tag{A.8}$$

$$\Psi_{ij}(\xi) = \sum_{n=0}^{\infty} A_{jn} (-2\,\xi)^n \frac{i+1}{i+n+1}, \tag{A.9}$$

with a_{jn} and A_{jn} given by equations (A.2) and (A.3), respectively.

A.3 Auxiliary function $g(\xi)$

Calculations of function ψ_{ij} from Appendix A.2 involve integral

$$g(\xi) = \int_0^{\xi} \ln(1+2x)\,\frac{dx}{x}. \tag{A.10}$$

We repeat here for completeness the method of calculations of this integral from Nagirner & Poutanen (1994). It is possible to write a relation between the values of this function on $\xi < 1/2$ and $\xi > 1/2$. Let us define for that the auxiliary function for $\xi \le 1$

$$g_*(\xi) = g(\xi/2) = \int_0^{\xi} \ln(1+x)\,\frac{dx}{x}. \tag{A.11}$$

It can be presented by series

$$g_*(\xi) = \begin{cases} \displaystyle\sum_{n=1}^{\infty} (-1)^{n-1} \frac{\xi^n}{n^2} & \text{if } \xi \le \xi_* < 1, \\ \displaystyle\frac{\pi^2}{12} + \ln 2\,\ln\xi + \sum_{k=0}^{\infty} \frac{(1-\xi)^{k+2}}{k+2} \sum_{m=1}^{k+1} \frac{1}{2^m m} & \text{if } \xi_* \le \xi \le 1. \end{cases} \tag{A.12}$$

As ξ_* we can take 0.8 – 0.9. Then

$$g(\xi) = \begin{cases} g_*(2\,\xi) & \text{if } 0 \le \xi \le 1/2, \\ \displaystyle\frac{\pi^2}{12} & \text{if } \xi = 1/2, \\ \displaystyle\frac{\pi^2}{6} + \frac{1}{2}\ln^2(2\,\xi) - g_*(1/2\,\xi) & \text{if } \xi \ge 1/2. \end{cases} \tag{A.13}$$

A.4 Asymptotic expansions of functions χ_{jn} and Δ_{jn} in the Thomson limit

Using Taylor expansion (A.8) of functions ψ_{0n} for small arguments, it is easy to get an expansion of functions χ_{0n} in the Thomson limit $x\gamma \ll 1$:

$$\chi_{0n}(x,\gamma) = \gamma^n \sum_{l=0}^{\infty} (-2x\gamma)^l \, a_{0l} \, \kappa_{n+l+1}, \tag{A.14}$$

where

$$\begin{aligned} \kappa_l &= \frac{(1+\beta)^{l+1} - (1-\beta)^{l+1}}{2\beta(l+1)} = \sum_{k=0}^{\mathrm{int}(l/2)} \frac{l!\,\beta^{2k}}{(2k+1)!\,(l-2k)!} \\ &= \frac{(1+\beta)^l}{l+1} \sum_{k=0}^{l} \frac{1}{[\gamma(1+\beta)]^{2k}} \end{aligned} \tag{A.15}$$

and int(x) is the integer part of x. A few first functions are

$$\begin{aligned} &\kappa_1 = 1, \quad \kappa_2 = 1 + \frac{1}{3}\beta^2, \quad \kappa_3 = 1 + \beta^2, \quad \kappa_4 = 1 + 2\beta^2 + \frac{1}{5}\beta^4, \\ &\kappa_5 = 1 + \frac{10}{3}\beta^2 + \beta^4, \quad \kappa_6 = 1 + 5\beta^2 + 3\beta^4 + \frac{1}{7}\beta^6, \quad \kappa_7 = 1 + 7\beta^2 + 7\beta^4 + \beta^6. \end{aligned} \tag{A.16}$$

The first three terms of the expansion (A.14) are as follows: Function Δ_{00} coincides with χ_{00}, and functions Δ_{01} and Δ_{02} can be obtained using definitions (1.27) and expansion (A.14). For Δ_{01}, we get

$$\Delta_{01} = -\beta \sum_{l=0}^{\infty} (-2x\gamma)^l a_{0l} \zeta_{l+1} \approx -\frac{\beta}{3}\left[1 - 4x\gamma + \frac{78}{5}(x\gamma)^2\left(1 + \frac{\beta^2}{5}\right)\right], \tag{A.17}$$

where

$$\begin{aligned} \zeta_l &= \frac{\kappa_{l+1} - \kappa_l}{\beta^2} = \sum_{k=0}^{\mathrm{int}[(l-1)/2]} \frac{2k+2}{(2k+3)!}\beta^{2k} \frac{l!}{(l-1-2k)!}, \\ \zeta_1 &= \frac{1}{3}, \quad \zeta_2 = \frac{2}{3}, \quad \zeta_3 = 1 + \frac{1}{5}\beta^2, \quad \zeta_4 = \frac{4}{3} + \frac{4}{5}\beta^2, \\ \zeta_5 &= \frac{5}{3} + 2\beta^2 + \frac{1}{7}\beta^4, \quad \zeta_6 = 2 + 4\beta^2 + \frac{6}{7}\beta^4. \end{aligned} \tag{A.18}$$

Respectively for Δ_{02}, we have

$$\Delta_{02} = \beta^2 \sum_{l=0}^{\infty} (-2x\gamma)^l \, a_{0l} \, \Lambda_{l+1} \approx -\frac{4}{15}\beta^2 (x\gamma)\left(1 - \frac{39}{5}x\gamma\right), \tag{A.19}$$

where

$$\Lambda_l = \frac{1}{2\beta^2}\left[3\frac{\kappa_l - 2\kappa_{l+1} + \kappa_{l+2}}{\beta^2} - \kappa_l\right] = \sum_{k=1}^{\mathrm{int}(l/2)} \frac{l!}{(l-2k)!(2k)!}\frac{2k}{(2k+1)(2k+3)}\beta^{2(k-1)},$$

$$\Lambda_1 = 0, \quad \Lambda_2 = \frac{2}{15}, \quad \Lambda_3 = \frac{2}{5}, \quad \Lambda_4 = \frac{4}{5} + \frac{4}{35}\beta^2. \tag{A.20}$$

Similarly, for functions χ_{1n}, using expansions (A.9) we get:

$$\begin{aligned}\chi_{1n}(x,\gamma) &= \gamma^{n+1}\sum_{l=0}^{\infty}(-2x\gamma)^l\,(\gamma A_{1l} + x A_{2l})\,\kappa_{n+l+2} \\ &= \gamma^n\left[\gamma^2\kappa_{2+n} + \sum_{l=1}^{\infty}(-2x\gamma)^l\left(\gamma^2 A_{1l}\,\kappa_{n+l+2} - \frac{A_{2\,l-1}}{2}\kappa_{n+l+1}\right)\right].\end{aligned} \tag{A.21}$$

Functions Δ_{1n} can then be obtained using definitions (1.50):

$$\begin{aligned}\Delta_{10} &= \chi_{10} \approx 1 + \frac{4}{3}p^2 - \frac{x\gamma}{5}\left(42\gamma^2 - 27 - 2\beta^2\right), \\ \Delta_{11} &= -p\sum_{l=0}^{\infty}(-2x\gamma)^l\,(\gamma A_{1l} + x A_{2l})\,\zeta_{l+2} \approx -\beta\left\{\frac{2}{3}\gamma^2 - \frac{x\gamma}{5}\left[21\gamma^2(1+\beta^2/5) - 4\right]\right\}, \\ \Delta_{12} &= p\beta\sum_{l=0}^{\infty}(-2x\gamma)^l\,(\gamma A_{1l} + x A_{2l})\,\Lambda_{l+2} \approx \frac{2}{15}\beta^2\left[\gamma^2 - \frac{3x\gamma}{5}\left(21\gamma^2 - 2\right)\right].\end{aligned} \tag{A.22}$$

For functions χ_{2n}, we can write the expansion

$$\begin{aligned}\chi_{2n}(x,\gamma) &= \gamma^n\sum_{l=0}^{\infty}(-2x\gamma)^l\left[\left(\gamma^4 A_{4l} - \gamma^2 A_{7l}\right)\kappa_{n+l+3} - \gamma^2 A_{5l}\,\kappa_{n+l+2} + A_{6l}\,\kappa_{n+l+1}\right] \\ &\approx \gamma^n\left[\frac{7}{5}\gamma^4\kappa_{3+n} - \frac{\gamma^2}{10}(3\kappa_{3+n} + 2\kappa_{2+n}) + \frac{1}{10}\kappa_{1+n}\right],\end{aligned} \tag{A.23}$$

where we kept only the zeroth term in $x\gamma$ of the series. Expansions for Δ_{2n} can then be obtained using definitions (1.50):

$$\begin{aligned}\Delta_{20} &= \chi_{20} \approx 1 + \frac{2}{15}p^2\left(21\gamma^2 + 4\right), \\ \Delta_{21} &= -\beta\sum_{l=0}^{\infty}(-2x\gamma)^l\left[\left(\gamma^4 A_{4l} - \gamma^2 A_{7l}\right)\zeta_{l+3} - \gamma^2 A_{5l}\,\zeta_{l+2} + A_{6l}\,\zeta_{l+1}\right] \\ &\approx -\beta\left[1 + \frac{2}{75}p^2\left(63\gamma^2 + 34\right)\right], \\ \Delta_{22} &= \beta^2\sum_{l=0}^{\infty}(-2x\gamma)^l\left[\left(\gamma^4 A_{4l} - \gamma^2 A_{7l}\right)\Lambda_{l+3} - \gamma^2 A_{5l}\,\Lambda_{l+2} + A_{6l}\,\Lambda_{l+1}\right] \\ &\approx p^2\frac{1}{75}\left(42\gamma^2 - 11\right).\end{aligned} \tag{A.24}$$

Let us now discuss the properties of functions χ^*_{1n}. The series expansion can be easily obtained from the definition (1.89) and series (A.9):

$$\chi^*_{1n}(x,\gamma) \;=\; \gamma^{n+2}\sum_{l=0}^{\infty}(-2x\gamma)^l A_{1l}\,\kappa_{n+l+3}. \tag{A.25}$$

For Δ^*_{1k} we get:

$$\begin{aligned}
\Delta^*_{10} &= \chi^*_{10} \approx \gamma^2\left(1+\beta^2\right),\\
\Delta^*_{11} &= -\gamma p\sum_{l=0}^{\infty}(-2x\gamma)^l A_{1l}\,\zeta_{l+3} \approx -\gamma p\,(1+\beta^2/5),\\
\Delta^*_{12} &= p^2\sum_{l=0}^{\infty}(-2x\gamma)^l A_{1l}\,\Lambda_{l+3} \approx \frac{2}{5}p^2.
\end{aligned} \tag{A.26}$$

The series expansion for functions $\chi^\perp_{1n}$ is:

$$\begin{aligned}
\chi^\perp_{1n}(x,\gamma) &= \frac{\gamma^{n+1}}{p}\sum_{l=0}^{\infty}(-2x\gamma)^l A_{1l}\left(\kappa_{n+l+2}-2\gamma^2\,\kappa_{n+l+3}+\gamma^2\kappa_{n+l+4}\right)\\
&= \frac{2}{3}\gamma^{n+1}p\sum_{l=0}^{\infty}(-2x\gamma)^l A_{1l}\left(\beta^2\Lambda_{n+l+2}-\kappa_{n+l+2}\right).
\end{aligned} \tag{A.27}$$

For $\Delta^\perp_{1k}$ we get:

$$\Delta^\perp_{11} = \frac{1}{2}\chi^\perp_{10} \approx -\frac{1}{3}\gamma p\,(1+\beta^2/5), \tag{A.28}$$

$$\Delta^\perp_{12} = \frac{1}{2p}\left(\gamma\chi^\perp_{10}-\chi^\perp_{11}\right) = \frac{1}{3}p^2\sum_{l=0}^{\infty}(-2x\gamma)^l A_{1l}\,\left[\Lambda_{l+2}-\Lambda_{l+3}+\zeta_{l+2}\right] \approx \frac{2}{15}p^2.$$

A.5 Eliminating cancellations in redistribution functions

If formulae (1.138), (1.139) and (1.140) are used as they stand, numerical cancellations appear at certain regions of parameter space. For example if x and x_1 are small, the quantities a_- and a_+, $1/a_-$ and $1/a_+$, are close to each other. Also a combination containing a sum of d_-/a_-^3 and d_+/a_+^3 minus double the difference $1/a_-$ and $1/a_+$ has a cancellation. Therefore it is useful to rewrite the expressions in a form not containing those cancellations. The cancellations appearing in (1.138) were dealt with in Nagirner & Poutanen (1993). Defining

$$u = a_+ - a_- = \frac{(x+x_1)(2\gamma+x_1-x)}{a_-+a_+}, \quad v = a_-a_+, \tag{A.29}$$

they got

$$R_0 = \frac{2}{Q} + \frac{u}{v}\left(1 - \frac{2}{q}\right) + u\frac{(u^2 - Q^2)(u^2 + 5v)}{2q^2v^3} + u\frac{Q^2}{q^2v^2}. \tag{A.30}$$

Using definitions (A.29), we get from (1.139) and (1.140)

$$R_\Sigma = (a_- + a_+)\left[\frac{2u}{Q^3} + \frac{1}{v}\left(1 - \frac{2}{q}\right) + \frac{(u^2 - Q^2)(u^2 + 3v)}{2q^2v^3} + \frac{Q^2}{q^2v^2}\right], \tag{A.31}$$

$$R_\Pi = \frac{1}{2Q^5}\left[u^2(u^2 + 4v) + 2b^2\right] + \frac{1}{2Q}\left(1 - \frac{4}{q}\right) + \frac{u}{q^2v}. \tag{A.32}$$

Another loss of accuracy occurs in the $u^2 - Q^2$ term, when γ is close to $\gamma_*(x, x_1, \mu)$. We can use the following formulae (Nagirner & Poutanen 1993):

$$\begin{aligned} u^2 - Q^2 &= 2rqCD_u, \quad D_u = (\gamma + x_1 - x + \gamma_*)(\gamma - \gamma_*), \\ C &= 2/[\gamma(\gamma + x_1 - x) + r + xx_1\mu + v]. \end{aligned} \tag{A.33}$$

A.6 Boundaries

The redistribution functions R_0, R_Σ, R_Π and R_1, R_2 are defined within the interval of photon and electron energies and scattering angles satisfying the relation $|\cos\theta| \le 1$, where $\cos\theta$ is given by equation (1.107). These limits were discussed in Nagirner & Poutanen (1994), but we repeat them here for completeness. For fixed photon energies and scattering angle, we already got the limits on the electron energies given by equation (1.110), $\gamma \ge \gamma_*(x, x_1, \mu)$. If we are interested in the interval of scattered photon energies for the fixed x_1, γ and μ, we have then $x^- \le x \le x^+$, where

$$x^\pm(x_1, \gamma, \mu) = x_1\,\frac{\mu + \gamma(\gamma + x_1)(1 - \mu) \pm p\,(1 - \mu)\,a_+}{1 + 2\,\gamma\,x_1\,(1 - \mu) + x_1^2\,(1 - \mu)^2}. \tag{A.34}$$

If the energy of the scattered photon x is fixed, the initial photon x_1 lies in the interval

$$\begin{aligned} &x_1^- \le x_1 \le x_1^+ \quad \text{if } 0 \le x\,(1 - \mu) \le \gamma - p, \\ &x_1 > x_1^- \qquad\quad \text{if } \gamma - p \le x\,(1 - \mu) \le \gamma + p, \end{aligned} \tag{A.35}$$

where

$$x_1^\pm(x, \gamma, \mu) = x\,\frac{\mu + \gamma(\gamma - x)(1 - \mu) \pm p\,(1 - \mu)\,a_-}{1 - 2\,\gamma\,x\,(1 - \mu) + x^2\,(1 - \mu)^2}. \tag{A.36}$$

In equations (A.34) and (A.36), the quantities $a_\pm$ are defined by equations (1.119). If $|x - x_1| \le 2xx_1$, the quantity $\gamma_*(x, x_1, \mu)$ as a function of μ has a minimum

$$\gamma_{\min} = 1 + (x - x_1 + |x - x_1|)/2 \tag{A.37}$$

at $\mu = \mu_{\min} = 1 - |x - x_1|/xx_1$, while in the opposite case, $|x - x_1| \ge 2xx_1$, the function is monotonic with the minimum reached at the boundary $\mu = -1$ (see

Figure A.1). Correspondingly, the limits of variations of μ depend on the photon energies x, x_1 and the electron energy γ and are given by

$$\mu_{\rm m} \le \mu \le \mu_+, \tag{A.38}$$

where

$$\begin{aligned}
\mu_{\rm m}(x, x_1, \gamma) &= \begin{cases} -1 & \text{if } |x - x_1| \ge 2\, x\, x_1, \\ -1 & \text{if } |x - x_1| \le 2\, x\, x_1 \text{ and } \gamma \ge \gamma_*(x, x_1, -1), \\ \mu_- & \text{if } |x - x_1| \le 2\, x\, x_1 \text{ and } \gamma_{\rm min} \le \gamma \le \gamma_*(x, x_1, -1), \end{cases} \\
\mu_-(x, x_1, \gamma) &= 1 - \frac{q_+}{x\, x_1}, \\
\mu_+(x, x_1, \gamma) &= 1 - \frac{q_-}{x\, x_1} = 1 - \frac{(x - x_1)^2}{x\, x_1\, q_+}
\end{aligned} \tag{A.39}$$

and

$$q_\pm = p^2 + \gamma\,(x_1 - x) \pm p\,\sqrt{(\gamma + x_1 - x)^2 - 1}. \tag{A.40}$$

The quantity $\gamma_\star(x, x_1, -1)$ is the minimum electron energy needed to scatter a photon backwards (i.e. $\mu = -1$) from x_1 to x:

$$\gamma_*(x, x_1, -1) = \left[x - x_1 + (x + x_1)\,\sqrt{1 + 1/x x_1}\right]/2. \tag{A.41}$$

For the angle-averaged redistribution function, the lower limit on the electron energy is:

$$\gamma_\star(x, x_1) = \begin{cases} \gamma_*(x, x_1, -1) & \text{if } |x - x_1| \ge 2\, x\, x_1, \\ \gamma_{\rm min} & \text{if } |x - x_1| \le 2\, x\, x_1. \end{cases} \tag{A.42}$$

The limits of variation of the scattered photon energy x as a function of incident photon energy x_1 and γ can be found by inverting equation (A.42). We obtain

$$x^-(x_1, \gamma) \le x \le x_{\rm m}(x_1, \gamma), \tag{A.43}$$

where

$$\begin{aligned}
x_{\rm m}(x_1, \gamma) &= \begin{cases} \gamma + x_1 - 1 & \text{if } 1 \le \gamma \le 1 + \dfrac{2x_1^2}{1 - 2x_1} \text{ and } x_1 < 1/2, \\ x^+(x_1, \gamma) & \text{if } 1 + \dfrac{2x_1^2}{1 - 2x_1} \le \gamma \text{ and } x_1 < 1/2, \\ \gamma + x_1 - 1 & \text{if } x_1 \ge 1/2, \end{cases} \\
x^\pm(x_1, \gamma) &= x_1\,(\gamma \pm p)\,/\,(\gamma \mp p + 2\, x_1)\,.
\end{aligned} \tag{A.44}$$

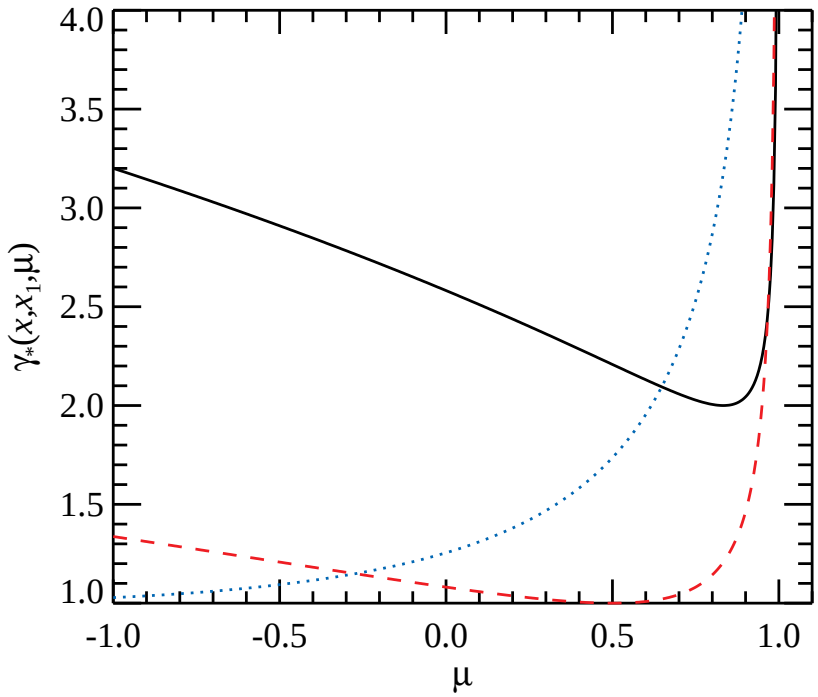

Figure A.1: The dependence of the function $\gamma_*(x, x_1, \mu)$ on μ. The energy of the incident photon is $x_1 = 2$. The solid curve is for $x = 3$, the dashed curve is for $x = 1$ (both cases correspond to $|x - x_1| < 2xx_1$), and the dotted curve is for $x = 0.3$ (for which $|x - x_1| > 2xx_1$).

A.7 Relation between the Compton redistribution functions for photons and electrons

The redistribution functions defined by equations (5.18) and (5.26) can be written as

$$\overline{R}_{\rm ph}(x,x_1,\gamma_1)=\frac{1}{4\pi^2}p_1\int p d\gamma d^2\Omega\delta(\gamma_1+x_1-\gamma-x)\int d^2\Omega_1 d^2\omega_1 F\delta(\boldsymbol{p}_1+\boldsymbol{x}_1-\boldsymbol{p}-\boldsymbol{x}), \tag{A.45}$$

$$\overline{R}_{\rm e}(\gamma,\gamma_1,x_1)=\frac{1}{4\pi^2}x_1\int x dx d^2\omega\delta(\gamma_1+x_1-\gamma-x)\int d^2\Omega_1 d^2\omega_1 F\delta(\boldsymbol{p}_1+\boldsymbol{x}_1-\boldsymbol{p}-\boldsymbol{x}). \tag{A.46}$$

We see that the inner integrals are identical in both expressions. Because of rotational symmetry, the only angle left in the calculation after performing the integrals over $d^2\Omega_1 d^2\omega_1$ is the angle between the momenta of outgoing particles. Therefore we can write $d^2\Omega = d^2\omega = 2\pi d\zeta$, where $\zeta = \boldsymbol{\Omega}\cdot\boldsymbol{\omega}$. We also see that $d\gamma\,\delta(\gamma_1 + x_1 - \gamma - x) = dx\,\delta(\gamma_1 + x_1 - \gamma - x)$, so we find from equations (A.45) and (A.46) that the redistribution functions are related as

$$pp_1\overline{R}_{\rm e}(\gamma,\gamma_1,x_1)=xx_1\overline{R}_{\rm ph}(x,x_1,\gamma_1), \tag{A.47}$$

where one of the energies/momenta has to be replaced from the condition $x+\gamma = x_1+\gamma_1$.

A.8 Isotropic Compton redistribution function

The isotropic Compton redistribution function defined in equation (5.18) can be written as an integral over the scattering angle (Nagirner & Poutanen 1994)

$$\overline{R}_{\rm ph}(x,x_1,\gamma_1)=\int_{\mu_m}^{\mu_+}R(x,x_1,\gamma_1,\mu)\,d\mu=T(x,x_1,\gamma_1,\mu)\Big|_{\mu_{\rm m}}^{\mu_+}. \tag{A.48}$$

The limits of integration are given by equations (A.39) in Section A.6, with γ substituted by γ_1.

The angle-dependent redistribution function $R(x,x_1,\gamma_1,\mu)$ was first derived by Aharonian & Atoyan (1981), see also Prasad et al. (1986) and Nagirner & Poutanen (1993). Similar functions for anisotropic electrons were derived in Chapter 1. The angle-averaged function was obtained by Jones (1968), but the presented expressions are very cumbersome and the loss of accuracy occurs for small photon energies and large electron energies. An alternative function given by Brinkmann (1984) and Nagirner & Poutanen (1994) does not suffer from these problems. We use here the latter expressions. The primitive function $T(x,x_1,\gamma_1,\mu)$ can be ex-

pressed through functions of one argument as

$$T(x,x_1,\gamma_1,\mu) = -\frac{2}{xx_1}Q + \sqrt{\frac{w}{2}}\left\{\frac{4}{xx_1}H_0 + w\left(1+\frac{1}{xx_1}\right)H_1 + \frac{H}{A(h_-)A(h_+)}\left[w + \frac{1}{2x^2x_1^2}\left(2\frac{H^2}{w} - (x-x_1)^2\right)\right]\right\}, \quad \text{(A.49)}$$

where $w = 1-\mu$ and $Q = \sqrt{(x-x_1)^2 + 2xx_1w}$. The functions H are given by the differences

$$H = A(h_-) - A(h_+), \quad H_n = A_n(h_-) - A_n(h_+), \quad \text{(A.50)}$$

where

$$A(h) = \sqrt{1+h}, \qquad h_+ = [(\gamma_1+x_1)^2 - 1]\,w/2, \qquad h_- = [(\gamma_1 - x)^2 - 1]\,w/2. \quad \text{(A.51)}$$

The zeroth function A_0 is

$$A_0(h) = \begin{cases} \ln(\sqrt{h} + \sqrt{1+h})/\sqrt{h} & \text{if } h \geq 0, \\ \arcsin(\sqrt{-h})/\sqrt{-h} & \text{if } h \leq 0, \end{cases} \quad \text{(A.52)}$$

while the others can be expressed through its derivatives as

$$A_n(h) = (-2)^n \frac{|2n-1|}{(2n-1)!!} A_0^{(n)}(h), \quad \text{(A.53)}$$

and can be computed by the recurrent relation

$$A_{n+1}(h) = \frac{1}{h}\left[\frac{2n+1}{|2n-1|}A_n(h) - \frac{1}{A^{2n+1}(h)}\right], \quad \text{(A.54)}$$

or for $|h| \leq 1$ via series

$$A_n(h) = \frac{|2n-1|}{(2n-1)!!}\sum_{k=0}^{\infty}\frac{(2n+2k-1)!!}{(2k)!!}\frac{(-h)^k}{2n+2k+1}. \quad \text{(A.55)}$$

Direct computations using (A.50) lead to numerical cancellations at small photon energies $x, x_1 \ll 1$. Nagirner & Poutanen (1994) describe in details how they should be dealt with.

A.9 Moments of the Compton redistribution function

The moments of the photon redistribution function given by equation (6.32) can be written explicitly using equation (5.14) as

$$\overline{x_1^i}\,\overline{s}_0(x) = \frac{3}{16\pi}\frac{2}{\lambda_C^3 N_e}\frac{1}{x}\int \frac{d^3p}{\gamma}\frac{d^3p_1}{\gamma_1}\frac{d^3x_1}{x_1}\,x_1^i\,\tilde{n}_e(\boldsymbol{p})\,F\,\delta^4, \quad \text{(A.56)}$$

where we have denoted $\delta^4 = \delta(\underline{p}_1 + \underline{x}_1 - \underline{p} - \underline{x})$ for brevity. We now define (Nagirner & Poutanen 1994)

$$\langle x_1^i \rangle \, s_0(\xi) = \frac{3}{16\pi} \frac{1}{\xi} \int \frac{d^3x_1}{x_1} \frac{d^3p_1}{\gamma_1} \, x_1^i \, F \, \delta^4 \tag{A.57}$$

and

$$\Psi_i(x, \gamma) = \frac{1}{4\pi\gamma x^{i+1}} \int d^2\Omega \; \xi \, \langle x_1^i \rangle \, s_0(\xi), \tag{A.58}$$

where $\xi = \underline{p} \cdot \underline{x}$. Using equations (A.57) and (A.58), we get for equation (A.56)

$$\overline{x_1^i} \, \overline{s}_0(x) = 4\pi \frac{2}{\lambda_C^3 N_e} \, x^i \int \tilde{n}_e(p) \, p^2 \, dp \, \Psi_i(x, \gamma). \tag{A.59}$$

Analytical expressions for Ψ_i along with asymptotic formulae for different limiting cases can be found in Nagirner & Poutanen (1994). For calculating $\dot{x}_c$ and $D_{ph}(x)$ using equations (6.33) we need terms like $\overline{(x_1 - x)^i} \, \overline{s}_0(x)$, for $i = 1, 2$, which are simply

$$\overline{(x_1 - x)} \, \overline{s}_0(x) = 4\pi \frac{2}{\lambda_C^3 N_e} \, x \int \tilde{n}_e(p) \, p^2 \, dp \, (\Psi_1 - \Psi_0), \tag{A.60}$$

$$\overline{(x_1 - x)^2} \, \overline{s}_0(x) = 4\pi \frac{2}{\lambda_C^3 N_e} \, x^2 \int \tilde{n}_e(p) \, p^2 \, dp \, (\Psi_2 - 2\Psi_1 + \Psi_0). \tag{A.61}$$

We now rewrite the moments of the electron redistribution function given by equation (6.17) using equation (5.22)

$$\overline{\gamma_1^i} \, \overline{s}_0(p) = \frac{3}{16\pi} \frac{2}{\lambda_C^3 N_{ph}} \frac{1}{\gamma} \int \frac{d^3x}{x} \frac{d^3x_1}{x_1} \frac{d^3p_1}{\gamma_1} \, \gamma_1^i \, \tilde{n}_{ph}(\boldsymbol{x}) \, F \, \delta^4. \tag{A.62}$$

We can define quantities analogous to equations (A.57) and (A.58):

$$\langle \gamma_1^i \rangle \, s_0(\xi) = \frac{3}{16\pi} \frac{1}{\xi} \int \frac{d^3x_1}{x_1} \frac{d^3p_1}{\gamma_1} \gamma_1^i \, F \, \delta^4 \tag{A.63}$$

and

$$\Phi_i(x, \gamma) = \frac{1}{4\pi x \gamma^{i+1}} \int d^2\omega \; \xi \, \langle \gamma_1^i \rangle \, s_0(\xi). \tag{A.64}$$

Equation (A.62) then takes the form

$$\overline{\gamma_1^i} \, \overline{s}_0(p) = 4\pi \frac{2}{\lambda_C^3 N_{ph}} \gamma^i \int \tilde{n}_{ph}(x) \, x^2 \, dx \, \Phi_i(x, \gamma), \tag{A.65}$$

while the terms needed for calculating $\dot{\gamma}_c$ and $D_e(\gamma)$ using equation (6.21) are

$$\overline{(\gamma_1 - \gamma)} \, \overline{s}_0(p) = 4\pi \frac{2}{\lambda_C^3 N_{ph}} \gamma \int \tilde{n}_{ph}(x) \, x^2 \, dx \, (\Phi_1 - \Phi_0), \tag{A.66}$$

$$\overline{(\gamma_1 - \gamma)^2} \, \overline{s}_0(p) = 4\pi \frac{2}{\lambda_C^3 N_{ph}} \gamma^2 \int \tilde{n}_{ph}(x) \, x^2 \, dx \, (\Phi_2 - 2\Phi_1 + \Phi_0). \tag{A.67}$$

From considerations of energy conservation one would expect a relation between the rates (A.60), (A.61) and (A.66), (A.67). To see this, consider the quantities $x\,(\Psi_1 - \Psi_0)$ and $\gamma\,(\Phi_1 - \Phi_0)$ entering equations (A.60) and (A.66):

$$x\,(\Psi_1 - \Psi_0) = \frac{1}{4\pi\gamma x}\int d^2\Omega\ \xi\,\langle x_1 - x\rangle s_0(\xi), \tag{A.68}$$

where

$$\langle x_1 - x\rangle\, s_0(\xi) = \frac{3}{16\pi}\frac{1}{\xi}\int \frac{d^3x_1}{x_1}\frac{d^3p_1}{\gamma_1}(x_1 - x)\,F\,\delta^4. \tag{A.69}$$

Analogously for electrons

$$\gamma\,(\Phi_1 - \Phi_0) = \frac{1}{4\pi x\gamma}\int d^2\omega\ \xi\,\langle\gamma_1 - \gamma\rangle\, s_0(\xi), \tag{A.70}$$

$$\langle\gamma_1 - \gamma\rangle\, s_0(\xi) = \frac{3}{16\pi}\frac{1}{\xi}\int \frac{d^3x_1}{x_1}\frac{d^3p_1}{\gamma_1}(\gamma_1 - \gamma)\,F\,\delta^4. \tag{A.71}$$

Due to the energy conservation δ-function, $x_1 - x = \gamma - \gamma_1$, and we thus get

$$\langle x_1 - x\rangle\, s_0(\xi) = -\langle\gamma_1 - \gamma\rangle\, s_0(\xi). \tag{A.72}$$

Also, after performing the integrals over $d^3x_1\,d^3p_1$ in equations (A.69) and (A.71) the only remaining angle that $\langle x_1 - x\rangle s_0(\xi)$ and $\langle\gamma_1 - \gamma\rangle s_0(\xi)$ can depend on is the one between the incoming photon and electron momenta. Therefore in equations (A.68) and (A.70) we can write $d^2\Omega = d^2\omega = 2\pi d\zeta$, $\zeta = \mathbf{\Omega}\cdot\boldsymbol{\omega}$ and conclude that

$$x\,(\Psi_1 - \Psi_0) = -\gamma\,(\Phi_1 - \Phi_0). \tag{A.73}$$

Using the same arguments one can show that

$$x^2\,(\Psi_2 - 2\Psi_1 + \Psi_0) = \gamma^2\,(\Phi_2 - 2\Phi_1 + \Phi_0). \tag{A.74}$$

We can thus use the analytic expressions for Ψ_i for calculating the rates $\dot{\gamma}_{\rm c}$ and $D_{\rm e}(\gamma)$ for electrons as well as photons. Note that since $\Psi_0 = \Phi_0$ we also have analytic expressions for calculating the total scattering cross-section for electrons through equation (A.65), setting $i = 0$.

Bibliography

Abdo, A. A., Ackermann, M., Ajello, M., et al. 2009a, ApJ, 706, L138

Abdo, A. A., Ackermann, M., Arimoto, M., et al. 2009b, Science, 323, 1688

Abramowicz, M. A., Chen, X., Kato, S., Lasota, J.-P., & Regev, O. 1995, ApJ, 438, L37

Aharonian, F. A. & Atoyan, A. M. 1981, Ap&SS, 79, 321

Amsler, C. et al. 2008, Phys. Lett., B667, 1

Arutyunyan, G. A. & Nikogosyan, A. G. 1980, Sov. Phys. – Doklady, 25, 918

Band, D., Matteson, J., Ford, L., et al. 1993, ApJ, 413, 281

Baring, M. 1987, MNRAS, 228, 695

Baring, M. G. & Harding, A. K. 1997, ApJ, 491, 663

Belmont, R. 2009, A&A, 506, 589

Belmont, R., Malzac, J., & Marcowith, A. 2008, A&A, 491, 617

Beloborodov, A. M. 1999, ApJ, 510, L123

Beloborodov, A. M. 2000, ApJ, 539, L25

Beloborodov, A. M. 2003a, ApJ, 585, L19

Beloborodov, A. M. 2003b, ApJ, 588, 931

Beloborodov, A. M. 2010, MNRAS, 407, 1033

Belyaev, S. T. & Budker, G. I. 1956, Dokl. Adac. Nauk SSSR, 107, 807

Berestetskii, V. B., Lifshitz, E. M., & Pitaevskii, V. B. 1982, Quantum electrodynamics (Oxford: Pergamon Press)

Bjornsson, C. 1985, MNRAS, 216, 241

Blumenthal, G. R. & Gould, R. J. 1970, Reviews of Modern Physics, 42, 237

Boettcher, M. & Schlickeiser, R. 1997, A&A, 325, 866

Bonometto, S. & Rees, M. J. 1971, MNRAS, 152, 21

Brinkmann, W. 1984, JQSRT, 31, 417

Chang, J. S. & Cooper, G. 1970, Journal of Computational Physics, 6, 1

Churazov, E., Gilfanov, M., & Revnivtsev, M. 2001, MNRAS, 321, 759

Coppi, P. S. 1992, MNRAS, 258, 657

Coppi, P. S. 1999, in Astronomical Society of the Pacific Conference Series, Vol. 161, High Energy Processes in Accreting Black Holes, ed. J. Poutanen & R. Svensson, 375–403

Coppi, P. S. & Blandford, R. D. 1990, MNRAS, 245, 453

Crusius, A. & Schlickeiser, R. 1986, A&A, 164, L16

Crusius-Waetzel, A. R. & Lesch, H. 1998, A&A, 338, 399

Daigne, F. & Mochkovitch, R. 2002, MNRAS, 336, 1271

de Groot, S. R., van Leeuwen, W. A., & van Weert, C. G. 1980, Relativistic kinetic equation (Amsterdam: North-Holland)

Derishev, E. V., Kocharovsky, V. V., & Kocharovsky, V. V. 1999a, A&A, 345, L51

Derishev, E. V., Kocharovsky, V. V., & Kocharovsky, V. V. 1999b, ApJ, 521, 640

Dermer, C. D. & Liang, E. P. 1989, ApJ, 339, 512

Dermer, C. D., Miller, J. A., & Li, H. 1996, ApJ, 456, 106

Dirac, P. A. M. 1930, Proc. Cambridge Phil. Soc., 26, 361

Esin, A. A., McClintock, J. E., & Narayan, R. 1997, ApJ, 489, 865

Fabian, A. C., Guilbert, P. W., Motch, C., et al. 1982, A&A, 111, L9

Frankel, N. E., Hines, K. C., & Dewar, R. L. 1979, Phys. Rev. A, 20, 2120

Ghirlanda, G., Celotti, A., & Ghisellini, G. 2003, A&A, 406, 879

Ghisellini, G. & Celotti, A. 1999, ApJ, 511, L93

Ghisellini, G., Celotti, A., & Costamante, L. 2002, A&A, 386, 833

Ghisellini, G., Guilbert, P. W., & Svensson, R. 1988, ApJ, 334, L5

Ghisellini, G., Haardt, F., & Svensson, R. 1998, MNRAS, 297, 348

Ghisellini, G. & Svensson, R. 1991, MNRAS, 252, 313

Giannios, D. 2008, A&A, 480, 305

Gierlinski, M., Zdziarski, A. A., Done, C., et al. 1997, MNRAS, 288, 958

Gierliński, M., Zdziarski, A. A., Poutanen, J., et al. 1999, MNRAS, 309, 496

Ginzburg, V. L., Sazonov, V. N., & Syrovatskii, S. I. 1968, Uspekhi Fiz. Nauk, 94, 63

Ginzburg, V. L. & Syrovatskii, S. I. 1965, ARA&A, 3, 297

Ginzburg, V. L. & Syrovatskii, S. I. 1969, ARA&A, 7, 375

Goodman, J. 1986, ApJ, 308, L47

Gould, R. J. & Schréder, G. P. 1967, Physical Review, 155, 1404

Grove, J. E., Johnson, W. N., Kroeger, R. A., et al. 1998, ApJ, 500, 899

Haardt, F. & Maraschi, L. 1993, ApJ, 413, 507

Haardt, F., Maraschi, L., & Ghisellini, G. 1994, ApJ, 432, L95

Jauch, J. M. & Rohrlich, F. 1976, The theory of photons and electrons. The relativistic quantum field theory of charged particles with spin one-half (New York: Springer)

Jones, F. C. 1968, Physical Review, 167, 1159

Kanbach, G., Straubmeier, C., Spruit, H. C., & Belloni, T. 2001, Nature, 414, 180

Katarzyński, K., Ghisellini, G., Svensson, R., & Gracia, J. 2006, A&A, 451, 739

Kershaw, D. S. 1987, Journal of Quantitative Spectroscopy and Radiative Transfer, 38, 347

Kershaw, D. S., Prasad, M. K., & Beason, J. D. 1986, Journal of Quantitative Spectroscopy and Radiative Transfer, 36, 273

Kobayashi, S. & Sari, R. 2001, ApJ, 551, 934

Landau, L. D. 1937, J. Exp. Theor. Phys., 7, 203

Le Roux, E. 1961, Annales d'Astrophysique, 24, 71

Lifshitz, E. M. & Pitaevskii, L. P. 1981, Physical kinetics (Oxford: Pergamon Press)

Lightman, A. P. & Zdziarski, A. A. 1987, ApJ, 319, 643

Ling, J. C., Wheaton, W. A., Wallyn, P., et al. 1997, ApJ, 484, 375

Lithwick, Y. & Sari, R. 2001, ApJ, 555, 540

Magdziarz, P. & Zdziarski, A. A. 1995, MNRAS, 273, 837

Malzac, J. & Belmont, R. 2009, MNRAS, 392, 570

Malzac, J., Beloborodov, A. M., & Poutanen, J. 2001, MNRAS, 326, 417

Marcowith, A. & Malzac, J. 2003, A&A, 409, 9

McConnell, M., Forrest, D., Ryan, J., et al. 1994, ApJ, 424, 933

McConnell, M. L., Zdziarski, A. A., Bennett, K., et al. 2002, ApJ, 572, 984

McCray, R. 1969, ApJ, 156, 329

Mészáros, P. & Rees, M. J. 2000a, ApJ, 541, L5

Mészáros, P. & Rees, M. J. 2000b, ApJ, 530, 292

Moderski, R., Sikora, M., Coppi, P. S., & Aharonian, F. 2005, MNRAS, 363, 954

Møller, C. 1932, Ann. Phys. (Leipzig), 14, 568

Motch, C., Ilovaisky, S. A., & Chevalier, C. 1982, A&A, 109, L1

Nagirner, D. I. & Loskutov, V. M. 1999, Astrophysics, 42, 206

Nagirner, D. I. & Poutanen, J. 1993, A&A, 275, 325

Nagirner, D. I. & Poutanen, J. 1994, Single Compton scattering, Vol. 9 (Amsterdam: Harwood Academic Publishers), 1–83

Nagirner, D. I. & Poutanen, J. 2001, A&A, 379, 664

Narayan, R., Mahadevan, R., & Quataert, E. 1998, in Theory of Black Hole Accretion Disks, ed. M. A. Abramowicz, G. Bjornsson, & J. E. Pringle (Cambridge: Cambridge University Press), 148

Narayan, R. & Yi, I. 1995, ApJ, 452, 710

Nava, L., Ghirlanda, G., Ghisellini, G., & Celotti, A. 2010, arXiv:1004.1410

Nayakshin, S. & Melia, F. 1998, ApJS, 114, 269

Ochelkov, I. P., Prilutskii, O. F., Rozental, I. L., & Usov, V. V. 1979, Relativistic kinetics and hydrodynamics (Moscow: Atomizdat)

Pacholczyk, A. G. 1970, Radio astrophysics. Nonthermal processes in galactic and extragalactic sources (San Francisco: Freeman)

Paczynski, B. 1986, ApJ, 308, L43

Panaitescu, A. & Mészáros, P. 2000, ApJ, 544, L17

Pe'er, A., Mészáros, P., & Rees, M. J. 2006, ApJ, 642, 995

Pe'er, A. & Waxman, E. 2005, ApJ, 628, 857

Pilla, R. P. & Shaham, J. 1997, ApJ, 486, 903

Piran, T. 2004, Reviews of Modern Physics, 76, 1143

Piran, T., Shemi, A., & Narayan, R. 1993, MNRAS, 263, 861

Pomraning, G. C. 1973, The equations of radiation hydrodynamics (Oxford: Pergamon Press)

Poutanen, J. 1994, PhD thesis, University of Helsinki

Poutanen, J. 1998, in Theory of Black Hole Accretion Disks, ed. M. A. Abramowicz, G. Björnsson, & J. E. Pringle (Cambridge: Cambridge University Press), 100–122

Poutanen, J. & Coppi, P. S. 1998, Physica Scripta T, 77, 57

Poutanen, J., Krolik, J. H., & Ryde, F. 1997, MNRAS, 292, L21

Poutanen, J. & Svensson, R. 1996, ApJ, 470, 249

Prasad, M. K., Kershaw, D. S., & Beason, J. D. 1986, Appl. Phys. Lett., 48, 1193

Preece, R. D., Briggs, M. S., Mallozzi, R. S., et al. 2000, ApJS, 126, 19

Preece, R. D., Briggs, M. S., Pendleton, G. N., et al. 1996, ApJ, 473, 310

Press, W. H., Teukolsky, S. A., Vetterling, W. T., & Flannery, B. P. 1992, Numerical recipes in FORTRAN. The art of scientific computing (Cambridge: University Press, 2nd ed.)

Pruet, J. & Dalal, N. 2002, ApJ, 573, 770

Rees, M. J. 1967, MNRAS, 136, 279

Roland, J., Hanisch, R. J., Veron, P., & Fomalont, E. 1985, A&A, 148, 323

Rybicki, G. B. & Lightman, A. P. 1979, Radiative processes in astrophysics (New York: Wiley-Interscience)

Ryde, F. 2004, ApJ, 614, 827

Ryde, F. 2005, ApJ, 625, L95

Sazonov, S. Y. & Sunyaev, R. A. 1998, ApJ, 508, 1

Scheuer, P. A. G. 1968, ApJ, 151, L139

Schopper, R., Lesch, H., & Birk, G. T. 1998, A&A, 335, 26

Schott, G. A. 1907, Phil. Mag., 13, 189

Spitkovsky, A. 2008a, ApJ, 673, L39

Spitkovsky, A. 2008b, ApJ, 682, L5

Stern, B. 1999, in Astronomical Society of the Pacific Conference Series, Vol. 161, High Energy Processes in Accreting Black Holes, ed. J. Poutanen & R. Svensson, 277

Stern, B. E., Begelman, M. C., Sikora, M., & Svensson, R. 1995a, MNRAS, 272, 291

Stern, B. E. & Poutanen, J. 2004, MNRAS, 352, L35

Stern, B. E. & Poutanen, J. 2006, MNRAS, 372, 1217

Stern, B. E. & Poutanen, J. 2008, MNRAS, 383, 1695

Stern, B. E., Poutanen, J., Svensson, R., Sikora, M., & Begelman, M. C. 1995b, ApJ, 449, L13

Sunyaev, R. A. & Zeldovich, Y. B. 1972, Comments on Astrophysics and Space Physics, 4, 173

Svensson, R. 1982, ApJ, 258, 321

Svensson, R. 1987, MNRAS, 227, 403

Svensson, R. 1999, in Astronomical Society of the Pacific Conference Series, Vol. 161, High Energy Processes in Accreting Black Holes, ed. J. Poutanen & R. Svensson, 361–374

Twiss, R. Q. 1958, Australian Journal of Physics, 11, 564

Vurm, I. & Poutanen, J. 2008, International Journal of Modern Physics D, 17, 1629

Vurm, I. & Poutanen, J. 2009, ApJ, 698, 293

Wardziński, G. & Zdziarski, A. A. 2001, MNRAS, 325, 963

Weinberg, S. 1973, Gravitation and Cosmology: Principles and Applications of the General Theory of Relativity (New York: Wiley-Interscience)

Westfold, K. C. 1959, ApJ, 130, 241

Woods, E. & Loeb, A. 1995, ApJ, 453, 583

Yuan, F. 2003, ApJ, 594, L99

Yuan, F. & Zdziarski, A. A. 2004, MNRAS, 354, 953

Zdziarski, A. A. 1988, ApJ, 335, 786

Zdziarski, A. A. & Gierliński, M. 2004, Prog. Theor. Phys. Suppl., 155, 99

Zdziarski, A. A., Grove, J. E., Poutanen, J., Rao, A. R., & Vadawale, S. V. 2001, ApJ, 554, L45

Zdziarski, A. A., Johnson, W. N., Poutanen, J., Magdziarz, P., & Gierlinski, M. 1997, in ESA SP-382: The Transparent Universe, ed. C. Winkler, T. J.-L. Courvoisier, & P. Durouchoux (Noordwijk: ESA), 373

Zdziarski, A. A. & Lightman, A. P. 1985, ApJ, 294, L79

Zdziarski, A. A., Lubinski, P., & Smith, D. A. 1999, MNRAS, 303, L11

Zdziarski, A. A., Poutanen, J., Paciesas, W. S., & Wen, L. 2002, ApJ, 578, 357

Zeldovich, Y. B. & Sunyaev, R. A. 1969, Ap&SS, 4, 301